

# Palaeoseismological analyses of northern and central Germany

Von der Naturwissenschaftlichen Fakultät der  
Gottfried Wilhelm Leibniz Universität Hannover

zur Erlangung des Grades  
Doktorin der Naturwissenschaften  
(Dr. rer. nat.)

genehmigte Dissertation  
von  
Katharina Müller, M. Sc.

2022

Referentin: Prof. Dr. rer. nat. Jutta Winsemann

Korreferent: Prof. Dr. rer. nat. habil. Manfred Frechen

Tag der Promotion 15.02.2022

## Abstract

Northern Germany is an intraplate region and has been regarded as a low seismicity area for a long time. However, historic sources show the occurrence of several significant natural earthquakes in northern and central Germany since the 10th century. In recent years natural earthquakes as well as earthquakes in the vicinity of active gas fields, likely to have been associated with the recovery of hydrocarbons, have been repeatedly instrumentally recorded in northern Germany. In central Germany, which is exposed to a higher earthquake hazard than northern Germany, historically and instrumentally recorded earthquakes accumulate in a N-S trending zone. However, the seismic record of Germany is limited and solely goes back to the year 800 CE. Long periods of seismic quiescence alternating with fault activity for a short geological period of time can falsify the seismic hazard of an intraplate region. Seismic hazard can be underestimated because of seismic quiescence or overestimated because of the detection of periodical clustering, migrating and infrequent seismicity. Therefore, palaeoseismology is the missing link for an accurate assessment of the seismic hazard estimation of a continental low strain area like Germany.

Northern and central Germany were repeatedly affected by glaciations and periglacial processes during the Pleistocene. The main difficulty is to distinguish the vast glaciotectonic deformation structures that are present in northern Germany from neotectonic deformation structures. Processes like cryoturbation, depositional loading in water saturated sediments and rapid rates of deposition can generate soft-sediment deformation structures that may also be mistaken for earthquake-induced structures. The analysis of neotectonic activity in northern and central Germany is challenging because recently observed vertical crustal movements along NW-SE-striking faults do not commonly correspond to visible morphological features and fault scarps are rapidly destroyed by climatic conditions.

Seven WNW-ESE trending major basement faults with a high potential for reactivation due to glacial isostatic adjustment were analysed with regard to neotectonic fault activity. In addition, in central Germany the controversially discussed seismically active part of the Regensburg-Leipzig-Rostock fault system between Leipzig and Cheb and surroundings was analysed with regard to pre-historic activity. Deformation bands and seismites in Palaeogene and Pleistocene deposits exposed in sand and gravel pits are indicators for neotectonic activity. Luminescence dating, shear-wave reflection seismics, electrical resistivity tomography and lineament analysis were applied to support neotectonic activity in the study area.

Evidence for neotectonic movements, indicated by the occurrence of deformation bands in Middle to Late Pleistocene sediments, was identified along five of the seven major basement faults that were analysed in northern Germany. Evidence was found at the Aller Fault, the Halle Fault, the Harz Boundary Fault, the Steinhuder Meer Fault and the Osning Thrust. In the area around the Regensburg-Leipzig-Rostock fault system neotectonic movements are indicated by deformation bands in Palaeocene and Middle Pleistocene sediments at fault intersections of mainly NW-SE oriented faults like the Lusatian Thrust and the Finne-Gera-Jáchymov fault system and fault intersections of minor faults in the vicinity to the cities Leipzig and Dresden.

It was possible to estimate the timing of neotectonic activity of faulted Pleistocene sediments by means of luminescence dating at two basement faults (Harz Boundary Fault, Steinhuder Meer Fault). The estimated ages of faulted debris-flow deposits at the Harz Boundary Fault ( $15.2 \pm 0.8$  and  $14.2 \pm 0.8$  ka) point to fault movements after  $\sim 15$  ka corresponding with the reactivation of the Osning Thrust. The estimated age of growth strata at the Steinhuder Meer Fault ( $189 \pm 5$  ka and  $158 \pm 4$  ka) indicates fault movements in Middle Pleistocene Saalian times. At the Harz Boundary Fault shear-wave reflection seismic surveys and electrical resistivity tomography profiles support the neotectonic activity in the Lateglacial. The timing of fault movements implies that the seismicity in northern and parts of central Germany is likely induced by varying lithospheric stress conditions related to glacial isostatic adjustment. For the Harz Boundary Fault and the Osning Thrust this is supported by numerical simulations of Coulomb failure stress variations. Thus, the faults can be classified as glacially-induced faults.

Along the Regensburg-Leipzig-Rostock fault system, focal mechanisms of deep-seated earthquakes partly show NW-SE trending nodal planes. The focal mechanisms indicate activity along NW-SE oriented faults that intersect the N-S striking Regensburg-Leipzig-Rostock fault system. This supports the seismotectonic importance of NW-SE oriented faults and intersecting faults in the study area of northern and central Germany.

**Keywords:** Palaeoseismology, intraplate earthquakes, soft-sediment deformation structures (SSDS), seismites, deformation bands, Middle to Late Pleistocene, glacial isostatic adjustment (GIA), glacially-induced faults (GIFs), northern and central Germany

## Zusammenfassung

Norddeutschland ist eine Intraplattenregion und wurde lange Zeit als ein Gebiet mit geringer Seismizität angesehen. Historische Quellen zeigen jedoch, dass in Nord- und Mitteldeutschland seit dem 10. Jahrhundert mehrere bedeutende natürliche Erdbeben aufgetreten sind. In den letzten Jahren wurden in Norddeutschland wiederholt natürliche Erdbeben und Erdbeben in der Nähe aktiver Gasfelder instrumentell aufgezeichnet, die wahrscheinlich mit der Förderung von Kohlenwasserstoffen zusammenhängen. In Mitteldeutschland, das eine höhere Erdbebengefährdung als Norddeutschland aufweist, häufen sich die historischen und instrumentell aufgezeichneten Erdbeben in einer N-S streichenden Zone. Allerdings ist die seismische Aufzeichnung Deutschlands limitiert und reicht nur bis in das Jahr 800 n. Chr. zurück. Lange Perioden seismischer Ruhe im Wechsel mit Störungsaktivität über einen kurzen geologischen Zeitraum können die seismische Gefährdung einer Intraplattenregion verfälschen, die durch seismische Ruhe unterschätzt oder durch den Nachweis von periodisch auftretender, wandernder Seismizität überschätzt werden kann. Daher ist die Paläoseismologie das fehlende Glied für eine genaue Abschätzung der seismischen Gefährdung eines kontinentalen Niedrigspannungsgebietes, wie Deutschland.

Während des Pleistozäns waren Nord- und Mitteldeutschland von Vergletscherungen und periglazialen Bedingungen betroffen. Die Herausforderung besteht darin, die vorhandenen glazitektonischen Verformungsstrukturen von neotektonischen Strukturen zu unterscheiden. Darüber hinaus können Prozesse wie Kryoturbation und Auflast wassergesättigter Sedimente Deformationsstrukturen in unverfestigten Sedimenten erzeugen, die mit Strukturen verwechselt werden können, die durch seismische Wellen entstehen. Zudem ist die Analyse neotektonischer Aktivität in Nord- und Mitteldeutschland schwierig, da die beobachteten vertikalen Krustalbewegungen entlang der NW-SE verlaufenden Störungen meist nicht sichtbare morphologische Merkmale zeigen und Bruchstufen aufgrund der klimatischen Bedingungen schnell zerstört werden.

Sieben WNW-ESE orientierte Hauptstörungszonen, die aufgrund der isostatischen Ausgleichsbewegung Skandinaviens ein hohes Reaktivierungspotenzial aufweisen, wurden auf neotektonische Aktivität untersucht. Darüber hinaus wurde in Mitteldeutschland der kontrovers diskutierte seismisch aktive Teil des Regensburg-Leipzig-Rostock-Störungssystems zwischen Leipzig und Cheb hinsichtlich prähistorischer Aktivität analysiert. Indikatoren für neotektonische Aktivität sind Deformationsbänder und Seismite in paläogenen und pleistozänen Sedimenten, die in Sandgruben aufgeschlossen sind. Zusätzlich wurden Lumineszenzdatierung, Scherwellenreflexionsseismik, elektrische Widerstandstomographie und Lineamentanalysen eingesetzt, um die Hinweise auf neotektonische Aktivität zu untermauern.

Hinweise auf neotektonische Bewegungen in mittel- bis spätpleistozänen Sedimenten konnten identifiziert werden. Diese waren entlang von fünf der untersuchten sieben Hauptstörungszonen in Norddeutschland aufgeschlossen. Diese Deformationsstrukturen wurden in Sandgruben entlang der Allertal-Störung, der Halle-Störung, der Harznordrand-Störung, der Steinhuder Meer-Störung und der Osning-Störung gefunden. Im Bereich des Regensburg-Leipzig-Rostock-Störungssystems sind neotektonische Bewegungen durch Deformationsbänder in paläozänen und mittelpleistozänen Sedimenten angezeigt. Diese waren an Störungskreuzungspunkten von hauptsächlich NW-SE orientierten Störungen wie der Lausitzer-Störung und dem Finne-Gera-Jáchymov-Störungssystem sowie an Kreuzungen von Nebenstörungen in der Nähe der Städte Leipzig und Dresden zu finden.

An zwei Hauptstörungszonen (Harznordrand-Störung, Steinhuder Meer-Störung) konnte mittels Lumineszenzdatierung der Zeitpunkt der neotektonischen Aktivität abgeschätzt werden. Das ermittelte Alter von versetzten Schuttstromablagerungen an der Harznordrand-Störung ( $15,2 \pm 0,8$  ka und  $14,2 \pm 0,8$  ka) zeigt Bewegungen nach  $\sim 15$  ka an und stimmt damit zeitlich mit dem Alter der Reaktivierung der Osning-Störung überein. Das ermittelte Alter von syntektonisch abgelagerten Sedimenten an der Steinhuder Meer-Störung ( $189 \pm 5$  ka und  $158 \pm 4$  ka) deutet auf eine pleistozäne saalezeitliche Aktivität hin. An der Harznordrand-Störung konnte die neotektonische Aktivität im Spätglazial durch gemessene Scherwellenreflexionsseismik- und elektrische Widerstandstomographieprofile bestätigt werden. Der Zeitpunkt der Störungsbewegungen impliziert, dass die Seismizität in Nord- und Teilen Mitteldeutschlands durch unterschiedliche lithosphärische Spannungszustände ausgelöst wurde, die im Zusammenhang mit der glazialen Ausgleichsbewegung stehen. Für die Harznordrand-Störung und die Osning-Störung wird dies durch numerische Simulationen der Coulomb-Spannungsänderungen unterstützt. Somit können die Störungen als glazial reaktivierte Störungen klassifiziert werden. Entlang des Regensburg-Leipzig-Rostock-Störungssystems zeigen Herdflächenlösungen, zum Teil NW-SE streichende Nodalflächen. Die Herdflächenlösungen weisen somit auf Aktivität entlang der NW-SE orientierten Störungen hin, die das N-S streichende Regensburg-Leipzig-Rostock-Störungssystem kreuzen. Dies unterstützt die seismotektonische Bedeutung von NW-SE orientierten Störungen und Störungskreuzungen in Nord- und Mitteldeutschland.

**Schlagwörter:** Paläoseismologie, Intraplatten-Erdbeben, Deformationsstrukturen in unverfestigten Sedimenten (SSDS), Seismite, Deformationsbänder, Mittel- bis Spätpleistozän, glaziale Ausgleichsbewegung (GIA), glazial reaktivierte Störungen (GIFs), Nord- und Mitteldeutschland



## List of Abbreviations

<b>ANU-ICE</b>	Ice history model	<b>Ma</b>	Million years
<b>BGR</b>	Federal Institute for Geosciences and Natural Resources	<b>MGCZ</b>	Mid-German Crystalline Zone
<b>BFB</b>	Broad Fourteens Basin	<b>MIS</b>	Marine Isotope Stages
<b>BK fs</b>	Bergen-Klingenthal fault system	<b>MLF</b>	Marienbader Fault
<b>cal kyr BP</b>	Calibrated kiloyears before present	<b>M<sub>L</sub></b>	Local magnitude
<b>CB</b>	Cheb Basin	<b>M<sub>w</sub></b>	Moment magnitude
<b>CE</b>	Common Era	<b>MSK scale</b>	Medvedev-Sponheuer-Karnik scale
<b>CEBS</b>	Central European Basin System	<b>NDB</b>	Norwegian Danish Basin
<b>D</b>	Saalian (Drenthe) ice sheet	<b>NGB</b>	North German Basin
<b>DF</b>	Debris flow	<b>NEGB</b>	Northeast German Basin
<b>CFS</b>	Coulomb failure stress	<b>NPR Lineament</b>	Naab-Pritzwalk-Rostock Lineament
<b>CMP stacking</b>	Common Mid-Point stacking	<b>OSL</b>	Optical Stimulated Luminescence
<b>DEM</b>	Digital Elevation Model	<b>PB</b>	Polish Basin
<b>D<sub>e</sub></b>	Equivalent dose	<b>RLRfs</b>	Regensburg-Leipzig-Rostock fault system
<b>D<sub>R</sub></b>	Dose rate	<b>RLRZ</b>	Regensburg-Leipzig-Rostock Zone
<b>E</b>	Elsterian ice sheet	<b>PGFs</b>	Postglacial faults
<b>ECRIS</b>	European Cenozoic Rift System	<b>PPZ</b>	Počátky-Plesná-Zone
<b>EMS</b>	European Macroseismic Scale	<b>PREM</b>	Preliminary Reference Earth Model
<b>ER</b>	Eger Rift	<b>P-wave</b>	Primary wave
<b>ERT</b>	Electrical Resistivity Tomography	<b>SAR protocol</b>	Single-Aliquot Regenerative- Dose protocol
<b>FD-migration</b>	Finite-difference migration	<b>SB</b>	Subhercynian Basin
<b>FGJ fault system</b>	Finne-Gera-Jáchymov fault system	<b>SF</b>	Seismic facies
<b>FK filters</b>	Frequency-wavenumber filters	<b>SH-waves</b>	Horizontally polarized shear waves
<b>GERSEIS</b>	BGR Geodata Service	<b>S<sub>Hmax</sub></b>	Maximum horizontal stress
<b>GIA</b>	Glacial Isostatic Adjustment	<b>RSEf</b>	Reichenbach-Schöneck-Erlbach Fault
<b>GIFs</b>	Glacially-Induced Faults	<b>SSDS</b>	Soft-sediment deformation structure
<b>GIS</b>	Geographic Information System	<b>STZ</b>	Sorgenfrei-Tornquist Zone
<b>GPS</b>	Global Positioning System	<b>SXNET</b>	Sachsennetz
<b>GPR</b>	Ground Penetrating Radar	<b>TESZ</b>	Trans-European Suture Zone
<b>Gy</b>	SI derived unit: Absorbed dose of ionizing radiation (1 J kg <sup>-1</sup> = 1 Gy (Gray))	<b>TLUBN</b>	Thüringer Landesamt für Umwelt, Bergbau und Naturschutz
<b>HBF</b>	Harz Boundary Fault	<b>TSN</b>	Thüringer Seismologisches Netz
<b>ICE-6G_C</b>	Global ice model version 6 with Antarctic component	<b>TTZ</b>	Teisseyre-Tornquist Zone
<b>IRSL</b>	Infrared Stimulated Luminescence	<b>TWT</b>	Two-Way-Travel time
<b>ISB</b>	Intramontane Saale Basin	<b>TZ</b>	Transition Zone
<b>I<sub>0</sub></b>	Epicentral Intensity	<b>WEBNET</b>	Westböhmennetz
<b>ka</b>	Thousand years	<b>WNB</b>	West Netherlands Basin
<b>LfULG</b>	Landesamt für Umwelt, Landwirtschaft und Geologie	<b>Wa1</b>	Saalian (Warthe1) ice sheet
<b>LGM</b>	Last Glacial Maximum	<b>Wa2</b>	Saalian (Warthe2) ice sheet
<b>LIAG</b>	Leibniz Institut für Angewandte Geophysik	<b>W</b>	Weichselian ice sheet
<b>LSB</b>	Lower Saxony Basin		

---

## Table of Contents

<b>Abstract</b>	I
<b>Zusammenfassung</b>	II
List of Abbreviations	III
Table of Contents	IV
<b>1. Introduction</b>	1
1.1 Motivation	1
1.2 Aim of this work and key research questions	2
1.3 Intraplate seismicity in Germany	3
1.4 Fault tectonics	6
1.5 Deformation processes and deformation structures	10
<b>2. Geological setting</b>	14
2.1 Crustal structure of northern central Europe	14
2.2 Geological evolution of the study area	15
2.3 Major faults in the study area	15
2.4 Pleistocene glaciations	20
2.5 Lithospheric stress field and glacial isostatic adjustment	22
<b>3. Methods</b>	24
3.1 Selection of outcrops	24
3.2 Fieldwork	24
3.3 Luminescence dating	26
3.4 Shear-wave reflection seismics	29
3.5 Electrical resistivity tomography	30
3.6 Coulomb failure stress modelling	31
3.7 Lineament analysis	32
<b>4. References</b>	33
<b>5. Overview of this thesis - Publications and their content</b>	46
<b>Publication 1</b>	49
Structural style and neotectonic activity along the Harz Boundary Fault, northern Germany: A multimethod approach integrating geophysics, outcrop data and numerical simulations	
<b>Supplementary data</b>	84
to Publication 1	
<b>Publication 2</b>	90
Glacially-induced faults in Germany	

<b>Publication 3</b>	111
The challenge to distinguish soft-sediment deformation structures (SSDS) formed by glaciotectonic, periglacial and seismic processes in a formerly glaciated area: a review and synthesis	
<b>Publication 4</b>	133
Re-examination and neotectonic analysis of the N-S trending Regensburg-Leipzig-Rostock fault system between Leipzig and Cheb	
<b>6. Synthesis and Discussion</b>	179
6.1 Neotectonic fault activity in northern and central Germany	179
6.2 Timing of fault activity	181
6.3 Challenges and geological indicators of young fault activity at blind faults	183
<b>7. Conclusions</b>	185
<b>8. References</b>	187
<b>9. Appendix</b>	196
9.1 Supplementary data to luminescence dating (Steinhuder Meer Fault)	196
9.2 Outcrop locations	199
<b>Acknowledgements</b>	210
<b>Curriculum Vitae</b>	211
<b>List of Publications</b>	212

# 1. Introduction

## 1.1 Motivation

For a long time, intraplate earthquakes were not in the research focus because they account for only 5% of the global seismic energy release (Talwani 2014). Due to the rarity of intraplate earthquakes, the database is limited. With the development of improved methods such as palaeoseismological analyses, denser seismic networks and improved near-surface geophysical techniques like georadar, ERT and reflection seismics it became possible to better detect and analyse intraplate fault systems and their hazard potential.

In general, intraplate earthquakes occur at pre-existing zones of weakness like fault zones, suture zones, failed rifts, and other tectonic boundaries (Sykes 1978). Depending on the regional stress field and the orientation of local stress concentrators, like intersecting faults, buried plutons or rift pillows, stress increases which can cause intraplate seismicity (Gangopadhyay and Talwani 2003). Intraplate earthquakes or earthquakes in stable continental regions show more complex spatial and temporal patterns compared to earthquakes at plate boundaries (Fig. 1). They occur due to the release of elastic energy caused by local stress or fault strength variations in a pre-stressed lithosphere (Calais et al. 2016). The tectonic loading rates of intraplate earthquakes in low strain areas are negligible (Calais et al. 2016). Earthquakes in stable continental areas can occur in regions with no significant seismicity. This assumption might be caused by very long recurrence intervals. They may occur as single events or as earthquake clusters in a short period of time, which is followed by a long time of quiescence. Their hypocentres may migrate between faults (Fig. 1) (Li et al. 2009; Liu et al. 2011; Talwani 2017). Without significant tectonic loading, earthquakes can occur repeatedly on a weakened fault zone (Li et al. 2009) caused by a complex system of interacting faults that spread over a wide area (Fig. 1) (Stein et al. 2015).

Thus, the variations of seismicity in space and time are a challenge for a seismic hazard estimation in intraplate areas. Due to the long recurrence intervals of intraplate earthquakes, fault systems can be falsely classified as inactive. Furthermore, the short observation periods of intraplate earthquakes in Germany since 800 CE, did not deliver a comprehensive view of the true seismic activity in this area. In low-strain areas commonly 8000-11000 years are needed to reveal a uniform seismicity. Shorter observation intervals may deliver a biased view on the seismicity in an intraplate area (e.g. Swafford and Stein 2007; Stein et al. 2015).

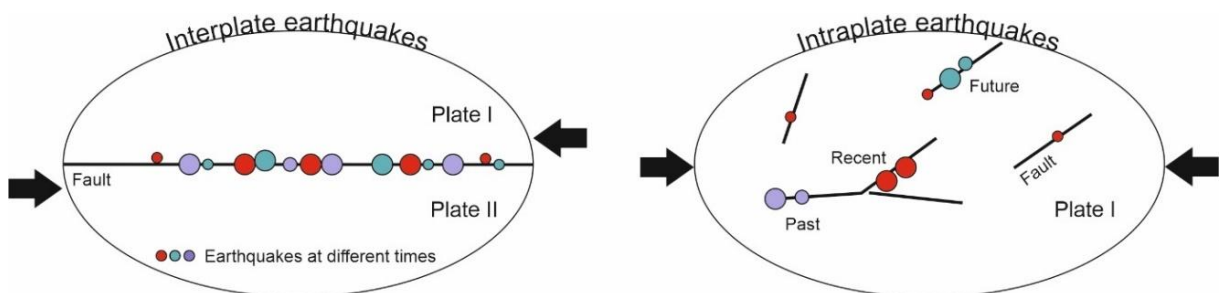


Figure 1: Schematic model of the different behaviour of interplate and intraplate seismicity (modified after Liu et al. 2011).

For a seismic hazard classification of a stable continental area like Germany, challenges associated with intraplate earthquakes are: 1) the long recurrence intervals between earthquakes, 2) the migration of hypocentres along faults (Fig. 1), and 3) the absence of visible morphological features like fault scarps or shutter ridges.

Palaeoseismological analyses can solve some of these problems and allow to extend the seismic record into the geological past in order to better derive earthquake recurrence intervals. Palaeoseismology is the study of the size, location and timing of pre-historic earthquakes based on the geological and geomorphic record (McCalpin 2009). These analyses help to extend the earthquake catalogue into the geological past and hence they are a helpful method for the understanding of intraplate seismicity.

### **1.2 Aim of this work and key research questions**

This doctoral thesis is based on two research projects 'Palaeoseismic investigation of northern Germany' and 'Palaeoseismic and tectonic investigation of a section of the Regensburg-Rostock Fault Zone and concept design for a trench for palaeoseismic analyses' both funded by the Federal Institute for Geosciences and Natural Resources (BGR).

To understand the controlling factors of intraplate earthquakes in the low strain area of northern and central Germany, the analysis of pre-historic earthquakes is necessary. With the current level of knowledge, the distribution of seismicity in plate interiors might be more heterogeneous as indicated by existing palaeoseismological analyses, instrumentally detected seismicity and measurements of geodetic strain rates (cf. Calais et al. 2016). Systematic palaeoseismological studies will deliver new evidence for fault activity and hence they are an important contribution for the understanding of the seismic and structural evolution of faults. To extent the limited number of palaeoseismological studies in northern and central Germany (e.g. Hoffmann and Reicherter 2011; Brandes et al. 2012; Brandes and Winsemann 2013) systematic palaeoseismological analyses were conducted in northern and central Germany.

The aim of this study was to analyse seven major fault zones (Aller Fault, Elbe Lineament, Gardelegen Fault, Halle Fault, Harz Boundary Fault, Osning Thrust and Steinhuder Meer Fault) in northern Germany and a section of the seismically active Regensburg-Leipzig-Rostock (RLR) fault system in central Germany, in order to find indications for Pleistocene to Holocene palaeo-earthquakes or at least neotectonic fault activity. This helps to extend the historic earthquake catalogue into the geological past and is necessary for a better assessment of the seismicity in northern and central Germany. This can help to reduce uncertainties caused by the short seismic record and improves the accuracy of published seismic hazard maps of Germany (e.g. Grünthal et al. 1998) with an extended pre-historic seismic record (e.g. Stein et al. 2015).

The study area of northern and central Germany, which appear to differ in the degree of seismicity, are compared in this study with respect to their palaeo-earthquake and neotectonic activity. This will deliver new insights into the seismic pattern and spatial distribution of earthquakes along fault systems. The results are important for the assessment of the seismic hazard potential in northern and central Germany and are relevant for the search for a suitable repository for nuclear waste, future hydrocarbon recovery and geothermal projects. They are also transferable to geologically similar, seismically active intraplate regions worldwide, e.g. in North America, Scandinavia and Russia.

Key research questions of this palaeoseismological study are:

### **Which of the major faults in northern and central Germany show evidence for neotectonic fault activity?**

Several major faults and fault systems were analysed: the Aller Fault, the Elbe Lineament, the Gardelegen Fault, the Halle Fault, the Harz Boundary Fault, the Osning Thrust, the Steinhuder Meer Fault and the area around the RLR fault system with the Lusatian Thrust and the Finne-Gera-Jáchymov (FGJ) fault system, in order to detect geological evidence for neotectonic fault movements.

### **What is the timing of neotectonic fault activity in the study area?**

The timing of fault activity in this study is estimated using geochronological methods like luminescence dating (OSL/IRSL) of unconsolidated Pleistocene sediments. This is possible if growth strata is developed, or if the depositional ages of faulted sediments and overlying post-tectonic sediments can be derived.

### **What are reliable geological indicators of young fault activity at blind faults and what are the challenges with the interpretation of such structures?**

Soft-sediment deformation structures (SSDS) developed in Pleistocene and Holocene sediments, can be used as indicators for seismic activity. However, there are several mechanisms such as depositional loading, glacial loading and periglacial processes that produce similar types of SSDS, which can be easily mistaken for seismites. Therefore, it is important to use clear criteria to recognize seismites in the field. Creeping faults that do not emit seismic waves are a special challenge in palaeoseismological analyses. In this study deformation bands are used as indicators for fault activity to overcome these limitations.

## **1.3 Intraplate seismicity in Germany**

Germany is a low strain area with a rather small seismic record (e.g. Leydecker and Kopera 1999; Leydecker 2011). It is a rigid continental area far from active plate boundaries. Continental areas commonly show a uniform stress field over hundreds of kilometres. In large parts of the stable European continent a homogeneous NW to NNW compressional stress regime exists (Müller et al. 1992; Heidbach et al. 2016). Measurements of the geodetic velocity field of central Europe show the rigidity and a low intraplate deformation rate of  $0.4 \text{ mm yr}^{-1}$  (Nocquet and Calais 2003) that was later lowered to  $0.2 \text{ mm yr}^{-1}$  (Nocquet 2012). Nevertheless, low strain rates of stable continental areas are prone for intraplate earthquakes (Johnston 1989).

Until today, the observed major seismicity in Germany accumulates in three zones of crustal weakness: the Rhine Rift Valley, the Swabian Alp, and eastern Thuringia/western Saxony (Grünthal et al. 1998). However, even in seismically calm areas, like northern Germany, historic and instrumentally detected earthquakes are observed (Fig. 2).



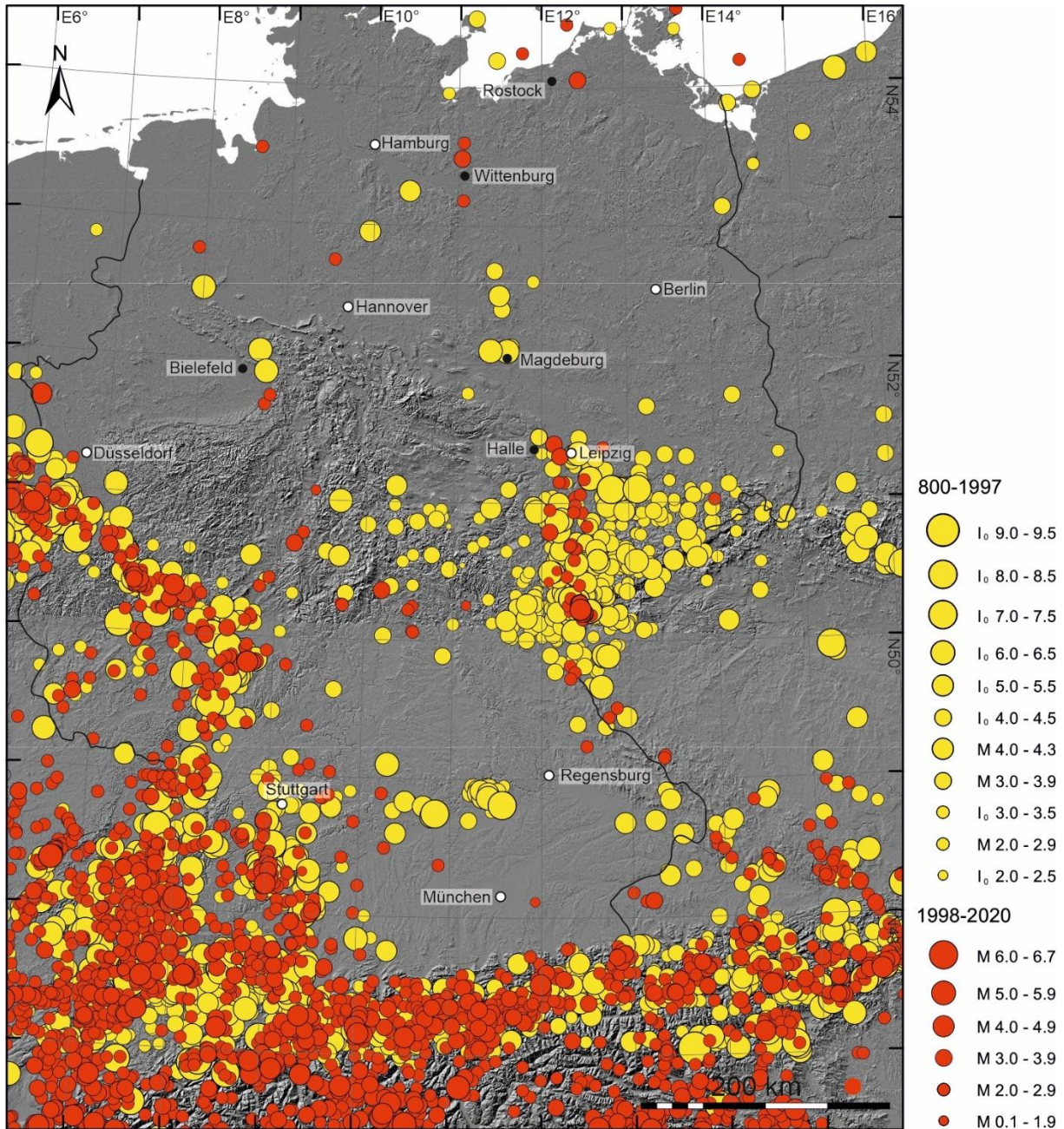


Figure 2: Tectonic earthquakes in Germany between 800 and 2020 (modified from GERSEIS 2020).

### 1.3.1 State of the art - Seismicity in northern and central Germany

Despite the intraplate setting, continuing seismic activity has been observed in historic times and is currently instrumentally detected.

Several historic earthquakes occurred in northern Germany since 800 CE (Fig. 2). Historic earthquakes between 997 and 1576 occurred in the Altmark area and in the vicinity of Magdeburg with epicentral intensities of IV to VI (Leydecker 2011). In the area of Bielefeld and near Oerlinghausen two earthquakes with epicentral intensities of VI occurred in 1612 and 1767. Between 1578 and 1670 earthquakes with epicentral intensities of III - (3.5) to IV - (4.5) are observed near Merseburg, Halle and Halle/Weißenfels (Fig. 2) (Leydecker 2011).

Many of the epicentres of recent earthquakes in northern Germany cluster in the vicinity of active gas fields and have been interpreted as a consequence of hydrocarbon recovery (Dahm et al. 2007, 2015). Earthquakes without an anthropogenic trigger have also been recorded, such as the more recent Wittenburg event in 2000 with a magnitude of  $M_L$  3.2 and the Rostock earthquake in 2001 with a magnitude of  $M_L$  3.4 (Leydecker 2011). Furthermore, between 2000 and 2018 seven deep earthquakes with hypocentre depths of 17.0 – 31.4 km were registered in northern Germany with magnitudes of  $M_L$  1.7 – 3.1 (Brandes et al. 2019).

In contrast, central Germany is more seismically active (Fig. 2). The area around Leipzig, the Vogtland and northwestern Bohemia is one of three areas in Germany/Czech Republic with increased seismic activity (Grünthal et al. 1998; Grünthal et al. 2018). A number of historic earthquakes with epicentral intensities of up to VII have occurred in these regions during the last 1200 years (Fig. 2) (Leydecker 2011; Grünthal and Wahlström 2012). The most prominent historic seismic event is the *Mid-German Earthquake* that occurred in 1872 near the city of Gera, with an epicentral intensity of VII (von Seebach 1873; Grünthal and Wahlström 2012). In a N-S oriented zone, called the RLR fault system, several historic earthquakes with epicentral intensities of up to VII (Leydecker 2011; Grünthal and Wahlström 2012) and instrumentally detected earthquakes and earthquake swarms occurred frequently (Korn et al. 2008; Fischer et al. 2014; Dahm et al. 2018; TLUBN 2020). Recently, two distinct earthquakes in the Halle/Leipzig area in 2015 and 2017 attracted attention. They reached magnitudes of  $M_w$  3.2 and  $M_w$  2.8 and focal depths of 29.0 km and 26.0 km respectively (Dahm et al. 2018).

### *Palaeoseismic record of northern and central Germany*

Palaeoseismic events are listed in the ‘Palaeoseismic Database of Germany and Adjacent Regions’ (PalSeisDB v1.0) (Hürtgen 2017). However, only a few palaeoseismological studies have been carried out in northern Germany so far. In general, these studies have focused on a single fault or have been restricted to a certain region. Evidence for palaeo-earthquakes and neotectonic activity is provided in Brandes et al. (2012) and Brandes and Winsemann (2013) for the Osning Thrust. SSDS and deformation bands in mixed alluvial-aeolian Late Pleistocene sediments indicate young tectonic activity in this location. Ludwig (2011), Hoffmann and Reicherter (2012) and Pisarska-Jamrózy et al. (2018, 2019) found evidence for seismic activity in Middle to Late Pleistocene sediments along the southwestern coast of the Baltic Sea. Further studies of Hübscher et al. (2004), Stackebrandt (2008) Brandes and Tanner (2012), Brandes et al. (2011, 2018a, b), Grube (2019a, b) and Huster et al. (2020), also indicate higher neotectonic activity in northern Germany than previously thought.

Palaeoseismological studies along the RLR fault system were carried out in the Cheb Basin (Czech Republic, NW Bohemia) (e.g. Bankwitz et al. 2003a; Štěpančíková et al. 2019) and several studies provide evidence for neotectonic fault activity in this area. A fault scarp at the Plesná Fault displaces Pleistocene river terrace deposits and points to Pleistocene fault activity (Bankwitz et al. 2003b; Peterek et al. 2011). Trench studies at the Marienbader Fault indicate repeated movements along several faults since the Oligocene. The youngest fault movement was documented in Holocene sediments. The fault movement caused a maximum displacement of ~0.4 m. In combination with the surface rupture length, an earthquake with a magnitude of up to  $M_w$  6.3 to 6.5 was estimated (Štěpančíková et al. 2019). In addition, SSDS in Pliocene deposits also indicate earthquake activity (Bankwitz et al. 2003a).



## 1.4 Fault tectonics

The lithosphere is divided into a seismic brittle and a predominantly aseismic ductile regime (Fig. 3). These two regimes can be present at a fully developed deep reaching fault system in the lithosphere (Huntington et al. 2018), where an upper crustal brittle fault passes into a ductile shear zone at greater depth (Sibson 1977; Scholz 2002). In continental interiors, with rocks that are rich in quartz and feldspar, the transition from the brittle to the plastic regime is wide and stretches from  $\sim 300$  to  $\sim 450$  °C when quartz and feldspar start to behave plastic (e.g. Fossen and Cavalcante 2017). Brittle deformation occurs in the upper lithosphere where frictional processes occur along faults, which is controlled by the material properties of quartz (Brandes and Tanner 2020). This thesis focuses on the brittle zone of a fault that is shown in blue in Figure 3.

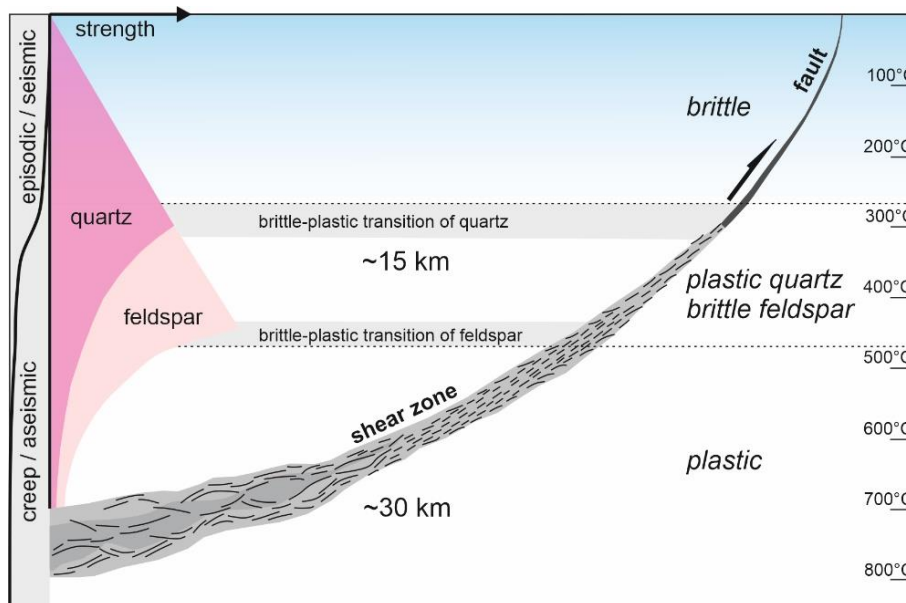


Figure 3: Fault evolution with depth. Depending on the heat flow in the lithosphere, a fault behaves brittle to plastic. This is controlled by material properties of quartz and feldspar minerals in the continental crust (modified after Fossen and Cavalcante 2017; Brandes and Tanner 2020).

### 1.4.1 Faults in the upper lithosphere

A fault zone represents a discontinuity in a rock volume that accommodates slip and acts as the source of seismic waves that are emitted during rupture. Thus, a fault zone is the key structure for the understanding of earthquake processes.

Faults represent lithological heterogeneous zones of localized brittle deformation in the upper continental crust. They are not discrete planes but rather zones of deformed rocks with a complex internal structure (e.g. Wibberley et al. 2008; Childs et al. 2009). A fault represents a 3D structure with a principal slip surface that accommodates slip and a surrounding volume of crushed rocks that accumulate strain through time (e.g. Shipton and Cowie 2001). A fully developed fault zone is characterised by a fault core, a damage zone and a process zone (Fig. 4) (e.g. Shipton and Cowie 2001). The fault core generally consists of gouge, cataclasite or ultracataclasite with several sub-parallel principal slip surfaces that can behave seismic or aseismic, which are surrounded by a zone of intensely fractured and damaged rocks that acts rather passively in slip accommodation (Ben-Zion and Sammis 2003; Shipton et al. 2006; Faulkner et al. 2010). In low porosity rocks the fault core is often fine-grained and it is surrounded by a fracture-dominated damage zone,

whereas in high porosity rocks low porosity deformation bands develop (Shipton et al. 2006; Fossen et al. 2007; Faulkner et al. 2010).

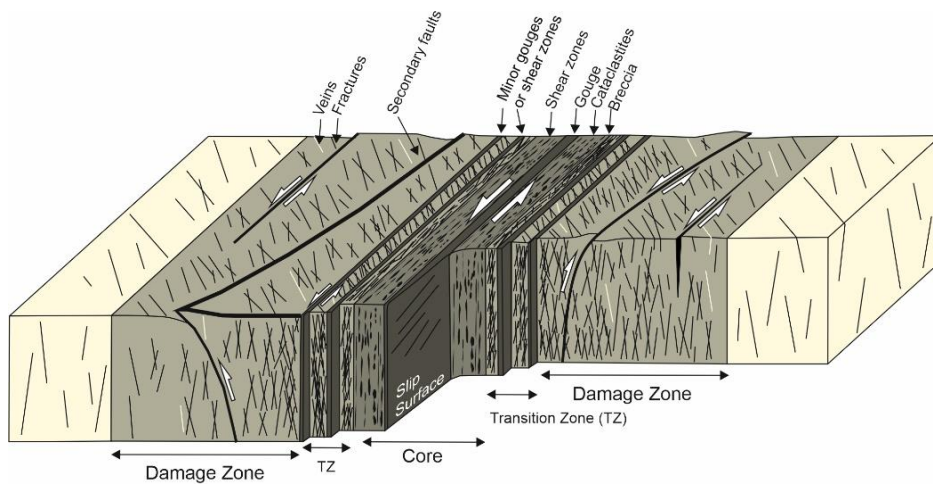


Figure 4: Schematic model of a fault zone showing the main fault elements (fault core and damage zone). Alterations of fault elements from fault core and damage zones characterise the transition zone (modified after Choi et al. 2016).

The size of the damage zone depends on the lithology of the host rock and scales linearly with the throw of the fault and the fault length (Cowie and Scholz 1992a). Ahead from the fault tip the process zone temporarily forms. Here, the displacement of faults decreases to zero (Cowie and Scholz 1992b). The process zone scales linearly with fault length and is internally characterised by microfractures that increase with approximation to the fault (Vermilye and Scholz 1998).

### *Deformation bands*

Deformation bands are small-scale structural elements in the upper crust that have a close relationship to faults. The term 'deformation band' was first applied by Aydin (1978) and Aydin and Johnson (1978). Deformation bands are tabular zones of local deformation that can occur in unconsolidated porous, sandy sediments and porous sedimentary rocks (Fossen et al. 2007). The bands define a millimetre- to centimetre-thick zone of deformation with small offsets that represent the equivalents to faults and fractures in porous material (Fossen et al. 2007). Faults commonly form in non-porous material. In contrast to deformation bands, faults with small offsets are distinct features and the deformation concentrates on the fault surface. The various types of tabular deformation zones that occur are governed by factors such as porosity, mineralogy, grain size and grain shape, lithification, state of stress and burial depth (Fossen et al. 2007).

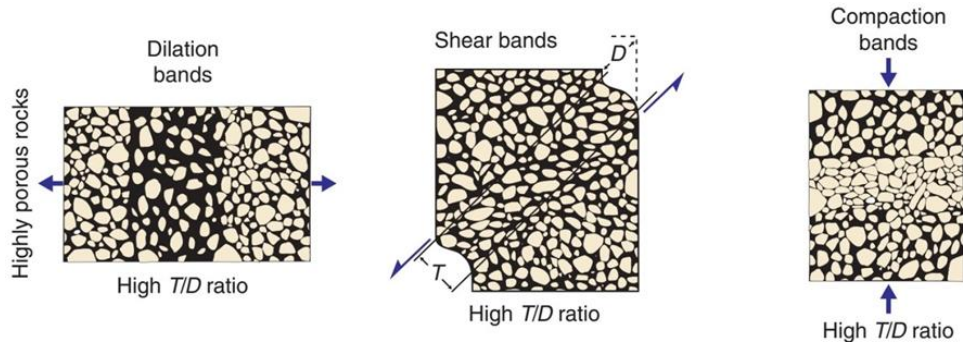


Figure 5: Kinematic classification of deformation bands. T, thickness; D, displacement (from Fossen 2010a).

Two different classifications exist for deformation bands. On the one hand they can be classified kinematically as dilation bands, shear bands, compaction bands and a hybrid of these types (Fig. 5) (e.g. Aydin et al. 2006). On the other hand, deformation bands can also be classified according to their characteristic deformation mechanism.

The most important deformation mechanisms are granular flow, cataclasis, phyllosilicate smearing, dissolution and cementation (Fossen 2010b). Depending on the deformation mechanisms, the principal types of deformation bands are disaggregation bands, phyllosilicate bands, cataclastic bands and solution and cementation bands (Fig. 6) (Fossen et al. 2007). Fossen et al. (2010a) showed differences in disaggregation bands that formed syndepositionally in soft sediments and due to tectonic activity in sandstones. Synsedimentary bands are associated with SSDS, whereas tectonic bands are typically clustered in the vicinity of faults. Tectonic bands are often affected by cataclasis, have a consistent orientation and commonly form conjugate sets (Fossen et al. 2010a).

Recent studies show that near-surface deformation bands that formed in unconsolidated sediments can develop due to earthquakes along active basement faults (Cashman et al. 2007; Brandes et al. 2018a, b). The majority of deformation bands are shear bands, which can be affected by compaction (compaction shear-bands) (Fossen et al. 2007).

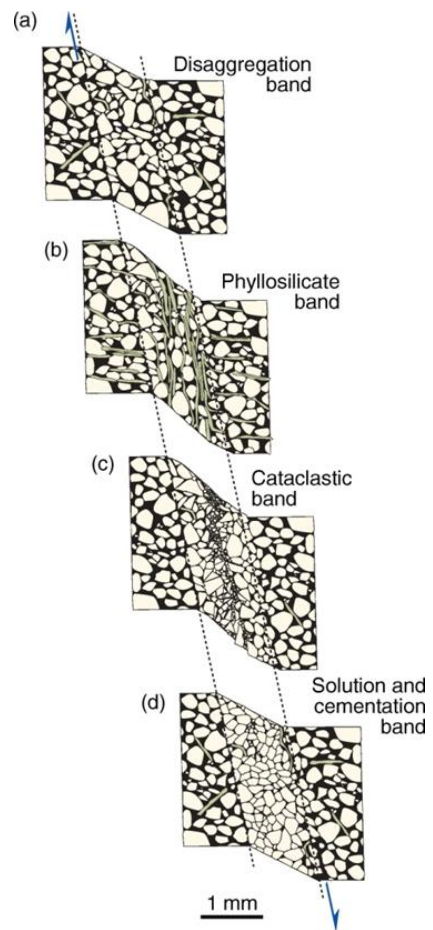


Figure 6: The principal types of deformation bands according to the deformation mechanism (from Fossen 2010a).

### **1.4.2 Active faults and earthquakes**

Fault activity can be expressed as rupture process (stick-slip) or aseismic creep in a critically stressed lithosphere.

#### *Brittle rupture processes*

Fault rupture is a sudden failure process on faults that emits seismic waves. The earthquakes occur due to the sudden release of elastic strain that was accumulated in the rigid plate in interseismic phases. If a critical shear stress ( $\tau_{crit}$ ) is exceeded, the fault fails and crustal blocks slip. After this rupture process the fault locks again and new stress accumulates in the interseismic phase. Therefore, seismicity can be regarded as a cycle of stress build-up (e.g. Brandes and Tanner 2020). The Mohr-Coulomb criterion describes the frictional behaviour and the slip processes on fault zones and is expressed by:

$$\tau_{crit} = c + \mu \sigma_N$$

where  $\tau_{crit}$  is the critical shear stress,  $c$  is the cohesion,  $\mu$  the friction coefficient and  $\sigma_N$  is the normal stress (Scholz 2002).

#### *Seismic cycle*

Repeating earthquakes caused by tectonic loading and relaxation processes can be described by earthquake recurrence models. The perfectly periodic model (Reid-type) (Fig. 7a) describes a proportional and constant strain release, a constant co-seismic slip and a constant recurrence interval, which leads to a perfectly periodic earthquake interval. In this model the time and the slip of the earthquake are predictable (Scholz 2002). In the time-predictable model (Fig. 7b) an earthquake is triggered when the critical stress level is reached but the co-seismic slip differs. The previous co-seismic slip rate and the magnitude of an earthquake predicts the time of the next earthquake (Shimazaki and Nakata 1980). In contrast, the slip predictable model (Fig. 7c) assumes that the accumulated strain of the previous earthquake is released. The co-seismic slip can be predicted from the time since the last earthquake which occurred. However, the time cannot be predicted (Shimazaki and Nakata 1980).

In nature, most earthquake cycles cannot be reduced to one of these simplified models. Despite intraplate earthquakes are less frequent in comparison to earthquakes at plate boundaries, the basic physical mechanisms are the same and consist of stress build-up and stress release. A major difference between interplate and intraplate earthquakes is the complex system of fault networks in continental areas (Liu et al. 2011). Whereas quasi-periodic earthquakes are concentrated at plate boundaries loaded by a steady rate of plate motion, intraplate faults are loaded from the far field and the strain is distributed over a system of interacting faults. Therefore, the loading rates are not time predictive and earthquakes can migrate to another fault system (Liu et al. 2011).

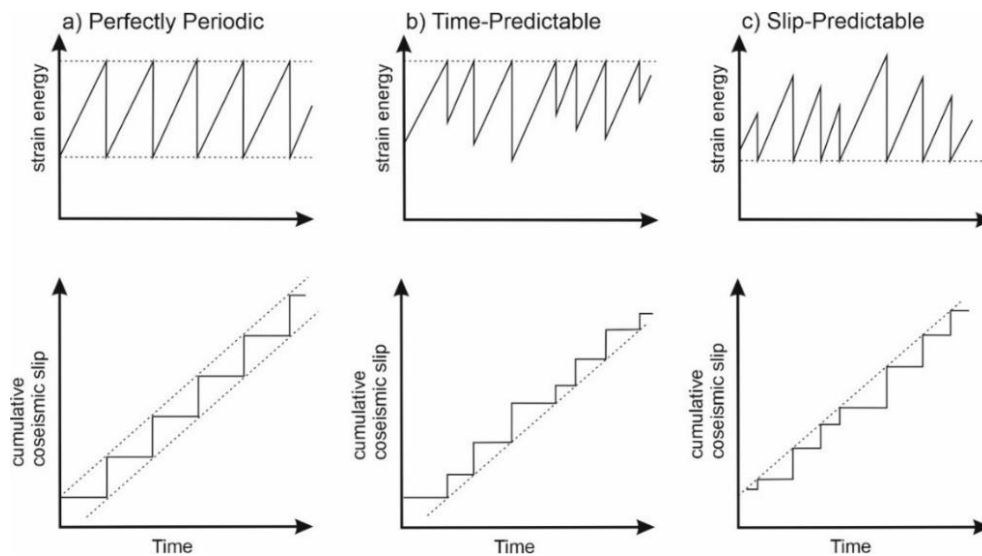


Figure 7: Strain release models for earthquakes. (a) Reid-type (perfectly periodic), (b) Time-Predictable, (c) Slip-Predictable (modified after Reid 1910, Shimazaki and Nakata 1980, Scholz 2002).

### *Creep processes*

Locked faults can rupture and emit seismic waves, besides unlocked faults can creep aseismically (Scholz 2002; Harris 2017; Kaduri et al. 2017; Brandes and Tanner 2020). Creep processes along faults are not restricted to short creep events (seconds to minutes) after an earthquake, creeping or aseismic slip can rather occur over long-time intervals (several decades) (Harris 2017). Along a fault zone there are locked segments next to unlocked creeping segments which is e.g. observed along the San Andreas Fault (USA) or the North Anatolian Fault (Turkey) (e.g. Scholz 2002; Harris 2017; Kaduri et al. 2017). Whether a fault ruptures or behaves aseismically is controlled by several geochemical and geophysical processes. Harris (2017) summarised these processes which include frictional resistance of the specific rock types, chemical reactions, dilation of dry rocks, elevated pore pressure, elevated temperatures, the fault geometry or a combination of these factors.

Palaeoseismological studies commonly fail to detect creeping faults, especially in low strain areas like Germany. Without the passage of seismic waves, no seismites can be formed. However, the development of deformation bands can be a hint to active tectonics if these bands are developed in young sediments and show the same strike like the active basement fault (e.g. Brandes et al. 2018a, b).

## **1.5 Deformation processes and deformation structures**

Seismogenic and non-seismogenic fault activity can produce different deformation structures in unconsolidated sediments in the study area of northern and central Germany. Common structures are shear-deformation bands, folds, various SSDS, ice-wedge casts and involutions. However, these deformation structures were formed by different processes. Deformation processes include neotectonic deformation processes, glaciotectonic deformation processes and periglacial processes. Using SSDS as indicators for past seismic activity must be done with caution. Otherwise

the seismic hazard potential might be overestimated. The following text describes the potential deformation processes that could have affected the unconsolidated sediments in northern and central Germany and introduces the different structural elements (Publication 3).

### **1.5.1 Neotectonic processes**

Several definitions of neotectonic exist. According to Pavlides (1989) neotectonic is *'the study of young tectonic events (deformation of upper crust), which have occurred or are still occurring in a given region after its final orogeny (at least for recent orogenies) or more precisely after its last significant reorganisation'*. Becker (1993) defined the neotectonic period in central and northern Europe to start in the early Late Miocene when most of the tectonic characteristics changed. In this thesis 'neotectonic processes' or 'neotectonic deformation' is used to mean post-Miocene tectonic seismogenic or non-seismogenic movements along major basement faults

Neotectonic fault activity is usually analysed on the basis of palaeoseismological studies that commonly rely on the identification of SSDS or seismites. However, the variety of different trigger mechanisms for SSDS (Publication 3) requires more robust tools. Deformation bands are such a tool in palaeoseismology to detect neotectonic deformation processes because they are a strong indicator for active faults. Unlike glaciotectonically induced shear-deformation bands that form in near-surface sediments, deformation bands caused by neotectonics often affect the whole sedimentary succession and show the same orientation as the nearby basement faults (Fig. 8a) (Brandes et al. 2018a). Deformation bands might be also formed by cryoturbation processes. In this case they reflect the local near-surface extension and contraction of the sediments related to freeze and thaw processes (Bertran et al. 2019).

Seismic events can lead to liquefaction and fluidization of sediments depending on the earthquake magnitude and strength of the substrate (Rodríguez-Pascua et al. 2000). However, no unambiguous geological indicator for past earthquake activity exists (Publication 3). The most common SSDS originating from seismic waves are load casts, pseudonodules and flame structures, which are mainly related to liquefaction (Van Loon 2009; Van Loon and Pisarska-Jamroży 2014). Brittle deformation and water-escape structures (e.g. sand volcanoes and hydrofractures) related to fluidization can also occur due to seismic waves (Fig. 8b) (Brandes and Winsemann 2013).

### **1.5.2 Glaciotectonic processes**

Glaciotectonic deformation structures were induced by the Middle and Late Pleistocene advances of the Scandinavian ice sheets and occur frequently in northern and central Germany (Fig. 8c, d, e, f). The processes and products of glaciotectonic deformation have been studied in great detail during the last decades (e.g. Van der Wateren et al. 2000; McCarrol and Rijdsdijk 2003; Bennett et al. 2004; Phillips et al. 2008; Phillips and Merritt 2008; Gehrman and Harding 2018). Deformation styles include proglacial compressional structures that form at the margin of an ice sheet and subglacial extensional deformation beneath the ice sheet (Hart and Boulton 1991). Different deformation structures commonly develop due to stress field variations caused by the advancing ice sheet.



Proglacial deformation leads to the formation of large-scale contractional structures such as folds, reverse and thrust faults (Aber and Ber 2007; Phillips et al. 2008; Gehrman and Harding 2018). Subglacial deformation is highly variable in style and intensity and can result in normal faulting and the formation of horst and graben structures as well as heterogeneous folds, SSDS and ductile shearing, which is associated with the formation of a subglacial shear zone (e.g. Menzies 2000; Van der Wateren et al. 2000; Piotrowski et al. 2004; Lee and Phillips 2008; Phillips and Merritt 2008). The initial water content of the deformed sediments governs the pattern of deformation within the shear zone (Phillips et al. 2008).



Figure 8: Deformation structures that developed in northern Germany due to different trigger processes. The different symbols show possible triggers that lead to similar structures. (a) Deformation band in Middle Pleistocene sand caused by neotectonic fault movements; (b) Sand volcano in Late Pleistocene sediments caused by palaeo-earthquakes; (c) Fold structures in Middle Pleistocene sand developed in a subglacial shear zone; (d) Fold structures in Middle Pleistocene sand developed in a subglacial shear zone; (e) Conjugate deformation bands with normal displacement in Middle Pleistocene sand overlain by a thick till

bed caused by ice sheet loading; (f) Deformation bands with reverse displacement in Middle Pleistocene sand caused by an advancing ice sheet; (g) Ice-wedge cast in Middle Pleistocene sand caused by freeze and thaw processes; (h) Involutions in Middle Pleistocene sand caused by freeze and thaw processes.

### ***1.5.3 Periglacial processes***

The periglacial environment is the marginal zone of an ice sheet that is not directly influenced by the glacier but is affected by permafrost (French 2017). Large parts of the study area were affected by periglacial conditions. Cryoturbation is a widely used term for different deformation structures that develop in unconsolidated sediments under periglacial climate conditions (Edelman et al. 1936) and refers to freeze and thaw processes (Washburn 1980; French 2017). Cryostatic pressure and gravity are processes that produce cryoturbation structures and cause soil movements (Bockheim and Tarnocai 1998), differential frost heave and loading (Ogino and Matsuoka 2007).

Common deformation structures are ice-wedge casts and involutions (Fig. 8g, h). Ice wedges are massive, generally wedge-shaped bodies with a downward-pointing apex. They are composed of foliated or vertically banded ice (Harry 1988). Ice wedges occur in thermal contraction cracks in which hoar frost forms. Water from melting snow then penetrates these cracks. The formation of an ice wedge takes many years and is caused by thermal cracking of the ground during rapid cooling events (Weise 1983). Ice-wedge casts are remaining structures that indicate permafrost in the Pleistocene sediments. An ice-wedge cast fills the space formerly occupied by ice. They are recognised as the most precise and widespread indicators of past periglacial conditions and permafrost (Péwé 1973).

Periglacial involutions often have swirl-like or teardrop patterns (Bockheim and Tarnocai 1998). Involution and convolute bedding describe comparable structures that originate from liquefaction (Vandenberghe 2013). Evidence of involutions has been widely reported from past or present periglacial environments with permafrost or deep seasonal frost (Ogino and Matsuoka 2007; Vandenberghe 2013).



## 2. Geological setting

### 2.1 Crustal structure of northern central Europe

Central Europe is built of a complex mosaic of terranes that have been assembled throughout Phanerozoic times (Ziegler 1990). It can be subdivided into two geological domains: The northeastern area with a stable Precambrian platform (craton), also known as the East European Platform, and the southern area that comprises a series of crustal blocks that were attached during the Caledonian and Variscan orogenic cycles (Ziegler 1990; Franke 1993) including several deformation phases like closures of ocean basins, terrane accretions, post-collisional crustal shortening and post-orogenic collapses (e.g. Kröner et al. 2008). These two geological domains are separated by the NW-SE trending Trans-European Suture zone (TESZ), which is separated into a northern segment called the Sorgenfrei-Tornquist Zone and a southern segment called the Teisseyre-Tornquist Zone (Pharaoh 1999, 2006).

Rocks that were deformed during the Variscan Orogeny form the continental crust of central Europe and thus of the study area. Traditionally, in central Europe, the Variscan orogenic belt is subdivided into three zones, originally defined by Kossmat (1927) as the so-called Rheno-Hercynian, Saxo-Thuringian and Moldanubian zone (Fig. 9). This subdivision is mainly based on the rock types and the degree of their metamorphism. The Saxo-Thuringian zone is situated at the northern boundary of the Bohemian Massif, which forms part of the Moldanubian zone. In the Northwest the Saxo-Thuringian is flanked by the Mid-German Crystalline Zone that separates the Rheno-Hercynian from the Saxo-Thuringian zone (Franke 2000; Kroner et al. 2007). These zones of the Variscan belt represent different terranes that were accreted at the southern margin of



Laurentia and Baltica during the Caledonian and the Variscan Orogeny (Torsvik and Cocks 2017). The study area forms part of the Rheno-Hercynian zone, the Mid-German Crystalline Zone, the Saxo-Thuringian zone and the Moldanubian zone with the Tepla-Barrandian zone of the Central European Variscides (Fig. 9).

Figure 9: Overview of the European Variscides subdivided into three zones: the Rheno-Hercynian, Saxo-Thuringian and Moldanubian zone. Eger Rift: ER; Teisseyre-Tornquist Zone: TTZ; Mid-German Crystalline Zone: MGCZ (modified after McCann 2008) and the maximum extent of the Middle to Late Pleistocene Elsterian (E), Saalian Drenthe (D), Warthe 1 (Wa1), Warthe 2 (Wa2) and Weichselian (W) ice sheets (modified after Lang et al. 2018; Winsemann et al. 2020).

### **2.2 Geological evolution of the study area**

In the Late Carboniferous, the convergence between Gondwana and Laurussia changed from N-S directed collision to an E-W orientation, which led to the development of dextral continental shears (e.g. the Tornquist-Teisseyre Zone) (McCann 2008). After the Variscan Orogeny in Late Carboniferous and Permian times, slab delamination led to a higher heat flow and thermal thinning of the crust accompanied with strong volcanic activity. During the Permian, the compressional and transpressional stress state changed into extension. Rift processes due to thermal contraction of the lithosphere occurred (e.g. Gast and Gundlach 2006; McCann 2008). Major structural elements included N-S trending normal faults. Thermal subsidence characterised the rift basin throughout the entire Mesozoic (e.g. Van Wees et al. 2000). The rotation of the Iberian Peninsula (Kley and Voigt 2008) in the Late Cretaceous caused a re-organisation of the stress field that changed from extension to compression. This led to a distinct tectonic inversion phase in the Late Cretaceous to Early Palaeocene (e.g. Kockel 2003; Mazur et al. 2005). The inversion of the stress field led to the reactivation of several faults e.g. the Harz Boundary Fault, the Osning Thrust, the Gardelegen Fault and the Lusatian Thrust (Franzke et al. 2004; Voigt et al. 2006) and basement blocks like the Bohemian Massif were upthrust (Ziegler and Dézes 2006). Many extensional structures, such as normal fault arrays and graben systems, were transformed into compressional features (Kockel 2003). The inversion phase has been discussed in detail in Baldschuhn et al. (1991) and Kley and Voigt (2008).

### **2.3 Major faults in the study area**

The study area of northern Germany comprises the federal states of Lower Saxony, Saxony-Anhalt and parts of North Rhine-Westphalia. The study area of central Germany comprises Saxony, and parts of Thuringia and Brandenburg.

#### ***2.3.1 Northern Germany***

Northern Germany forms part of the Central European Basin System (CEBS). After the end of the Variscan Orogeny, the CEBS evolved out of a Carboniferous Variscan foreland basin (Betz et al. 1987). Today, the CEBS consists of several sub-basins, such as the Lower Saxony Basin, the Subhercynian Basin and the Northeast German Basin (Publication 2, Fig. 2). As a consequence of different tectonic phases, northern Germany is characterised by a dense fault array with several major faults (oriented NW-SE) and fault zones with minor faults, oriented NE-SW or NNE-SSW (Reicherter et al. 2005; Lohr et al. 2007). Distinct NW-SE and WNW-ESE oriented major faults in northern Germany are the Aller Fault, the Elbe Lineament, the Gardelegen Fault, the Halle Fault, the Harz Boundary Fault, the Osning Thrust and the Steinhuder Meer Fault (Fig. 10). The palaeoseismological analysis of these faults is described in Publications 1 and 2.

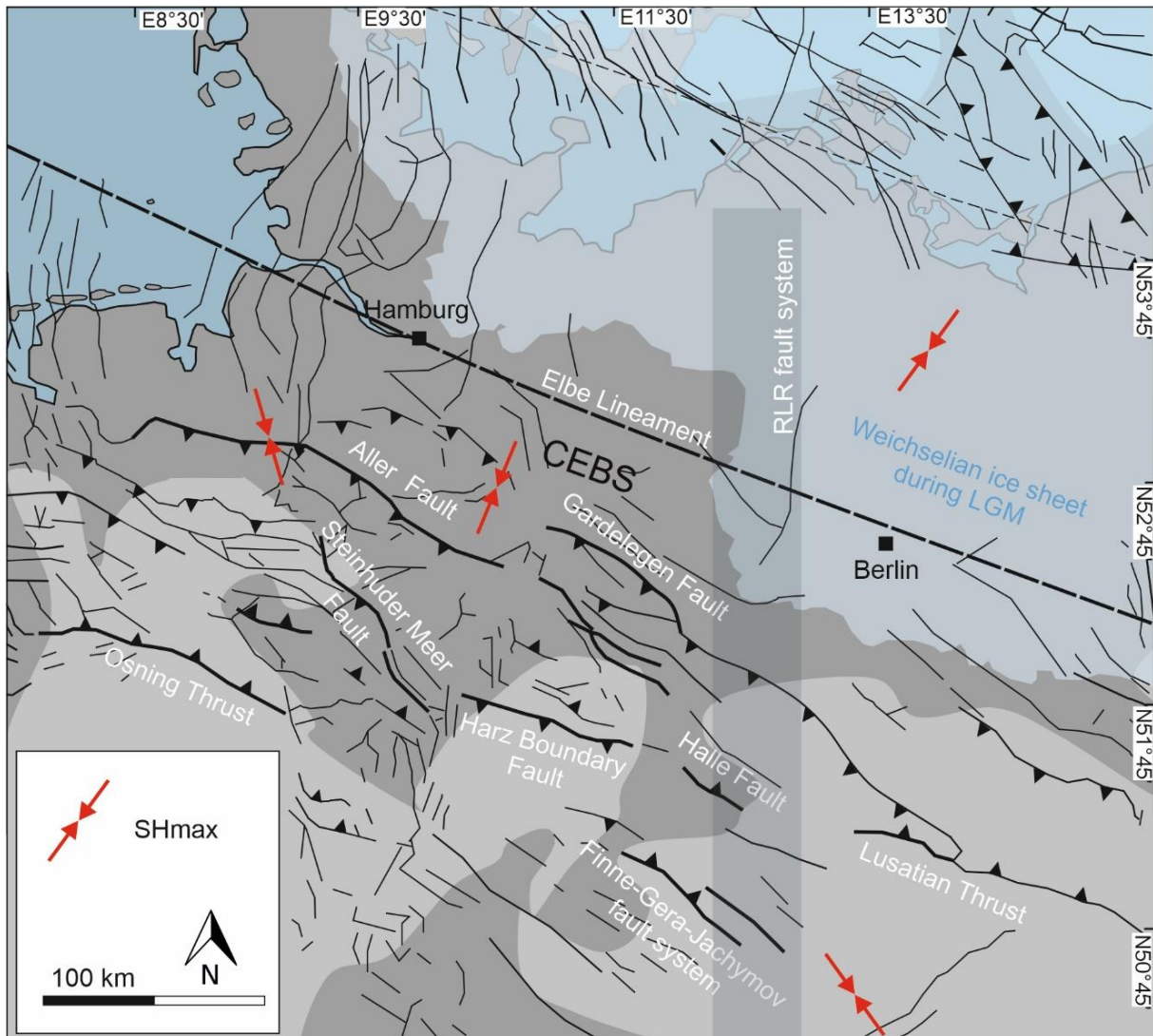


Figure 10: Fault map of the study area in northern and central Germany with the Central European Basin System (CEBS) (dark grey) and the analysed faults. Regensburg-Leipzig-Rostock fault system: RLR fault system; Last Glacial Maximum: LGM. Red arrows show the recent stress field orientation based on Marotta et al. (2000, 2002), Reicherter et al. (2005) and Heidbach et al. (2016). Map is based on Kley and Voigt (2008) and Scheck-Wenderoth and Lamarche (2005).

### *The Aller Fault*

The Aller Fault trends NW-SE and extends from the Magdeburg area across Lower Saxony into the area of Oldenburg over a distance of 250 km (Fig. 10). From a tectonic point of view, the Aller Fault is a complex inversion structure (Jubitz et al. 1991; Kockel 2003) that underwent multiphase tectonic evolution with extension in the Triassic and Jurassic followed by contraction and inversion in the Cretaceous (Best 1996; Lohr et al. 2007). Initial normal fault movements along the south-eastern part of the Aller Fault during the Late Triassic are indicated by the development of thick growth-strata packages, e.g. as shown on geological cross-sections in Baldschuhn et al. (1996). Normal faulting prevailed throughout the Mesozoic and ended in the Early Cretaceous (Albian) (Best and Zirngast 2002). Contraction and inversion followed (Best and Zirngast 2002). Comparable observations were also made for the central part of the Aller Fault by Lohr et al. (2007). These authors provided a detailed kinematic analysis based on seismic reflection data.

Initial extension in the Late Triassic was directed NNE-SSW and created normal faults. This phase was followed by an E-W extension in the Middle Jurassic that led to transtensional movements along the central part of the Aller Fault. In the Cretaceous, E-W contraction occurred during the Santonian to Campanian, and N-S contraction occurred during the Coniacian to Maastrichtian. This contraction partially prevailed into the Palaeocene (Lohr et al. 2007).

### *The Elbe Lineament*

The Elbe Lineament represents two different NW-SE fault zones in central Europe, the northern Elbe Line and the southern Elbe Line (Franke and Hoffmann 1999a). The northern part of the Elbe Line extends from the southern North Sea called the *Lower Elbe Line* (Franke and Hoffmann 1999a; Abramovitz and Thybo 2000; Tesauro et al. 2007), across northern Germany (Rabbel et al. 1995) and into Poland where it includes the Cracow-Lubliniec Zone (Franke and Hoffmann 1999a). The southern Elbe Line trends from Hamburg towards Dresden into the Czech Republic and comprises the Wittenberg, Haldensleben and Gardelegen faults (Franke and Hoffmann 1999a). This set of faults is named Elbe Fault System in Scheck et al. (2002).

The northern Elbe Line has been analysed and is referred to as the Elbe Lineament in this thesis (Fig. 10). This segment of the Elbe Lineament strikes NW-SE parallel to the Teisseyre-Tornquist Zone and represents an important geological boundary (Rabbel et al. 1995; Tesauro et al. 2007). The Elbe Lineament is a ~800 km long major crustal structure in northern Germany (Scheck et al. 2002). It is interpreted as a deep crustal structure characterised by a drop in the p-wave velocity (e.g. Franke and Hoffmann 1999a; Scheck et al. 2002) and appears subordinated in geophysical analyses within the Mesozoic and Cenozoic rocks (Franke and Hoffmann 1999a). Strong changes in the crustal thickness and composition have been observed (Tesauro et al. 2007). The Elbe Lineament has been interpreted either as a major strike-slip fault that defines the NE extent of eastern Avalonia and the southwestern margin of the Baltic Shield (Tanner and Meissner 1996) or as an intra-Avalonian subterranean boundary (Krawczyk et al. 2008). It separates the Holstein Block in the north from the Pompeckj and Niedersachsen Block in the south (Rabbel et al. 1995). Deep seismic surveys indicate frequently occurring listric faults, which may be the result of recent tectonic movements (Franke and Hoffmann 1999b).

### *The Gardelegen Fault*

The Gardelegen Fault is an approximately 70 km long and NW-SE oriented Permo-Carboniferous structure reactivated during the Late Cretaceous inversion of the NE German Basin (Publication 2, Fig. 2) (Kossow and Krawczyk 2002). It is part of the southern Elbe Line that trends from Hamburg towards Dresden (Fig. 10) (Franke and Hoffmann 1999a; Scheck et al. 2003). The Gardelegen reverse fault, has a pronounced listric geometry, a vertical offset of 5-6 km (Otto 2003) and soles out into a subhorizontal detachment at a depth of 20 to 25 km (DEKORP Basin Research Group 1999; Kossow and Krawczyk 2002; Kley and Voigt 2008; Kley 2013).

### *The Halle Fault*

The Halle Fault has a significant structural role because it separates two tectonic units: The Merseburg-Scholle and the Halle-Wittenberg-Scholle (Schwab et al. 2006). The fault is approximately 40 km long and trends NW-SE to E-W (Fig. 10). It underwent multiphase tectonic evolution and is interpreted as an Early Permian strike-slip fault (Rappsilber 2003) that was reactivated as a reverse fault in Late Cretaceous times (Rappsilber 2003; Schwab et al. 2006; Kley and Voigt 2008). The Halle Fault belongs to the NE-SW-trending intramontane Saale Basin, a local basin related to the Variscan Orogen (Publication 2, Fig. 2) (Rappsilber 2003). It is interpreted as a transtensional strike-slip basin that developed in the Late Carboniferous to Early Permian and is filled with material derived from the Variscan Orogen (Rappsilber 2003).

### *The Harz Boundary Fault*

The Harz Boundary Fault is a major structural element of the CEBS. The fault has a length of approximately 90 km and strikes WNW-ESE (Fig. 10). The Harz Boundary Fault is a key element of intraplate deformation during the Late Cretaceous inversion phase. It separates the Palaeozoic rocks of the Harz Mountains from the Mesozoic sedimentary rocks of the Subhercynian Basin (von Eynatten et al. 2008; Voigt et al. 2008). In the hanging wall of the Harz Boundary Fault, a large fault-propagation fold developed above the tip of the Harz Boundary Fault that reached the seafloor not before the Late Coniacian (Voigt et al. 2006). In the Early Campanian, rock fragments composed of Palaeozoic rocks were shed from the Harz Mountains (von Eynatten et al. 2008), implying ongoing unroofing of the fault-propagation fold. These observations indicate a major phase of tectonic activity along the Harz Boundary Fault between the Coniacian and the Campanian, which is also supported by apatite fission track dating from the Harz Mountains (Kley and Voigt 2008). A comprehensive kinematic analysis of the Harz Boundary Fault was published by Franzke and Schmidt (1993), but there is an ongoing debate about the general nature of the Harz Boundary Fault. It is either interpreted as a wrench fault system (Wrede 1988, 2008) or as a dip-slip thrust (Voigt et al. 2006). Depending on the kinematics of the Harz Boundary Fault, the Subhercynian Basin is regarded as a wrench fault basin (Wrede 1988) or as a piggy-back basin on the top of a basement thrust system (Voigt et al. 2006), which has similarities with foreland basins (Brandes et al. 2013).

### *The Osning Thrust*

The Osning Thrust is a WNW-ESE oriented thrust system located at the southern margin of the Lower Saxony Basin (Publication 2, Fig. 2). This fault system is referred to as 'Osning Thrust', 'Osning Zone' or 'Osning Lineament' (Drozdzewski 1988; Baldschuhn and Kockel 1999) and has a length of approximately 115 km (Fig. 10). The first movements along the Osning Fault probably took place in the Late Triassic (Baldschuhn and Kockel 1999). At that time the Osning Fault was a NNE-dipping normal fault (Baldschuhn and Kockel 1999). In the Coniacian, the inversion of the Lower Saxony Basin began (Kockel 2003). During this inversion, the fill of the basin was overthrust southwards along the Osning Thrust onto the Münsterland Block (Baldschuhn and Kockel 1999), and the former normal fault was transformed into a thrust fault.

### *The Steinhuder Meer Fault*

The tectonic history of the Steinhuder Meer Fault is poorly documented. It is assumed to be 50 – 70 km long, but the exact length of the fault trace is difficult to define due to the close connection to the Bokeloh salt structure (Fig. 10). Cross-sections shown in Kley et al. (2008) and Müller et al. (2016) relate the Steinhuder Meer Fault to deep-seated faults in the pre-Permian basement. The thickness distribution of potential growth strata along the fault shown in Baldschuhn et al. (1996), implies potential normal fault movements in the Middle Jurassic followed by reverse movements in Late Cretaceous times. Reverse faulting led to the formation of a tight fault propagation fold in the area of the Stemmer Berg as indicated on a cross-section shown in Baldschuhn et al. (1996).

### **2.3.2 Central Germany**

During Late Carboniferous to Early Permian, Variscan intramontane basins developed and were filled with debris from the Variscan Orogen and volcanic rocks. Subsequently, Palaeozoic and Mesozoic rocks were accumulated in major sedimentary basins, which are dominated by Permian to Triassic rocks and Cretaceous sediments (Pälcher and Walter 2008).

Besides NE-SW oriented faults, the regional fault pattern in central Germany is dominated by NW-SE oriented faults (e.g. Siegert et al. 1901; Dalmer and Credner 1901; Weise et al. 1913; Zimmermann and Liebe 1930; Picard et al. 1937; Gläßer et al. 1995; Gläßer and Wiefel 1999), including among others, the distinct Lusatian Thrust, the Finne Fault and the Gera-Jáchymov Fault (Fig. 10). Furthermore, photolineations derived from orthophotos, DEMs and measured gravity anomalies are interpreted to point to deep seated N-S and E-W striking structures (Grünthal et al. 1985; Kämpf et al. 1991; Bram and Hirschmann 1992; Bankwitz et al. 1998; Behr et al. 2002; Bankwitz et al. 2003b; Pohl et al. 2006). Many major faults intersect with the N-S trending zone in the area around Leipzig, Gera, Zwickau and in the Cheb Basin, which results in a complex subsurface structure (e.g. Skamletz et al. 2000) and fault pattern. The investigations at the RLR fault system and the Lusatian Thrust are described in Publication 4.

### *Regensburg-Leipzig-Rostock (RLR) fault system*

The RLR fault system is commonly interpreted as a N-S trending sinistral shear zone (Bankwitz et al. 2003b; Schneider 2004; Neunhöfer 2009). It is a roughly ~ 700 km long and ~ 40 km wide network of faults (Bankwitz et al. 2003b). Based on satellite images the RLR fault system was traced from the area of Regensburg passing through the Vogtland and the region of Leipzig further to the north up to the area of Rostock at the Baltic Sea coast (Fig. 10) (e.g. Grünthal et al. 1985; Kämpf et al. 1991; Kämpf et al. 1992; Bankwitz et al. 2003b). The fault system consists of a set of N-S trending sub-parallel faults composed of en-échelon segments (Bram and Hirschmann 1992; Bankwitz et al. 2003b; Neunhöfer and Hemmann 2005; Pohl et al. 2006). Due to the segmentation of several short lineaments, Pohl et al. (2006) excluded the possibility that the RLR fault system represents a strike-slip zone, but point to normal fault mechanisms with an oblique component. The N-S trending lineaments do not represent a sharp block boundary but rather form a bundle of N-S directed short lineaments.

### *The Lusatian Thrust*

The Lusatian Thrust represents one of the key faults in central Europe. It is part of the Elbe Fault Zone, which shows repeated phases of fault activity since the Late Carboniferous (Scheck et al. 2002). The Lusatian Thrust has a maximum vertical offset of 500 – 1000 m and is 80 – 100 km long (Krentz and Stanek 2015). It is the boundary between the Lusatian Block and the Elbe Zone between the Ještěd Ridge (Czech Republic) and Dresden Klotzsche (Fig. 10). In the northeast of Dresden Klotzsche, the Elbe Zone is flanked by the Großenhainer Fault (Wendt et al. 1996; Krentz et al. 2010). Near Dresden the position of the fault is not well constrained (e.g. cf. Bankwitz 1971; Voigt 2009; Krentz and Stanek 2015; Käßner et al. 2020). The Lusatian Thrust is characterised by several short segments that are offset by neotectonically active younger Cenozoic, NE-SW oriented faults (e.g. the Borsberg Fault, the Ebersbacher Fault, the Stráž fault system) (Bankwitz 1971; Krentz 2008; Krentz and Stanek 2015; Käßner et al. 2020). From southeast to northwest the fault characteristics (e.g. offset, dip of the fault) change, which causes a separation of the fault in different segments: namely the Elbesandsteingebirge Segment, Lusatian Segment, Ještěd Segment and Jizera Segment. The curved geometry of the fault is interpreted to result from a multiphase tectonic evolution of the different fault segments (Käßner et al. 2020; Krentz et al. 2020). The main phase of fault activity was in the Late Cretaceous to Palaeogene (Kley and Voigt 2008; Krentz 2008; Krentz and Stanek 2015).

### *The Finne-Gera-Jáchymov (FGJ) fault system*

The Finne-Gera-Jáchymov (FGJ) fault system is a ~ 10 km wide and ~ 250 km long, tectonically significant fault system with several parallel fault segments. The fault system incorporates the Kyffhäuser-Crimmitschau Fault in the northwest, the Finne Fault in the southwest and the Gera-Jáchymov Fault in the southeast (Fig. 10). One of the most important fault segment, is the Roter Kamm Fault, which is a normal fault with a throw of ~ 580 m (Hiller and Schuppan 2008; Berger et al. 2011). The polyphase evolution of the FGJ fault system started with the Variscan Orogeny (Bankwitz et al. 1993; Berger et al. 2011). Based on geophysical datasets (such as seismic, gravimetric and magnetic data) this zone is interpreted to represent a distinct deep-seated fault system between the Franconian Line in the south and the southern Elbe Line in the north (Bankwitz and Bankwitz 1991; Haupt and Conrad 1991). Major faults frequently intersect in the area around Gera, Posterstein and Zwickau, which results in a complex subsurface structure (Skamletz et al. 2000). The N-S oriented RLR fault system intersects with the NW-SE oriented FGJ fault system near the city of Gera (Publication 4, Fig. 2).

## **2.4 Pleistocene glaciations**

During the Pleistocene, Germany was transgressed by three major glaciations referred to as the Elsterian, Saalian and Weichselian glaciations (Fig. 9) (Ehlers et al. 2011) and thus affected by glacial loading and unloading stresses. Repeated ice advances led to the deformation of near-surface sediments and sedimentary rocks in many areas of northern and central Europe (e.g. Eissmann 1987, 1995, 2002; Aber and Ber 2007; Ehlers et al. 2011; Winsemann et al. 2020). Three ice advances during the Elsterian glaciation have been recorded in the study area (Knoth 1995; Eissmann 2002; Ehlers et al. 2011). The maximum extent of the Elsterian ice sheet in central



## 2. Geological setting

Germany is recorded from Bad Schandau and represents the southernmost advance of the ice sheets during the Middle Pleistocene (Eissmann 2002). These ice sheets advanced from northerly and north-easterly directions (Eissmann 2002) and are correlated with Marine Isotope Stages MIS 12 and MIS 10 (Fig. 11) (Lang et al. 2012; Roskosch et al. 2015).

*MIS stages* represent oscillating warm and cold periods in the Earth's palaeoclimate, which are based on marine oxygen isotope data reflecting temperature changes in the ocean (e.g. Wright 2001). The data is often derived from the  $\delta^{18}\text{O}/^{16}\text{O}$  ratio of ice cores and benthic foraminifera. Even numbers represent high  $\delta^{18}\text{O}$  values and are typical for cold climates. Odd numbers represent low  $\delta^{18}\text{O}$  values and are typical for warm periods (e.g. Wright 2001).

Marine Isotop Stages	Northwest Europe		Northern Germany					
	Huijzer & Vandenberghe 1998; Cohen & Gibbard 2020		Böse et al. 2012; Roskosch et al. 2015; Lang et al. 2018		Litt et al. 2007			
MIS 1	Holocene		Holocene		Holocene			
MIS 2	Late Pleistocene	Lateglacial	Weichselian		Weichselian			
MIS 3		Periglacial						
MIS 4								
MIS 5d-a								
MIS 5e		Early Glacial				Eemian	Eemian	Eemian
MIS 6	Middle Pleistocene	Saalian		Saalian		Warthe Drenthe		
MIS 7				Saalian		Dömnitz		
MIS 8				Saalian		Fuhne		
MIS 9				Holsteinian		Holsteinian		
MIS 10				Elsterian		Elsterian		
MIS 11				Holsteinian		Cromerian		Ruhme
MIS 12				Elsterian		Elsterian		

Figure 11: Chronostratigraphy of the Pleistocene in north-western Europe. The blue arrows represent ice advances. Please note that different stratigraphic charts exist for northwestern Europe and Germany.

Three major ice advances with several sub-phases occurred during the Saalian glaciation (Eissmann 2002; Litt et al. 2007; Ehlers et al. 2011; Lang et al. 2018). These repeated ice advances are commonly correlated with MIS 6 and are referred to as the Drenthe and Warthe ice advances (Fig. 11) (Litt et al. 2007; Ehlers et al. 2011; Lang et al. 2018). However, there is also evidence for an ice advance during MIS 8 (see discussion in Roskosch et al. 2015). In central Germany, the maximum extent of the Saalian ice sheets reached the area around Meißen (Eissmann 2002; Lang et al. 2018). These Saalian ice sheets advanced from northerly, north-easterly and easterly directions (Lang et al. 2018). The younger Saalian Warthe ice advances did not reach as far as the older Saalian and Elsterian ice sheets (Fig. 9).

The Late Pleistocene Weichselian ice sheets did not cross the Elbe river and did not reach the study area of central Germany and phased periglacial conditions prevailed in the study area (Eissmann 2002; Reinecke 2006; Litt et al. 2007; Meinsen et al. 2014). Three main ice-marginal positions are known in northeastern Germany from the Weichselian glaciation. The peak of the Eurasian ice sheet in global ice volume, often referred to as the Last Glacial Maximum (LGM), occurred at around 21-20 ka during MIS 2 (Hughes et al. 2016), although it does not correspond with the maximum ice extent in northeastern Germany. The maximum extent of the Weichselian



ice sheet in northeastern Germany was reached at around 30 ka (Hardt et al. 2016), while further west in Mecklenburg and Schleswig-Holstein the maximum ice extent was reached at around 24 ka (Böse et al. 2012). The ice margin position was located northeast of the Elbe Lineament, whereby the Elbe Valley acted as a major valley for meltwater flows (Ehlers et al. 2011; Lang et al. 2019). The ice subsequently melted back rapidly and a standstill phase during the down wasting period occurred, which was later followed by a third minor re-advance (Lüthgens and Böse 2011; Hardt et al. 2016; Hardt and Böse 2018).

### 2.5 Lithospheric stress field and glacial isostatic adjustment

Collisional forces from the Alpine orogeny and the Atlantic ridge push affect the stress field in northern and central Germany (Marotta et al. 2001, 2002, 2004; Kaiser et al. 2005). Caused by the rotation of the Iberian Peninsula, a key tectonic phase in Germany was the Late Cretaceous/Palaeogene inversion phase when major basement faults were reactivated (Lohr et al. 2007; Kley and Voigt 2008). After this inversion phase, the stress field in northern Germany was N-S to NE-SW oriented and rotated counter clockwise from NE-SW to NW-SE in the Neogene (Kley and Voigt 2008). The present-day stress field is characterised by NW-SE compression and NE-SW extension (Heidbach et al. 2016). The recent stress field in northern Germany has a fan-shaped pattern (Fig. 10) (Marotta et al. 2000; Reicherter et al. 2005). Grünthal and Stromeyer (1994) showed that the Bohemian Massif deflects the regional stress field and  $S_{Hmax}$  changes from a NW-SE orientation in the south to a NE-SW orientation in the north (Fig. 10). Similar observations were made by Roth and Fleckenstein (2001) and Heidbach et al. (2016).

From the Pleistocene onwards to the present day, the stress field is influenced by the post glacial rebound of Fennoscandia (Nocquet 2012). This rebound also affects the area outside the former glaciated area (Brandes et al. 2015). Ice loading and unloading during the Middle and Late Pleistocene in northern central Europe led to visco-elastic relaxation of the mantle-lithosphere system (Stewart et al. 2000). These uplift and subsidence processes are called glacial isostatic adjustment (GIA) (e.g. Steffen et al. 2014).

GIA can have a strong impact on the neotectonic activity of an area. Predominantly, the deglaciation related stress field changes caused a reactivation of pre-existing faults as so-called postglacial faults (PGFs) or glacially-induced faults (GIFs). This has been demonstrated for Scandinavia for the Late Pleistocene Weichselian ice sheet cover (Mörner 1978; Arvidsson 1996; Dehls et al. 2000) and northern Germany that was located outside the former ice sheet (Brandes et al. 2012; 2015).

Before the glaciation of an area, in a thrust fault regime, the maximum ( $\sigma_1$ ) and intermediate ( $\sigma_2$ ) principal stresses are oriented nearly horizontally (Fig. 12a) and the minimum principal stress ( $\sigma_3$ ) is nearly vertically oriented. Existing faults are close to failure. During glaciation, a bowl-shaped depression occurs below the centre of an ice sheet due to elastic crustal flexure as a result of the crustal loading and the outward flow of the deep mantle material away from the maximal ice load (Fig. 12b) (Stewart et al. 2000). Existing faults are inactive and stabilised. When the ice retreats, crustal unloading is faster than the crustal loading during the ice advance (Fig. 12c) (Stewart et al. 2000) because the ice sheet melts much faster than it develops. The minimum principal stress ( $\sigma_3$ ) rapidly decreases without ice loading but the lithospheric bending stress ( $\sigma_1$ ) remains constant (Steffen et al. 2014). The rapid release of vertical stress leads to a fast crustal rebound during deglaciation and the resulting stress changes can trigger earthquakes in intraplate settings (e.g. Grollmund and Zoback 2001).

## 2. Geological setting

A glacial forebulge develops in front of the ice sheet due to the flexure of the lithosphere (e.g. Kiden et al. 2002). The forebulge area is characterised by uplift and extension (Stewart et al. 2000). The WNW-ESE striking faults in northern Germany were susceptible for reactivation under the GIA induced stress field. In this case the GIA-induced stress field matches to the palaeo-stress field under which these faults formed. The reactivation potential of faults running parallel to the former ice margins is the greatest. The WNW-ESE trending major basement faults analysed in this study thus have a high potential for neotectonic reactivation (Brandes et al. 2015).

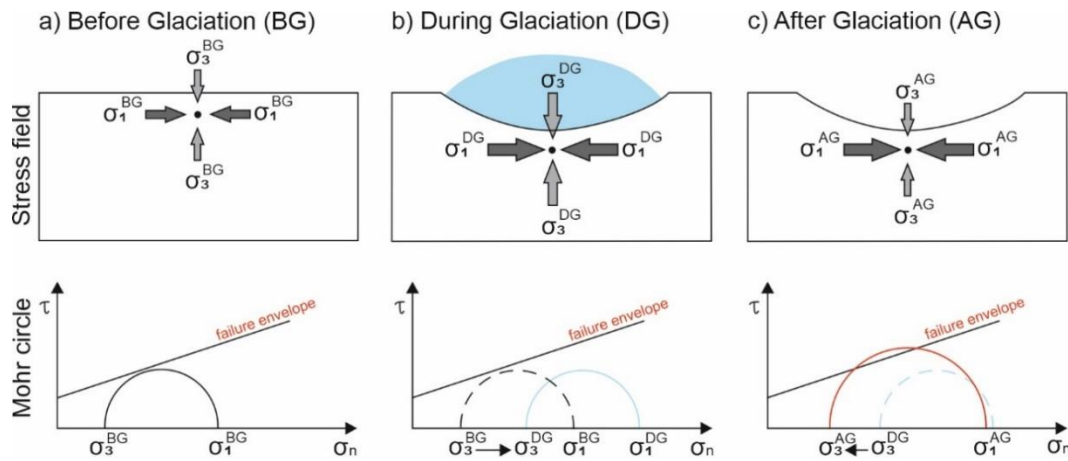


Figure 12: Schematic model of the fault stability in a compressional stress regime during a glacial cycle. (a) Initial stress state without surface load; (b) Stress state with surface load; (c) Stress state without surface load leading to rebound and stress release. With  $\sigma_1$ : maximum principal stress,  $\sigma_3$ : minimum principal stress,  $\sigma_n$ : normal stress. The dashed circles represent the previous stress situation (modified from Steffen et al. 2014).

## 3. Methods

### 3.1 Selection of outcrops

Quaternary deposits commonly serve as archives for young fault movements. Natural outcrops of Pleistocene and Holocene sediments are rare in northern and central Germany. A systematic problem in northern and central Germany is that young (Holocene) sediments are difficult to access. Commonly they are not of economic interest and not exploited. Natural outcrops of Pleistocene sediments are almost absent and trench studies of all major basement faults are very time consuming and expensive. Therefore, Pleistocene sediments were analysed in sand and gravel pits located in the vicinity of major basement faults.

All sand and gravel pits in the study area were identified from satellite images. Geological maps (scale 1:25 000 and 1:50 000) and the related reports were used to estimate the depositional ages of the exposed sediments. Altogether 156 sand and gravel pits were identified for further analyses (Fig. 13). All pits are listed in the Appendix in Tables A6-A13.

### 3.2 Fieldwork

Fieldwork was carried out along major basement faults in northern and central Germany in the 156 sand and gravel pits and one sinkhole mainly exposing Middle to Late Pleistocene deposits (Fig. 13). During fieldwork the depositional environment and deformation structures were investigated.

The Middle to Late Pleistocene deposits serve as artificial outcrops which were investigated to seek for evidence for palaeo-earthquakes and neotectonic fault activity. All pits with distances up to 10 km from the major basement fault were selected for the analysis in northern Germany resulting in a 20-km-wide study area around each fault trace. At the Harz Boundary Fault only the sand and gravel pits north of the fault were investigated within a 20-km-wide area. South of the fault no outcrops of appropriate Pleistocene sediments are present. Pits along the RLR fault system were investigated in a fieldwork area of ~22800 km<sup>2</sup> independent from the fault pattern between Leipzig, Aue, Halle and Dresden whereas the Lusatian Thrust and the FGJ fault system represent major faults in this area.

#### 3.2.1 Sedimentological analysis

A sedimentological analysis of the exposed sediments based on sedimentary facies and facies associations was carried out to reconstruct the depositional environment. Sedimentary facies were defined on the basis of grain size, bed thicknesses, bed contacts, bed geometry and internal sedimentary structures. Photos were used to document further details of the sedimentary facies. Based on the sedimentary facies and the geometry of the deposits, architectural elements of the exposed sedimentary systems were identified. The larger-scale facies architecture and deformation structures were mapped from photo panels. The main palaeo-current directions were determined from cross bedding.

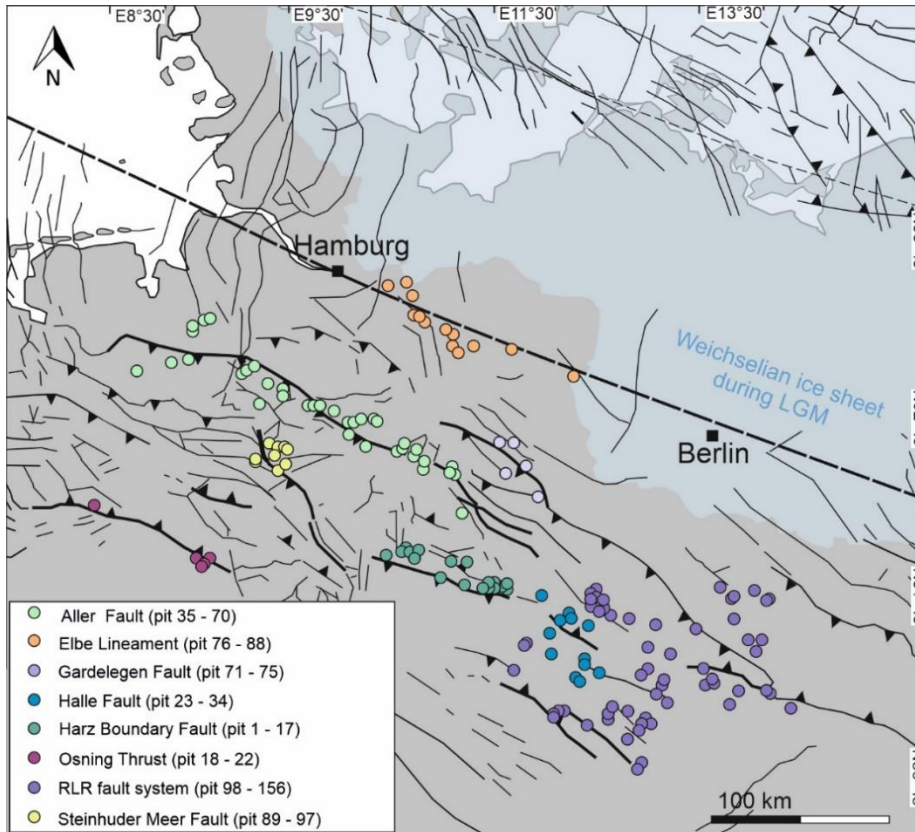


Figure 13: Map of the major fault systems in northern and central Germany with the location of sand and gravel pits analysed. All pits are listed in the Appendix in Tables A6-A13. Map is based on Kley and Voigt (2008) and Scheck-Wenderoth and Lamarche (2005).

### 3.2.2 Structural analysis

The structural analysis of each entire outcrop is necessary to provide a robust interpretation of the deformation structures exposed. The identification and classification of the different deformation structures like folds, normal and reverse faults, deformation bands with normal and reverse displacements or SSDS caused by liquefaction and/or fluidization processes is the basis for correctly identified driving processes. A detailed description of these processes is shown in Publication 3. During the structural analysis, the fabric of the SSDS, the position within the sedimentary succession and the orientation of the structures, using a geological compass, have been acquired.

All measurements were executed using the Clar method, which allows the orientation and dip of a plane to be deduced in one single process. This is especially useful for measuring fabrics in unconsolidated sediments where the structures might otherwise be destroyed. The orientation of tectonic fabrics and sedimentary structures was measured with a standard Freiberg compass (GeKom model from Breithaupt, Kassel).

Knowledge of the orientation of the deformation structures like faults, deformation bands and folds, is required for a correct interpretation and a subsequent palaeo-stress field analysis. The orientation of tectonic fabrics and deformation structures are displayed as stereographic projections (lower hemisphere equal area projection).

### 3.3 Luminescence dating

Luminescence dating is crucial in palaeoseismological studies of Holocene and Late Pleistocene sediments as it is one of the best geochronological methods to derive the age of unconsolidated sediments. The major aim of palaeoseismological studies is to derive the timing of faulting (McCalpin 2009) and thus luminescence dating is an ideal technique to derive the age of the fault movement (Rittenour 2008; Rhodes 2011). Samples are taken from tectonically disturbed and overlying undisturbed sediments to estimate the time of deformation. However, the dating of glacial sediments is challenging because the deposits may have been poorly bleached. In addition, the uncertainty of individual luminescence ages typically ranges between 5 - 10% (Duller 2008), which limits the age estimate for Middle Pleistocene fault movements.

#### 3.3.1 Basic concept of luminescence dating

Luminescence dating yields absolute ages that indicate the last time when sediments were exposed to the sunlight. In most cases, this represents the depositional age of sediments (Aitken 1998). The luminescence signal is accumulated through time when the sediment is deposited. The basic concept behind the luminescence method is the increase of radiation damage in the crystal lattice of nonconductive minerals, e.g. quartz and feldspar (Fig. 14) (Bøtter-Jensen et al. 2003; Fuchs and Owen 2008). These minerals are natural dosimeters that accumulate the amount of radiation, which they were exposed over time. Energy is trapped and released in the crystals over a certain period of time (Aitken 1985). Due to natural radiation in the sediment, energy is added to electrons in the crystal, which move from a lower to a higher energy level. Some of these electrons can be trapped in a metastable state in crystal defects between these two energy levels. By adding energy in the form of light or temperature these electrons drop back to a lower energy level by emitting photons. This light emission is named luminescence. Luminescence dating measures the intensity of the light emitted, which is proportional to accumulated dose and time since deposition (Duller 2008).

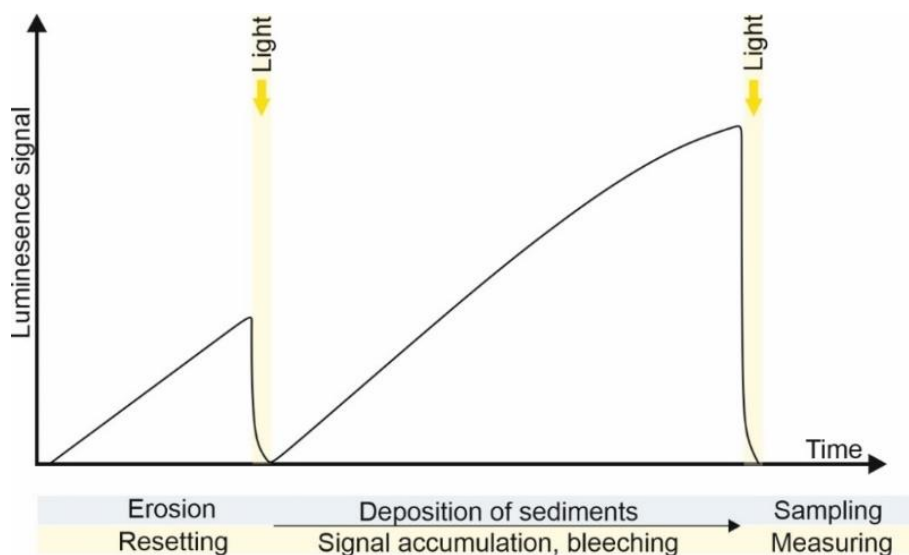


Figure 14: Accumulation of the luminescence signal through time (modified after Aitken 1998).

By measuring the luminescence signal in the laboratory, the optical stimulation is imitated by light stimulation. The emitted photons are counted by applying a photomultiplier. Afterwards, the natural luminescence signal is bleached and the used aliquot is irradiated again. The measured luminescence signal forms a growth curve. By interpolating the natural luminescence signal, the past radiation dose is estimated. This is equivalent to the accumulated energy since the last bleaching of the sediment, referred to as the equivalent dose ( $D_e$  in Gy). The dose rate ( $D_R$  in Gy  $ka^{-1}$ ), measured by gamma spectrometry of the background radiation of the sedimentary system, describes the annual dose rate of the surrounding environment including cosmic radiation and allows the calculation of the time since the last exposure to sunlight prior to deposition. More details are given in Aitken (1998) and Preusser et al. (2008).

The following equation is used for age calculation:

$$\text{Age (ka)} = \frac{\text{Equivalent dose } (D_e)(\text{Gy})}{\text{Dose rate } (D_R)(\text{Gy ka}^{-1})}$$

#### **3.3.2 Sample preparation**

##### *Determination of the dose rate*

To detect the background radiation of the sedimentary system dose rate determination was conducted. The radionuclide concentrations of uranium ( $^{235}\text{U}$ ,  $^{238}\text{U}$ ), thorium ( $^{232}\text{Th}$ ), and potassium ( $^{40}\text{K}$ ) were measured using high-resolution gamma spectrometry. 700 g of the sediment surrounding each sample were dried (130 °C) homogenized and packed into so-called Marinelli-beakers. To achieve an equilibrium between Radon and its daughter nuclides, the samples were stored for at least six weeks before measuring. The radiation dose rates were calculated by using the conversion factors of Guérin et al. (2011) and the beta attenuation factors of Mejdahl (1979). An  $a$ -value of  $0.04 \pm 0.01$  for quartz and an  $a$ -value of  $0.09 \pm 0.02$  for feldspar were used (Rees-Jones 1995). The in-situ water content of all samples was measured and used for the calculation of the attenuation caused by the contained water and hence for the correction of the  $\alpha$ -,  $\beta$ - and  $\gamma$ -dose rates. The cosmic dose rate was calculated considering altitude, geomagnetic latitude and sediment thickness according to Prescott and Hutton (1994).

##### *Determination of the equivalent dose*

The preparation of the samples for luminescence measurements was carried out under subdued red light in the luminescence laboratory at the Leibniz Institute of Applied Geophysics (LIAG). The outer ends (2 cm) of the undisturbed material in cylinders were removed to exclude any sediment that was exposed to light. For the luminescence measurement 50 - 100 g of the sample material was dried at  $\leq 50$  °C and chemically treated with 10% hydrochloric acid (HCl) until the reaction stopped. Afterwards, 200 ml disodium oxalate ( $\text{Na}_2\text{C}_2\text{O}_4$ ) was added for 2 hours and 30% hydrogen peroxide ( $\text{H}_2\text{O}_2$ ) was added for 12 hours in order to dissolve carbonates, break up aggregates and to eliminate the organic matter. Depending on the grain size the sample material was treated differently as described below:

#### A) Fine-grained samples

The grain fraction of 4 - 11  $\mu\text{m}$  was separated to measure the luminescence signal of quartz and polymineral fine grains. For the quartz aliquots, a part of the sample was treated with 40% hexafluorosilicic acid ( $\text{H}_2\text{SiF}_6$ ) to remove minerals other than quartz (Prasad 2000; Fuchs et al. 2005). Finally, the polymineralic and quartz aliquots were mounted on aluminium discs to measure the luminescence signal.

#### B) Coarse-grained samples

Coarse-grained samples were sieved before they were chemically treated to obtain the following fractions:  $>250 \mu\text{m}$ ,  $200 - 250 \mu\text{m}$ ,  $150 - 200 \mu\text{m}$ ,  $100 - 150 \mu\text{m}$ ,  $<100 \mu\text{m}$ . The fraction  $150 - 200 \mu\text{m}$  was chosen for further analysis. A separation of feldspar and quartz minerals was implemented by using sodium polytungstate ( $2.62 \text{ g cm}^{-3}$ ). This procedure was implemented twice more with densities of  $2.58 \text{ g cm}^{-3}$  and  $2.70 \text{ g cm}^{-3}$ . Sodium polytungstate with a density of  $2.58 \text{ g cm}^{-3}$  was used for the separation of potassium feldspar and plagioclase and a density of  $2.70 \text{ g cm}^{-3}$  was used for the separation of quartz and heavy minerals. For the quartz aliquots, a part of the sample was treated with 40% hexafluorosilicic acid ( $\text{H}_2\text{SiF}_6$ ) to remove the outer layers of the minerals affected by  $\alpha$  radiation. Finally, the feldspar aliquots were mounted on stainless steel discs using silicone to measure the luminescence signal.

#### **3.3.3 Luminescence measurements**

Feldspar and quartz luminescence signals were measured with two automated Risø TL/OSL readers (DA-20) with calibrated  $^{90}\text{Sr}/^{90}\text{Y}$  beta sources ( $1.48 \text{ GBq} = 40 \text{ mCi}$  and  $2.96 \text{ GBq} = 80 \text{ mCi}$ ) delivering between  $0.08$  and  $0.09 \text{ Gy s}^{-1}$ . Polyminerals were used for infrared stimulated luminescence (IRSL) dating, where only the feldspar is stimulated by pulsed IR light-emitting diodes (LED) with wavelengths of  $870 \text{ nm}$ . To detect a stable IRSL signal with reduced anomalous fading, the feldspar signal was detected in the off-periods of each pulsed cycle with a Schott BG39/Corning 7-59 filter combination (Tsukamoto et al. 2006; 2017). The pulsed IR stimulation was performed at  $50 \text{ }^\circ\text{C}$  ( $\text{IR}_{50}$ ). The used protocols measurement parameters and ages are shown in Publication 1 for the Harz Boundary Fault and the Appendix 9.1 for the Steinhuder Meer Fault.

The quartz signal was stimulated by blue LED diodes, emitting at  $470 \text{ nm}$  and detected through a Hoya U-340 filter. A single-aliquot regenerative dose (SAR) protocol after Murray and Wintle (2000) was applied for equivalent dose ( $D_e$ ) determination (see Publication 1).

#### *Fading tests and age calculations*

Fading tests are necessary because feldspar minerals are affected by a phenomenon called anomalous fading, where a tunnelling-induced loss of trapped electrons occurs (Wintle 1973; Spooner 1994). This phenomenon can lead to an underestimation of the age (Wintle 1973; Jain et al. 2015). Therefore, a fading correction for feldspar aliquots, was performed by determining the anomalous fading rate under laboratory conditions (Huntley and Lamothe 2001). For young samples (up to  $50 \text{ ka}$ ), age correction models relating to the 'linear part' of the dose response curve



are used (Huntley and Lamothe 2001). Fading rates ( $g$ -values) were determined by using 8 aliquots using the log-decay model (Huntley and Lamothe 2001).

The fading-uncorrected pulsed  $IR_{50}$  feldspar ages and quartz ages were calculated using the mean  $D_e$  value of all accepted aliquots. The fading corrected age of feldspar samples was calculated by using the R-Luminescence Package (R version 3.3.2), which is based on Huntley and Lamothe (2001). The OSL ages were calculated by dividing the equivalent dose ( $D_e$ ) by the total dose rate ( $D_R$ ).

#### 3.4 Shear-wave reflection seismics

Shallow seismic reflection methods are excellent tools to obtain a high-resolution image of the subsurface (e.g. Winsemann et al. 2009, 2011; Brandes et al. 2011; Lang et al. 2012; Polom et al. 2013) and for the detection and analysis of near-surface faults (e.g. Campbell et al. 2010; Wadas et al. 2016) and lithological contrasts. This method was already successfully applied in palaeoseismological studies and can image faults in unconsolidated sediments (e.g. Harris 2009; Ghose et al. 2013). The shear-wave reflection system uses horizontally polarized shear waves (SH-waves) and has a non-invasive source and receiver design (Krawczyk et al. 2013; Polom et al. 2013). The achieved maximum target depth of the SH-waves is nearly 70 m in the study area. Shear-wave seismic surveys were measured at the Harz Boundary Fault to support the structural analysis (Figs 15, 16). In the Mesozoic rocks of the Subhercynian Basin a vertical resolution of 4 m was obtained and in the Palaeozoic rocks of the Harz Mountains a resolution of 5 m was achieved. The acquisition and used set-up are described in detail in Publication 1.



Figure 15: Shear-wave reflection seismic investigation at the Harz Boundary Fault.



The seismic interpretation is based on the definition and analysis of seismic facies, which are relying on the external geometry, internal reflector configuration and seismic facies parameters, which include the amplitude, polarity, continuity and density of the individual reflectors (Roksandić 1978). Distinctive differences in the shear-wave velocities and shot gather examples at significant seismic facies changes were used for the interpretation of the seismic data, supported by geological maps, outcrop and borehole data. Shear-wave interval velocities and shear-wave refraction inversion results support the interpretation (see Publication 1).

Difficulties are caused by the special geological situation along the Harz Boundary Fault. Due to the steeply dipping lithological units, the vertical to steeply dipping beds are not directly imaged. The 70° limit of the applied FD-migration (Yilmaz 1987) results in a limitation of the reflection seismic method to image steeply dipping structures. Therefore, the fault traces and lithological units are interpreted based on reflector disruptions and secondary wavelet effects caused by changes in signature patterns.

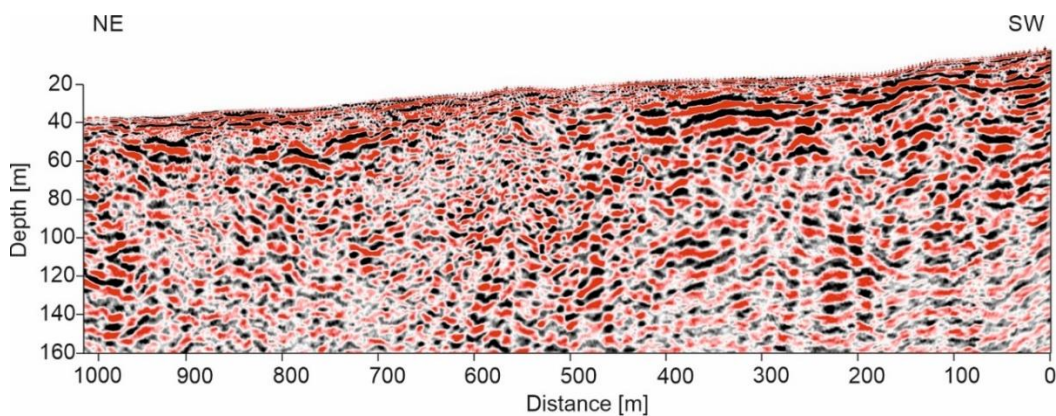


Figure 16: Shear-wave reflection seismic profile at the Harz Boundary Fault.

### 3.5 Electrical resistivity tomography

Electrical resistivity tomography (ERT) is a non-invasive geophysical method to analyse the upper 10 m of the near-surface (Lowrie 2007). Several studies show the possibility to visualize fault zones with ERT profiles (e.g. Galli et al. 2006; Vanneste et al. 2008; Nabi et al. 2020; Meng et al. 2020). ERT uses electric currents which are transferred via electrodes into the subsurface to measure the conductivity. An array of regularly spaced current and potential electrodes are used. Different configurations can be applied such as the Wenner configuration, which is best adapted for lateral profiling, the Schlumberger and the double-dipole configuration (Fig. 17). The acquisition and used set-up are described in Publication 1.

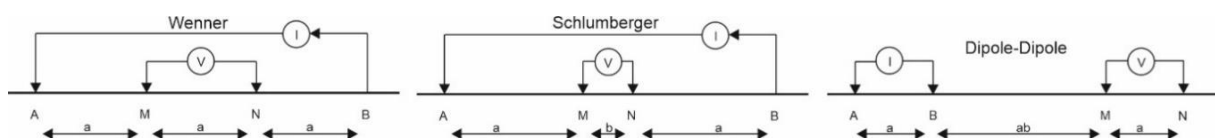
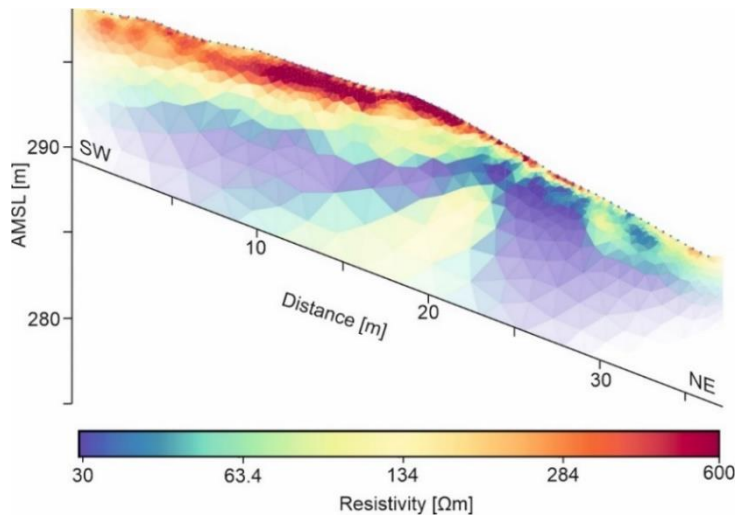


Figure 17: Electrode configurations: Wenner, Schlumberger and Dipole-Dipole. A and B represent the current electrodes and M and N are the potential electrodes (modified after Garofalo 2014).

The current electrodes transfer the electric current into the subsurface and the potential electrodes measure the potential difference. Based on the potential difference, resistivities are calculated (Kearey et al. 2002; Lowrie 2007). The results are displayed in form of a resistivity image that reflects material properties and water content in the near-subsurface (Fig. 18).

Due to the detection of density contrasts, caused by different porosities of various materials and thus compaction and water saturations, it is possible to image near-surface faults and hence this



method is a useful tool in palaeoseismological studies. The porosity is the major control of the resistivity of the deposits or rocks. Generally, the resistivity increases as porosity decreases (Kearey et al. 2002). The interpretation is based on porosity variations in the fault zone caused by compaction and shearing.

Figure 18: ERT profile at the Harz Boundary Fault.

### 3.6 Coulomb failure stress modelling

To analyse the glacially-induced reactivation potential of faults at the end of the Late Pleistocene Weichselian glaciations, numerical simulations were carried out, based on the approaches of Wu (2004) and Steffen et al. (2006). These finite-element simulations describe the process of GIA together with Coulomb failure stress (CFS) calculations (Publication 1). Assuming that the analysed faults were close to failure before glaciation, a change in the CFS can be observed during and after the deglaciation phase. The numerical simulations were carried out by Dr. Holger Steffen, Landmåteriet, Sweden.

Two types of models were used for numerical simulation with and without a lateral homogeneous structure. Laterally homogeneous models that vary only with depth, are commonly used in GIA modelling. The basic model with a laterally homogeneous structure has a lithospheric thickness of 90 km, an upper mantle viscosity of  $5 \times 10^{20}$  Pa s and a lower mantle viscosity of  $2 \times 10^{21}$  Pa s. Additionally, models that vary in one of these three parameters were tested. Hence, four laterally homogeneous models were analysed. Also 140 km lithospheric thickness,  $8 \times 10^{20}$  Pa s upper mantle viscosity and  $2 \times 10^{22}$  Pa s lower mantle viscosity were applied. All values represent reliable estimates based on GIA studies of Fennoscandia (Lambeck et al. 2010; Zhao et al. 2012; Kierulf et al. 2014). Although, these laterally homogeneous models can explain the GIA process in Fennoscandia, they are not supported by seismic results that point to lateral variations in the deep subsurface. Thus, additionally two models with a laterally heterogeneous structure were tested. The models vary in lithospheric thickness (90 km and 140 km) and use a three-dimensional (3D) mantle viscosity structure of the seismic tomography model by Grand et al. (1997), which is converted based on the method of Wu et al. (2013). For the ice load history part, two different ice history models were used that were available and that are commonly applied in GIA studies. The

first is the North-European part of the global ice model ICE-6G\_C (Argus et al. 2014; Peltier et al. 2015), while the other is a combination of the so-called ANU-ICE history models for the British Isles (Lambeck 1995) and Fennoscandia (Lambeck et al. 2010).

#### **3.7 Lineament analysis**

Using lineament analysis, neotectonic activity can be investigated by a visual analysis of geomorphological structures on the Earth's surface. The term 'lineament' was introduced by Hobbs (1904). O'Leary et al. (1976) deliver the most comprehensive treatment of the topic and define a lineament as a mappable, simple, or composite linear feature of a surface. This definition includes that the elements of a lineament are aligned in a rectilinear or slightly curvilinear relationship and differ from the pattern of adjacent structures. A lineament is supposed to reflect a subsurface phenomenon (O'Leary et al. 1976). Thus, lineaments are linear, structurally distinct zones that can extend through several tectonic levels of the Earth's crust. The term photolineament is used for linear or slightly curved geological structures in the landscape that were extracted by using satellite data or aerial photos of the Earth's surface (e. g. Van der Pluijm and Marshak 2004; Murawski and Meyer 2017). Two types of lineaments exist. Positive lineaments can be expressed by e.g. dykes, fault scarps and ridges. Negative lineaments are depressions, river valleys as well as faults and shear zones. The basic approach for a lineament analysis is the employment of a digital elevation model (DEM) or a pan-chromatic satellite image. In general, lineament interpretations have to be considered with care and they are often not very robust because of artifacts of sunlight on the surface (Van der Pluijm and Marshak 2004).

Using a Geographic Information System (GIS) analysis of DEMs is a well-established method and has been successfully applied in many studies (e.g. Grohmann 2004; Abdullah et al. 2010). The advantage of DEM data to satellite data is that the azimuth and inclination of illumination can be adapted and changed during analyses. Using the GIS, eight shaded relief maps were created with lighting 20° above the horizon. For automatic lineament extraction, the LINE module of the software PCI Geomatica was used. This module extracts linear features from an image and transforms the polylines into vector segments. The procedure and the used parameters are described in Publication 4.

## 4. References

- Abdullah A, Akhir JM, Abdullah I (2010) Automatic mapping of lineaments using shaded relief images derived from digital elevation model (DEMs) in the Maran - Sungai Lembing area, Malaysia. *Electron J Geotech Eng* 15:949-958, <https://doi.org/10.3390/geosciences11050183>
- Aber JS, Ber A (2007) Glaciotectonism. In: Van der Meer JJM (ed), *Developments in Quaternary Science*, 6, Elsevier, Amsterdam, p 246
- Abramovitz T, Thybo H (2000) Seismic images of Caledonian, lithosphere-scale collision structures in the southeastern North Sea along Mona Lisa Profile 2. *Tectonophysics* 317:27-54
- Aitken MJ (1985) *Thermoluminescence dating*. Academic Press, London, p 551
- Aitken MJ (1998) *Introduction to optical dating: the dating of Quaternary sediments by the use of photon-stimulated luminescence*. Oxford University Press, Oxford, New York, p 267
- Argus DF, Peltier W, Drummond R, Moore AW (2014) The Antarctica component of postglacial rebound model ICE-6G\_C (VM5a) based on GPS positioning, exposure age dating of ice thicknesses, and relative sea level histories. *Geophys J Int* 198:537-563
- Arvidsson R (1996) Fennoscandian earthquakes: Whole crustal rupturing related to postglacial rebound. *Science* 274:744-746
- Aydin A (1978) Small faults formed as deformation bands in sandstone. In: Byerlee JD, Wyss M (eds), *Rock Friction and Earthquake Prediction, Contributions to Current Research in Geophysics (CCRG)*, 6, Birkhäuser, Basel, pp 913-930
- Aydin A, Johnson AM (1978) Development of faults as zones of deformation bands and as slip surfaces in sandstone. *Pure Appl Geophys* 116:931-942
- Aydin A, Borja RI, Eichhubl P (2006) Geological and mathematical framework for failure modes in granular rock. *J Struct Geol* 28:83-98
- Baldschuhn R, Best G, Kockel F (1991) Inversion tectonics in the north-west German basin. Generation, accumulation, and production of Europe's hydrocarbons. *Spec Publ Eur Assoc Petroleum Geosci* 1:149-159
- Baldschuhn R, Binot F, Fleig S, Kockel F (1996) *Geotektonischer Atlas von Nordwest-Deutschland und dem deutschen Nordsee-Sektor*. *Geol Jb A* 153:3-95
- Baldschuhn R, Kockel F (1999) Das Osning-Lineament am Südrand des Niedersachsen-Beckens. *ZDGG* 150:673-695
- Bankwitz P (1971) Geologische Auswertung von geodätisch ermittelten rezenten Krustenbewegungen im Gebiet der DDR. *Petermanns Geogr Mitt* 115:130-140
- Bankwitz P, Bankwitz E (1991) Tektonische Aspekte der Erdkrustenentwicklung im Raum Erzgebirge-Vogtland. In: *Kurzfassungen der Vorträge und Poster, Geologisch-Tektonischer Bau der Gera-Jáchymov Störungszone und die daran gebundenen Uranlagerstätten, Stratigraphie, Tektonik, Metallogenie, Umweltengineering*. Gera/Thüringen. *Kurzfassungen der Vorträge und Poster*, p 1
- Bankwitz P, Grossand U, Bankwitz E (1993) Krustendeformation im Bereich der Finne-Kyffhäuser-Gera-Jáchymov-Zone. *Z Geol Wiss* 21:3-20
- Bankwitz P, Wetzel HU, Kämpf H (1998) Fototektonische Interpretation des Schwarmbeben- und Quellengebietes am NW-Rand des Böhmisches Massivs. *Publ Deutsch Ges Photogrammetrie und Fernerkundung* 6:95-102
- Bankwitz P, Bankwitz E, Bräuer K, Kämpf H, Störr M (2003a) Deformation structures in Plio- and Pleistocene sediments (NW Bohemia, Central Europe). In: Van Rensberger P, Hillis RR, Maltman AJ, Morley CK (eds), *Subsurface Sediment Mobilization*. *Geol Soc London, Spec Publ* 216:73-93
- Bankwitz P, Schneider G, Kämpf H, Bankwitz E (2003b) Structural characteristics of epicentral areas in Central Europe: study case Cheb Basin (Czech Republic). *J Geodyn* 35:5-32
- Becker A (1993) An attempt to define a "neotectonic period" for central and northern Europe. *Geol Rundsch* 82:67-83

- Behr HJ, Conrad W, Muller A, Trzebski R (2002) Compilation, Linsser filtering and interpretation of the gravity map of Germany and adjacent regions at a scale of 1:1000000. *Z Geol Wiss* 30:385-402
- Bennett MR, Huddart D, Waller RI, Midgley NG, Gonzalez N, Tomio N (2004) Styles of ice-marginal deformation at Hagafellsjökull-Eystrí, Iceland during the 1998/99 winter-spring surge. *Boreas* 33:97-107
- Ben-Zion Y, Sammis CG (2003) Characterization of fault zones. *Pure Appl Geophys* 160:677-715
- Berger HJ, Felix M, Görne S, Koch E, Krentz E, Förster A, Förster HJ, Konietzky H, Lunow C, Walter K, Schütz H, Stanek K, Wagner S (2011) Tiefengeothermie Sachsen. Landesamt für Umwelt, Landwirtschaft und Geologie 9, Dresden, p 108
- Bertran P, Font M, Giret A, Manchuel K, Sicilia D (2019) Experimental soft-sediment deformation caused by fluidization and intrusive ice melt in sand. *Sedimentology* 66:1102-1117
- Best G (1996) Floßtektonik in Nordwestdeutschland. Erste Ergebnisse reflexionsseismischer Untersuchungen an der Salzstruktur "Oberes Allertal". *Zeitschrift der Dtsch Gesellschaft für Geowissenschaften* 147:455-464
- Best G, Zirngast M (2002) Die strukturelle Entwicklung der exhumierten Salzstruktur "Oberes Allertal". *Geol Jahrb Sonderheft A1*, 142:100
- Betz D, Führer F, Greiner G, Plein E (1987) Evolution of the Lower Saxony Basin. *Tectonophysics* 137:127-170
- Bockheim JG, Tarnocai C (1998) Recognition of cryoturbation for classifying permafrost-affected soils. *Geoderma* 81:281-293
- Böse M, Lüthgens C, Lee JR, Rose J (2012) Quaternary glaciations of northern Europe. *Quat Sci Rev* 44:1-25
- Bøtter-Jensen L, McKeever SWS, Wintle AG (2003) *Optically Stimulated Luminescence Dosimetry*. Elsevier, Amsterdam, p 355
- Bram K, Hirschmann G (1992) Ergebnisse geowissenschaftlicher Umfelduntersuchungen - KTB Report 92-3, Schweizerbartsche Vertragsbuchhandlung, Hannover, p 260
- Brandes C, Polom U, Winsemann J (2011) Reactivation of basement faults: interplay of ice sheet advance, glacial lake formation and sediment loading. *Basin Res* 23:53-64
- Brandes C, Tanner DC (2012) Three-dimensional geometry and fabric of shear deformation bands in unconsolidated Pleistocene sediments. *Tectonophysics* 518:84-92
- Brandes C, Winsemann J, Roskosch J, Meinsen J, Tanner DC, Frechen M, Steffen H, Wu P (2012) Activity along the Osning Thrust in Central Europe during the Lateglacial: ice sheet and lithosphere interactions. *Quat Sci Rev* 38:49-62
- Brandes C, Schmidt C, Tanner DC, Winsemann J (2013) Paleostress pattern and salt tectonics within a developing foreland basin (north-western Subhercynian Basin, northern Germany). *Int J Earth Sci* 102:2239-2254
- Brandes C, Winsemann J (2013) Soft-sediment deformation structures in NW Germany caused by Late Pleistocene seismicity. *Int J Earth Sci* 102:2255-2274
- Brandes C, Steffen H, Steffen R, Wu P (2015) Intraplate seismicity in northern Central Europe is induced by the last glaciation. *Geology* 43:611-614
- Brandes C, Igel J, Loewer M, Tanner DC, Lang J, Müller K, Winsemann J (2018a) Visualization and analysis of shear deformation bands in unconsolidated Pleistocene sand using ground-penetrating radar: Implications for paleoseismological studies. *Sediment Geol* 367:135-145
- Brandes C, Steffen H, Sandersen PBE, Wu P, Winsemann J (2018b) Glacially induced faulting along the NW segment of the Sorgenfrei-Tornquist Zone, northern Denmark: implications for neotectonics and Lateglacial fault-bound basin formation. *Quat Sci Rev* 189:149-168
- Brandes C, Plenefisch T, Tanner DC, Gestermann N, Steffen H (2019) Evaluation of deep crustal earthquakes in northern Germany - Possible tectonic causes. *Terra Nova* 31:83-93
- Brandes C, Tanner DC (2020) Fault mechanics and earthquakes. In: Tanner DC, Brandes C (eds), *Understanding Faults*. Elsevier, Amsterdam, pp 11-80
- Calais E, Camelbeeck T, Stein S, Liu M, Craig TJ (2016) A new paradigm for large earthquakes in stable continental plate interiors. *Geophys Res Lett* 43:10-621

- Campbell FM, Ghisetti F, Kaiser AE, Green AG, Horstmeyer H, Gorman AR (2010) Structure and evolution of the seismically active Ostler Fault Zone (New Zealand) based on interpretations of multiple high-resolution seismic reflection profiles. *Tectonophysics* 495:195-212
- Cashman SM, Baldwin JN, Cashman KV, Swanson K, Crawford R (2007) Microstructures developed by coseismic and aseismic faulting in near-surface sediments, San Andreas fault, California. *Geology* 35:611-614
- Childs C, Manzocchi T, Walsh JJ, Bonson CG, Nicol A, Schöpfer MP (2009) A geometric model of fault zone and fault rock thickness variations. *J Struct Geol* 31:117-127
- Choi JH, Edwards P, Ko K, Kim YS (2016) Definition and classification of fault damage zones: A review and a new methodological approach. *Earth Sci Rev* 152:70-87
- Cohen KM, Gibbard PL (2020) Global chronostratigraphical correlation table for the last 2.7 million years v. 2019, V3, doi: 10.17632/dtsn3xn3n6.3
- Cowie PA, Scholz CH (1992a) Physical explanation for the displacement-length relationship of faults using a post-yield fracture mechanics model. *J Struct Geol* 14:1133-1148
- Cowie PA, Scholz CH (1992b) Displacement-length scaling relationship for faults: data synthesis and discussion. *J Struct Geol* 14:1149-1156
- Dahm T, Krüger F, Stammer K, Klinge K, Kind R, Wylegalla K, Grasso JR (2007) The 2004  $M_w$  4.4 Rotenburg, northern Germany, earthquake and its possible relationship with gas recovery. *Bull Seismol Soc Am* 97:691-704
- Dahm T, Cesca S, Hainzl S, Braun T, Krüger F (2015) Discrimination between induced, triggered and natural earthquakes close to hydrocarbon reservoirs: A probabilistic approach based on the modeling of depletion-induced stress changes and seismological source parameters. *J Geophys Res* 120:2491-2509
- Dahm T, Heimann S, Funke S, Wendt S, Rappsilber I, Bindi D, Plenefisch T, Cotton F (2018) Seismicity in the block mountains between Halle and Leipzig, Central Germany: centroid moment tensors, ground motion simulation, and felt intensities of two  $M \approx 3$  earthquakes in 2015 and 2017. *J Seismol* 22:985-1003
- Dalmer K, Credner H (1901) Erläuterungen zur geologischen Spezialkarte des Königreichs Sachsen. Blatt 5341 Wilkau-Haßlau. 2 Edition, Königliches Finanzministerium, Leipzig, p 79
- Dehls JF, Olesen E, Olsen L, Blikra, LH (2000) Neotectonic faulting in northern Norway; the Stuaragurra and Nordmannvikdalen postglacial faults. *Quart Sci Rev* 19:1447-1460
- DEKORP-BASIN and Group R (1999) Deep crustal structure of the Northeast German basin: new DEKORP-BASIN '96 deep profiling results. *Geology* 27:55-58
- Drozdowski G (1988) Die Wurzel der Osning-Überschiebung und der Mechanismus herzynischer Inversionsstörungen in Mitteleuropa. *Geol Rundsch* 77:127-141
- Duller GAT (2008) Luminescence Dating: Guidelines on Using Luminescence Dating in Archaeology. English Heritage, Swindon, p 43
- Edelman CH, Florschütz F, Jeswiet J (1936) Über spätpleistozäne frühholozäne kryoturbate Ablagerungen in den östlichen Niederlanden. *Verh Geol Serie* 11:301-336
- Ehlers J, Grube A, Stephan HJ, Wansa S (2011) Pleistocene glaciations of North Germany - new results. In: Ehlers J, Gibbard PL, Hughes PD (eds), *Quaternary Glaciations: Extent and Chronology - A Closer Look: Developments in Quaternary Science*, 1 Edition, 15:149-162
- Eissmann L (1987) Lagerungsstörungen im Lockergebirge. Exogene und endogene Tektonik im Lockergebirge des nördlichen Mitteleuropas. *Geophys Veröff KMU Leipzig* 3:7-77
- Eissmann L (1995) Sachsen. In: Benda L (ed), *Das Quartär Deutschlands*. Gebrüder Borntraeger, Berlin, Stuttgart, pp 171-198
- Eissmann L (2002) Quaternary geology of eastern Germany (Saxony, Saxon-Anhalt, south Brandenburg, Thüringia), type area of the Elsterian and Saalian stages in Europe. *Quat Sci Rev* 21:1275-1346
- von Eynatten H, Voigt T, Meier A, Franzke HJ, Gaupp R (2008) Provenance of Cretaceous clastics in the Subhercynian Basin: constraints to exhumation of the Harz Mountains and timing of inversion tectonics in Central Europe. *Int J Earth Sci* 97:1315-1330
- Faulkner DR, Jackson CAL, Lunn RJ, Schlische RW, Shipton ZK, Wibberley CAJ, Withjack MO (2010) A review of recent developments concerning the structure, mechanics and fluid flow properties of fault zones. *J Struct Geol* 32:1557-1575



- Fischer T, Horálek J, Hrubcová P, Vavryčuk V, Bräuer K, Kämpf H (2014) Intra-continental earthquake swarms in West-Bohemia and Vogtland: a review. *Tectonophysics* 611:1-27
- Fossen H, Schultz RA, Shipton ZK, Mair K (2007) Deformation bands in sandstone: a review. *J Geol Soc* 164:755-769
- Fossen H (2010a) Deformation bands and fractures in porous rocks. In: Fossen H (ed), *Structural Geology*, Cambridge University Press, pp 141-148
- Fossen H (2010b) Deformation bands formed during soft-sediment deformation: Observations from SE Utah. *Mar Pet Geol* 27:215-222
- Fossen H, Cavalcante GCG (2017) Shear zones - A review. *Earth Sci Rev* 171:434-455
- Franke D (1993) The southern border of Baltica - a review of the present state of knowledge. *Precambrian Res* 64:419-430
- Franke D, Hoffmann N (1999a) Das Elbe-Lineament - bedeutende Geofraktur oder Phantomgebilde? - Teil 1: Die Referenzgebiete. *Z Geol Wiss* 27:279-318
- Franke D, Hoffmann N (1999b) Das Elbe-Lineament - bedeutende Geofraktur oder Phantomgebilde? - Teil 2: Regionale Zusammenhänge. *Z Geol Wiss* 27:319-350
- Franke W (2000) The mid-European segment of the Variscides: tectonostratigraphic units, terrane boundaries and plate tectonic evolution. *Geol Soc Lon Spec Pub* 179:35-61
- Franzke HJ, Schmidt D (1993) Die mesozoische Entwicklung der Harznordrandstörung-Makrogefügeuntersuchungen in der Aufrichtungszone. *Zbl Geol Paläont Teil I*: 1443-1457
- Franzke H-J, Voigt T, von Eynatten H, Brix MR, Burmester G (2004). Geometrie und Kinematik der Harznordrandstörung, erläutert an Profilen aus dem Gebiet von Blankenburg. *Geowiss Mitt Thüringen* 11:39-62
- French HM (2017) *The periglacial environment*. John Wiley and Sons. 4 Edition, Chichester, p 544
- Fuchs M, Straub J, Zöller L (2005) Residual luminescence signals of recent river flood sediments: a comparison between quartz and feldspar of fine- and coarse-grain sediments. *Anc TL* 23:25-30
- Fuchs M, Owen LA (2008) Luminescence dating of glacial and associated sediments: review, recommendations and future directions. *Boreas* 37:636-659
- Galli P, Bosi V, Piscitelli S, Giocoli A, Scionti V (2006) Late Holocene earthquakes in southern Apennine: paleoseismology of the Caggiano fault. *Int J Earth Sci* 95:855-870
- Gangopadhyay A, Talwani P (2003) Symptomatic features of intraplate earthquakes. *Seismol Res Lett* 74:863-883
- Garofalo F (2014) Physically constrained joint inversion of seismic and electrical data for near surface applications. Dissertation, Politecnico di Torino, Italy, p 151
- Gast R, Gundlach T (2006) Permian strike slip and extensional tectonics in Lower Saxony, Germany. *Dtsch Ges Geowiss* 157:41-56
- Gehrmann A, Harding C (2018) Geomorphological Mapping and Spatial Analyses of an Upper Weichselian Glacitectonic Complex Based on LiDAR Data, Jasmund Peninsula (NE Rügen), Germany 8:208-232
- GERSEIS (2020) Geodatendienst für Erdbeben in Deutschland. URL: [https://www.bgr.bund.de/DE/Themen/Erdbeben-Gefahrdungsanalysen/Seismologie/Seismologie/Seis-Online/gerseis\\_node.html](https://www.bgr.bund.de/DE/Themen/Erdbeben-Gefahrdungsanalysen/Seismologie/Seismologie/Seis-Online/gerseis_node.html). (Accessed 16.12.2020)
- Ghose R, Carvalho J, Loureiro A (2013) Signature of fault zone deformation in near-surface soil visible in shear wave seismic reflections. *Geophys Res Lett* 40:1074-1078
- Gläßer W, Hänel M, Hecht G, Hiller W, Katzschmann L, Mädler J, Michel C, Pustal I, Seidel G, Wiefel H (1995) Erläuterungen zur geologischen Karte 1:25000 von Thüringen. Blatt 5040 Altenburg. 2 Edition, Thüringer Landesanstalt für Geologie, Weimar, p 288
- Gläßer W, Wiefel H (1999) Erläuterungen zur Geologischen Karte 1:25000 von Thüringen. Blatt 5041 Langenleuba-Niederhain, 2 Edition, Thüringer Landesanstalt für Geologie, Weimar, p 212
- Grand SP, Van Der Hilst RD, Widiyantoro S (1997) Global seismic tomography: A snapshot of convection in the Earth. *Geol Soc Am* 7:1-7
- Grollmund B, Zoback MD (2001) Did deglaciation trigger intraplate seismicity in the New Madrid Seismic Zone? *Geology* 29:175-178

- Grohmann CH (2004) Morphometric analysis in Geographic Information Systems: applications of free software GRASS and R. *Comput Geosci* 30:1055-1067, <https://doi.org/10.1016/j.cageo.2004.08.002>
- Grube A (2019a) Palaeoseismic structures in Quaternary sediments of Hamburg (NW Germany), earthquakes evidence during the younger Weichselian and Holocene. *Int J Earth Sci* 108:845-861
- Grube A (2019b) Palaeoseismic structures in Quaternary sediments, related to an assumed fault zone north of the Permian Peissen-Gnutz salt structure (NW Germany) – Neotectonic activity and earthquakes from the Saalian to the Holocene. *Geomorphology* 328:15-27
- Grünthal G, Bankwitz P, Bankwitz E, Bednarek J, Guterch B, Schenk V, Schenková Z, Zeman A (1985) Seismicity and geological features of the eastern part of the West European Platform. *Gerlands Beitr Geophys* 94:276-289
- Grünthal G, Stromeyer D (1994) The recent crustal stress field in Central Europe sensu lato and its quantitative modelling. *Neth J Geosci* 73:173-180
- Grünthal G, Mayer-Rosa D, Lenhardt WA (1998) Abschätzung der Erdbebengefährdung für die D-A-CH-Staaten-Deutschland, Österreich, Schweiz. *Bautechnik* 75:753-767
- Grünthal G, Wahlström R (2012) The European-Mediterranean earthquake catalogue (EMEC) for the last millennium. *J Seismol* 16:535-570
- Grünthal G, Stromeyer D, Bosse C, Cotton F, Bindi D (2018) The probabilistic seismic hazard assessment of Germany-version 2016, considering the range of epistemic uncertainties and aleatory variability. *Bull Earthq Eng* 16:4339-4395
- Guérin G, Mercier N, Adamiec G (2011) Dose-rate conversion factors: update. *Anc TL* 29:5-8
- Hardt J, Lühgens C, Hebenstreit R, Böse M (2016) Geochronological (OSL) and geomorphological investigations at the presumed Frankfurt ice marginal position in northeast Germany. *Quat Sci Rev* 154:85-99
- Hardt J, Böse M (2018) The timing of the Weichselian Pomeranian ice marginal position south of the Baltic Sea: a critical review of morphological and geochronological results. *Quat Int* 478:51-58
- Harris JB (2009) Hammer-impact SH-wave seismic reflection methods in neotectonic investigations: General observations and case histories from the Mississippi Embayment, USA. *J Earth Sci* 20:513-525
- Harris RA (2017) Large earthquakes and creeping faults. *Rev Geophys* 55:169-198
- Harry DG (1988) Ground ice and permafrost. *Advances in Periglacial Geomorphology*. Wiley, Chichester, pp 113-149
- Hart JK, Boulton GS (1991) The interrelation of glaciotectonic and glacio-depositional processes within the glacial environment. *Quat Sci Rev* 10:335-350
- Haupt M, Conrad W (1991) Die Störungszone von Gera-Jáchymov aus Sicht der Potentialfelder. In: Kurzfassungen der Vorträge und Poster, Geologisch-Tektonischer Bau der Gera-Jáchymov Störungszone und die daran gebundenen Uranlagerstätten, Stratigraphie, Tektonik, Metallogenie, Umweltengineering. Gera/Thüringen. Kurzfassungen der Vorträge und Poster, p 11-12
- Heidbach O, Rajabi M, Reiter K, Ziegler M (2016) World stress map 2016. *Science* 277:1956-62
- Hiller A, Schuppan W (2008) Geologie und Uranbergbau im Revier Schlema-Alberoda. *Bergbau in Sachsen, Sächsisches Landesamt für Umwelt und Geologie* 14, p 171
- Hobbs WH (1904) Lineaments of the Atlantic border region. *GSA Bull* 15:483-506
- Hoffmann G, Reicherter K (2012) Soft-sediment deformation of Late Pleistocene sediments along the southwestern coast of the Baltic Sea (NE Germany). *Int J Earth Sci* 101:351-363
- Hughes AL, Gyllencreutz R, Lohne ØS, Mangerud J, Svendsen JI (2016) The last Eurasian ice sheets – a chronological database and time-slice reconstruction, DATED-1. *Boreas* 45:1-45
- Huijzer B, Vandenberghe J (1998) Climatic reconstruction of the Weichselian Pleniglacial in northwestern and central Europe. *J Quat Sci* 13:391-417
- Huntington, KW, Klepeis KA, with 66 community contributors (2018) Challenges and opportunities for research in tectonics: Understanding deformation and the processes that link Earth systems, from geologic time to human time. A community vision document

- submitted to the U.S. National Science Foundation. University of Washington, pp 84, <https://doi.org/10.6069/H52R3PQ5>
- Huntley DJ, Lamothe M (2001) Ubiquity of anomalous fading in K-feldspars and the measurement and correction for it in optical dating. *Can J Earth Sci* 38:1093-1106
- Huster H, Hübscher C, Seidel E (2020) Impact of Late Cretaceous to Neogene plate tectonics and Quaternary ice loads on supra-salt deposits at Eastern Glückstadt Graben, North German Basin. *Int J Earth Sci* 109:1029-1050
- Hübscher C, Lykke-Andersen H, Hansen MB, Reicherter K (2004) Investigating the structural evolution of the western Baltic. *Eos Trans Am Geophys Union* 85:115-115
- Hürtgen J (2017) The First Paleoseismic Database of Germany and Adjacent Regions PalSeisDB v1.0, Dissertation, Rheinisch-Westfälischen Technischen Hochschule Aachen, p 478
- Jain M, Buylaert JP, Thomsen KJ, Murray AS (2015) Further investigations on 'non-fading in K-Feldspar. *Quat Int* 362:3-7
- Johnston AC (1989) The seismicity of "stable" continental interiors. In: Gregersen S, Basham PW (eds), *Earthquakes at North Atlantic Passive Margins: Neotectonics and Post-Glacial Rebound*, NATO ASI Series C, Mathematical and Physical Sciences, 563-579
- Jubitz K-B, Beutler G, Schwab G, Stackebrandt W (1991) Zur Strukturentwicklung des Spaltendiapirs der Allertalzone (Subherzyne Senke). *Z Geol Wiss* 19:421-409
- Kaduri M, Gratier JP, Renard F, Çakir Z, Lasserre C (2017) The implications of fault zone transformation on aseismic creep: Example of the North Anatolian Fault, Turkey. *J Geophys Res* 122:4208-4236
- Kaiser A (2005) Neotectonic modelling of the North German Basin and adjacent areas a tool to understand postglacial landscape evolution? *Z Dtsch Ges Geowiss* 156:357-366
- Kaiser A, Reicherter K, Hübscher C, Gajewski D (2005) Variation of the present-day stress field within the North German Basin-insights from thin shell FE modeling based on residual GPS velocities. *Tectonophysics* 397:55-72
- Kämpf H, Franzke H-J, Neunhöfer H, Märtens P, Röllig G, Schauer M (1991) Zur strukturellen Bedeutung der Nord-Süd-Bruchstörungszone Plauen/Klingenthal - Altenberg/Gera - Leipzig/Halle - Dessau/Bernburg. In: *Geologisch-tektonischer Bau der Gera-Jachymov (Joachimsthal)-Störungszone und die daran gebundenen Uranlagerstätten - Kurzfassungen der Vorträge und Poster*, pp 12-13
- Kämpf H, Bräuer K, Koch H, Malkovský M, Strauch G, Weinlich FH, Weise S (1992) Vulkanismus-Mineralwässer-Seismizität im Bereich der Marienbaden Störungszone. *Münchberger Gneismasse und ihr geologischer Rahmen*. In: *Exkursionsführer Jahrestagung der Gesellschaft für Geowissenschaften, Falkenstein/Vogtland*, pp 129-155
- Käßner A, Stanek KP, Lapp M (2020) Post-Variscan tectonic and landscape evolution of the Elbe Fault Zone and the Lusatian Block based on apatite fission-track data and geomorphologic constraints. *Geomorphology* 355:106860
- Kearey P, Brooks M, Hill I (2002) *An Introduction to Geophysical Exploration*. 3 Edition, Blackwell, Oxford, p 262
- Kiden P, Denys L, Johnston P (2002). Late Quaternary sea-level change and isostatic and tectonic land movements along the Belgian-Dutch North Sea coast: geological data and model results. *J Quat Sci* 17:535-546
- Kierulf HP, Steffen H, Simpson MJR, Lidberg M, Wu P, Wang H (2014) A GPS velocity field for Fennoscandia and a consistent comparison to glacial isostatic adjustment models. *J Geophys Res Solid Earth* 119:6613-6629
- Kley J, Franzke HJ, Jähne F, Krawczyk C, Lohr T, Reicherter K, Scheck-Wenderoth M, Sippel J, Tanner D, van Gent H (2008) Strain and stress. In: Littke R, Bayer U, Gajewski D, *Dynamics of Complex Intracontinental Basins: The Central European Basin System*. Springer Berlin, Heidelberg, pp 97-124
- Kley J and Voigt T (2008) Late Cretaceous intraplate thrusting in central Europe: Effect of Africa-Iberia-Europe convergence, not Alpine collision. *Geology* 36:839-842
- Kley J (2013) Saxonische Tektonik im 21. Jahrhundert. *Z Dtsch Ges Geowiss* 164:295-311
- Knoth W (1995) Sachsen-Anhalt. In: Benda L (ed), *Das Quartär Deutschlands*, Gebrüder Bornträger, Berlin, pp 148-170

- Kockel F (2003) Inversion structures in Central Europe - Expressions and reasons, an open discussion. *Neth J Geosci* 82:351-366
- Korn M, Funke S, Wendt S (2008) Seismicity and seismotectonics of West Saxony, Germany - new insights from recent seismicity observed with the Saxonian seismic network. *Studia Geophys et Geod* 52:479-492
- Kossmat F (1927) Gliederung des varistischen Gebirgsbaues. *Abh Sächs Geol Landesamt* 1:1-39
- Kossow D, Krawczyk CM (2002) Structure and quantification of processes controlling the evolution of the inverted NE-German Basin. *Mar Pet Geol* 19:601-618
- Krawczyk CM, McCann T, Cocks LRM, England RW, McBride JH, Wybraniec S (2008) Caledonian tectonics. In: McCann T (ed), *The Geology of Central Europe. Precambrian and Paleozoic*, 1. Geol Soc London, pp 303-381
- Krawczyk CM, Polom U, Beilecke T (2013) Shear-wave reflection seismics as a valuable tool for near-surface urban applications. *Lead Edge* 32:256-263
- Krentz O (2008) Postvariszische tektonische Entwicklung. In: Pälcher W, Walter H (eds), *Geologie von Sachsen - Geologischer Bau und Entwicklungsgeschichte*, Schweizenbart, Stuttgart, pp 472-478
- Krentz O, Lapp M, Seibel B, Bahrt W (2010) Bruchtektonik. In: Autorenkollektiv (eds), *Die geologische Entwicklung der Lausitz*. Vattenfall Europe Mining AG, Cottbus, pp 137-160
- Krentz O, Stanek K (2015) Die Lausitzer Überschiebung zwischen Meißen und Jeschken – neue Aspekte. *Ber Naturforsch Ges Oberlausitz* 23:123-137
- Krentz O, Mlčoch B, Mrázová Š, Nádaskay R, Rommel A, Sidorinová T, Skácelová Z, Tomanová Petrová P, Valečka J, Voigt T (2020) Geologie des Sächsisch-Böhmischen Kreidebeckens zwischen Erzgebirge und Jeschken. In: Mrázová Š, Tomanová Petrová P, Krentz O (eds), *ResiBil – Wasserressourcenbilanzierung und - Resilienzbewertung im Ostteil des sächsisch-tschechischen Grenzraumes*, Tschechischer Geologischer Dienst, Prag, p 104
- Kroner U, Hahn T, Romer RL, Linnemann U (2007) The Variscan orogeny in the Saxo-Thuringian zone - heterogenous overprint of Cadomian/Paleozoic Peri-Gondwana crust. *Spec Pap Geol Soc Am* 423:153-172
- Kröner U, Mansy J-L, Mazur S, Aleksandrowski P, Hann HP, Huckriede H, Lacquement F, Lamarche J, Pharaoh TC, Zedler D, Zeh A, Zulauf G (2008) Variscan Tectonics. In: McCann T (ed), *The Geology of Central Europe*. Geol Soc London 559-664
- Lambeck K (1995) Late Devensian and Holocene shorelines of the British Isles and North Sea from models of glacio-hydro-isostatic rebound. *J Geol Soc London* 152:437-448
- Lambeck K, Purcell A, Zhao J, Svensson NO (2010) The Scandinavian Ice Sheet: from MIS 4 to the end of the Last Glacial Maximum. *Boreas* 39:410-435
- Lang J, Winsemann J, Steinmetz D, Polom U, Pollok L, Böhner U, Serangeli J, Brandes C, Hampel A, Winghart S (2012) The Pleistocene of Schöningen, Germany: a complex tunnel valley fill revealed from 3D subsurface modelling and shear wave seismics. *Quat Sci Rev* 39:86-105
- Lang J, Lauer T, Winsemann J (2018) New age constraints for the Saalian glaciation in northern central Europe: implications for the extent of ice sheets and related proglacial lake systems. *Quat Sci Rev* 180:240-259
- Lang J, Alho P, Kasvi E, Goseberg N, Winsemann J (2019) Impact of Middle Pleistocene (Saalian) glacial lake-outburst floods on the meltwater-drainage pathways in northern central Europe: insights from 2D numerical flood simulation. *Quat Sci Rev* 209:82-99
- Lee JR, Phillips ER (2008) Progressive soft sediment deformation within a subglacial shear zone – a hybrid mosaic-pervasive deformation model for Middle Pleistocene glaciotectionised sediments from eastern England. *Quat Sci Rev* 27:1350-1362
- Leydecker G, Kopera JR (1999) Seismological hazard assessment for a site in Northern Germany, an area of low seismicity. *Eng Geol* 52:293-304
- Leydecker G (2011) Erdbebenkatalog für die Bundesrepublik Deutschland mit Randgebieten für die Jahre 800 bis 2008. *Geol Jb E* 59, Hannover, p 198
- Li Q, Liu M, Stein S (2009) Spatiotemporal complexity of continental intraplate seismicity: insights from geodynamic modeling and implications for seismic hazard estimation. *Bull Seismol Soc Am* 99:52-60

- Litt T, Behre KE, Meyer KD, Stephan HJ, Wansa S (2007) Stratigraphische Begriffe für das Quartär des norddeutschen Vereisungsgebietes. *E&G Quat Sci J* 56:7-65
- Liu M, Stein S, Wang H (2011) 2000 years of migrating earthquakes in North China: How earthquakes in midcontinents differ from those at plate boundaries. *Lithosphere* 3:128-132
- Lohr T, Krawczyk CM, Tanner DC, Samiee R, Endres H, Oncken O, Trappe H, Kukla PA (2007) Strain partitioning due to salt: insights from interpretation of a 3D seismic data set in the NW German Basin. *Basin Res* 19:579-597
- Lowrie W (2007) *Fundamentals of Geophysics*. 2 Edition, Cambridge University Press, New York, p 381
- Ludwig AO (2011) Zwei markante Stauchmoränen: Peski/Belarusland und Jasmund, Ostseeinsel Rügen/Nordostdeutschland - Gemeinsame Merkmale und Unterschiede. *E & G - Quat Sci J* 60:464-487
- Lüthgens C, Böse M (2011). Chronology of Weichselian main ice marginal positions in north-eastern Germany. *E & G - Quat Sci J* 60:236-247
- Marotta AM, Bayer U, Thybo H (2000) The legacy of the NE German Basin – Reactivation by compressional buckling. *Terra Nova* 12:132–140
- Marotta AM, Bayer U, Scheck M, Thybo H (2001) The stress field below the NE German Basin: effects induced by the Alpine collision. *Geophys J Int* 144:F8-F12
- Marotta AM, Bayer U, Thybo H, Scheck M (2002) Origin of regional stress in the North German basin: Results from numerical modeling. *Tectonophysics* 360:245-264
- Marotta AM, Mitrovica JX, Sabadini R, Milne G (2004) Combined effects of tectonics and glacial isostatic adjustment on intraplate deformation in central and northern Europe: applications to geodetic baseline analyses. *J Geophys Res: Solid Earth* 109:B1
- Mazur S, Scheck-Wenderoth M, Krzywiec P (2005) Different modes of the Late Cretaceous Early Tertiary inversion in the North German and Polish basins. *Int J Earth Sci* 94:782-798
- McCalpin, JP (2009) *Paleoseismology*, 2 Edition, *Int Geophys Ser* 95, pp 613
- McCann T (2008) *The Geology of Central Europe*. Volume I: Precambrian and Palaeozoic, *Geol Soc London* pp 1-20
- McCarroll D, Rijdsdijk KF (2003) Deformation styles as a key for interpreting glacial depositional environments. *J Quat Sci* 18:473-489
- Meinsen J, Winsemann J, Roskosch J, Brandes C, Frechen M, Dultz S, Böttcher J (2014) Climate control on the evolution of Late Pleistocene alluvial-fan and aeolian sand-sheet systems in NW Germany. *Boreas* 43:42-66
- Mejdahl V (1979) Thermoluminescence dating: beta-dose attenuation in quartz grains. *Archaeometry* 21:61-72
- Meng F, Zhang G, Qi Y, Zhou Y, Zhao X, Ge K (2020) Application of combined electrical resistivity tomography and seismic reflection method to explore hidden active faults in Pingwu, Sichuan, China. *Open Geosci* 12:174-189
- Menzies J (2000) Micromorphological analyses of microfabrics and microstructures indicative of deformation processes in glacial sediments. *Geol Soc London Spec Publ* 176:245-257
- Mörner NA (1978) Faulting, fracturing, and seismicity as functions of glacio-isostasy in Fennoscandia. *Geology* 6:41-45
- Müller B, Zoback ML, Fuchs K, Mastin L, Gregersen S, Pavoni N, Stephansson O, Ljunggren C (1992) Regional patterns of tectonic stress in Europe. *J Geophys Res* 97:11783-11803
- Müller C, Jähne-Klingberg F, von Goerne G, Binot F, Röhling H-G (2016) Vom geotektonischen Atlas („Kockel-Atlas“) zu einem 3D-Gesamtmodell des Norddeutschen Beckens: Basisinformationen zum tieferen Untergrund von Norddeutschland. *Z Dtsch Ges Geowiss* 167:65-106
- Murawski H, Meyer W (2017) *Geologisches Wörterbuch*. 12 Edition, Springer-Verlag, Berlin, p 220
- Murray AS, Wintle AG (2000) Luminescence dating of quartz using an improved single-aliquot regenerative-dose protocol. *Radiat Meas* 32:57-73
- Nabi A, Liu X, Gong Z, Ali A (2020) Electrical resistivity imaging of active faults in palaeoseismology: case studies from Karachi Arc, southern Kirthar Fold Belt, Pakistan. *NRIAG J Astron and Geophys* 9:116-128

- Neunhöfer H, Hemmann A (2005) Earthquake swarms in the Vogtland/Western Bohemia region: spatial distribution and magnitude-frequency distribution as an indication of the genesis of swarms? *J Geodyn* 39:361-385
- Neunhöfer H (2009) Erdbeben in Thüringen, eine Bestandsaufnahme. *Z Geol Wiss* 37:1-14
- Nocquet JM, Calais E (2003) Crustal velocity field of western Europe from permanent GPS array solutions, 1996–2001. *Geophys J Int* 154:72-88
- Nocquet JM (2012) Present-day kinematics of the Mediterranean: A comprehensive overview of GPS results. *Tectonophysics* 579:220-242
- Ogino Y, Matsuoka N (2007) Involutions resulting from annual freeze - thaw cycles: a laboratory simulation based on observations in northeastern Japan. *Permafrost Periglacial Process* 18:323-335
- O’Leary DW, Freidman JD, Pohn AH (1976) Lineament, linear, lineation: Some proposed new standards for old terms. *GSA Bull* 87:1463-1469
- Otto V (2003) Inversion-related features along the southeastern margin of the North German Basin (Elbe Fault System). *Tectonophysics* 373:107-123
- Pälcher W, Walter H (2008) *Geologie von Sachsen – Geologischer Bau und Entwicklungsgeschichte*. Schweizerbart’sche Verlagsbuchhandlung, Stuttgart, p 535
- Pavlidis SB (1989) Looking for a definition of neotectonics. *Terra Nova* 1:233-235
- Peltier W, Argus D, Drummond R (2015) Space geodesy constrains ice age terminal deglaciation: The global ICE-6G\_C (VM5a) model. *J Geophys Res: Solid Earth* 120:450-487
- Peterek A, Reuther CD, Schunk R (2011) Neotectonic evolution of the Cheb Basin (Northwestern Bohemia, Czech Republic) and its implications for the late Pliocene to recent crustal deformation in the western part of the Eger Rift. *Z Geol Wiss* 39:335-365
- Péwé TL (1973) Ice wedge casts and past permafrost distribution in North America. *Geoforum* 4:15-26
- Pharaoh TC (1999) Palaeozoic terranes and their lithospheric boundaries within the Trans-European Suture Zone (TESZ): a review. *Tectonophysics* 314:17-41
- Pharaoh TC, Winchester JA, Verniers J, Lassen A, Seghedi A (2006) The western accretionary margin of the East European Craton: an overview. *Mem Geol Soc Lon* 32:291–311
- Phillips ER, Lee JR, Burke H (2008) Progressive proglacial to subglacial deformation and syntectonic sedimentation at the margins of the Mid-Pleistocene British Ice Sheet: evidence from north Norfolk, UK. *Quat Sci Rev* 27:1848-1871
- Phillips E, Merritt J (2008) Evidence for multiphase water-escape during rafting of shelly marine sediments at Clava, Inverness-shire, NE Scotland. *Quat Sci Rev* 27:988-1011
- Piotrowski JA, Larsen NK, Junge FW (2004) Reflections on soft subglacial beds as a mosaic of deforming and stable spots. *Quat Sci Rev* 23:993-1000
- Picard E, Naumann E, Ihnen K (1937) *Erläuterungen zur geologischen Karte von Preußen und benachbarten deutschen Ländern*. Blatt 4439 Brehna. 2 Edition, Preußische Geologische Landesanstalt, Berlin, p 78
- Pisarska-Jamroży M, Belzyt S, Börner A, Hoffmann G, Hüneke H, Kenzler M, Obst K, Rother H, Van Loon AT (2018) Evidence from seismites for glacio-isostatically induced crustal faulting in front of an advancing land-ice mass (Rügen Island, SW Baltic Sea). *Tectonophysics* 745:338-348
- Pisarska-Jamroży M, Woźniak PP (2019) Debris flow and glacio-isostatic induced soft-sediment deformation structures in a Pleistocene glaciolacustrine fan: the southern Baltic Sea coast, Poland. *Geomorphology* 326:225-238
- Pohl D, Wetzell H-U, Grünthal G (2006) Tektonische Untersuchungen im Raum Vogtland-Leipzig mit Hilfe von Fernerkundung. *Geoinformatik, Erdbebenbeobachtung, Vorträge*, 26, pp 277-286
- Polom U, Bagge M, Wadas S, Winsemann J, Brandes C, Binot F, Krawczyk CM (2013) Surveying near-surface depocentres by means of shear wave seismics. *First Break* 3:63-75
- Prasad S (2000). HF treatment for the isolation of fine grain quartz for luminescence dating. *Anc TL* 18:15-17
- Prescott JR, Hutton JT (1994) Cosmic ray contributions to dose rates for luminescence and ESR dating: large depths and long-term time variations. *Radiat Meas* 23:497-500



- Preusser F, Degering D, Fuchs M, Hilgers A, Kadereit A, Klasen N, Krbetschek M, Richter D, Spencer JQG (2008) Luminescence dating: basics, methods and applications. *E&G Quat Sci J* 57:95-149
- Rabbel W, Förste K, Schulz A, Bittner R, Röhl J, Reichert JC (1995) A high-velocity layer in the lower crust of the North German Basin. *Terra Nova* 7:327-337
- Rappsilber I (2003) Struktur und Entwicklung des nördlichen Saale-Beckens (Sachsen-Anhalt): Geophysik und Geologie. Dissertation, Martin-Luther-Universität Halle-Wittenberg p 118
- Rees-Jones J (1995) Optical dating of young sediments using fine-grain quartz. *Anc TL* 13:9-14
- Reicherter K, Kaiser A, Stackebrandt W (2005) The post-glacial landscape evolution of the North German Basin: morphology, neotectonics and crustal deformation. *Int J Earth Sci* 94:1083-1093
- Reid HF (1910) The California earthquake of April 18, 1906. Report of the (California) State Earthquake Investigation Commission, vol. 2, The mechanics of the earthquake, Washington, p 192
- Reinecke V (2006) Untersuchung zur jungpleistozänen Reliefentwicklung und Morphodynamik im nördlichen Harzvorland. *Aachen Geogr Arb* 43:1-170
- Rittenour TM (2008) Luminescence dating of fluvial deposits: applications to geomorphic, palaeoseismic and archaeological research. *Boreas* 37:613-635
- Rhodes EJ (2011) Optically stimulated luminescence dating of sediments over the past 200,000 years. *Annu Rev Earth Planet Sci* 39:461-488
- Rodríguez-Pascua MA, Calvo JP, De Vicente G, Gómez-Gras D (2000) Soft-sediment deformation structures interpreted as seismites in lacustrine sediments of the Prebetic Zone, SE Spain, and their potential use as indicators of earthquake magnitudes during the Late Miocene. *Sediment Geol* 135:117-135
- Roksandić MM (1978) Seismic facies analysis concepts. *Geophys Prospect* 26:383-398
- Roskosch J, Winsemann J, Polom U, Brandes C, Tsukamoto S, Weitkamp A, Bartholomäus WA, Henningsen D, Frechen M (2015) Luminescence dating of ice-marginal deposits in northern Germany: evidence for repeated glaciations during the Middle Pleistocene (MIS 12 to MIS 6). *Boreas* 44:103-126
- Roth F, Fleckenstein P (2001) Stress orientations found in north-east Germany differ from the West European trend. *Terra Nova* 13:289-296, <https://doi.org/10.1046/j.1365-3121.2001.00357.x>
- Scheck M, Bayer U, Otto V, Lamarche J, Banka D, Pharaoh T (2002) The Elbe Fault System in North Central Europe - a basement controlled zone of crustal weakness. *Tectonophysics* 360:281-299
- Scheck M, Bayer U, Lewerenz B (2003) Salt movements in the Northeast German Basin and its relation to major post-Permian tectonic phases - results from 3D structural modelling, backstripping and reflection seismic data. *Tectonophysics* 361:277-299
- Scheck-Wenderoth M, Lamarche J (2005) Crustal memory and basin evolution in the Central European Basin System-new insights from a 3D structural model. *Tectonophysics* 397:143-165
- Schneider G (2004) Erdbeben. Eine Einführung für Geowissenschaftler und Bauingenieure. Spektrum Akademischer Verlag, München, p 246
- Scholz CH (2002) The mechanics of earthquakes and faulting. 2 Edition, Cambridge University Press, pp 471
- Schwab U, Herold U, Rappsilber I, Thomae M (2006) Geologischer Überblick zur Halle – Störung. In: Rappsilber I (ed), Halle Störung. *Mitt Geol Bergwesen Sachsen-Anhalt* 10:9-12
- von Seebach K (1873) Das Mitteldeutsche Erdbeben vom 6. März 1872: Ein Beitrag zu der Lehre von den Erdbeben. Verlag von Haessel, Leipzig, p 188
- Shimazaki K, Nakata T (1980) Time-predictable recurrence model for large earthquakes. *Geophys Res Lett* 7:279-282
- Shipton ZK, Cowie PA (2001) Damage zone and slip-surface evolution over  $\mu\text{m}$  to km scales in high-porosity Navajo sandstone, Utah. *J Struct Geol* 23:1825-1844

- Shipton ZK, Soden AM, Kirkpatrick JD, Bright AM, Lunn RJ (2006) How thick is a fault? Fault displacement-thickness scaling revisited. In: Abercrombie R (ed), *Earthquakes: Radiated Energy and the Physics of Faulting*, pp. 193-198
- Sibson RH (1977) Fault rocks and fault mechanisms. *J Geol Soc* 133:191-213
- Siegert T, Sterzel T, Credner H (1901) Erläuterungen zur geologischen Spezialkarte des Königreichs Sachsen. Blatt 5240 Zwickau-Werdau. 2. Edition, Königliches Finanzministerium, Leipzig, p 142
- Skamletz J, Korn M, Forkmann B, Göthe W (2000) A temporary network for seismological monitoring in West-Saxony: first results. *Studia Geophys et Geod* 44:142-157
- Spooner NA (1994) The anomalous fading of infrared-stimulated luminescence from feldspars. *Radiat Meas* 23:625-632
- Stackebrandt W (2008) Zur Neotektonik der Niederlausitz. *Z Dtsch Gesell Geowiss* 159:117-122
- Steffen H, Kaufmann G, Wu P (2006) Three-dimensional finite-element modeling of the glacial isostatic adjustment in Fennoscandia. *Earth Planet Sci Lett* 250:358-375
- Steffen R, Steffen H, Wu P, Eaton DW (2014) Stress and fault parameters affecting fault slip magnitude and activation time during a glacial cycle. *Tectonics* 33:1461-1476
- Stein S, Liu M, Camelbeeck T, Merino M, Landgraf A, Hintersberger E, Kübler S (2015) Challenges in assessing seismic hazard in intraplate Europe. *Geol Soc Lon Spec Publ* 432:13-28
- Štěpančíková P, Fischer T, Stemberk JJ, Nováková L, Hartvich F, Figueiredo PM (2019) Active tectonics in the Cheb Basin: youngest documented Holocene surface faulting in Central Europe? *Geomorphology* 327:472-488
- Stewart IS, Sauber J, Rose J (2000) Glacio-seismotectonics: ice sheets, crustal deformation and seismicity. *Quat Sci Rev* 19:1367-1389
- Swafford L, Stein S, Mazzotti S (2007) Limitations of the short earthquake record for seismicity and seismic hazard studies. *Spec Pap Geol Soc Am* 425:49-58
- Sykes LR (1978) Intraplate seismicity, reactivation of preexisting zones of weakness, alkaline magmatism, and other tectonism postdating continental fragmentation. *Rev Geophys* 16:621-688
- Talwani P (2014) *Intraplate earthquakes*. Cambridge University Press, New York, pp 338
- Talwani P (2017) On the nature of intraplate earthquakes. *J Seismol* 21:47-68
- Tanner B, Meissner R (1996) Caledonian deformation upon southwest Baltica and its tectonic implications: alternatives and consequences. *Tectonics* 15:803-312
- Tesauro M, Kaban MK, Cloetingh SA, Hardebol NJ, Beekman F (2007) 3D strength and gravity anomalies of the European lithosphere. *Earth Planet Sci Lett* 263:56-73
- TLUBN (2020) Kartendienst Seismologie in Mitteldeutschland. URL: <http://www.tlug-jena.de/erdbeben> (Accessed 1.11.2020)
- Torsvik TH, Cocks LRM (2017) The integration of palaeomagnetism, the geological record and mantle tomography in the location of ancient continents. *Geol Mag* 156:242-260
- Tsukamoto S, Denby PM, Murray AS, Bøtter-Jensen L (2006) Time-resolved luminescence from feldspars: new insight into fading. *Radiat Meas* 41:790-795
- Tsukamoto S, Kondo R, Lauer T, Jain M (2017) Pulsed IRSL: A stable and fast bleaching luminescence signal from feldspar for dating Quaternary sediments. *Quat Geochronol* 41:26-36
- Vandenberghe J (2013) Cryoturbation Structures. In: Elias SA (ed), *The Encyclopedia of Quaternary Science*, 3, Elsevier, Amsterdam, pp 430-435
- Vanneste K, Verbeeck K, Petermans T (2008) Pseudo-3D imaging of a low-slip-rate, active normal fault using shallow geophysical methods: the Geleen fault in the Belgian Maas River valley. *Geophysics* 73:B1-B9
- Van der Pluijm BA, Marshak S (2004) *Earth Structures. An introduction to structural geology and tectonics*, 2 Edition, Norton and Company, New York, p 656
- Van der Wateren FM, Kluiving SJ, Bartek LR (2000) Kinematic indicators of subglacial shearing. In: Maltman AJ, Hubbard B, Hambrey MJ (eds), *Deformation of Glacial Materials*. *Geol Soc London Spec Publ* 176:259-278
- Van Loon AJ (2009) Soft-sediment deformation structures in siliciclastic sediments: an overview. *Geologos* 15:3-55

- Van Loon AJ, Pisarska-Jamroży M (2014) Sedimentological evidence of Pleistocene earthquakes in NW Poland induced by glacio-isostatic rebound. *Sediment Geol* 300:1-10
- Van Wees JD, Arche A, Bejedorff CG, López-Gómez J, Cloetingh SA (1998) Temporal and spatial variations in tectonic subsidence in the Iberian Basin (eastern Spain): inferences from automated forward modelling of high-resolution stratigraphy (Permian–Mesozoic). *Tectonophysics* 300:285-310
- Van Wees JD, Stephenson RA, Ziegler PA, Bayer U, McCann T, Dadlez R, Gaupp R, Narkiewicz F, Scheck M (2000) On the origin of the southern Permian Basin, Central Europe. *Mar Pet Geol* 17:43-59
- Vermilye JM, Scholz CH (1998) The process zone: a microstructural view of fault growth. *J Geophys Res* 103:12223-12237
- Voigt T, Wiese F, von Eynatten H, Franzke H-J, Gaupp R (2006) Facies evolution of syntectonic Upper Cretaceous deposits in the Subhercynian Cretaceous Basin and adjoining areas (Germany). *Z Dtsch Ges Geowiss* 157:203-244
- Voigt T (2009) Die Lausitz-Riesengebirgs-Antiklinalzone als kreidezeitliche Inversionsstruktur: Geologische Hinweise aus den umgebenden Kreidebecken. *Z Geol Wiss* 37:15-39
- Wadas SH, Polom U, Krawczyk CM (2016) High-resolution shear wave seismic reflection as a tool to image near-surface subsidence structures - a case study in Bad Frankenhausen, Germany. *Solid Earth* 7:1491-1508
- Washburn AL (1980) Permafrost features as evidence of climatic change. *Earth Sci Rev* 15:327-402
- Weise W, Uhlemann A, Dalmer K, Credner H (1913) Erläuterungen zur geologischen Spezialkarte des Königreichs Sachsen. Blatt 5439 Treuen-Herlasgrün. 2. Edition, Königliches Finanzministerium, Leipzig, p 58
- Weise OR (1983) Das Periglazial. Geomorphologie und Klima in gletscherfreien, kalten Regionen. Gebrüder Bornstraeger, Berlin Stuttgart, p199
- Wendt S, Mittag R, Forkmann B, Berger H-J, Krentz O, Witthauer B, Eilers H, Neumann E (1996) Seismologische Übersichtskarte des Freistaates Sachsen. 1: 400 000, 1. Edition, Sächsisches Landesamt für Umwelt und Geologie, Freiberg
- Wibberley CA, Yielding G, Di Toro G (2008) Recent advances in the understanding of fault zone internal structure: a review. *Geol Soc London Spec Publ* 299:5-33
- Winsemann J, Hornung JJ, Meinsen J, Asprien U, Polom U, Brandes C, Bußmann M, Weber C (2009) Anatomy of a subaqueous ice-contact fan and delta complex, Middle Pleistocene, north-west Germany. *Sedimentology* 56:1041-1076
- Winsemann J, Brandes C, Polom U, Weber C (2011) Depositional architecture and deformation pattern of Middle Pleistocene ice marginal deposits in north-western Germany: a synoptic overview. *E & G - Quat Sci J* 60:212-235
- Winsemann J, Koopmann H, Tanner DC, Lutz R, Lang J, Brandes C, Gaedicke C (2020) Seismic interpretation and structural restoration of the Heligoland glaciotectionic thrust-fault complex: implications for multiple deformation during (pre-) Elsterian to Warthian ice advances into the southern North Sea Basin. *Quat Sci Rev* 227:106068
- Wintle AG (1973) Anomalous fading of thermo-luminescence in mineral samples. *Nature* 245:143-144
- Wrede V (1988) Der nördliche Harzrand - flache Abscherbahn oder wrench-fault-system. *Geol Rundsch* 77:101-107
- Wrede V (2008) Nördliche Harzrandstörung: Diskussionsbeiträge zu Tiefenstruktur, Zeitlichkeit und Kinematik. *ZDGG* 159:293-316
- Wright JD (2001) Paleo-oceanography: Cenozoic Climate – Oxygen Isotope Evidence. In: Steele J, Thorpe S, Turekian K (eds), *Encyclopedia of Ocean Sciences*, Academic Press, pp 415-426
- Wu P (2004) Using commercial finite element packages for the study of earth deformations, sea levels and the state of stress. *Geophys J Int* 158:401-408
- Wu P, Wang H, Steffen H (2013) The role of thermal effect on mantle seismic anomalies under Laurentia and Fennoscandia from observations of Glacial Isostatic Adjustment. *Geophys J Int* 192:7-17

- Yilmaz O (1987) Seismic Data Processing: Society of Exploration Geophysicists, Tulsa, Oklahoma 2:82-153
- Zhao S, Lambeck K, Lidberg M (2012) Lithosphere thickness and mantle viscosity inverted from GPS-derived deformation rates in Fennoscandia. *Geophys J Int* 190:278-292
- Ziegler PA (1990) Geological Atlas of the Western and Central Europe, 2 Edition. Shell International PetroleumMaatschappij B. V. the Hague, pp 239
- Ziegler PA, Dèzes P (2006) Crustal evolution of western and central Europe. *Geol Soc Lon Mem* 32:43-56
- Zimmermann E, Liebe KT (1930) Erläuterungen zur geologischen Karte von Preußen und benachbarten deutschen Ländern. Blatt 5138 Gera. 3 Edition, Preußisch geologische Landesanstalt, Berlin, p 80

## 5. Overview of this thesis – Publications and their content

The results of this study are subdivided into four publications, which have been submitted to international, peer-reviewed journals and a peer-reviewed book.

### Publication 1:

#### **Structural style and neotectonic activity along the Harz Boundary Fault, northern Germany: A multimethod approach integrating geophysics, outcrop data and numerical simulations**

by Katharina Müller, Ulrich Polom, Jutta Winsemann, Holger Steffen, Sumiko Tsukamoto, Thomas Günther, Jan Igel, Thomas Spies, Thomas Lege, Manfred Frechen, Hans-Joachim Franzke and Christian Brandes, published in *International Journal of Earth Sciences*, (2020), 109, 1811-1835.

This publication focuses on the Harz Boundary Fault, which is a key structure in northern Germany that is classified as a GIF. New evidence for neotectonic activity along the Harz Boundary Fault is presented and the structural style of the fault is discussed. For the fault analysis a multimethod approach was used, integrating outcrop data, luminescence dating, shear-wave seismic surveys, ERT profiles and numerical simulations. A recent sinkhole at the Harz Boundary Fault exposes a planar fault surface that cuts through unconsolidated debris-flow deposits. The outcrop data in combination with the seismic data give evidence for a splay fault system with steep back-thrusts. The lateral extent of the fault was mapped with ERT profiles. The timing of fault movement was estimated by means of optically stimulated luminescence dating of the faulted debris-flow deposits using both quartz and feldspar minerals. Numerical simulations of GIA-related changes in the Coulomb failure stress regime at the Harz Boundary Fault underpin the assumption that the fault was reactivated during the Lateglacial due to stress changes induced by the decay of the Late Pleistocene (Weichselian) Fennoscandian ice sheet.

*Own contributions: Fieldwork, geophysical measurement assistance, luminescence dating, interpretation of data, manuscript preparation, figure preparation*

### Publication 2:

#### **Glacially-induced faults in Germany**

by Katharina Müller, Jutta Winsemann, David C. Tanner, Thomas Lege, Thomas Spies and Christian Brandes published in Steffen H, Olesen, O and Sutinen R (eds), *Glacially-Triggered Faulting*, Cambridge University Press (2021).

This publication gives an overview of evidence of neotectonic fault activity in northern Germany and draws a connection to lithospheric stress field changes induced by the decay of the Fennoscandian ice sheet. This article presents major faults in northern Germany that show evidence of neotectonic activity. The timing of fault movements implies that the seismicity in northern Germany is most likely induced by varying lithospheric stress conditions related to GIA and some faults can be thus classified as GIFs. Along the Aller Fault, the Halle Fault, the Harz

Boundary Fault, the Steinhuder Meer Fault and the Osning Thrust evidence of neotectonic fault activity was observed. All these faults are oriented parallel to the margin of the former Pleistocene ice sheets. For the Osning Thrust and the Harz Boundary Fault, this is supported by numerical simulations of GIA related stress field changes. GIA processes are also a likely driver for the historic and parts of the recent fault activity.

*Own contributions: Fieldwork, interpretation of data, manuscript preparation, figure preparation*

### **Publication 3:**

#### **The challenge to distinguish soft-sediment deformation structures (SSDS) formed by glaciotectonic, periglacial and seismic processes in a formerly glaciated area: a review and synthesis**

by Katharina Müller, Jutta Winsemann, Małgorzata Pisarska-Jamroży, Thomas Lege, Thomas Spies and Christian Brandes, published in Steffen H, Olesen O and Sutinen R (eds), *Glacially-Triggered Faulting*, Cambridge University Press (2021).

This publication forms the basis for the palaeoseismological analyses in northern and central Germany. This article reviews the use of SSDS as palaeo-earthquake indicators in formerly glaciated and periglacial areas, like northern and central Germany. In regions that were affected by glaciations and periglacial processes, the use of SSDS as palaeo-earthquake indicators is challenging and the interpretation must be done with care. Earthquakes are only one trigger mechanism of many that can cause liquefaction and/or fluidization of sediments, which leads to the formation of sand volcanoes, clastic dykes, flame structures, load structures or ball-and-pillow structures. Criteria for seismically triggered SSDS are outlined. The use of deformation bands that occur in the vicinity of basement faults in combination with SSDS is a certain indicator for palaeo-earthquakes.

*Own contributions: Evaluation and synthesis of literature, manuscript preparation, figure preparation*

### **Publication 4:**

#### **Re-examination and neotectonic analysis of the N-S trending Regensburg-Leipzig-Rostock fault system between Leipzig and Cheb**

by Katharina Müller, Jutta Winsemann, Diethelm Kaiser, Thomas Spies, Thomas Lege, Christian Brandes, submitted to *International Journal of Earth Sciences*.

This manuscript shows the importance of NW-SE oriented faults and fault intersections and demonstrates that indicators of neotectonic fault activity are rare and difficult to observe also in seismically active areas. The focus is placed on the seismically active RLR fault system with its significant seismicity in a N-S trending zone between the cities of Leipzig and Cheb. A key aspect is that this fault system is far from being understood. In this study, new evidence for neotectonic fault activity between Leipzig and Cheb is presented. The palaeoseismological analysis is based



on fieldwork data collected in outcrops composed of Cenozoic deposits, DEM lineament analysis, intensive literature research, which is combined with earthquake datasets and fault maps. At five locations, evidence for post-Palaeogene fault activity is indicated by the formation of deformation bands implying that faults in this area are active at least since the Palaeogene. The deformation bands developed at intersecting faults. This matches with the hypothesis that fault intersections act as stress concentrators, where seismic activity concentrates. Potential trigger mechanisms for fault re-activation, such as GIA and the formation and drainage of large Pleistocene ice-dammed lakes and whether the RLR fault system is a deep-seated active shear zone are discussed.

*Own contributions: Fieldwork, evaluation and synthesis of literature, DEM analysis, interpretation of data, manuscript preparation, figure preparation*

## Publication 1

This chapter has been published as Müller et al. 2020,  
International Journal of Earth Sciences, 109, 1811-1835.  
[doi.org/10.1007/s00531-020-01874-0](https://doi.org/10.1007/s00531-020-01874-0)

### **Structural style and neotectonic activity along the Harz Boundary Fault, northern Germany: A multimethod approach integrating geophysics, outcrop data and numerical simulations**

Katharina Müller<sup>1</sup>, Ulrich Polom<sup>2</sup>, Jutta Winsemann<sup>1</sup>, Holger Steffen<sup>3</sup>, Sumiko Tsukamoto<sup>2</sup>, Thomas Günther<sup>2</sup>, Jan Igel<sup>2</sup>, Thomas Spies<sup>4</sup>, Thomas Lege<sup>4</sup>, Manfred Frechen<sup>2</sup>, Hans-Joachim Franzke<sup>5</sup> and Christian Brandes<sup>1</sup>

<sup>1</sup>Institut für Geologie, Leibniz Universität Hannover, Callinstraße 30, 30167 Hannover, Germany

<sup>2</sup>Leibniz Institute for Applied Geophysics (LIAG), Stilleweg 2, 30655 Hannover, Germany

<sup>3</sup>Lantmäteriet, Geodetic Infrastructure Referenssystem, Lantmäterivägen 2C, 80102 Gävle, Sweden

<sup>4</sup>Bundesanstalt für Geowissenschaften und Rohstoffe (BGR), Stilleweg 2, 30655 Hannover, Germany

<sup>5</sup>Institut für Geologie und Paläontologie der Technischen Universität Clausthal, Leibnizstraße 10, 38678 Clausthal-Zellerfeld, Germany

Corresponding Author: Katharina Müller, Institut für Geologie, Leibniz Universität Hannover, Callinstraße 30, 30167 Hannover, Germany

Email: [mueller@geowi.uni-hannover.de](mailto:mueller@geowi.uni-hannover.de)

## Abstract

We present new evidence for neotectonic activity along the Harz Boundary Fault, a Cretaceous reverse fault that represents a key structure in northern Germany. For the fault analysis we use a multimethod approach, integrating outcrop data, luminescence dating, shear wave seismics, electrical resistivity tomography (ERT) and numerical simulations.

A recent sinkhole at the SSW-ward dipping and WNW - ESE striking Harz Boundary Fault exposes a NNE-ward dipping and WNW - ESE striking planar fault surface that cuts through unconsolidated debris-flow deposits thus pointing to young Lateglacial tectonic activity. The fault shows a polyphase evolution with initial normal fault movement and a later reactivation as an oblique fault with reverse and strike-slip components. Shear wave seismic profiles were acquired to analyse the geometry of the fault and show that the Harz Boundary Fault is steeply-dipping and likely has branches. Partly, these branches propagate into overlying alluvial-fan deposits that are probably Pleniglacial to Lateglacial in age. The outcrop data in combination with the seismic data give evidence for a splay fault system with steep back-thrusts. One of these back-thrusts is most likely the NNE-ward dipping fault that is exposed in the sinkhole. The lateral extent of the fault was mapped with electrical resistivity tomography (ERT) profiles. The timing of fault movement was estimated based on optically stimulated luminescence dating of the faulted debris-flow deposits using both quartz and feldspar minerals. Consistent feldspar and quartz ages indicate a good bleaching of the sediment prior to deposition. The results imply fault movements post-dating ~15 ka. Numerical simulations of GIA-related changes in the Coulomb failure stress regime at the Harz Boundary Fault underpin the assumption that the fault was reactivated during the Lateglacial due to stress changes induced by the decay of the Late Pleistocene (Weichselian) Fennoscandian ice sheet.

**Keywords:** Harz Boundary Fault, neotectonics, northern Germany, glacial isostatic adjustment (GIA), electrical resistivity tomography (ERT), shear wave seismics, luminescence dating, numerical simulations, Lateglacial

## Introduction

The analysis of the neotectonic activity of northern Germany is challenging because fault scarps that could point to past seismic events are rarely developed due to the low slip rates and climate conditions (Kaiser 2005). In general, this region is commonly regarded as a low seismicity area (Leydecker and Kopera 1999). However, there is evidence for several seismic events during the last 1200 years (Leydecker 2011). In addition, the palaeoseismological studies that were carried out in northern Germany (e.g., Hübscher et al. 2004; Brandes and Tanner 2012; Hoffmann and Reicherter 2012; Brandes et al. 2011, 2012b; Brandes and Winsemann 2013; Brandes et al. 2018a; Pisarska-Jamroży et al. 2018, 2019; Grube 2019a, b) also point to a higher seismic activity than previously thought. Al Hseinat and Hübscher (2017) recently found faults in the Baltic Sea, which dissect Pleistocene deposits and therefore point to young tectonic activity. This questions the status of a low seismicity area and its earthquake hazard. For a profound seismic hazard assessment, it is thus necessary to re-evaluate the past seismic activity and tectonic movements as well as the probability of earthquakes in northern Germany.

Collisional forces from the Alpine orogeny and the Atlantic ridge push affect the stress field in northern Germany (Marotta et al. 2001, 2002, 2004; Kaiser et al. 2005). Evidence for active faults in northern Germany is rare but recent tectonic earthquakes were recorded e.g., east of Hamburg in 2000 (magnitude of  $M_w$  3.1; Bock et al. 2002) and in the Leipzig/Halle area in 2015 and 2017 (magnitude of  $M_w$  3.2 and 2.8; Dahm et al. 2018). Many of the historic earthquakes concentrate along major Cretaceous reverse faults and were possibly triggered by lithospheric stress changes due to glacial isostatic adjustment (Brandes et al. 2015). The approximately 90 km long Harz Boundary Fault (Fig. 1) is one of these Cretaceous reverse faults and represents a key structure in northern Germany. There is a controversial discussion about the nature of the Harz Boundary Fault. Two different interpretations co-exist, a wrench fault system and a frontal thrust model (Wrede 1988, 2008, 2009 and Voigt et al. 2009). The frontal thrust model is meanwhile well supported by field evidence from investigations along the Harz Boundary Fault (Flick 1986; Franzke et al. 1995; Kley et al. 2008). More recently, Paul (2019) discussed the role of dissolution and migration of Zechstein salt for basin-wide subsidence and uplift in the Harz foreland area and the Harz Mountains.

The aim of this study is to visualize the structural style of the fault zone at the northern Harz Boundary with shear wave seismic and electrical resistivity tomography (ERT) profiles and to analyse the neotectonic activity of the fault. Tectonic evidence of young fault movements along the Harz Boundary Fault were already published by Franzke et al. (2015). The study benefits from a recent sinkhole at the Harz Boundary Fault, which exposes a NNE-ward dipping and WNW - ESE striking planar fault plane with several slip surfaces that cuts through unconsolidated debris-flow deposits (Franzke et al. 2015). In this study we use an expanded dataset. We image the faults in a shear wave seismic profile and mapped the lateral extent of the fault in the sinkhole using electrical resistivity tomography (ERT) profiles. We estimate the timing of fault activity by means of luminescence dating of faulted periglacial debris-flow deposits and use numerical simulations of glacial isostatic adjustment (GIA)-related changes of Coulomb failure stress to support the estimated ages.

## **Geological setting**

The study area is located in northern Germany and belongs to the Subhercynian Basin, which lies directly north of the Harz Mountains and forms a subbasin of the Central European Basin System (CEBS) (Fig. 1a, b). The geological evolution of northern Germany is characterised by different tectonic processes (Lohr et al. 2007; Kley et al. 2008). In Permian and Triassic times E-W transtension/extension took place, which was followed by NNE-SSW extension in the Jurassic to Early Cretaceous. The Late Cretaceous is characterised by an NE-SW to NNE-SSW compression. The Late Cretaceous contraction lasted into the Palaeogene (Lohr et al. 2007). This led to crustal shortening in the study area and as a result, local thrust-related basement uplifts such as the Flechtingen High and the Harz Mountains formed. In addition, a widespread reactivation of faults occurred. This tectonic inversion phase was discussed in detail by Baldschuhn et al. (1991), Kockel (2003), Kley and Voigt (2008) and Kley et al. (2008).

### **The Harz Boundary Fault and the Subhercynian Basin**

A key element of the Late Cretaceous inversion phase and intraplate deformation in northern Germany is the Harz Boundary Fault that separates the Palaeozoic rocks of the Harz Mountains from the Mesozoic sedimentary rocks of the Subhercynian Basin (von Eynatten et al. 2008; Voigt et al. 2008) (Fig. 1c). Modelling results of Kaiser et al. (2005) predict a modern fault slip rate of 0.08 mm/yr for the Harz Boundary Fault. The Subhercynian Basin trends WNW-ESE and is approximately 100 km long and 50 km wide. It is bounded to the SSW by the Harz Boundary Fault and to the NNE by the Flechtingen basement high (Stackebrandt 1986). The basin has a twofold evolution that started with extensional movements in the early Permian. Extension prevailed throughout the Mesozoic. In Late Cretaceous times, the Subhercynian Basin was transformed into a kind of foreland basin controlled by the overthrusting of the Harz basement block (Franzke et al. 2004; Voigt et al. 2006; Kley et al. 2008; Brandes et al. 2013).

### ***Pleistocene deposits***

During the Pleistocene, northern Germany was influenced by three major ice advances referred to as the Elsterian, Saalian and Weichselian glaciations. The Harz foreland was affected by the Elsterian and Saalian glaciations (Fig. 1a; Reinecke 2006; Ehlers et al. 2011; Lang et al. 2018, 2019). The Elsterian ice advances probably reached the study area during Marine Isotope Stages MIS 12 and 10 (Roskosch et al. 2015), leaving meltwater sediments and two Elsterian tills (Feldmann 2002; Elsner 2003; Lang et al. 2012). Subsequently fluvial sediments were deposited (Weymann et al. 2005; Reinecke 2006). These fluvial deposits are covered by Saalian glacial sediments (Weymann et al. 2005), which are probably MIS 6 in age (Litt et al. 2007; Lang et al. 2018, 2019). During the Late Pleistocene Weichselian glaciation, the ice sheets did not cross the Elbe River (Ehlers et al. 2011) and periglacial conditions prevailed in northwestern and central Germany (Reinecke 2006; Kasse et al. 2007; Litt et al. 2007; Meinsen et al. 2014; Lehmkuhl et al. 2016).

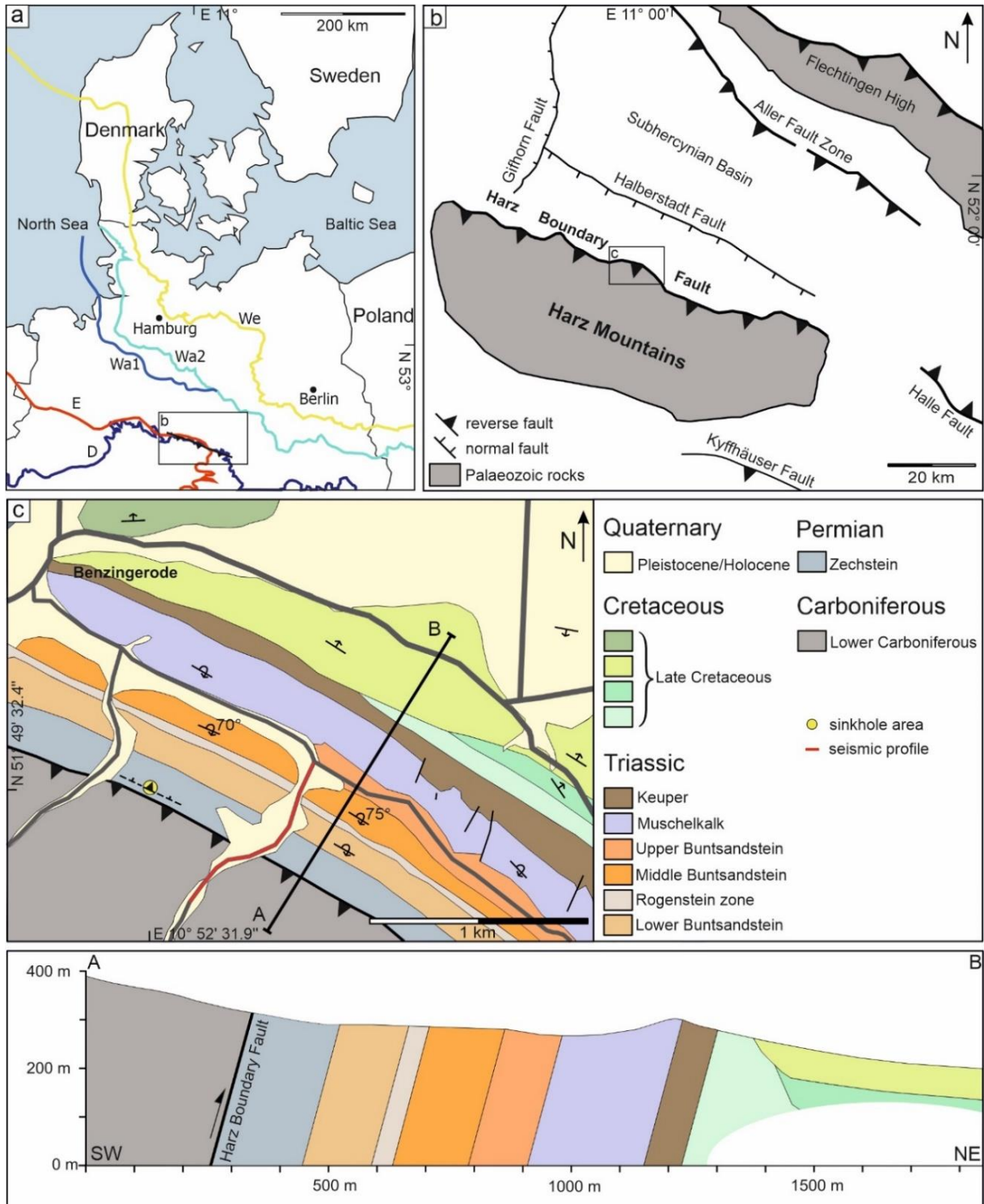


Figure 1: Location of the study area in northern Germany; a) Maximum extents of the Elsterian (E), Saalian (D: Drenthe; Wa1: Warthe 1 and Wa2: Warthe 2) and Weichselian (We) ice sheets are shown in red, light- and dark-blue and yellow (modified after Ehlers et al. 2011; Roskosch et al. 2015; Lang et al. 2018; Winsemann et al. 2020); b) Close-up view of the study area showing major fault systems; c) Geological map of the study area with geological cross-section (modified after Schröder et al. 1927).

Periglacial Late Pleniglacial to Lateglacial deposits in the study area consist of alluvial, mass-flow and aeolian deposits (Fig. 2) (Bode et al. 2003; Weymann et al. 2004; Reinecke 2006; Litt and Wansa 2008; Krauß et al. 2016; Lehmkuhl et al. 2016). On hillslopes different mass-flow deposits



accumulated that are commonly referred to as periglacial cover beds ('periglaziale Deckschichten'; Reinecke 2006; Litt and Wansa 2008). These periglacial mass-flow deposits are generally subdivided into three main depositional units referred to as basal layer ('Basislage'), middle layer ('Mittellage') and main layer ('Hauptlage') (Reinecke 2006; Litt and Wansa 2008; Bullmann 2010). The basal layer directly overlies bedrock and is commonly characterised by a high clast content. The middle layer is partly rich in reworked loess. The main layer forms the top of these periglacial mass-flow deposits and may contain Laacher See tephra. The main layer is partly overlain by loess (Fig. 2). However, not all depositional units are always present. In general, the age of these mass-flow deposits is poorly constrained and based on an uncertain correlation with dated deposits of the Harz foreland area (Fig. 2; Reinecke 2006; Litt and Wansa 2008; Bullmann 2010). The main layer probably formed during the younger Dryas, as indicated by the presence of reworked Laacher See tephra (Reinecke 2006; Bullmann 2010), which is a marker horizon for the late Allerød (van den Bogaard 1995; Reinecke 2006). During the Holocene, a stabilizing vegetation cover rapidly formed on hillslopes (Litt et al. 2007), preventing further mass-flow events.

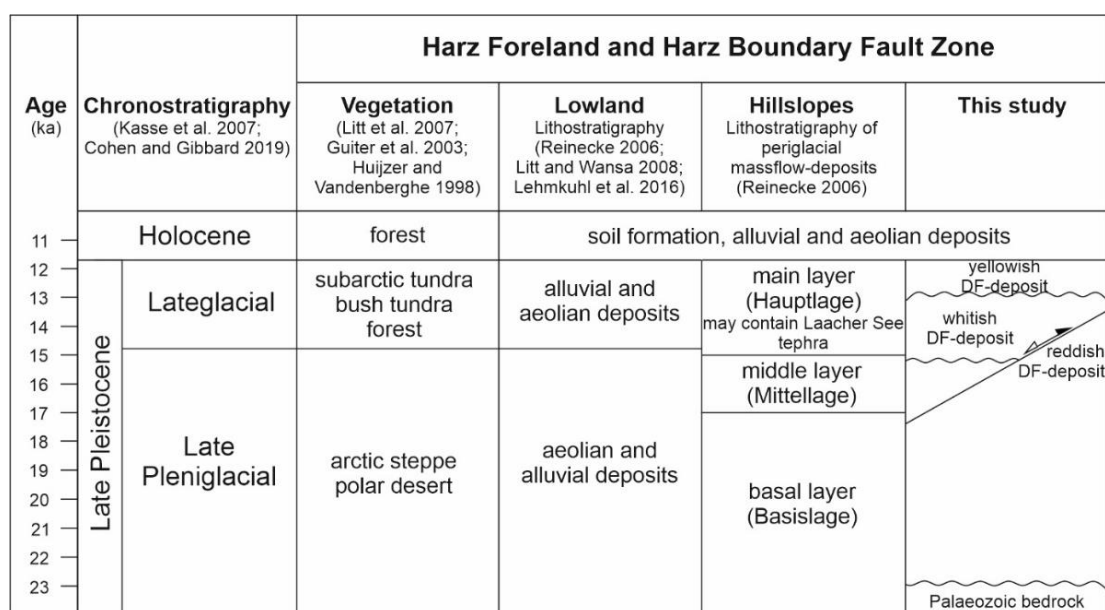


Figure 2: Stratigraphy of Late Pleistocene periglacial deposits. DF= Debris flow.

### Sinkholes

At the southern margin of the Subhercynian Basin, north of the Harz Boundary Fault, several sinkholes occur due to dissolution processes in the steeply-dipping sulphate rocks that belong to the Zechstein Werra sequence (Schröder and Dahlgrün 1927; Franzke et al. 2015). Approximately 30 m north of the Harz Boundary Fault a recent sinkhole (likely developed around the year 2013) (N51°49'32.4"E10°52'31.9"), exposes a NNE-ward dipping and WNW - ESE striking planar fault plane with several slip surfaces (Figs. 1c, 3). This fault displaces two debris-flow deposits that differ in colour and composition (Fig. 3). The fault tip is sealed by a younger thin debris-flow deposit.

## Methods

This study is based on outcrop data, electrical resistivity tomography (ERT) profiles, a high-resolution shear wave seismic profile, luminescence dating, and numerical simulations. Field work included sedimentological and structural analyses of outcrops and sampling for luminescence dating (Fig. 3a). The luminescence dating was performed at the Leibniz Institute for Applied Geophysics (LIAG).

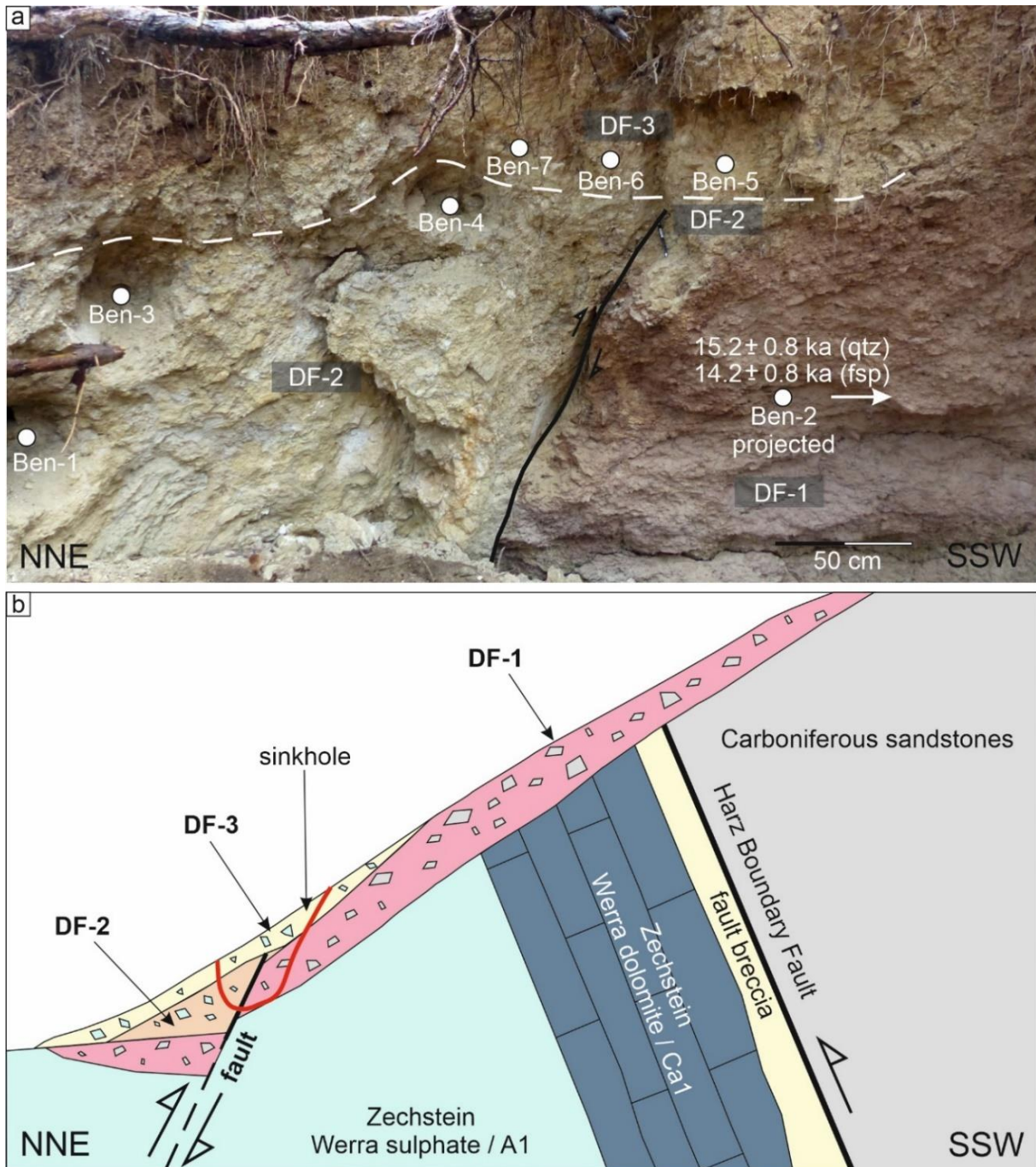


Figure 3: Sinkhole above the Zechstein Werra-evaporites; a) Fault surface in Lateglacial debris-flow deposits and location of OSL samples; b) Schematic profile of the Harz Boundary Fault zone near Benzingerode with the location of the sinkhole (based on Franzke et al. 2015).

## Electrical resistivity tomography (ERT)

Four electrical resistivity tomography (ERT) profiles were acquired to map the lateral extent of the NNE-dipping fault exposed in the sinkhole. The ERT method is very suitable to detect near-surface faults (e.g., Caputo et al. 2003; Vanneste 2008; Gélis et al. 2010).

The profiles are 40 m (profile 1) and 30 m (profiles 2, 3, 4) long and trend  $\sim$  NE-SW, perpendicular to the Harz Boundary Fault and to the fault in the sinkhole (Fig. 4). Profiles 1 to 3 were measured NW of the sinkhole. Profile 4 was measured SE of the sinkhole (Fig. 4). Electrodes were spaced at a distance of 0.5 m to resolve small and shallow structures. GPS positions of the electrodes were acquired using a total station and provided accurate elevations for the inversion process that reconstructs the subsurface resistivity. To incorporate the rough topography, we used the finite-element method with an irregular triangle mesh implemented in the software BERT (Günther et al. 2006).

For the ERT measurements, we applied the dipole-dipole array that provides the best resolution and the Wenner array for deep penetration. We combined several base dipole lengths ( $a=1, 2, 4$  and  $8$ ) and dipole separations of  $n=1$  through  $6$ . The resulting high-quality data could be fitted with root-mean-square errors between 2 and 4%.

Samples were taken from debris-flow DF-1 and DF-2 to measure their resistivities in the laboratory. The sediments were inserted in a sample holder and measured under different water saturations using a 4 point light 10 W Lippmann device.

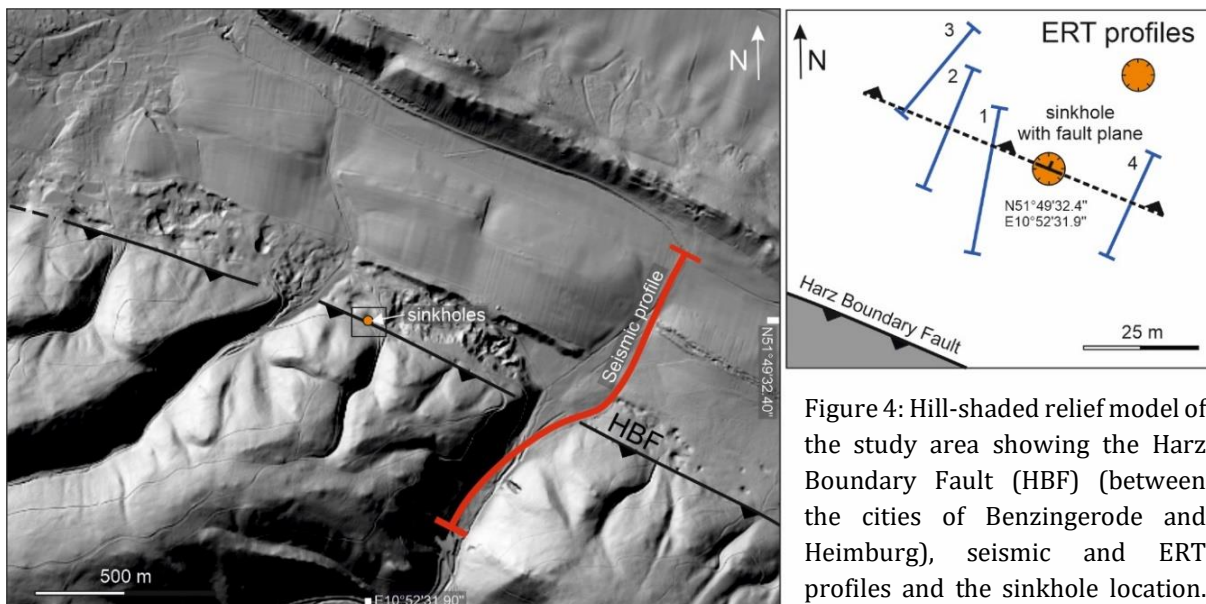


Figure 4: Hill-shaded relief model of the study area showing the Harz Boundary Fault (HBF) (between the cities of Benzingerode and Heimbürg), seismic and ERT profiles and the sinkhole location. The DEM is based on data from the

Landesamt für Vermessung und Geoinformation Sachsen-Anhalt (GeoBasis-DE / LVerGeo LSA, 2016) (1 m grid, vertical resolution:  $\pm 0.2$  m).

## Shear wave seismics

One shear wave seismic reflection profile was acquired to analyse the shallow subsurface structure of the Harz Boundary Fault zone in high-resolution. The profile is approximately 1 km

long and oriented perpendicular to the Harz Boundary Fault (Figs. 1c, 4). The shear wave vibroseis method (Crawford et al. 1960; Ghose et al. 1996; Polom et al. 2013), using a linear frequency modulated seismic source signal of 20–160 Hz over 10 s duration, was applied. For a fast data acquisition in high-resolution, a land streamer unit with 120 transverse horizontal (SH) geophones (10 Hz resonance frequency) at 1 m interval and an electrodynamic-driven SH shaker source system was used (Polom et al. 2011). The achieved maximum target depth of the SH-waves is nearly 70 m. The recording configuration was a so-called asymmetric varying split-spread set-up. Two sweeps with alternating polarity were initiated at each source location.

In contrast to the commonly used compression waves (P-waves) of exploration seismics, shear waves only propagate in solid material. Shear waves cannot propagate in liquids or gases of the pore space, where the shear modulus is zero. Therefore, e.g., the groundwater level does not affect the shear wave propagation, resulting in significantly lower velocities and an improved resolution compared to P-waves. On the other hand, as result of the low velocities, the penetration depth is significantly lower compared to P-waves.

The acquired seismic data underwent a standard processing procedure by using the VISTA software (version 10.028, Schlumberger). During the processing, first a quality assessment, a geometry fitting and a vibroseis correlation were carried out. The next steps of the processing procedure were the vertical stacking of records, an automatic gain control for amplitude scaling and the application of band pass and frequency-wavenumber (FK) filters. Afterwards interactive velocity analysis, common mid-point (CMP) stacking, and a finite-difference (FD) time migration were applied. The last step of the processing was the time-to-depth conversion using a data-driven 2D velocity function.

## **Sampling**

Seven samples were taken from the faulted sediments, which are exposed in the sinkhole (N51°49'32.4" E10°52'31.9"), close to the Harz Boundary Fault (Figs. 1c, 3). In general, debris-flow deposits are difficult to date (e.g., Döhler et al. 2018), especially carbonate-rich debris-flows that are poor in quartz and feldspar minerals. Therefore, as many samples as necessary were taken to obtain a good coverage of the debris-flow deposits.

One sample (Ben-2) was taken from the basal reddish debris-flow (DF-1) in the footwall south of the exposed fault trace. Three more samples (Ben-1, Ben-3, Ben-4) are derived from the hanging-wall block north of the fault surface (lower whitish debris-flow deposit; DF-2). Three further samples (Ben-5, Ben-6, Ben-7) were taken from the yellowish debris-flow (DF-3) that seals the fault tip (Fig. 3a). The sample material of Ben-1 was too poor for luminescence dating because not enough material of the required grain-size was obtained during sample preparation.

During the sampling procedure opaque metal tubes with a length of 10 cm and a diameter of 5 cm were hammered into the freshly cleaned sediment surface and closed with aluminium foil to avoid light exposure. Additionally, samples (700 g) for dose rate determination were taken from the surrounding sediment at each sample position.

## Luminescence dating

For age determination of the fault movements, we performed luminescence dating on fine-grained (4-11  $\mu\text{m}$ ) quartz minerals and polymineralic material for feldspar measurements. Additional technical information about the method is given in the supplementary files.

## Numerical simulations

To analyse the glacially-induced fault reactivation potential, numerical simulations were carried out in form of three-dimensional (3D) finite-element (FE) simulations that describe the process of GIA together with Coulomb failure stress (CFS) calculations. Input parameters to a GIA model are generally (i) the Earth's structure and rheology in the subsurface down to the core-mantle boundary and (ii) the ice load history of the last glaciation. Our models are based on the flat-Earth approach described by Wu (2004), Steffen et al. (2006) and Brandes et al. (2018b). The FE software ABAQUS (ABAQUS 2018) is applied to create a 3D earth model with a size of 60,000 km  $\times$  60,000 km (horizontally)  $\times$  2891 km (depth to core-mantle boundary). A centre block of 4500 km  $\times$  4500 km  $\times$  2891 km size represents our study area, the lithosphere and mantle of Fennoscandia, while the frame allows mantle material to flow outside this area minimizing any associated numerical errors (Steffen et al. 2006). The element mesh in the centre has 50 km horizontal side length, while the frame has increasing side lengths from the centre to the edge to save run time and memory. In the vertical the model is subdivided in 18 layers of different thickness, whereas (model-dependent) 8 or 9 element layers build up the elastically behaving lithosphere. Here, the first 6 layers have 5 km thickness each for a more detailed analysis of the stress changes in the upper lithosphere. The visco-elastically behaving upper mantle down to 670 km has 4 or 5 element layers, and the lower mantle down to 2891 km depth 5 element layers. The Preliminary Reference Earth Model (PREM; Dziewonski and Anderson 1981) is applied to assign layer-dependent and volume-averaged values for density, shear modulus and Young's modulus. For further details, we refer the reader to Brandes et al. (2018b). Rigid boundary conditions fix the sides of the model. An ice history model is applied as ice thickness variations over the last two glacial cycles on the element surfaces of the earth model centre.

The setups of the ice and earth model partly affect the results. To show the spread of possible results that may lead to a range of uncertainties of the modelling, we test a variety of Earth and ice model combinations that are based on results of previous GIA studies, which represent the GIA process in Fennoscandia reasonably well.

The timing of possible fault reactivation depends on the Earth model composition according to previous studies (Brandes et al. 2012b, 2015, 2018b; Steffen et al. 2014b). Two types of models, with and without a laterally homogeneous structure, are used for numerical simulation. Laterally homogeneous models (i.e., they vary only with depth) are commonly used in GIA modelling. The basic model with laterally homogeneous structure has a lithospheric thickness of 90 km, an upper mantle viscosity of  $5 \times 10^{20}$  Pa s and a lower mantle viscosity of  $2 \times 10^{21}$  Pa s, but we additionally tested models that vary in one of these 3 parameters. Hence, we analysed 4 laterally homogeneous models. We also applied 140 km lithospheric thickness,  $8 \times 10^{20}$  Pa s upper mantle viscosity and  $2 \times 10^{22}$  Pa s lower mantle viscosity. All values represent viable estimates based on GIA studies of Fennoscandia (Lambeck et al. 2010; Zhao et al. 2012; Kierulf et al. 2014). Although these laterally homogeneous models can explain the GIA process in Fennoscandia well, they are not



supported by seismic results that point to lateral variations in the deep subsurface. We thus additionally tested two models with a laterally heterogeneous structure. The models vary in lithospheric thickness (90 and 140 km) and use a three-dimensional (3D) mantle viscosity structure, which is converted from the seismic tomography model by Grand et al. (1997) based on the method in Wu et al. (2013). For the ice load history part, two different ice history models were used that are available to us and that are commonly applied in GIA studies. The first is the North-European part of the global ice model ICE-6G\_C (Argus et al. 2014; Peltier et al. 2015) while the other is a combination of the so-called ANU-ICE history models for the British Isles (Lambeck 1995) and Fennoscandia (Lambeck et al. 2010).

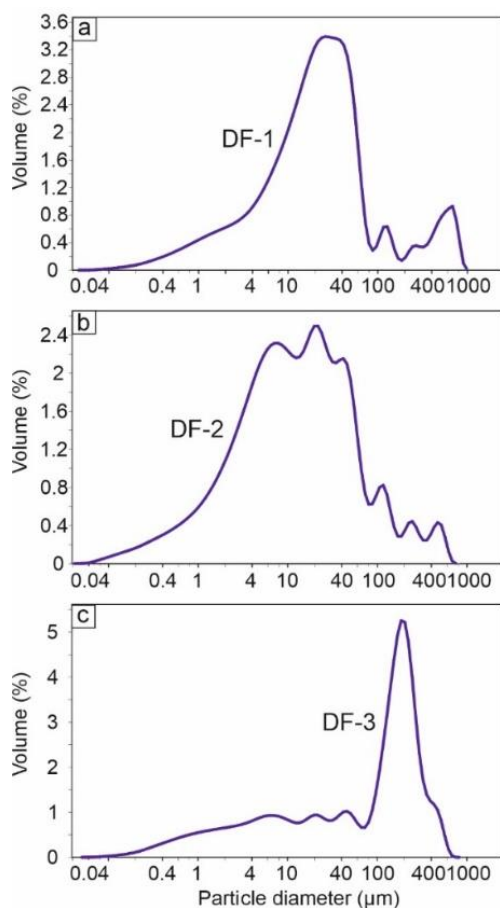
For each model combination we calculate deformation and stress changes due to GIA with the FE software following the procedure outlined in Wu (2004). Then we combine the GIA-induced stress changes with overburden and tectonic background stress to calculate the change in CFS ( $\delta\text{CFS}$ ) for the location of our study area. We test a compressional (thrust/reverse) stress regime for all GIA models. The CFS can be regarded as the simplest form of indication of possible reactivation of a fault as it represents the minimum stress required to reach faulting. Steffen et al. (2014a) found that the crust was critically stressed before glaciation which means that the CFS was about 0 MPa at that time. Hence, the  $\delta\text{CFS}$ , which is calculated relative to the CFS before glaciation, shows that a fault is stable when  $\delta\text{CFS}$  is negative, while positive values indicate fault instability and potential fault movements. A  $\delta\text{CFS}$  value of 0 MPa (a zero line) thus represents the threshold that separates zones of instability ( $>0$  MPa) and stability ( $<0$  MPa). We apply a CFS of 0 MPa before glaciation and optimally oriented faults, i.e., their strike and dip values promote faulting for a commonly used friction coefficient of 0.6. For a compressional stress regime, strike values are thus perpendicular to the maximum horizontal direction of the chosen tectonic background stress, while the corresponding optimal fault dip is approximately 30 degrees, respectively. We note that the Harz Boundary Fault strikes about WNW-ESE, which is almost in line with the maximum horizontal principal stress that is suggested from the World Stress Map (Heidbach et al. 2016). Therefore, the fault cannot be initially considered as optimally oriented for the tectonic background regime. However, GIA stresses can overprint tectonic stress fields and lead to rotation of principal stress directions (Wu 1997) so that a fault orientation close to optimal is possible. This is especially the case for small differences in the horizontal components of the principal stresses (Wu 1997) and thus important to consider for faults near the surface since GIA generates additional stresses of some 10 MPa (Wu 1997) contributing here largely to the overall stress budget.

Non-optimally oriented faults could also be activated under certain conditions. This is not part of this investigation, i.e., as this involves testing a large set of parameter combinations (strike and dip of the fault, depth, principal stress directions and their stress differences, friction parameter, pore fluid factor) and is thus left for future studies. We investigate the  $\delta\text{CFS}$  at a depth of 12.5 km for a thrust fault regime.

## Results

### Sedimentology

The sinkhole, in which the fault is exposed, formed in the steeply-dipping Zechstein Werra-sulphates that belongs to the Zechstein Z1 sequence (Schröder et al. 1927; Franzke et al. 2015), approximately 30 m north (Figs. 1c, 4) of the Harz Boundary Fault. The position of the Harz Boundary Fault is taken from the geological map (scale 1:25 000) (Schröder et al. 1927).



According to Schröder and Dahlgrün (1927) the position of the Zechstein rocks can be determined with high accuracy and are almost overlain by debris-flow deposits in this area. The sinkhole has a depth of 2 m and a diameter of 3 m and exposes three different debris-flow deposits (Fig. 3a), which differ in colour, matrix and clast composition (Fig. 5a-c). The basal debris-flow deposit (DF-1) has a reddish silty matrix (Fig. 5a) and contains 60-70% angular greywacke clasts. This reddish debris-flow deposit is overlain by a whitish debris-flow deposit (DF-2) that contains 80% angular Zechstein clasts, embedded in a silty carbonaceous matrix (Fig. 5b). These two debris-flow deposits are displaced by the fault and are overlain by a yellowish debris-flow deposit (DF-3) that is ~30 cm thick and seals the fault. This uppermost debris-flow deposit has a silty to fine-grained sandy carbonaceous matrix (Fig. 5c) and contains 20% angular Zechstein clasts.

Figure 5: Grain-size distribution curves of the debris-flow matrix; a) Basal reddish debris-flow (DF-1; sample Ben-2); b) Whitish debris-flow (DF-2; sample Ben-3); c) Yellowish debris-flow (DF-3; sample Ben-6) that seals the tip of the fault.

### Structural geology

In the lower two debris-flow deposits (DF-1 and DF-2) a NNE-ward dipping and WNW-ESE striking planar fault is developed (Figs. 3, 6). The limited outcrop situation in the sinkhole does not allow to determine the exact offset along the fault. The normal offset of the reddish debris-flow (DF-1) must have been at least 150 cm, because the hanging-wall is not exposed in the sinkhole (Fig. 3). This normal fault offset was not fully compensated by the later reverse offset of the fault. At least 150 cm of normal offset remains after the reverse motion.

The fault is characterised by two small bends that separate the fault surface into three segments. The lower segment has an average dip of 76° and the middle segment has an average dip of 60°. In contrast, the upper segment shows a much steeper dip angle of 80° (Fig. 6c). Two sets of striations are developed on the fault surface (Fig. 6a, b). These striations indicate initial normal fault movements and a later reactivation of the fault as oblique fault with reverse and strike-slip



components (Fig. 6a, b). Similar fault kinematics of this fault were described by Franzke et al. (2015). The tip of the fault is sealed by the third yellowish debris-flow deposit (DF-3).

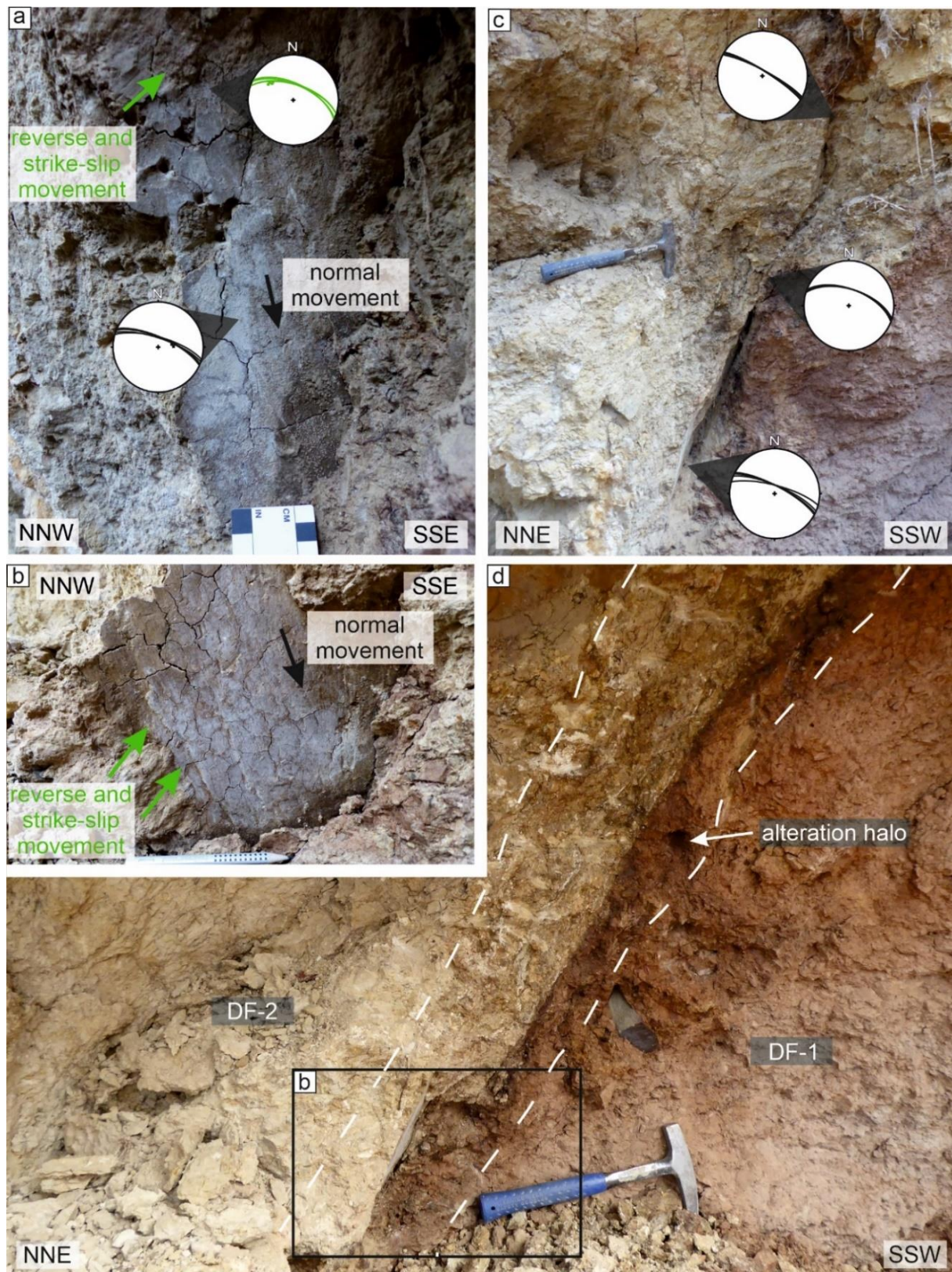
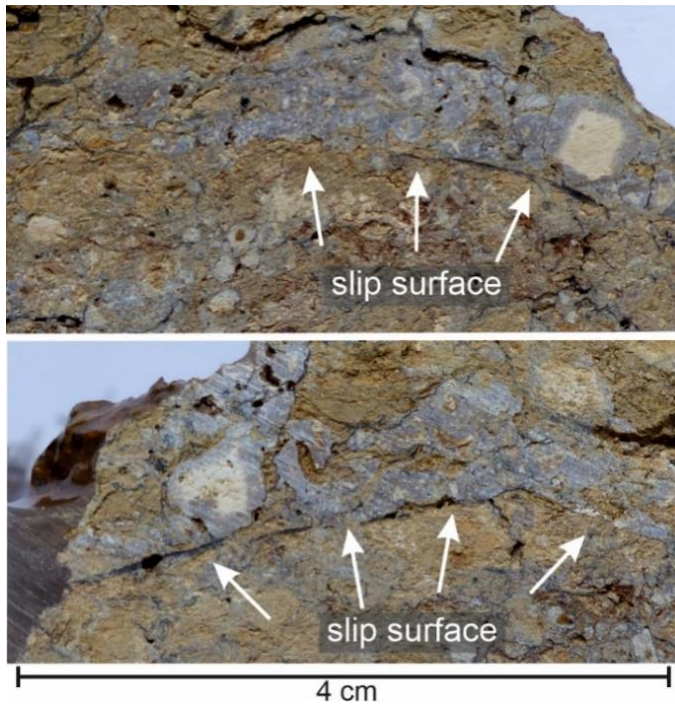


Figure 6: Structural data set of the exposed NNE-ward dipping fault in the sinkhole; a) Stereographic projections showing normal and reverse fault kinematics; b) Fault surface with normal and reverse kinematics; c) Stereographic projections of the normal fault component; d) Fault surface in debris-flow deposits with fault core and alteration halo.





The outcrop reveals that the fault has a complex structure, with a 7 - 9 cm thick core that contains several thin slip surfaces, which are characterised by polished and striated surfaces (Figs. 6d, 7), similar to fault cores shown in e.g., Faulkner et al. (2011) or Shipton and Cowie (2003). In addition, the fault core is partly flanked by an alteration halo (Fig. 6d). This alteration halo can be interpreted as part of the fault damage zone, which contains near-field fault-related deformation (Vermilye and Scholz 1998; Shipton and Cowie 2003). The damage zone is likely the product of rupture processes (cf. Kim et al. 2004).

Figure 7: Cross-section of the fault core material with slip surfaces.

### Electrical resistivity tomography (ERT)

Laboratory measurements show that the debris-flow material from the outcrop has high resistivities (1200  $\Omega\text{m}$  for DF-1 and 2000  $\Omega\text{m}$  for DF-2). This is caused by the very low water content of the samples (3-5 vol-%) due to the drying of the debris-flow deposits during the summer. As moisture was far below the expected in-situ conditions, we added some water to the samples resulting in about 20 vol% water. We then obtained similar resistivities slightly below 20  $\Omega\text{m}$  for both DF-1 and DF-2, so that they cannot be distinguished from each other. This is probably caused by their similar grain-size distribution and mineral composition. However, we expect secondary effects in electrical resistivity in the vicinity of the fault zone due to shearing or fracturing processes, which leads to variations in the porosity and thus to the water saturation of the deposits. Deposits with high porosity and thus a low water content are indicated by high resistivities, whereas deposits with low porosity and higher water content show low resistivities. Furthermore, we expect a contrast to the underlying Zechstein sulphates (gypsum), which resistivity is expected to be higher (>150  $\Omega\text{m}$  for undissolved and 50 - 100  $\Omega\text{m}$  for moderately dissolved gypsum according to Drahor (2019)).

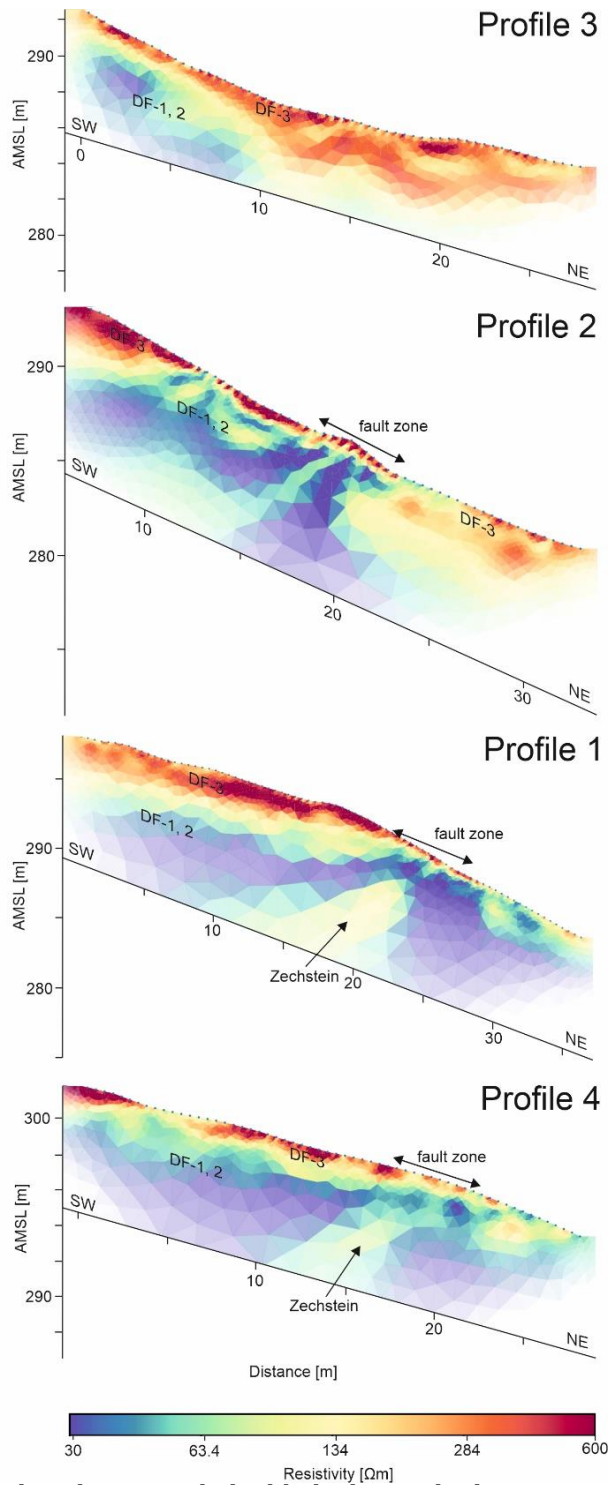


Figure 8: Measured ERT profiles. DF-1 to DF-3 refer to debris-flow deposits exposed in the sinkhole (Fig. 3). Note that the alpha shading represents the coverage (sum of absolute sensitivity values) and thus indicates the reliability of the structures.

*Interpretation*

The basal parts of all profiles are characterised by low electrical resistivities, which are probably caused by a relatively high water content (Ullrich et al. 2008) of debris-flow deposits DF-1 and DF-2, which have a fine-grained silty matrix (Fig. 5a, b). The central zone of higher resistivity (~60 - 130 Ωm) runs parallel to the strike direction of the small NNE-ward dipping fault that is exposed in the sinkhole. We interpret this resistivity pattern (mostly visible on profiles 1 and 4) as the offset Zechstein sulphates (gypsum) that is located 3 - 4 m below the surface (see schematic profile of Fig. 3b), whereas it is hardly detectable on profiles 2 and 3. The initial normal movements brought the hanging-wall block north of the fault in a position below the penetration depth of the ERT. The near-surface part of the fault is characterised by a complex structure with a several centimetre-thick alteration halo and a fault core that contains several parallel slip surfaces (Figs. 6d, 7). This heterogeneity is probably reflected in the resistivity pattern. The part of the higher resistivities (~60 - 130 Ωm) may represent the fault core that is characterised by sheared finer-grained material with less fractures and voids that are not completely water-saturated.

The alteration halo likely has a higher water content caused by a higher fracture density. Therefore, the surrounding lower resistivity values (30 - 60 Ωm) are interpreted as the flanking fault damage zone (Fig. 8).

The high electrical resistivity values (130 - 600 Ωm) in the uppermost parts of the ERT profiles can be explained by a low water content and low compaction of the youngest debris-flow deposit DF-3, which has a coarser-grained sandy to silty matrix (Fig. 5c).



### Shear wave seismic profile

The shear wave seismic profile was acquired and interpreted to image the near surface structure of the Harz Boundary Fault (Fig. 9). The location of the seismic profile is shown in Figures 1c and 4.

The profile runs roughly NE-SW and crosses the Harz Boundary Fault and the steeply-dipping Palaeozoic-Mesozoic rocks of the foreland (Figs. 1c, 9a, b). It is approximately 1 km long and was acquired 500 m SE of the sinkhole (Figs. 1c, 4).

The steeply-dipping, almost vertically oriented Permian and Triassic rocks represent a special challenge for seismic imaging. The 70° limit of the applied FD-migration (Yilmaz 1987) results in a limitation of the reflection seismic method to image steeply-dipping structures. Due to the survey geometry, the vertical to steeply-dipping beds north of the Harz Boundary Fault are not directly imaged. The fault traces and lithological units are interpreted based on reflector disruptions and secondary wavelet effects caused by changes in signature patterns.

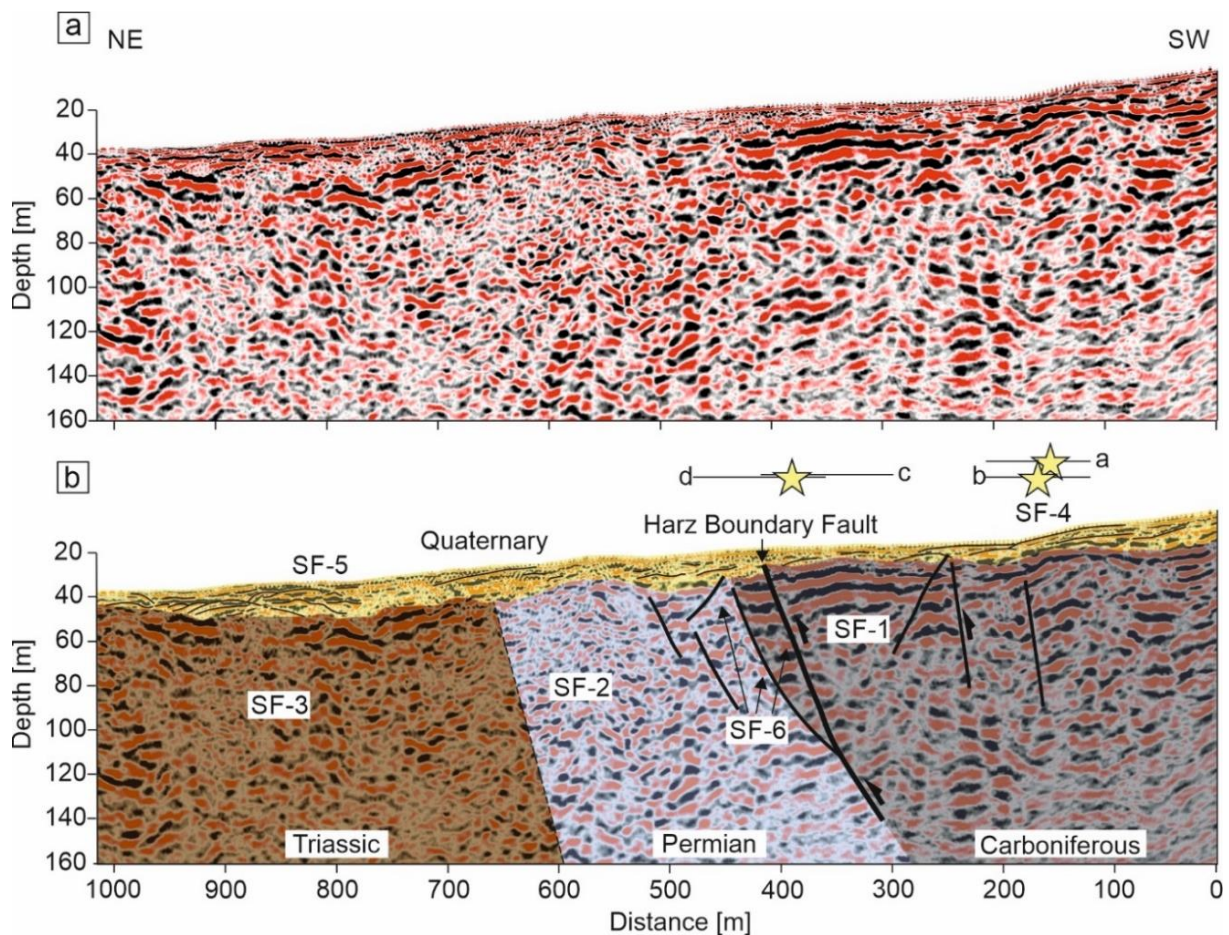


Figure 9: Shear wave seismic profile. For location see Figs. 1c and 4; a) Uninterpreted section; b) Interpreted section. The yellow stars show the shot point locations (a-d) shown in Figure 13.

## Seismic facies (SF)

Six different seismic facies (SF) can be distinguished in the seismic profile. These different seismic facies are characterised by using the external geometry and the internal reflector pattern (Fig. 10).

### Seismic facies 1

SF-1 is characterised by mainly horizontal to sub-horizontal parallel, continuous to partly discontinuous reflectors. Locally high amplitude reflectors are developed and partly the reflectors are transparent. In the upper part, the parallel reflectors are more continuous and locally dip in two directions and form a slightly curved pattern.

#### *Interpretation*

Based on the geological map of the study area, the parallel reflectors with higher amplitudes are interpreted as Carboniferous sandstones (cf. Schröder et al. 1927). Parts of the shallower dipping Carboniferous sandstones produce a clear reflector pattern that can be interpreted following the standard seismic interpretation workflow (e.g., Brandes et al. 2011). The changes in impedance are a result of bedding planes and fractures.

### Seismic facies 2

SF-2 is characterised by short discontinuous, thick and hummocky, partly weak to diffuse, and transparent low- partly high-amplitude reflectors.

#### *Interpretation*

The reflector pattern is characteristic for soluble Permian Zechstein rocks (e.g., Wadas 2016) interpreted as steeply-dipping Zechstein sulphates (cf. Schröder et al. 1927) north of the Harz Boundary Fault.

### Seismic facies 3

SF-3 is characterised by short hummocky, thick partly weak to diffuse discontinuous mostly high amplitude reflectors.

#### *Interpretation*

SF-3 represents the steeply-dipping sedimentary rocks of the Buntsandstein north of the Harz Boundary Fault (cf. Schröder et al. 1927). Lithological changes within the Buntsandstein rocks, e.g., the intercalated Rogenstein zone (~ 820-785 m on the profile) produced the different reflector pattern.

#### Seismic facies 4

SF-4 has a sheet-like external geometry and an internal mainly parallel, discontinuous to partly continuous closely spaced reflector pattern. Some of the reflectors are weak to slightly transparent. The lower boundary is erosive.

#### *Interpretation*

Based on the information taken from geological maps (Schröder et al. 1927) and regional stratigraphic studies (Bode et al. 2003) the closely spaced reflector pattern represents proximal Pleistocene alluvial-fan deposits. The sheet-like, slightly inclined geometry points to fan-head aggradation that resulted either from unchanneled debris-flow or stream-flow depositions (cf. Blair and McPherson 2009; Ventra and Nichols 2014; Franke et al. 2015).

#### Seismic facies 5

SF-5 has a mound-shaped external geometry and an internal concentric, mainly continuous to partly transparent reflector pattern. These mounds have a width of 20 to 100 m and are 3 to 13 m thick. They show an upslope-stepping, shingled stacking pattern that onlaps seismic facies SF-4. The lower boundary is characterised by partly discontinuous, slightly transparent and concave reflectors.

#### *Interpretation*

The mound-shaped geometry of these deposits points to a mid- or lower fan-environment, where depositional lobes were deposited below the intersection point from stream-flows, sheetfloods or debris-flows. The downslope deposition indicates a phase of fan progradation (cf. Blair and McPherson 2009; Meinsen et al. 2014; Franke et al. 2015). The upslope-stepping lobes may indicate a subsequent phase of aggradation and fan-trench backfilling (e.g., Ventra and Nichols 2014; Meinsen et al. 2014).

#### Seismic facies 6

SF-6 is characterised by mainly discontinuous short, subparallel high amplitude reflectors that show a regular offset pattern.

#### *Interpretation*

The reflectors result from density variations within the steeply-dipping rocks of the Harz Mountain foreland. Their discontinuous, short reflectors with the characteristic offset pattern points to displaced density variations in the subsurface and are therefore interpreted as faults (cf. Wadas et al. 2016).

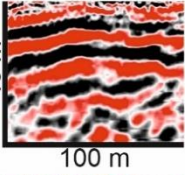
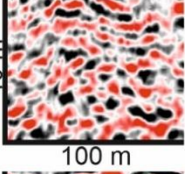
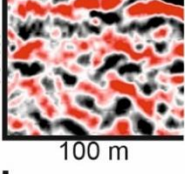
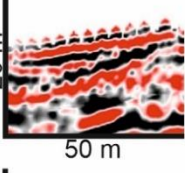
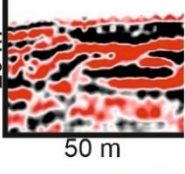
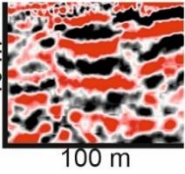
Seismic facies	Description	Geological interpretation
<p>SF-1</p> 	<p>Parallel to sub-horizontal, continuous to partly discontinuous partly transparent, partly high-amplitude reflectors</p>	<p>Carboniferous sandstones</p>
<p>SF-2</p> 	<p>Short hummocky, discontinuous, partly weak to diffuse and transparent, low-partly high-amplitude reflectors</p>	<p>Zechstein carbonates and sulphates</p>
<p>SF-3</p> 	<p>Short hummocky, discontinuous, thick, partly weak to diffuse, mostly high-amplitude reflectors</p>	<p>Buntsandstein sand- and limestones</p>
<p>SF-4</p> 	<p>Mainly parallel, discontinuous to partly continuous slightly transparent closely spaced, high-amplitude reflectors</p>	<p>Quaternary proximal alluvial-fan deposits</p>
<p>SF-5</p> 	<p>Shingled mound-shaped internal concentric, mainly continuous to partly transparent, partly high-amplitude reflectors</p>	<p>Quaternary lower to mid alluvial-fan deposits</p>
<p>SF-6</p> 	<p>Regular offset pattern of mainly subparallel high-amplitude reflectors</p>	<p>Faults</p>

Figure 10: Description and interpretation of the seismic facies.

### ***Larger-scale subsurface architecture and fault systems***

The visualization of the subsurface structure and the fault system is largely based on the shear wave profile (Fig. 9). The profile crosses the Harz Boundary Fault and covers parts of the foreland. In order to determine the vertical resolution of this seismic profile, the dominating frequencies were extracted from CMP 300-700 and 1300-1700 down to 500 ms TWT, which represents approximately a depth of 0-150 m (Fig. 11 a-c). The extracted frequencies are in a range of 30 Hz. For the SW part of the profile the frequency of 30 Hz, together with shear wave velocities of 600 m/s cause wavelengths of approximately 20 m and a resulting vertical resolution of about 5 m. In the NE part of the seismic profile, the shear wave velocities are lower with about 450 m/s, which results in a local vertical resolution of about 4 m. This is sufficient for the visualization of the structural elements related to the Harz Boundary Fault.



The seismic profile displays 6 different seismic facies. The lower seismic units comprise seismic facies 1-3, representing Carboniferous bedrock and steeply-dipping Permian and Triassic rocks (Fig. 9a, b; cf. Schröder et al. 1927). SF-1 is located in the SW part (~ 0 - 440 m) of the section. SF- 2 occurs in the central part (~ 440 - 740 m) and SF-3 in the NE part (~740 - 1000 m) of the profile (Fig. 9a, b).

The steeply-dipping rocks of partly SF-1, SF-2 and SF-3 do not allow a common analysis of the reflector pattern (cf. Yilmaz 1987). In this case the reflectors do not represent bedding planes, because the sedimentary succession was strongly tilted during the uplift of the Harz Mountains. The reflections result from lateral changes in the physical properties of the rocks, caused by faults, fractures and small-scale density variations within the individual lithological units (cf. Woolery et al. 1993). The prominent lateral changes in the reflector pattern from low-amplitude discontinuous to higher-amplitude discontinuous reflectors indicate the transition from the Upper Permian rocks to the rocks of the Lower to Middle Buntsandstein. The bedrock is unconformably overlain by 7-17 m thick Quaternary deposits (Fig. 9a, b), (SF-4 and SF-5) that most probably represent Pleniglacial to Lateglacial alluvial-fan deposits (Fig. 10; cf. Roskosch et al. 2012; Meinsen et al. 2014). SF-4 occurs in the upper ~10 m at the SW part (~700- 0) and SF-5 at the NE part (~1000 - 700 m) in the seismic profile (Fig. 9a, b). The stacking pattern indicates a prograding-retrograding fan system, which might have been controlled by changes in water discharge and sediment supply (cf. Meinsen et al. 2014).

SF-6 represents steeply-dipping Permian rocks, in which faults displace density variations. These systematic offsets allow to interpret faults on the seismic profile. Comparable structures and interpretations were presented by Wadas et al. (2016) for Permian Zechstein rocks close to Bad Frankenhausen. These faults occur in the SW part of the seismic profile within SF-1 and in a 300 m wide zone between SF-1 to SF-2 (~150 - 500 m). Several synthetic and antithetic reverse faults are mapped that partly propagate into the overlying Late Pleistocene alluvial-fan deposits (SF-4 and SF-5; Fig. 9a, b). These SSW-ward dipping thrusts and NNE-ward dipping faults form a splay fault system, which developed during the Cretaceous inversion phase. It is likely that the fault exposed in the sinkhole is one of these NNE-ward dipping back thrusts (Fig. 9a, b).

The seismic interval velocities (Fig. 11c) image the lithological changes along the seismic profile. The highest velocities in the SW correspond to the Carboniferous sandstones. Between 440 m and 270 m a significant decrease in the shear wave velocity is recorded, which images the transition between the Carboniferous sandstones and the Permian rocks. The floating decrease in the seismic interval velocity is caused by CMP ray velocity averaging and subsequent interpolation effects at the boundaries of the different lithologies and probably by the development of damage zones parallel to the faults of the splay fault system at the Harz Boundary (Figs. 1, 4, 9). The onset of lower shear wave interval velocities at approximately 600 m (Fig. 11c) images the boundary from the Permian rocks to the Triassic rocks.

The strong lateral change in seismic interval velocities (also referred to as layer inhomogeneity) is supported by the results of the shear wave refraction inversion (Fig. 11d) for a 2 layer model (one layer above the half-space). It is only based on the first break pick times (i.e., only one sample of a recorded trace) of all seismic traces recorded, which results in a simplified velocity-depth model. The upper layer represents the Quaternary alluvial-fan deposits and the weathering zone of the rocks and the lower layer represents the bedrocks of the Harz Mountains and the Harz foreland area (also referred to as half space layer). The colour coding shows the calculated refraction layer velocities, which vary from 200 m/s to 350 m/s for the upper layer (alluvial-fan

deposits), and from 1500 m/s in the SW to 516 m/s at the NE section of the profile. The strong velocity drop at about ~ 400 m indicates the location of the Harz Boundary Fault system and thus the boundary between the Carboniferous sandstones and the Permian rocks.

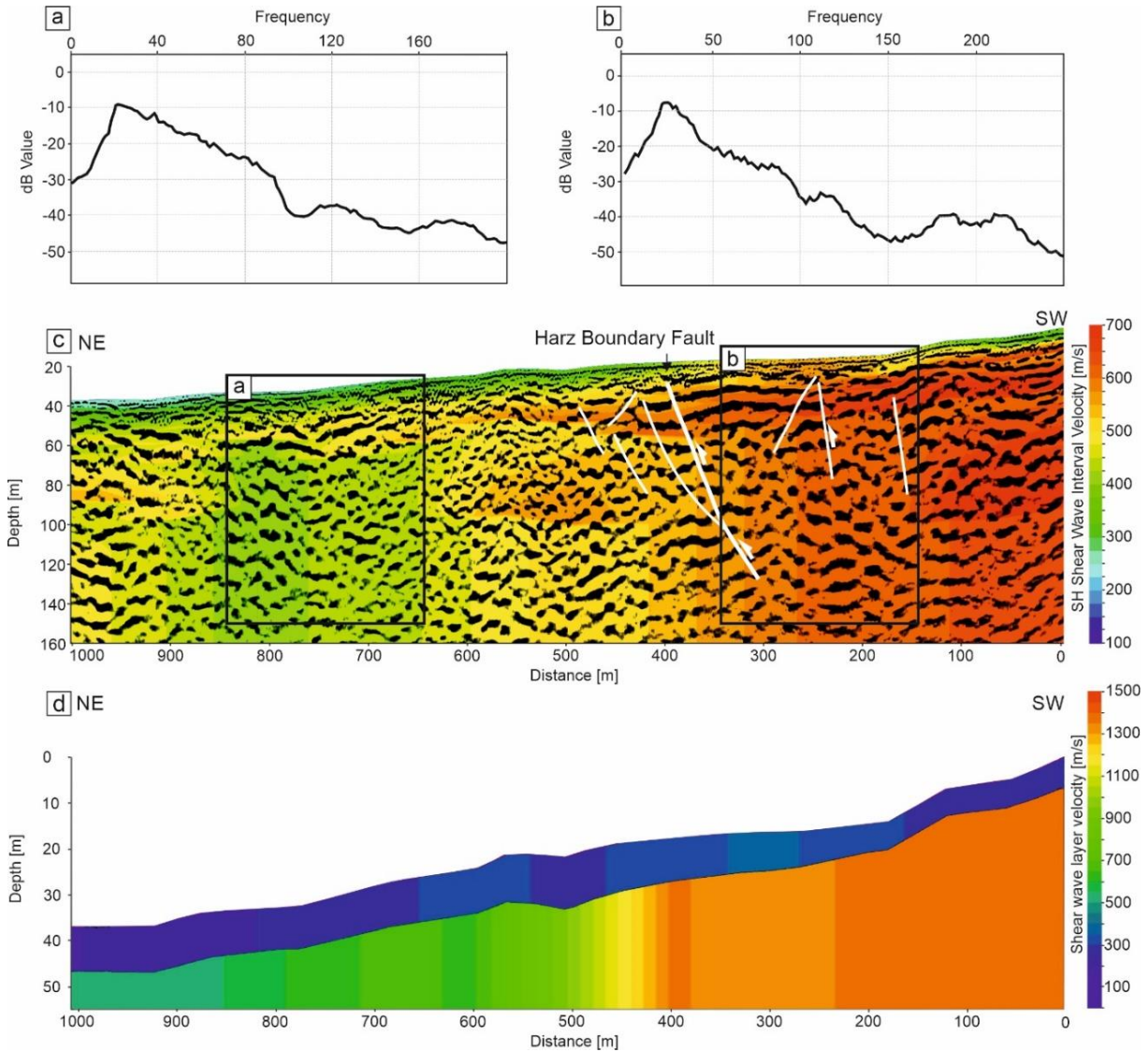


Figure 11: Local average amplitude spectra of the corresponding time section, shear wave interval velocities and shear wave refraction inversion results. a-b) Two extracted average amplitude spectra of the corresponding time section visualize the lateral change in the frequency response in the time range 0 - 500 ms TWT, which corresponds to a depth range of ~ 0-150 m. The dominating frequencies (~30 Hz) extracted from window a) CMP range 300-700 and corresponding shear wave velocities of ~ 600 m/s result in a vertical resolution of ~ 5 m; b) CMP range 1300-1700 and shear wave velocities of ~ 450 m/s result in a vertical resolution of ~ 4 m; c) Colour-coded seismic profile by shear wave interval velocities derived from reflection seismic stacking velocities. The lateral variations in velocities image the response of the lateral succession of steeply-dipping rock units. Due to the averaging of the incoming and outgoing raypath velocity at a vertical velocity boundary of different rock units by the CMP ray fan methodology, these boundaries are not imaged in a precise, sharp manner, only the change of the average values along a vertical boundary are imaged; d) Results of the shear wave refraction inversion for a 2 layer model (one layer above the half-space) based on the first break pick times of all seismic traces recorded. The upper layer represents the poorly consolidated Quaternary alluvial-fan deposits and the weathering zone of the rocks; the lower layer represents the bedrock (half space). The colour coding shows the calculated refraction layer velocities, which are varying from 200 m/s to 350 m/s for the upper layer, and from 1500 m/s (SW) to 516 m/s (NE) for the half space.

## Age calculation of the debris-flow deposits

### *Basal reddish debris-flow (DF-1)*

Sample (Ben-2) provided reliable luminescence ages. The dose recovery ratios  $0.93 \pm 0.01$  for the pulsed IR<sub>50</sub> signal and  $1.08 \pm 0.01$  for quartz OSL signal close to unity (0.9 - 1.1; Wintle and Murray 2006) show that the applied SAR protocols were suitable for the D<sub>e</sub> measurements.

The pulsed IR<sub>50</sub> signal of the fine grain fraction yielded a recycling ratio of  $1.04 \pm 0.03$  and the quartz OSL recycling ratio was  $1.02 \pm 0.05$ . The values are within 10% of unity (cf. Wintle and Murray 2006) and show that the SAR protocol corrected sensitivity changes successfully during the measurements.

Fading tests gave a mean g-value of  $1.4 \pm 0.2\%$ . The fading uncorrected pulsed IR<sub>50</sub> age ( $12.8 \pm 0.7$  ka) was fading corrected based on Huntley and Lamothe (2001). The fading corrected polymineral fine grain age (feldspar) is  $14.2 \pm 0.8$  ka.

The estimated luminescence ages from the reddish debris-flow deposits (Ben-2) for feldspar and quartz are in agreement;  $14.2 \pm 0.8$  ka (polymineral, feldspar) and  $15.2 \pm 0.8$  ka (quartz).

### *Whitish (DF-2) and yellowish debris-flow deposits (DF-3)*

No IRSL signal could be detected by measurements of the polymineral fine grain fraction of samples Ben-3 to 7. The quartz minerals (Ben-3, 4, 5, 6, 7) were regarded as in saturation. Chapot et al. (2012) showed that although the laboratory OSL dose response curve continued to grow, the natural OSL signal saturated at  $\sim 150$  Gy. Therefore, all quartz D<sub>e</sub> values  $> 150$  Gy were considered in saturation. Consequently, the calculated ages of samples Ben-3 to 7 are minimum ages of the deposits before transport (Table 1) or the samples were insufficiently exposed to daylight prior to deposition, which resulting in age overestimation.

The quartz and fading corrected feldspar ages are listed in Table 1.

Table 1: Quartz and feldspar luminescence ages from Benzingerode.

Sample	Debris-flow	quartz		feldspar		uncorr.	corr.
		D <sub>e</sub> (Gy)	Age (ka)	D <sub>e</sub> (Gy)	Age (ka)	Age (ka)	
Ben-2	DF-1	64.3±0.7	<b>15.2±0.8</b>	60.5±0.5	12.6±0.6	<b>14.2±0.8</b>	
Ben-3	DF-2	>378±12	>123±9	-	-	-	
Ben-4	DF-2	>273±13	>119±11	-	-	-	
Ben-5	DF-3	>217±7	>124±13	-	-	-	
Ben-6	DF-3	>356±11	>164±14	-	-	-	
Ben-7	DF-3	>285±5	>109±8	-	-	-	

## Numerical simulations

The results of the numerical simulations are shown in Figure 12. The coloured solid lines represent the results for the North-European part of the global ice model ICE-6G\_C and the dashed coloured lines for the ANU-ICE ice history model. The time when  $\delta\text{CFS}$  becomes positive the coloured lines cross the threshold from the stable zone into the unstable zone, which marks the onset of possible fault motion. Due to the relative character of the  $\delta\text{CFS}$  it is independent of how large (or small) the positive values of the  $\delta\text{CFS}$  are.

In a thrust-faulting regime (Fig. 12), the zero line is crossed mainly between 13.8 ka and 10.3 ka for the ICE-6G\_C ice model and between 13.2 ka and 6.3 ka for the ANU-ICE ice model, suggesting that a fault in 12.5 km depth became instable at that time and was probably reactivated. This timing falls into the deglaciation process of the Late Pleistocene Weichselian ice sheet and suggests a fault reactivation triggered by this process.

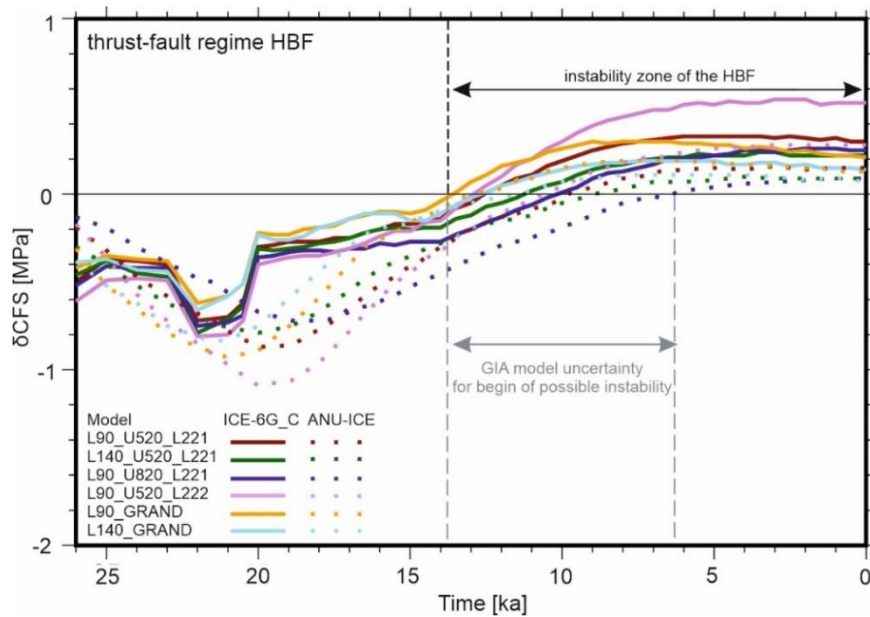


Figure 12: Modelling results for a thrust faulting stress regime with the development of the change in Coulomb failure stress at the Harz Boundary Fault over the last 26 ka in a depth of 12.5 km. The simulation was performed with two different ice history models. The solid lines represent the results for the North-European part of the global ice model ICE-6G\_C. The second ice history model (dashed lines) is the ANU-ICE ice history model. The first L is the lithospheric thickness being 90 or 140 km; U is the upper-

mantle viscosity with  $5 \times 10^{20}$  [520] or  $8 \times 10^{20}$  [820] Pa s; the second L is the lower-mantle viscosity with  $2 \times 10^{21}$  [221] or  $2 \times 10^{22}$  [222] Pa s; GRAND represents a laterally varying upper and lower-mantle viscosity model.

## Discussion

Central Europe was affected by repeated glaciations since the Middle Pleistocene (Ehlers et al. 2011; Roskosch et al. 2015; Lang et al. 2018). Loading and unloading by ice sheets influenced the lithosphere (Thorson 2000) and resulted in stress modifications (Wu 1997; Stewart et al. 2000), which may lead to the tectonic reactivation of regional fault systems (e.g., Brandes et al. 2011, 2012b, Brandes and Winsemann 2013; Brandes et al. 2015, Pisarska-Jamroży et al. 2019).

### Structural geology, electrical resistivity tomography and seismic interpretation

Similar to Franzke et al. (2015) we interpret the fault that is exposed in the sinkhole, as a result of neotectonic activity along the Harz Boundary Fault system. This small fault shows a WNW-ESE strike (Figs. 4, 6) that implies a close connection to the Harz Boundary Fault that has a similar strike as indicated on the geological map (Schröder et al. 1927). This interpretation is supported by the seismic data that show synthetic and antithetic faults (Fig. 9). The seismic profile gives evidence that the Harz Boundary Fault is not a discrete fault but rather represents a splay of several faults. Such a structure is typical for the bounding faults of major basement blocks. Comparable splay fault systems are well known from the Laramide uplifts in the USA (Erslev 1986; Neely and Erslev 2009; Yonkee and Weil 2015). The fault which is exposed in the sinkhole is probably a back thrust of this splay fault system (Fig. 9). Based on the ERT profiles the fault exposed in the sinkhole can be traced for at least 50 m parallel to the Harz Boundary Fault (Fig. 8).

The fault interpretation shown in Figure 9b is also supported by the analysis of the refracted shear waves. Based on four shot gather examples (Fig. 13) extracted at profile meter 158 m, 170 m and two at 390 m, the velocity structure is shown. The shot gathers at profile meter 158 and 170 (Fig. 13a, b) are located within the Carboniferous sandstones (cf. Schröder et al. 1927). The documented drop in the shear wave velocity is interpreted as a result of fracturing in a damage zone parallel to a fault. The refracted shear wave in the Carboniferous sandstones with a velocity of up to 1500 m/s (~1400 m/s at the position of the shot gathers in Fig. 13) is characterised by small interruptions in the potential damage zone of the Harz Boundary Fault, likely caused by fractures within the Carboniferous rocks (Fig. 13a). The fault interpretation is supported by reflector offsets. We interpret this fault as a branch that is located south of the main fault.

The shear wave velocity of up to 1500 m/s (corresponding to a P-wave velocity of > 3000 m/s) is characteristic for the Carboniferous sandstones below the poorly consolidated Pleistocene alluvial-fan deposits (Figs. 11, 13). Compared to the shot gathers shown in Figure 13 a-c the shot gather Figure 13d shows a significant drop in the shear wave velocity to 790 m/s, which points to a strong lithological contrast. We interpret this as indicator for the position of the main fault, between the high-velocity Carboniferous sandstones and the juxtaposed rather low-velocity Permian rocks.

The refracted shear wave signatures in the shot gather shown in Figure 13d also give evidence (by the disruption of the first break signature and backscattered Love surface waves) for a thin sliver of Permian Werra dolomite NE of the main fault that is also supported by the results of the shear wave refraction inversion (Fig. 11d, orange to yellow shear wave layer velocity zone at approximately 400 to 450 m; Fig. 11d). The results of the seismic refraction inversion (Fig. 11d) allow to delineate the different rock lithologies and match with the interval velocity coded seismic



profile (Fig. 11b). Both show a laterally decreasing pattern of high velocities in the SW and lower velocities in the NE, reflecting the lateral succession steeply-dipping rock units.

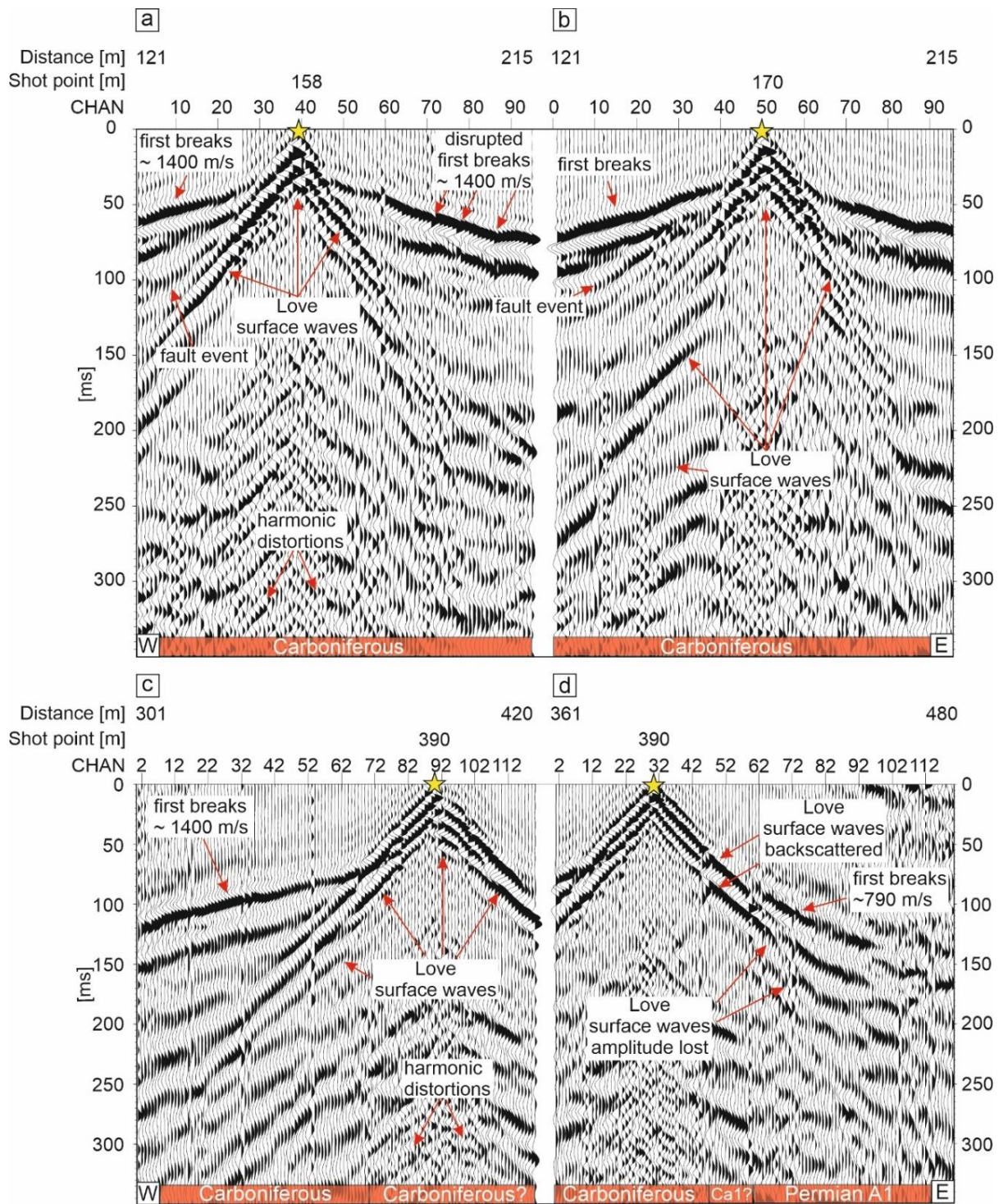


Figure 13: Four shot gather examples (Vibroseis Correlation, Automatic Gain Control 100 ms window, and Bandpass Filter 20-22-90-105 Hz applied) along profile meter 121-215 (a-b), profile meter 301-420 (c) and profile meter 361-480 (d). Recording duration is 350 ms. Channel numbers and distance along the profile are shown. Individual seismic source locations are labelled by a yellow star. The shot gathers at profile meter 158m (a) and 170 m (b) are located within the Carboniferous sandstones. The high shear wave velocity of nearly 1500 - 1400 m/s is characteristic for these sandstones. Small interruptions are caused by the potential damage zone of the Harz Boundary Fault. A significant drop in the shear wave velocity to

790 m/s points to a strong lithological contrast. The refracted waves also give evidence for a thin sliver of Permian Werra dolomite (Ca1) and Permian Werra sulphates (A1) (c, d). Further elements of the surrounding wave field like first breaks, Love surface waves and harmonic distortions are additionally denoted for differentiation. For location of shot point gather examples see Fig. 9b.

### **Timing of fault movements**

The results of luminescence dating show that the age of the lower reddish debris-flow deposit (DF-1) ranges between  $14.2 \pm 0.8$  ka (feldspar pulsed IR<sub>50</sub>) and  $15.2 \pm 0.8$  ka (quartz OSL). Since IR<sub>50</sub> signal of feldspar bleaches one order of magnitude slower than the quartz OSL, the agreement of ages indicates that both sediments were well bleached before deposition (Murray et al. 2012). The ages imply that fault movements took place after  $\sim 15$  ka. The younger yellowish debris-flow deposit (DF-3), that seals the tip of the fault, did not give reliable luminescence ages. The quartz minerals in the sediment are regarded as in saturation. However, it is likely that the uppermost debris-flow deposit is also Lateglacial in age. During the Holocene, a stabilizing vegetation cover rapidly developed on hillslopes most likely preventing erosion and mass movements (cf. Litt et al. 2007; Meinsen et al. 2014).

The age of the alluvial-fan deposits is unknown. Reinecke (2006) assumed a Late Pleniglacial to Lateglacial age for alluvial-fan deposits in the Harz foreland area. The study of Meinsen et al. (2014) from the Senne area implies that the onset of wide-spread alluvial-fan deposition started during the late Middle to Late Pleniglacial ( $29.3 \pm 3.2$  ka) and was probably related to the decreasing temperatures at the end of MIS 3. Strong progradation of alluvial fans correlates with early MIS 2, which is attributed to the decrease of a stabilizing vegetation cover, an increase in water discharge and runoff rates from the catchment areas. The subsequent phase of fan aggradation and retrogradation indicates decreasing discharge and an increase in sediment supply. Fan aggradation in the Senne area ceased at around  $19.6 \pm 2.1$  to  $18.7 \pm 1.9$  ka (Roskosch et al. 2012; Meinsen et al. 2014), when polar desert conditions began to establish, and arid conditions prevailed, resulting in the widespread deposition of aeolian loess, sand-sheets and dunes. This stacking pattern can also be observed in the alluvial-fan deposits of the study area (Seismic profile, SF-4 and 5), pointing to a similar age.

All estimated ages imply a Lateglacial fault activity and would correspond to the time interval of fault reactivation along the Osning thrust and the Sorgenfrei-Tornquist Zone (Brandes et al. 2012b; Brandes and Winsemann 2013; Brandes et al. 2018b).

### **Possible trigger for fault development**

#### ***Dissolution and migration of Zechstein rocks***

The sinkhole, in which the fault is exposed, developed above steeply-dipping sulphate rocks of the Zechstein Werra sequence (Fig. 4). The observed initial normal fault movement could therefore be related to dissolution processes and sinkhole formation (cf. Poppe et al. 2015) or gravitational deformation as a consequence of slope failure (cf. Gardner et al. 1999) and does not require a neotectonic trigger mechanism. Non-tectonic normal faults that were induced by dissolution processes are reported e.g., from SE Utah, (USA) (Guerrero et al. 2014). However, the reverse fault



movement, which is indicated on the fault surface by striations cannot be explained by slope failure. Recent experimental studies on sinkhole formation show the development of a set of ring faults (e.g., Poppe et al. 2015). We rule out that the observed fault belongs to such a sinkhole related ring fault system, because in the sinkhole only one fault is exposed and in a nearby sinkhole (a few m distance), no fault is exposed. Ring faults evolving during the sag process cannot explain the observed evolution of the fault in the sinkhole. In addition, based on ERT profiles and the seismic profile the lateral extent of the NNE-ward dipping fault was mapped (Fig. 8). The results point to a straight fault that runs parallel to the Harz Boundary Fault. Therefore, we rule out dissolution processes as a driver for fault evolution. Paul (2019) discussed the role of Zechstein salt dissolution and migration for basin-wide subsidence in the Harz foreland area. He assumes that no active tectonic uplift of the Harz Mountains has occurred since the Neogene and the apparent relative uplift is caused by subsidence of the foreland basins. As discussed before, we cannot rule out dissolution processes as a potential trigger for normal faulting. However, the two-fold fault kinematics with initial normal faulting followed by reverse and strike-slip movements is difficult to explain with dissolution. Collapse and block rotation processes cannot explain the striations with oblique reverse movement.

We rule out salt migration in the vicinity of the Harz Boundary Fault as proposed by Paul (2019), because cross-sections of Baldschuhn et al. (1996) show a salt weld directly north of the range front. The lack of a source layer with a significant thickness makes an effective salt migration unlikely in this part of the Subhercynian Basin.

### ***GIA as possible trigger for fault activity***

Comparable observations of young normal fault movements that were followed by reverse faulting were made by Brandes et al. (2012b) and Brandes and Winsemann (2013) at the Osning thrust. The kinematic behaviour is interpreted as a consequence of deformation in the area of the Late Pleistocene Weichselian glacial forebulge. The study area was affected by this forebulge, which was located several 100 kilometres in front of the ice sheet (Kiden et al. 2002; Nocquet et al. 2005; Busschers et al. 2008; Sirocko et al. 2008; Kierulf et al. 2014; Winsemann et al. 2015). The formation, migration and collapse of the glacial forebulge induced a complex stress pattern in the lithosphere that varied in space and time and could have caused the reactivation of pre-existing faults (cf. Stewart et al. 2000). Moreover, Wu (1997) has shown that GIA can lead to tensional stresses in the forebulge area, with values exceeding 10 MPa during full glaciation, although the tectonic background stress regime is thrusting.

The collapse of the forebulge is still ongoing in northern Germany. The recent maximum subsidence rate is 1.0 - 1.5 mm/yr at latitudes between 50.5 - 53°N (Frischbutter, 2001; Nocquet et al. 2005). The tectonic activity along the Harz Boundary Fault system is probably a consequence of the forebulge development and decay, comparable to the similar tectonic evolution as observed at the Osning thrust.

The forebulge area of the older, Middle Pleistocene ice sheets in northern Germany is not exactly known. The Elsterian and Saalian post-glacial re-directions of the rivers Weser and Leine, southwest of the study area, might have been caused by GIA (Winsemann et al. 2015).

With numerical simulations it is possible to analyse the interplay of glaciation-induced stress changes and fault reactivation (Wu and Hasegawa 1996a, b; Hetzel and Hampel 2005; Turpeinen

et al. 2008; Hampel et al. 2009; Steffen et al. 2014b; Hampel 2017). Modelling results of Grollmund and Zoback (2001) and Hampel et al. (2009) imply that post-glacial tectonic activity is possible in areas that are located outside former ice sheets.

Due to the ongoing collision of Europe and Africa, the most suitable results are delivered by a thrust-faulting regime model (Fig. 12), because in parts of northern Germany, recent horizontal compression occurs. The SHmax direction shows a fan-like pattern with small deviations from NW-SE in the western regions to NE-SW in the eastern regions (Marotta et al. 2001, 2002, 2004; Kaiser et al. 2005; Heidbach et al. 2016). Hence, based on the thrust-fault regime results, which imply fault activity after 13.8 - 6.3 ka, combined with the results of the luminescence dating of the debris-flow deposit, which imply fault activity after ~15 ka, it can be assumed that the reactivation as oblique reverse fault with strike-slip components, is probably triggered by the decay of the Late Pleistocene (Weichselian) ice sheet in the Lateglacial.

Based on field data and numerical simulations, Brandes et al. (2012b, 2015) showed that the Lateglacial seismicity and the historic earthquakes in northern Central Europe were triggered by stress changes related to GIA. The results of this study imply that the Harz Boundary Fault also underwent a similar reactivation during the decay of the Fennoscandian ice sheet.

## **Conclusion**

Based on outcrop analyses, luminescence dating, ERT profiles and shear wave seismic data we present new structural data of the Harz Boundary Fault and evidence for GIA-related neotectonic movements in this region. A sinkhole exposes a fault that is most likely related to the Harz Boundary Fault. The shear wave seismic profile shows that the Harz Boundary Fault is a splay fault system in this area. Luminescence dating of faulted debris-flow deposits indicates fault movements after ~15 ka. The timing points to movements along the Harz Boundary Fault system as a consequence of stress changes induced by the decay of the Late Pleistocene (Weichselian) Fennoscandian ice sheet. This assumption is supported by numerical simulations of GIA-related change in Coulomb failure stress. Modelling results for a compressional regime assumed for this area show that a possible reactivation of the Harz Boundary Fault was between 13.8 to 6.3 ka. This matches with the luminescence dating ( $14.2 \pm 0.8$  ka polymineral, feldspar;  $15.2 \pm 0.8$  ka quartz), which implies that fault movement occurred after ~15 ka and supports the idea that the Harz Boundary Fault system was reactivated during the Lateglacial. Furthermore, this time of fault movement matches also with data from the Osning thrust and the Sorgenfrei-Tornquist Zone.

## **Acknowledgements**

We thank Gösta Hoffmann, Christian Hübscher, Jonas Kley and Klaus Reicherter for their constructive reviews that helped to improve the manuscript. We thank Dieter Epping, Robert Meyer and Jan Bergmann Barrocas for supporting the ERT measurements. The ANU-ICE model parts were kindly provided by Kurt Lambeck and Anthony Purcell. This is an open access article distributed under the terms of the Creative Commons CC BY license.

## References

- Al Hseinat M and Hübscher C (2017) Late Cretaceous to recent tectonic evolution of the North German Basin and the transition zone to the Baltic Shield/southwest Baltic Sea. *Tectonophysics* 708:28-55
- Argus DF, Peltier W, Drummond R, Moore AW (2014) The Antarctica component of postglacial rebound model ICE-6G\_C (VM5a) based on GPS positioning, exposure age dating of ice thicknesses, and relative sea level histories. *Geophys J Int* 198:537-563
- Baldschuhn R, Best G, Kockel F (1991) Inversion tectonics in the north-west German basin. Generation, accumulation, and production of Europe's hydrocarbons. *Spec Publ Eur Assoc Petroleum Geosci* 1:149-159
- Baldschuhn R, Binot F, Fleig S, Kockel F (1996) Geotektonischer Atlas von Nordwest-Deutschland und dem deutschen Nordsee-Sektor. *Geol Jb A* 153:3-95
- Blair TC, McPherson JG (2009) Processes and forms of alluvial fans. In: Parsons AJ, Abrahams AD (eds), *Geomorphology of desert environments*, 2nd edn, Springer, Netherlands, pp 413-467
- Bock G, Wylegalla K, Stromeyer D, Grünthal G (2002) The Wittenburg Mw = 3.1 earthquake of May 19th, 2000: an unusual tectonic event in northeastern Germany. In: Korn M (ed), *Ten years of German regional seismic network (GRSN)*. Report 25 of the Senate Commission for Geosciences, Wiley-VCH, pp 220-226
- Bode R, Lehmkuhl F, Reinecke V, Hilgers A, Dresely V, Radtke U (2003) Holozäne fluviale Geomorphodynamik und Besiedlungsgeschichte in einem kleinen Einzugsgebiet am nördlichen Harzrand. *E&G Quat Sci J* 53:74-93
- van den Bogaard P (1995)  $^{40}\text{Ar}/^{39}\text{Ar}$  ages of sanidine phenocrysts from Laacher See Tephra (12.900 yr BP): Chronostratigraphic and petrological significance. *Earth Planet Sci Lett* 133:163-174
- Brandes C, Polom U, Winsemann J (2011) Reactivation of basement faults: interplay of ice-advance, glacial lake formation and sediment loading. *Bas Res* 23:53-64
- Brandes C, Tanner D (2012) Three-dimensional geometry and fabric of shear deformation bands in unconsolidated Pleistocene sediments. *Tectonophysics* 518-521:84-92
- Brandes C, Pollok L, Schmidt C, Wilde V, Winsemann J (2012a) Basin modelling of a lignite-bearing salt rim syncline: insights into rim syncline evolution and salt diapirism in NW Germany. *Basin Research* 24:699-716
- Brandes C, Winsemann J, Roskosch J, Meinsen J, Tsukamoto S, Frechen M, Tanner DC, Steffen H, Wu P (2012b) Activity along the Osning Thrust in Central Europe during the Late glacial: ice-sheet and lithosphere interactions. *Quat Sci Rev* 38:49-62
- Brandes C, Schmidt C, Tanner DC, Winsemann J (2013) Paleostress pattern and salt tectonics within a developing foreland basin (northwestern Subhercynian Basin, northern Germany). *Int J Earth Sci* 102:2239-2254
- Brandes C, Winsemann J (2013) Soft sediment deformation structures in NW Germany caused by Late Pleistocene seismicity. *Int J Earth Sci* 102:2255-2274
- Brandes C, Steffen H, Steffen R, Wu P (2015) Intraplate seismicity in northern Central Europe is induced by the last glaciation. *Geology* 43:611-614
- Brandes C, Igel J, Loewer M, Tanner DC, Lang J, Müller K, Winsemann J (2018a) Visualisation and analysis of shear-deformation bands in unconsolidated Pleistocene sand using ground-penetrating radar: Implications for paleoseismological studies. *Sediment Geol* 367:135-145
- Brandes C, Steffen H, Sandersen PBE, Wu P, Winsemann J (2018b) Glacially induced faulting along the NW segment of the Sorgenfrei-Tornquist Zone, northern Denmark: implications for neotectonics and Lateglacial fault-bound basin formation. *Quat Sci Rev* 189:149-168
- Bullmann H (2010) Eigenschaften und Genese periglazialer Deckschichten auf Carbonatgesteinen des Muschelkalks in einem Teilgebiet der ostthüringischen Triaslandschaft. Dissertation, Universität Leipzig
- Busschers FS, Van Balen RT, Cohen KM, Kasse C, Weerts HJT, Wallinga J, Bunnik FPM (2008) Response of the Rhine-Meuse fluvial system to Saalian ice-sheet dynamics. *Boreas* 37:377-398

- Caputo R, Piscitelli S, Oliveto A, Rizzo E, Lapenna V (2003) The use of electrical resistivity tomographies in active tectonics: examples from the Tyrnavos Basin, Greece. *J Geodyn* 36:19-35
- Chapot MS, Roberts HM, Duller GAT, Lai ZP (2012) A comparison of natural-and laboratory-generated dose response curves for quartz optically stimulated luminescence signals from Chinese Loess. *Radiat Meas* 47:1045-1052
- Cohen KM, Gibbard PL (2019) Global chronostratigraphical correlation table for the last 2.7 million years, version 2019 QI-500. *Quat Int* 500:20-31
- Crawford JM, Doty WEN, Lee MR (1960) Continuous signal seismograph. *Geophysics* 25:95-105
- Dahm T, Heimann S, Funke S, Wendt S, Rappsilber I, Bindi D, Plenefisch T, Cotton F (2018) Seismicity in the block mountains between Halle and Leipzig, Central Germany: centroid moment tensors, ground motion simulation, and felt intensities of two  $M \approx 3$  earthquakes in 2015 and 2017. *J Seismol* 22:1-19
- Döhler S, Terhorst B, Frechen M, Zhang J, Damm B (2018) Chronostratigraphic interpretation of intermediate layer formation cycles based on OSL-dates from intercalated slope wash sediments. *Catena* 162:278-290
- Drahor MG (2019) Identification of gypsum karstification using an electrical resistivity tomography technique: The case-study of the Sivas gypsum karst area. *Eng Geol* 252:78-98
- Dziewonski AM, Anderson DL (1981) Preliminary reference Earth model. *Phys Earth Planet Int* 25: 297-356
- Ehlers J, Grube A, Stephan HJ, Wansa S (2011) Pleistocene glaciations of North Germany - new results. In: Ehlers J, Gibbard PL, Hughes PD (ed), *Quaternary Glaciations: Extent and Chronology - A Closer Look: Developments in Quaternary Science*, 1st edn, 15:149-162
- Elsner H (2003) Verbreitung und Ausbildung Elster-zeitlicher Ablagerungen zwischen Elm und Flechtinger Höhenzug. *E&G Quat Sci J* 52:91-116
- von Eynatten H, Voigt T, Meier A, Franzke HJ, Gaupp R (2008) Provenance of Cretaceous clastics in the Subhercynian Basin: constraints to exhumation of the Harz Mountains and timing of inversion tectonics in Central Europe. *Int J Earth Sci* 97:1315-1330
- Erslev EA (1986) Basement balancing of Rocky Mountain foreland uplifts. *Geology*, 14:259-262
- Faulkner DR, Mitchell TM, Jensen E, Cembrano J (2011) Scaling of fault damage zones with displacement and the implications for fault growth processes. *J Geophys Res-Solid EA* 116:B5
- Feldmann L (2002) Das Quartär zwischen Harz und Allertal mit einem Beitrag zur Landschaftsgeschichte im Tertiär, Dissertation, TU Clausthal
- Flick H (1986) The Hercynian Mountains - a Postorogenic Overthrust Massif? - *Naturwissenschaften* 73:670-671
- Franke D, Hornung J, Hinderer M (2015) A combined study of radar facies, lithofacies and three-dimensional architecture of an alpine alluvial fan (Illgraben fan, Switzerland). *Sedimentology* 62:57-86
- Franzke HJ, Schmidt, D (1995) Die mesozoische Entwicklung der Harznordrandstörung - Makrogefügeuntersuchungen in der Aufrichtungszone. *Zbl Geol Paläont* 1:1443-1457
- Franzke HJ, Voigt T, von Eynatten H, Brix MR, Burmester G (2004) Geometrie und Kinematik der Harznordrandstörung, erläutert an Profilen aus dem Gebiet von Blankenburg. *Geowiss Mitt Thüringen* 11:39-62
- Franzke HJ, Hauschke N, Hellmund M (2015) Spät Pleistozäne bis früh Holozäne Tektonik in einem Karsttrichter im Bereich der Störungszone des Harznordrandes nahe Benzingerode (Sachsen-Anhalt). *Hall JB Geowiss* 37:1-10
- Frischbutter A (2001) Recent vertical movements (map 4). *Brand Geowiss Beitr* 8:27-31
- Gardner JV, Prior DB, Field ME (1999) Humboldt slide-a large shear-dominated retrogressive slope failure. *Mar Geol* 154:323-338
- Gélis C, Revil A, Cushing ME, Jougnot D, Lemeille F, Cabrera J, De Hoyos A, Rocher M (2010) Potential of electrical resistivity tomography to detect fault zones in limestone and argillaceous formations in the experimental platform of Tournemire, France. *Pure Appl Geophys* 167:1405-1418

- Ghose R, Brouwer J, Nijhof V (1996) A portable S-wave vibrator for high resolution imaging of the shallow subsurface. In: Extended Abstract, 59th EAGE Conference and Technical Exhibition, Amsterdam
- Grollmund B and Zoback MD (2001) Did deglaciation trigger intraplate seismicity in the New Madrid seismic zone? *Geology* 29:175-178
- Grand SP, Van Der Hilst RD, Widiyantoro S (1997) Global seismic tomography: A snapshot of convection in the Earth. *Geol Soc Am* 7:1-7
- Grube A (2019a) Palaeoseismic structures in Quaternary sediments of Hamburg (NW Germany), earthquakes evidence during the younger Weichselian and Holocene. *Int J Earth Sci* 108:845-861
- Grube A (2019b) Palaeoseismic structures in Quaternary sediments, related to an assumed fault zone north of the Permian Peissen-Gnutz salt structure (NW Germany) - Neotectonic activity and earthquakes from the Saalian to the Holocene. *Geomorphology* 328:15-27
- Guerrero J, Bruhn RL, McCalpin JP, Gutiérrez F, Willis G, and Mozafari M (2015) Salt-dissolution faults versus tectonic faults from the case study of salt collapse in Spanish Valley, SE Utah (USA). *Lithosphere*, 7:46-58
- Guitter F, Andrieu-Ponel V, de Beaulieu JL, Cheddadi R, Calvez M, Ponel P, Reille M, Keller T and Goeury C (2003) The last climatic cycles in Western Europe: a comparison between long continuous lacustrine sequences from France and other terrestrial records. *Quat Int* 111:59-74
- Günther T, Rücker C, Spitzer K (2006) Three-dimensional modelling and inversion of DC resistivity data incorporating topography - II. Inversion. *Geophys J Int* 166:506-517
- Hampel A, Hetzel R, Maniatis G, Karow T (2009) Three-dimensional numerical modeling of slip rate variations on normal and thrust fault arrays during ice cap growth and melting. *J Geophys Res* 114:B08406 <https://doi.org/10.1029/2008JB006113>
- Hampel A (2017) Response of faults to climate-induced changes of ice sheets, glaciers and lakes. *Geol Today* 33:12-18
- Heidbach O, Rajabi M, Reiter K, Ziegler M (2016) World stress map 2016. *Science* 277:1956-62
- Hetzel R and Hampel A (2005) Slip rate variations on normal faults during glacial-interglacial changes in surface loads. *Nature* 435:81-84
- Hoffmann G, Reicherter K (2012) Soft-sediment deformation of Late Pleistocene sediments along the southwestern coast of the Baltic Sea (NE Germany). *Int J Earth Sci* 101:351-363
- Hübscher C, Lykke-Andersen H, Hansen MB, Reicherter K (2004) Investigating the structural evolution of the western Baltic. *Eos Trans AGU* 85:115-115
- Huijzer B and Vandenberghe J (1998) Climatic reconstruction of the Weichselian Pleniglacial in northwestern and central Europe. *J Quat Sci* 13:391-417
- Huntley DJ and Lamothe M (2001) Ubiquity of anomalous fading in K-feldspars and the measurement and correction for it in optical dating. *Can J Earth Sci* 38:1093-1106
- Kaiser, A. (2005) Neotectonic modelling of the North German Basin and adjacent areas – a tool to understand postglacial landscape evolution? *Zeitschrift der deutschen Gesellschaft für Geowissenschaften* 156:357-366.
- Kaiser A, Reicherter K, Hübscher C and Gajewski D (2005) Variation of the present-day stress field within the North German Basin-insights from thin shell FE modeling based on residual GPS velocities. *Tectonophysics* 397:55-72
- Kasse C, Vandenberghe D, De Corta F, Van den Haute P (2007) Late Weichselian fluvio-aeolian sands and coversands of the type locality Grubbenvorst (southern Netherlands): sedimentary environments, climate record and age. *J Quat Sci* 22:695-708
- Kiden P, Denys L, Johnston P (2002) Late Quaternary sea-level change and isostatic and tectonic land movements along the Belgian-Dutch North Sea coast: geological data and model results. *J Quat Sci* 17:535-546
- Kierulf HP, Steffen H, Simpson MJR, Lidberg M, Wu P, Wang H (2014) A GPS velocity field for Fennoscandia and a consistent comparison to glacial isostatic adjustment models. *J Geophys Res Sol Ea* 119:6613-6629
- Kim YS, Peacock DC, Sanderson DJ (2004) Fault damage zones. *J Struct Geol* 26:503-517

- Kley J, Franzke HJ, Jähne F, Krawczyk C, Lohr T, Reicherter K, Scheck-Wenderoth M, Sippel J, Tanner D, van Gent H (2008) Strain and stress. In: Littke R, Bayer U, Gajewski D, Dynamics of Complex Intracontinental Basins: The Central European Basin System. Springer Berlin, Heidelberg, pp 97-124
- Kley J and Voigt T (2008) Late Cretaceous intraplate thrusting in central Europe: Effect of Africa-Iberia-Europe convergence, not Alpine collision. *Geology* 36:839-842
- Kockel F (2003) Inversion structures in Central Europe-Expressions and reasons, an open discussion. *Neth J Geosci* 82:351-366
- Krauß L, Zens J, Zeeden C, Schulte P, Eckmeier E, Lehmkuhl F (2016) A Multi-Proxy Analysis of two Loess-Paleosol Sequences in the Northern Harz Foreland, Germany. *Palaeogeogr Palaeoclimatol Palaeoecol* 461:401-417
- Lambeck K (1995) Late Devensian and Holocene shorelines of the British Isles and North Sea from models of glacio-hydro-isostatic rebound. *J Geol Soc Lond* 152:437-448
- Lambeck K, Purcell A, Zhao J, Svensson NO (2010) The Scandinavian Ice Sheet: from MIS 4 to the end of the Last Glacial Maximum. *Boreas* 39:410-435
- Lang J, Winsemann J, Steinmetz D, Polom U, Pollok L, Böhner U, Serangeli J, Brandes C, Hampel A, Winghart S (2012) The Pleistocene of Schöningen, Germany: a complex tunnel valley fill revealed from 3D subsurface modelling and shear wave seismics. *Quat Sci Rev* 39:86-105
- Lang J, Lauer T, Winsemann J (2018) New age constraints for the Saalian glaciation in northern central Europe: implications for the extent of ice sheets and related proglacial lake systems. *Quat Sci Rev* 180:240-259
- Lang J, Alho P, Kasvi E, Goseberg N, Winsemann J (2019) Impact of Middle Pleistocene (Saalian) glacial lake-outburst floods on the meltwater-drainage pathways in northern central Europe: insights from 2D numerical flood simulation. *Quat Sci Rev* 209:82-99
- Lehmkuhl F, Zens J, Krauß L, Schulte P, Kels H (2016) Loess-paleosol sequences at the northern European loess belt in Germany: distribution, geomorphology and stratigraphy. *Quat Sci Rev* 153:11-30
- Leydecker G, Kopera JR (1999) Seismological hazard assessment for a site in Northern Germany, an area of low seismicity. *Eng Geol* 52:293-304
- Leydecker G (2011) Erdbebenkatalog für Deutschland mit Randgebieten für die Jahre 800 bis 2008. *Geol Jb E* 59, Hannover
- Litt T, Behre KE, Meyer KD, Stephan HJ, Wansa S (2007) Stratigraphische Begriffe für das Quartär des norddeutschen Vereisungsgebietes. *E&G Quat Sci J* 56:7-65
- Litt T and Wansa S (2008) Quartär. In: Bachmann GH, Ehling BC, Eichner R, Schwab M (ed), *Geologie von Sachsen-Anhalt*, 1st eds, Schweizerbart, Stuttgart, pp 293-325
- Lohr T, Krawczyk CM, Tanner DC, Samiee R, Endres H, Oncken O, Trappe H, Kukla PA (2007) Strain partitioning due to salt: insights from interpretation of a 3D seismic data set in the NW German Basin. *Bas Res* 19:579-597
- Marotta AM, Bayer U, Scheck M, Thybo H (2001) The stress field below the NE German Basin: effects induced by the Alpine collision. *Geophys J Int* 144:F8-F12
- Marotta AM, Bayer U, Thybo H, Scheck M (2002) Origin of regional stress in the North German basin: Results from numerical modeling. *Tectonophysics*, 360:245-264
- Marotta AM, Mitrovica JX, Sabadini R, Milne G (2004) Combined effects of tectonics and glacial isostatic adjustment on intraplate deformation in central and northern Europe: applications to geodetic baseline analyses. *J Geophys Res: Sol Ea* 109:B1
- Meinsen J, Winsemann J, Roskosch J, Brandes C, Frechen M, Dultz S, Böttcher J (2014) Climate control on the evolution of Late Pleistocene alluvial-fan and aeolian sand-sheet systems in NW Germany. *Boreas* 43:42-66
- Murray AS, Thomsen KJ, Masuda N, Buylaert JP and Jain M (2012) Identifying well-bleached quartz using the different bleaching rates of quartz and feldspar luminescence signals. *Radiat Meas* 47:688-695
- Neely TG, Erslev EA (2009) The interplay of fold mechanisms and basement weaknesses at the transition between Laramide basement-involved arches, north-central Wyoming, USA. *J Struct Geol* 31:1012-1027

- Nocquet JM, Calais E, Parsons B (2005) Geodetic constraints on glacial isostatic adjustment in Europe. *Geophys Res Lett* 32:L06308
- Paul J (2019) Hat sich der Harz im jüngeren Tertiär und Quartär gehoben? *Z Dt Ges Geowiss* 170:95-107
- Peltier W, Argus D, Drummond R (2015) Space geodesy constrains ice age terminal deglaciation: The global ICE-6G\_C (VM5a) model. *J Geophys Res Sol Ea* 120:450-487
- Pisarska-Jamroży M, Belzyt S, Börner A, Hoffmann G, Hüneke H, Kenzler M, Obst K, Rother H, Van Loon T (2018) Evidence from seismites for glacio-isostatically induced crustal faulting in front of an advancing land-ice mass (Rügen Island, SW Baltic Sea). *Tectonophysics* 745:338- 348
- Pisarska-Jamroży M, Belzyt S, Börner A, Hoffmann G, Hüneke H, Kenzler M, Obst K, Rother H, Steffen H, Steffen R, Van Loon T (2019) The sea cliff at Dwasieden: soft-sediment deformation structures triggered by glacial isostatic adjustment in front of the advancing Scandinavian ice-sheet. *DEUQUASP* 2:61-67
- Polom U, Druivenga G, Grossmann E, Grüneberg S and Rode W (2011) Transportabler Scherwellenvibrator: Deutsches Patent und Markenamt. Patentschrift DE10327757B4
- Polom U, Bagge M, Wadas S, Winsemann J, Brandes C, Binot F and Krawczyk CM (2013) Surveying near-surface depocentres by means of shear wave seismics. *First Break* 31
- Poppe S, Holohan E P, Pauwels E, Cnudde V, Kervyn M (2015) Sinkholes, pit craters, and small calderas: Analog models of depletion-induced collapse analyzed by computed X-ray microtomography. *Geol Soc Am Bull* 127:281-296
- Reinecke V (2006) Untersuchung zur jungpleistozänen Reliefentwicklung und Morphodynamik im nördlichen Harzvorland. *Aachen Geogr Arb* 43:1-170
- Roskosch J, Tsukamoto S, Meinsen J, Frechen M, Winsemann J (2012) Luminescence dating of an Upper Pleistocene alluvial-fan and aeolian sandsheet complex: the Senne in the Münsterland Embayment, NW Germany. *Quat Geochronol* 10:94-101
- Roskosch J, Winsemann J, Polom U, Brandes C, Tsukamoto S, Weitkamp A, Bartholomäus WA, Henningsen D, Frechen M (2015) Luminescence dating of ice-marginal deposits in northern Germany: evidence for repeated glaciations during the Middle Pleistocene (MIS 12 to MIS 6). *Boreas* 44:103-126
- Schröder H, Fliegel G, Dahlgrün F, Beck G (1927) Geologische Karte von Preußen und benachbarten deutschen Ländern, 1:25.000, Blatt 4131 Derenburg, Preußisch Geologisches Landesamt, Berlin
- Schröder H, Dahlgrün F, (1927) Erläuterungen zur Geologische Karte von Preußen und benachbarten deutschen Ländern, Blatt 4131 Derenburg, Preußisch Geologisches Landesamt, Berlin
- Shipton ZK, Cowie PA (2003) A conceptual model for the origin of fault damage zone structures in high-porosity sandstone. *J Struct Geol* 25:333-344
- Sirocko F, Reicherter K, Lehné R, Hübscher C, Winsemann J, Stackebrandt W (2008) Glaciation, salt and the present landscape. In: Littke R, Bayer U, Gajewski D, Dynamics of Complex Intracontinental Basins: The Central European Basin System. Springer Berlin, Heidelberg, pp 97-124
- Stackebrandt W (1986) Beiträge zur tektonischen Analyse ausgewählter Bruchzonen der Subherzynen Senke. *Veröff Zentralinst Phys der Erde* 79, Potsdam
- Steffen H, Kaufmann G, Wu P (2006) Three-dimensional finite-element modeling of the glacial isostatic adjustment in Fennoscandia. *Earth Planet Sci Lett* 250:358-375
- Steffen R, Steffen H, Wu P and Eaton D W (2014a) Stress and fault parameters affecting fault slip magnitude and activation time during a glacial cycle. *Tectonics* 33:1461-1476
- Steffen R, Wu P, Steffen H and Eaton DW (2014b) On the implementation of faults in finite-element glacial isostatic adjustment models. *Computers & Geosciences* 62:150-159
- Stewart IS, Sauber J, Rose J (2000) Glacio-seismotectonics: ice sheets, crustal deformation and seismicity. *Quat Sci Rev* 19:1367-1389
- Thorson RM (2000) Glacial tectonics: a deeper perspective. *Quat Sci Rev* 19:1391-1398
- Turpeinen H, Hampel A, Karow T, Maniatis G (2008) Effect of ice sheet growth and melting on the slip evolution of thrust faults. *Earth Planet Sci Lett* 269:230-241



- Ullrich B, Günther T, Rücker C (2008) Electrical Resistivity Tomography Methods for Archaeological Prospection. In: Posluschny A, Lambers K, Herzog I (eds) Layers of Perception. Proceedings of the 35th International Conference on Computer Applications and Quantitative Methods in Archaeology (CAA) Berlin April 26 2007
- Vanneste K, Verbeeck K, Petermans T (2008) Pseudo - 3D imaging of low-slip-rate, active normal fault using shallow geophysical methods: The Geleen fault in the Belgian Maas river valley. *Geophysics* 73:B1-B9
- Ventra D, Nichols GJ (2014) Autogenic dynamics of alluvial fans in endorheic basins: Outcrop examples and stratigraphic significance. *Sedimentology* 61:767-791
- Vermilye JM, Scholz CH (1998) The process zone: A microstructural view of fault growth. *J Geophys Res-Solid EA* 103: 12223-12237
- Voigt T, Wiese F, von Eynatten H, Franzke HJ, Gaupp R (2006) Facies evolution of syntectonic Upper Cretaceous deposits in the Subhercynian Cretaceous Basin and adjoining areas (Germany). *German J Geol* 157:203-244
- Voigt T, von Eynatten H (2008) Field trip POST2–Syntectonic sedimentation in front of a late Cretaceous growth fault-the Harz Mountains and the adjacent Subhercynian Basin (Germany). In: Voigt T, von Eynatten H, Franzke HJ (2004) Excursion Guidebook: 26th Regional Meeting of the International Association of Sedimentologists (IAS) held Jointly with the SEPM-CES Sediment 2008 Meeting, Bochum, Germany, September 1-3 2008, Mecke Druck und Verlag 237:59-94
- Voigt T, von Eynatten H, Kley J (2009) Kommentar zu „Nördliche Harzrandstörung: Diskussionsbeiträge zu Tiefenstruktur, Zeitlichkeit und Kinematik“ von Volker Wrede *Z d Ges Geowiss* 159:293-316, *Z d Ges Geowiss* 160:93-99
- Wadas SH, Polom U, Krawczyk CM (2016) High-resolution shear wave seismic reflection as a tool to image near-surface subsosion structures - a case study in Bad Frankenhausen, Germany. *Solid Earth* 7:1491-1508
- Weymann HJ (2004) Die mittelpleistozäne Flussentwicklung im nord-östlichen Harzvorland. - Petrographie, Terrassenstratigraphie. *Geol Beitr Hannover* 6:3-116
- Weymann HJ, Feldmann L, Bombien H (2005) Das Pleistozän des nördlichen Harzvorlands - eine Zusammenfassung. *E&G Quat Sci J* 55:43-63
- Winsemann J, Lang J, Roskosch J, Polom U, Böhner U, Brandes C, Glotzbach C, Frechen M (2015) Terrace styles and timing of terrace formation in the Weser and Leine valleys, northern Germany: Response of a fluvial system to climate change and glaciations. *Quat Sci Rev* 123:31-57
- Winsemann J, Koopmann H, Tanner DC, Lutz R, Lang J, Brandes C, Gaedicke C (2020) Seismic interpretation and structural restoration of the Heligoland glaciotectionic thrust-fault complex: Implications for multiple deformation during (pre-) Elsterian to Warthian ice advances into the southern North Sea Basin. *Quat Sci Rev* 227:106068
- Wintle AG, Murray AS (2006) A review of quartz optically stimulated luminescence characteristics and their relevance in single-aliquot regeneration dating protocols. *Radiat Meas* 41:369- 391
- Woolery EW, Street RL, Wang Z, Harris JB (1993) Near-surface deformation in the New Madrid Seismic zone as imaged by high resolution SH-wave seismic methods. *Geophys Res Lett* 20:1615-1618
- Wrede V (1988) Der nördliche Harzrand. Flache Abscherbahn oder wrench-fault-system? *Int J Earth Sci* 77:101-114
- Wrede V (2008) Nördliche Harzrandstörung: Diskussionsbeiträge zu Tiefenstruktur, Zeitlichkeit und Kinematik. *Z dt Ges Geowiss* 159:293-316
- Wrede V (2009) Antwort auf den Kommentar von T. Voigt, H. von Eynatten and J. Kley zu „Nördliche Harzrandstörung: Diskussionsbeiträge zu Tiefenstruktur, Zeitlichkeit und Kinematik“. *Z dt Ges Geowiss* 160:100-106
- Wu P and Hasegawa HS (1996a) Induced stresses and fault potential in eastern Canada due to a realistic load: a preliminary analysis. *Geophys J Int* 127:215-229
- Wu P and Hasegawa HS (1996b) Induced stresses and fault potential in Eastern Canada due to a disc load: a preliminary analysis. *Geophys J Int* 125:415-430

- Wu P (1997) Effect of viscosity structure on fault potential and stress orientations in Eastern Canada. *Geophys J Int* 130:365-382
- Wu P (2004) Using commercial finite element packages for the study of earth deformations, sea levels and the state of stress. *Geophys J Int* 158:401-408
- Wu P, Wang H, Steffen H (2013) The role of thermal effect on mantle seismic anomalies under Laurentia and Fennoscandia from observations of Glacial Isostatic Adjustment. *Geophys J Int* 192:7-17
- Yilmaz O 1987 *Seismic Data Processing*: Society of Exploration Geophysicists, Tulsa, Oklahoma 2:82-153
- Yonkee W, and Weil AB (2015) Tectonic evolution of the Sevier and Laramide belts within the North American Cordillera orogenic system. *Earth Sci Rev* 150:531-593
- Zhao S, Lambeck K, Lidberg M (2012) Lithosphere thickness and mantle viscosity inverted from GPS-derived deformation rates in Fennoscandia. *Geophys J Int* 190:278-292

## Supplementary data to Publication 1

### **Structural style and neotectonic activity along the Harz Boundary Fault, northern Germany: A multimethod approach integrating geophysics, outcrop data and numerical simulations**

Katharina Müller<sup>1</sup>, Ulrich Polom<sup>2</sup>, Jutta Winsemann<sup>1</sup>, Holger Steffen<sup>3</sup>, Sumiko Tsukamoto<sup>2</sup>, Thomas Günther<sup>2</sup>, Jan Igel<sup>2</sup>, Thomas Spies<sup>4</sup>, Thomas Lege<sup>4</sup>, Manfred Frechen<sup>2</sup>, Hans-Joachim Franzke<sup>5</sup> and Christian Brandes<sup>1</sup>

<sup>1</sup>Institut für Geologie, Leibniz Universität Hannover, Callinstraße 30, 30167 Hannover, Germany

<sup>2</sup>Leibniz Institute for Applied Geophysics (LIAG), Stilleweg 2, 30655 Hannover, Germany

<sup>3</sup>Lantmäteriet, Geodetic Infrastructure Referenssystem, Lantmäterivägen 2C, 80102 Gävle, Sweden

<sup>4</sup>Bundesanstalt für Geowissenschaften und Rohstoffe (BGR), Stilleweg 2, 30655 Hannover, Germany

<sup>5</sup>Institut für Geologie und Paläontologie der Technischen Universität Clausthal, Leibnizstraße 10, 38678 Clausthal-Zellerfeld, Germany

## **Luminescence dating**

### **Dose rate determination**

The radionuclide concentrations of uranium (U), thorium (Th), and potassium (K) were measured using high-resolution gamma spectrometry. 700 g of the sediment surrounding each sample were dried (130 °C) homogenized and packed into so-called Marinelli-beakers. To achieve an equilibrium between radon and its daughter nuclides, the samples were stored for at least six weeks before measuring. The radiation dose rates were calculated by using the conversion factors of Guérin et al. (2011) and the beta attenuation factors of Mejdahl (1979). An a-value of  $0.04 \pm 0.01$  for quartz and an a-value of  $0.09 \pm 0.02$  for feldspar were used (Rees-Jones 1995). The in-situ water content of all samples was measured and used for the calculation of the attenuation caused by the contained water and therefore for the correction of the  $\alpha$ -,  $\beta$ - and  $\gamma$ -dose rates. The cosmic dose rate was calculated taking into account altitude, geomagnetic latitude and sediment thickness according to Prescott and Hutton (1994). The results of the dose rate determination are listed in Table S1.

### **Sample preparation**

The preparation of the samples for luminescence measurements was carried out under subdued red light in the luminescence laboratory. The outer ends (2 cm) of the undisturbed material in cylinders were removed to exclude any sediment that was exposed to light. For the luminescence

measurement 50 - 100 g of the sample material was dried at  $\leq 50^{\circ}\text{C}$  and chemically treated with 10% hydrochloric acid (HCl) until the reaction stopped. Afterwards, 200 ml disodium oxalate ( $\text{Na}_2\text{C}_2\text{O}_4$ ) was added for 2 hours and 30% hydrogen peroxide ( $\text{H}_2\text{O}_2$ ) was added for 12 hours to dissolve carbonates, break up aggregates and to eliminate the organic matter. Subsequently the grain fraction of 4 - 11  $\mu\text{m}$  was separated for luminescence measurement of quartz and polymineral fine grains. For the quartz aliquots, a part of the sample was treated with 40% hexafluorosilicic acid ( $\text{H}_2\text{SiF}_6$ ) to remove feldspar (Prasad 2000; Fuchs et al. 2005). Finally, the polymineralic and the quartz aliquots were mounted on aluminium discs for the luminescence measurement

Supplementary data to Publication 1

Table S1: Dosimetry results and dose rates for the samples from Benzingerode. For the feldspar samples, an a-value of  $0.09 \pm 0.02$  and for quartz an a-value of  $0.04 \pm 0.01$  was used.

Sample	Water content (%)	Depth (m)	Radionuclide concentrations			Dose rate				Total dose rate	
			Potassium (%)	Thorium (ppm)	Uranium (ppm)	$D_\alpha$ ( $\text{mGy a}^{-1}$ )	$D_\beta$ ( $\text{mGy a}^{-1}$ )	$D_\gamma$ ( $\text{mGy a}^{-1}$ )	$D_{\text{cosmic}}$ ( $\text{mGy a}^{-1}$ )	Feldspar ( $\text{mGy a}^{-1}$ )	Quartz ( $\text{mGy a}^{-1}$ )
<b>Ben-2</b>	10±5	1.8	2.24±0.12	12.00±0.64	3.27±0.18	1.21±0.22 0.56±0.13	2.53±0.09 2.53±0.14	1.43±0.08 1.43±0.09	0.22±0.2 0.22±0.2	4.81±0.24	4.24±0.21
<b>Ben-3</b>	7±4	0.84	1.11±0.07	4.97±0.29	4.88±0.26	0.51±0.13	1.64±0.12	0.95±0.09	0.22±0.2		3.06±0.20
<b>Ben-4</b>	7±4	1.03	0.65±0.04	2.52±0.17	4.45±0.24	0.42±0.12	1.15±0.11	0.68±0.08	0.22±0.2		2.28±0.19
<b>Ben-5</b>	4±2	0.93	0.53±0.04	2.32±0.16	2.79±0.16	0.28±0.10	0.84±0.09	0.49±0.08	0.22±0.2		1.75±0.17
<b>Ben-6</b>	7±4	0.94	0.78±0.05	2.90±0.19	3.40±0.19	0.34±0.11	1.13±0.10	0.64±0.08	0.22±0.2		2.17±0.18
<b>Ben-7</b>	8±4	0.83	0.94±0.06	3.74±0.23	4.35±0.23	0.44±0.12	1.40±0.11	0.80±0.08	0.22±0.2		2.61±0.19

## Luminescence measurements

Feldspar and quartz luminescence signals were measured with two automated Risø TL/OSL readers (DA-20) with calibrated  $^{90}\text{Sr}/_{90}\text{Y}$  beta sources (1.48 GBq = 40 mCi and 2.96 GBq = 80 mCi) delivering between 0.08 and 0.09 Gy s<sup>-1</sup>. Polyminerals were used for infrared stimulated luminescence (IRSL) dating, where only the feldspar is stimulated by pulsed IR light-emitting diodes (LED) with wavelengths of 870 nm. To detect a stable IRSL signal with reduced anomalous fading, the feldspar signal was detected in the off-periods of each pulsed cycle with a Schott BG39/Corning 7-59 filter combination (Tsukamoto et al. 2006; 2017). The quartz signal was stimulated by blue LED diodes, emitting at 470 nm and detected through a Hoya U-340 filter. A single-aliquot regenerative dose (SAR) protocol after Murray and Wintle (2000) was applied for equivalent dose ( $D_e$ ) determination (see Table S2).

Table S2: SAR protocol used for equivalent dose determination of feldspar and quartz samples (after Murray and Wintle 2000).

Step	Treatment	Observed	
	Feldspar IRSL (polymineral)	Quartz OSL	
1	Give dose	Give dose	
2	Preheat, 250°C, 60 s	Preheat, 240°C, 10 s	
3	Pulsed IRSL, 50°C, 500 s <sup>a</sup>	OSL, 125°C, 40 s	Lx
4	Test dose	Give test dose	
5	Preheat, 250°C, 60 s	Heat to 160°C	
6	Pulsed IRSL, 50°C, 500s <sup>a</sup>	OSL, 125°C, 40 s	Tx
7	Return to step 1	Return to step 1	

<sup>a</sup> 100  $\mu\text{s}$  on and 400  $\mu\text{s}$  off

### *Polymineral fine grain (feldspar)*

Only sample Ben-2 (DF-1) was dated using polymineral fine grain, because the other samples did not give a measurable feldspar signal. For the  $D_e$  determination a total of 8 aliquots were measured. For the measurement, a preheat temperature of 250°C for 60 s and a pulsed IRSL signal was used (Table S2). The pulsed IR stimulation was performed at 50°C (IR<sub>50</sub>). To reduce anomalous fading of the feldspar, the signal was only detected in the off-period of the light source, 21.5  $\mu\text{s}$  after the LED pulses were switched off (Tsukamoto et al. 2006, 2017; Jain et al. 2015).

Additionally, to check if the used protocol is suitable, a dose recovery test was carried out by using 4 aliquots. For the dose recovery ratio, the aliquots were bleached for 4 hours in the solar simulator. A dose close to the expected natural one was given and the same SAR protocol was applied to check if the given dose could be accurately recovered. The protocol is suitable, if the dose recovery ratio is within the range of 0.9-1.1 (Wintle and Murray 2006).

### *Fading tests*

Fading tests are necessary because feldspar minerals are affected by a phenomenon called anomalous fading, where a tunnelling-induced loss of trapped electrons occurred (Wintle 1973; Spooner 1994). This phenomenon can lead to an underestimation of the age (Wintle 1973; Jain et al. 2015). For feldspar aliquots, a fading correction was therefore performed by determining the anomalous fading rate under laboratory conditions (Huntley and Lamothe 2001). For young

samples (up to 50 ka) age correction models relating to the 'linear part' of the dose response curve are used (Huntley and Lamothe 2001). Fading rates (g-values) were determined by using 8 aliquots using the log-decay model (Huntley and Lamothe 2001).

### Quartz

A total of 8 quartz aliquots per sample were measured. The preheat temperature, which should be selected for accurate equivalent dose determination ( $D_e$ ) was determined by applying the preheat plateau test at six different preheat temperatures (160 - 260 °C) with a fixed low cutheat temperature at 160 °C (Fig. S1a). This low cutheat temperature is suggested for dating young samples (Madsen and Murray 2009). Additionally, a dose recovery test was performed (Fig. S1b). Details about this procedure are shown in Wintle and Murray (2006). According to the results we selected a preheat temperature of 240 °C for the quartz  $D_e$  measurement of sample Ben-2 (Fig. S1c) to Ben-7 using the SAR protocol shown in Table S2. Only sample Ben-2 gave a reliable quartz luminescence age. The other samples (Ben-3 to 7) were in saturation and did not give reliable quartz luminescence ages.

### Age calculation

The fading uncorrected pulsed IR<sub>50</sub> feldspar age and quartz ages were calculated using the mean  $D_e$  value of all accepted aliquots. The fading corrected age of feldspar sample Ben-2 was calculated by using the R-Luminescence Package (R version 3.3.2), which is based on Huntley and Lamothe (2001). The OSL ages were calculated by dividing the equivalent dose ( $D_e$ ) by the total dose rate ( $D_R$ ).

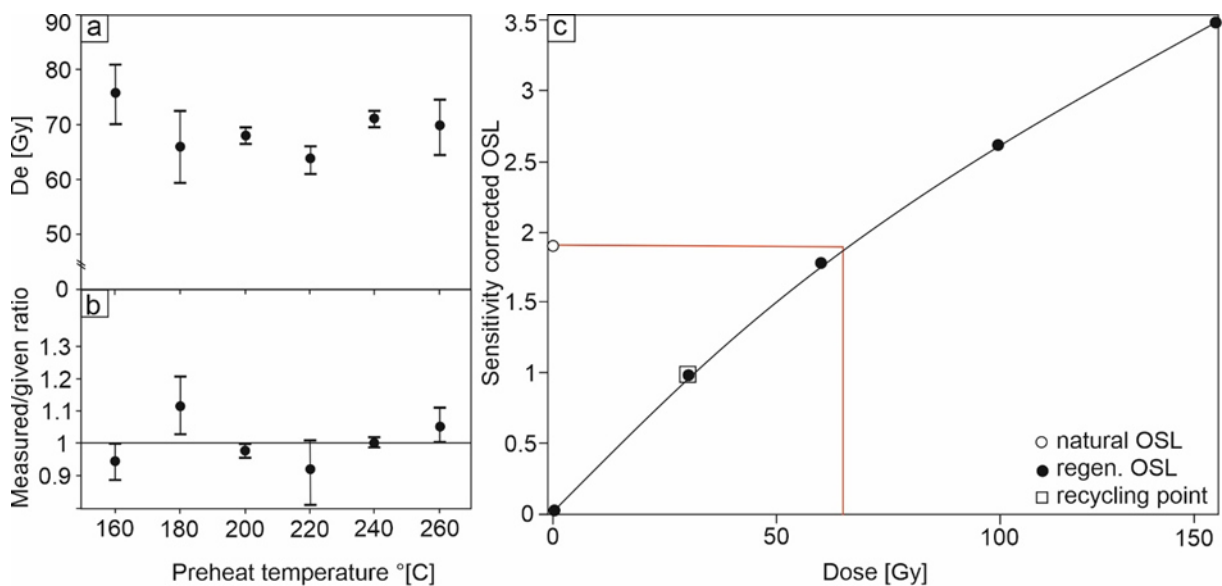


Figure S1: Performance tests for luminescence dating; a) preheat plateau test; b) dose recovery test and c)  $D_e$  determination of sample Ben-2. The preheat temperature of 240 °C was selected, which gave the dose recovery ratio closest to unity.



## References

- Fuchs M, Straub J, Zöller L (2005) Residual luminescence signals of recent river flood sediments: a comparison between quartz and feldspar of fine- and coarse-grain sediments. *Anc TL* 23:25-30
- Guérin G, Mercier N, Adamiec G (2011) Dose-rate conversion factors: update. *Anc TL* 29:5-8
- Huntley DJ, Lamothe M (2001) Ubiquity of anomalous fading in K-feldspars and the measurement and correction for it in optical dating. *Can J Earth Sci* 38:1093–1106
- Jain M, Buylaert JP, Thomsen KJ, Murray AS (2015) Further investigations on ‘non-fading’ in K-Feldspar. *Quat Int* 362:3-7
- Madsen AT and Murray AS (2009) Optically stimulated luminescence dating of young sediments: a review. *Geomorphology* 109:3-16
- Mejdahl V (1979) Thermoluminescence dating: Beta-dose attenuation in quartz grains. *Archaeometry* 21:61-72
- Murray AS, Wintle A G (2000) Luminescence dating of quartz using an improved single-aliquot regenerative-dose protocol. *Radiat Meas* 32:57-73
- Murray AS, Thomsen KJ, Masuda N, Buylaert JP and Jain M (2012) Identifying well-bleached quartz using the different bleaching rates of quartz and feldspar luminescence signals. *Radiat Meas* 47:688-695
- Prasad S (2000) HF treatment for the isolation of fine grain quartz for luminescence dating. *Anc TL* 18:15-17
- Prescott JR, Hutton JT (1994) Cosmic ray contributions to dose rates for luminescence and ESR dating: large depths and long-term time variations. *Radiat Meas* 23:497-500
- Rees-Jones J (1995) Optical dating of young sediments using fine-grain quartz. *Anc TL* 13:9-14
- Spooner NA (1994) The anomalous fading of infrared-stimulated luminescence from feldspars. *Radiat Meas* 23:625-632
- Tsukamoto S, Denby PM, Murray AS, Bøtter-Jensen L (2006) Time-resolved luminescence from feldspars: new insight into fading. *Radiat Meas* 41:790-795
- Tsukamoto S, Kondo R, Lauer T, Jain M (2017) Pulsed IRSL: A stable and fast bleaching luminescence signal from feldspar for dating Quaternary sediments. *Quat Geochronol* 41:26-36
- Wintle AG (1973) Anomalous fading of thermo-luminescence in mineral samples. *Nature* 245:143
- Wintle AG, Murray AS (2006) A review of quartz optically stimulated luminescence characteristics and their relevance in single-aliquot regeneration dating protocols. *Radiat Meas* 41:369–391

## Publication 2

This chapter has been published as Müller et al. 2021,  
In: Steffen H, Olesen O and Sutinen R (eds) Glacially-Triggered Faulting,  
Cambridge University Press

### Glacially-Induced Faults in Germany

Katharina Müller<sup>1</sup>, Jutta Winsemann<sup>1</sup>, David C. Tanner<sup>2</sup>, Thomas Lege<sup>3</sup>, Thomas Spies<sup>3</sup> and Christian Brandes<sup>1</sup>

<sup>1</sup>Institut für Geologie, Leibniz Universität Hannover, Callinstraße 30, 30167 Hannover, Germany

<sup>2</sup>Leibniz Institute for Applied Geophysics (LIAG), Stilleweg 2, 30655 Hannover, Germany

<sup>3</sup>Bundesanstalt für Geowissenschaften und Rohstoffe (BGR), Stilleweg 2, 30655 Hannover, Germany

Corresponding Author: Katharina Müller, Institut für Geologie, Leibniz Universität Hannover, Callinstraße 30, 30167 Hannover, Germany

Email: [mueller@geowi.uni-hannover.de](mailto:mueller@geowi.uni-hannover.de)

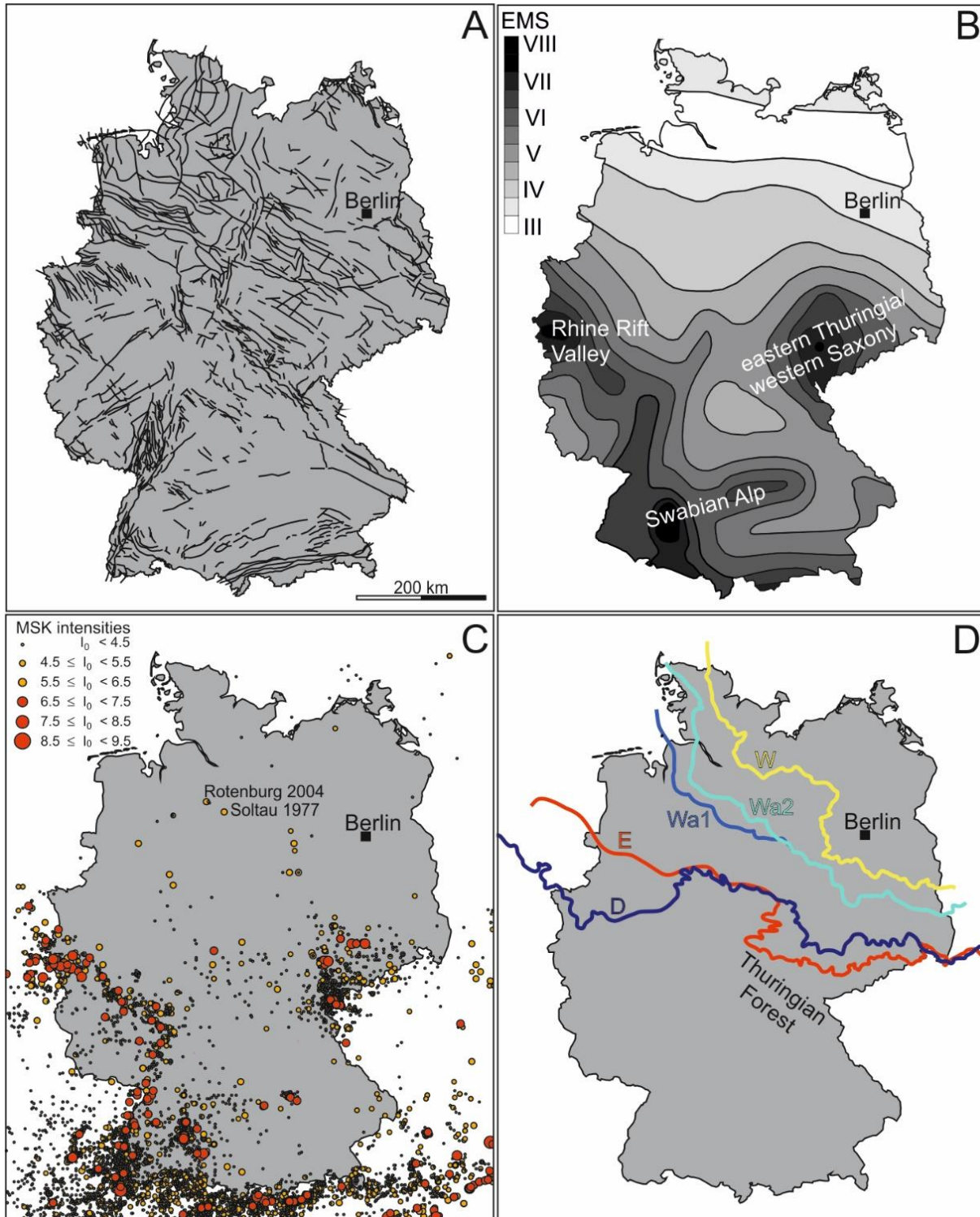
## Abstract

Germany is a geologically diverse, intraplate setting that was affected by several tectonic phases. This has caused a complex fault pattern. Despite the intraplate setting, significant palaeo-, historical, and recent seismicity has been observed on many faults, especially in three zones of crustal weakness: The Rhine Rift Valley, the Swabian Alp, and eastern Thuringia/western Saxony. Recent studies have shown that the low seismicity of northern Germany is characterised by fault activity caused by the decay of the Late Pleistocene (Weichselian) ice sheet. Several faults and fault systems show evidence of neotectonic activity, such as the Aller Valley Fault, Halle Fault system, Harz Boundary Fault, Steinhuder Meer Fault, Osning Thrust, all of which are oriented parallel to the margin of the Pleistocene ice sheets. The timing of fault movements implies that the seismicity in northern Germany is likely induced by varying lithospheric stress conditions related to glacial isostatic adjustment (GIA) and the faults can be thus classified as glacially-induced faults (GIFs). For the Osning Thrust, the Harz Boundary Fault and the Schaabe Fault, this is supported by numerical simulation of GIA-related stress field changes. GIA processes are also a likely driver for the historical and parts of the recent fault activity. The southern extent of GIA-induced fault reactivations caused by the decay of the Fennoscandian ice sheet is not clear. Modelling results imply the influence of GIA reached up to 230 km south of the former Weichselian ice sheet. GIA processes are also described for the Alps, but it is difficult to clearly distinguish between reactivation of faults in the foreland of the Alps due to the Alpine collision and GIA processes.

**Keywords:** Agricola Fault, Aller Valley Fault System, Coulomb Failure Stress (CFS) Modelling, Germany, Halle Fault System, Harz Boundary Fault, Langeland Fault, Lateglacial, Leine Valley Fault System, Osning Thrust, Prerow Fault Schaabe Fault, Steinhuder Meer Fault, Thor Suture, Weser Valley Fault System, Were Fault, Wiek Fault

## Introduction

The geological structure of Germany was shaped by terrane accretion during the Caledonian and Variscan orogenies in the Palaeozoic and subsequently overprinted by Late Palaeozoic, Mesozoic and Cenozoic tectonic phases. The latter include the inversion tectonics in Central Europe, the Alpine collision and the rift phase in the Rhine Valley. This polyphase tectonic history has created a complex fault pattern (Figure 1A). The majority of today's seismically active faults are concentrated in the Rhine Rift Valley, the Swabian Alp and eastern Thuringia/western Saxony, including the earthquake swarm area of the Vogtland (Figure 1B) (Grünthal et al., 1998).



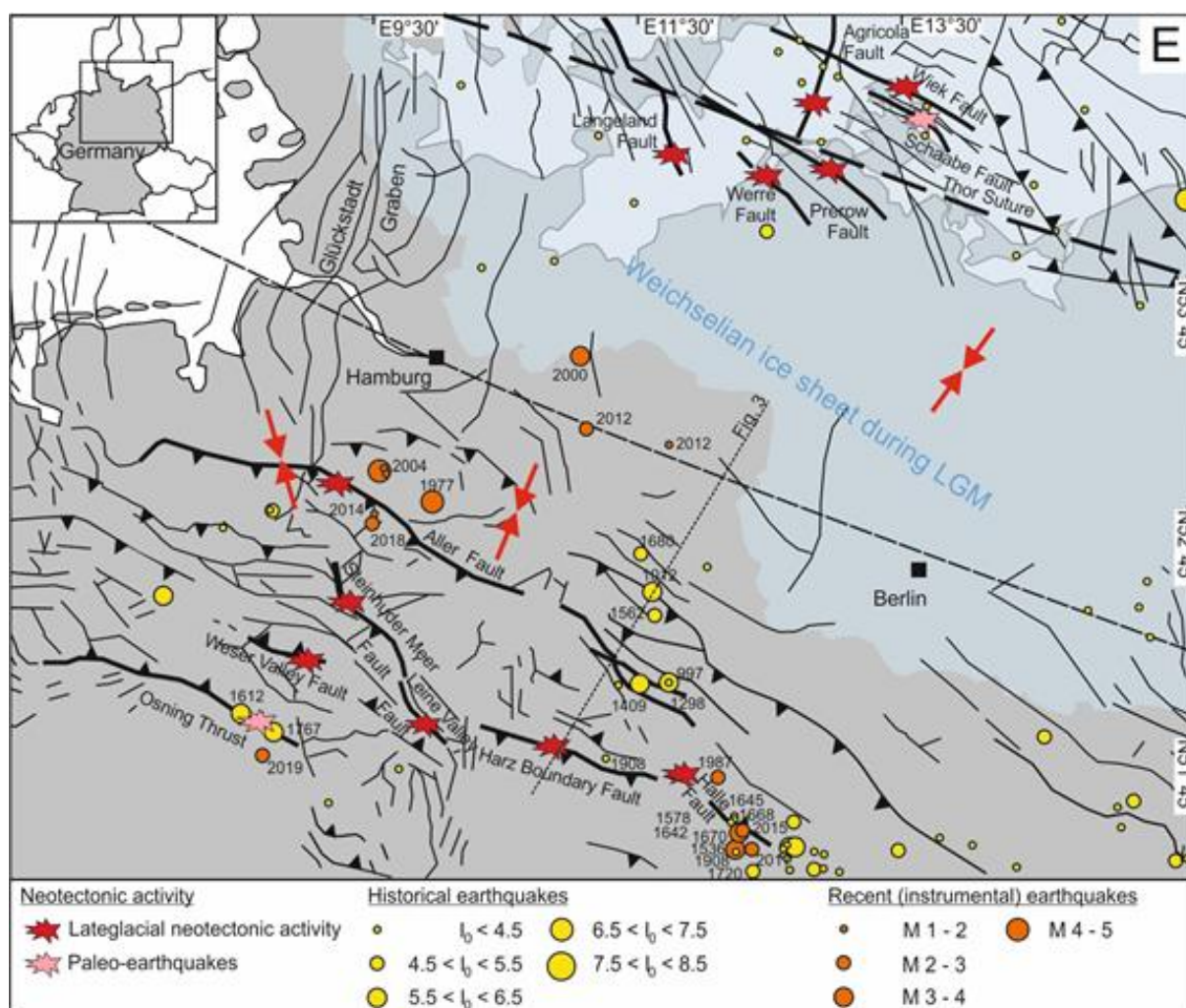


Figure 1: Map of Germany. (A) Major faults and fault systems in Germany (modified after Schulz, 2013). (B) Intensity-based earthquake hazard map. The greyscale displays the macro seismic intensities using the European Macroseismic Scale (EMS) (modified after Grünthal et al., 1998). (C) Map of earthquake epicentres and adjacent areas for the period 800–2008 CE (modified after Leydecker, 2011). (D) Maximum extents of the Elsterian (E), Saalian Drenthe (D), Warthe 1 (Wa1), Warthe 2 (Wa2) and Weichselian (W) ice sheets (modified after Winsemann et al., 2020). (E) Tectonic activity along major basement faults in northern Germany. Shown are neotectonic activity, historical earthquakes and recent earthquakes (modified after Brandes et al., 2015; faults from Kley & Voigt, 2008; Seidel et al., 2018; Elbe line from Scheck-Wenderoth & Lamarch, 2005). The red arrows show the recent stress field orientation taken from Marotta et al. (2000, 2002). The numbers represent the years of the earthquakes, which are listed in Table 1.

Historical earthquakes, with epicentral intensities of up to IX, have occurred in Germany during the last 1,200 years (Figure 1C) (Leydecker, 2011), indicating repeated fault activity. In the last 100 years, seismic activity has been instrumentally detected. Besides natural tectonic earthquakes, there have been several recent earthquakes in northern Germany, with epicentres near active gas fields that have been interpreted as the consequence of hydrocarbon exploitation (Dahm et al., 2007, 2015).

Recent studies have shown that northern Germany is characterised by a Lateglacial fault activity that is attributed to fault reactivation caused by the decay of the Late Pleistocene Weichselian ice sheet (Figure 1D, E) (Brandes et al., 2012). A study on fault-reactivation in intraplate areas controlled by ice sheet movements were published by Reicherter et al. (2005). In addition, along salt structures that reach near the Earth’s surface, e.g. the Schlieven and Marnitz salt pillows in

south-western Mecklenburg (Müller & Obst, 2008) and the Sperenberg and Rambow salt diapirs in Brandenburg (Stackebrandt, 2005, 2015), there is evidence of reactivated basement structures caused by glacial isostatic adjustment (GIA). See also the modelling study of Lang et al. (2014).

Numerical modelling studies imply that many faults in northern Germany became unstable due to glacial isostatic adjustment (GIA)-related stress-field changes (Brandes et al., 2012, 2015; Pisarska-Jamroży et al., 2019; Müller et al. 2020b). These findings raise the question of whether there are other glacially-induced faults (GIFs) in Germany.

GIFs have been documented in Fennoscandia over the last six decades (e.g. Kujansuu, 1964; Mörner, 1978), a region that was covered by large ice sheets during the Pleistocene. The occurrence of GIFs outside the former glaciated areas is a novelty and has a significant impact on the distribution of neotectonic activity in Germany (and other areas), as shown by the modelling results of Grollmund and Zoback (2001), Hampel et al. (2009), Brandes et al. (2015), Pisarska-Jamroży et al. (2019), (Müller et al. 2020b), and therefore requires re-evaluation. Potential GIFs can occur in northern and southern Germany, related to the Fennoscandian ice sheet (Figure 1D) and the Alpine ice cover, respectively.

The extent of the area prone to fault reactivation is not clear. The results of Brandes et al. (2015) imply a GIA influence as far south as the Thuringian Forest, located up to 230 km south of the former Weichselian ice sheet. Grützner et al. (2016), Vanneste et al. (2018) and van Balen et al. (2019) have discussed a potential GIA effect on the faults in the Lower Rhine Rift Valley. However, these faults were already active before the Pleistocene, and a clear reactivation due to GIA processes, e.g. supported by modelling studies, has not yet been shown. Therefore, this study focuses on northern Germany.

## **Geological Setting**

### **Main Geological Structures**

The geological evolution of Germany was significantly influenced by the Cadomian, Caledonian, Variscan and Alpine orogenies (McCann et al., 2008). The area consists of a terrane assemblage that was formed progressively during the closure of the Tornquist Sea, the Rhenohercynian Ocean and the Saxothuringian Ocean (Torsvik & Cocks, 2017). From north to south, Germany consists of the East Avalonian Terrane, the Saxothuringian Terrane (composed of Franconia and Thuringia) and the Moldanubian Terrane (Franke, 2000; Franke et al., 2017). The subdivision of the Variscan orogenic belt into three zones, as originally defined by Kossmat (1927), the so-called Rhenohercynian, Saxothuringian and Moldanubian zone, reflects this terrane assemblage (Figure 2A).



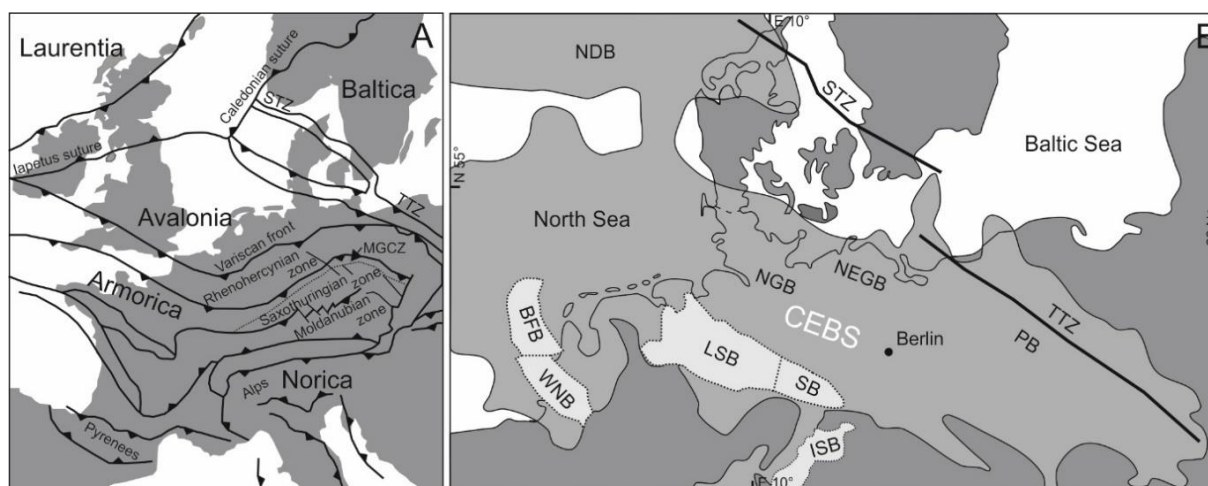


Figure 2: A) Tectonostratigraphic units of Germany. TTZ – Tornquist-Teisseyre Zone; STZ – Sorgenfrei-Tornquist Zone; MGCZ – Mid-German Crystalline Zone (modified after Meschede, 2015). B) Overview of the sedimentary basins in the study area; CEBS – Central European Basin System; NGB – North German Basin; NEGB – Northeast German Basin; NDB – Norwegian Danish Basin; PB – Polish Basin; BFB: Broad Fourteens Basin; LSB: Lower Saxony Basin; SB – Subhercynian Basin; WNB – West Netherlands Basin, ISB – intramontane Saale Basin (modified after Scheck-Wenderoth and Lamarch, 2005; Pharaoh et al., 2010).

### The Central European Basin System

Northern Germany forms part of the Central European Basin System (CEBS) (Figure 2B). After the Variscan Orogeny, the CEBS evolved on top of a Carboniferous Variscan foreland basin (Littke et al., 2008). During Permian times, after the filling of the peripheral foreland basin, a rift system developed (e.g. Gast & Gundlach, 2006). North-south-striking normal faults were the major structural elements. Strong subsidence in this area during the Mesozoic (e.g. van Wees et al., 2000) was followed by a tectonic inversion phase in Late Cretaceous to Early Palaeocene times (e.g. Mazur et al., 2005; Kley & Voigt, 2008). Within the CEBS an elongated zone of subsidence (the so-called Mid-German subsidence zone) has shown neotectonic activity since the Oligocene (Stackebrandt, 2004, 2015).

Today, the CEBS consists of several sub-basins such as the North German Basin, the Northeast German Basin, the Lower Saxony Basin and the Subhercynian Basin (Figure 2B). As a consequence of different tectonic phases mentioned above, northern Germany is characterised by a dense fault array with several major faults (striking NW-SE) and fault zones with minor faults striking NE-SW or NNE-SSW (Reicherter et al., 2005, see Figure 1A, E).

### Pleistocene Glaciations

From the Middle Pleistocene onwards, northern Germany was repeatedly influenced by glaciations (Ehlers et al., 2011; Figure 1D) and was therefore affected by stresses caused by glacial loading and unloading. The oldest ice advance may have reached the study area during the Cromerian (Marine Isotope Stage (MIS) 16?), or even earlier, during the Menapian (MIS 34) (Ehlers et al., 2011; Winsemann et al., 2020).

The following Middle Pleistocene glaciations are termed Elsterian and Saalian, where the latter is the younger. The Elsterian glaciation was characterised by three ice advances that are recorded in northern Germany (Eissmann, 2002; Ehlers et al., 2011). It probably can be correlated with

MIS 12 and/or MIS 10 (Roskosch et al., 2015; Lauer & Weiss, 2018). Three major ice advances with several sub-phases occurred during the Saalian glaciation (Eissmann, 2002; Ehlers et al., 2011; Lang et al., 2018; Winsemann et al., 2020). They are commonly correlated with MIS 6 and are referred to as the Drenthe and Warthe ice advances (Figure 1D; Ehlers et al., 2011; Lang et al., 2018; Winsemann et al., 2020). However, there is evidence for an ice advance during MIS 8, as well (Roskosch et al., 2015).

The Late Pleistocene Weichselian ice sheet did not cross the Elbe river, and thus periglacial conditions prevailed in northern Germany (Eissmann, 2002; Meinsen et al., 2014; Lehmkuhl et al., 2016). Three main ice marginal positions are known in northeastern Germany from the Weichselian glaciation. The peak of the Eurasian ice sheet in terms of global ice volume, often referred to as the last glacial maximum (LGM), occurred at around 21–20 ka (Hughes et al., 2016), but in northeastern Germany the maximum extent was reached at around 30 ka (Hardt et al., 2016), while further to the west, in Mecklenburg and Schleswig-Holstein, it was reached at around 24 ka (Böse et al., 2012) (Figure 1D, E). Subsequently, the ice rapidly melted and retreated. A standstill phase during the down-wasting period occurred, which was later followed by the third minor re-advance (Lüthgens & Böse, 2011; Hardt et al., 2016; Hardt & Böse, 2018).

### **The Stress Field**

The present-day stress field in the CEBS has a fan-shaped pattern (Marotta et al., 2002, 2004). The North German Basin is characterised by NW-SE compression and NE-SW extension (Reinecker et al., 2004; Heidbach et al., 2016), whereas the area of the Northeast German Basin shows a NE-SW compression. The major controls on the stress field, which have an effect on the faults in the CEBS, are the NW-SE-directed force induced by the North Atlantic ridge push and the N-S-directed force caused by the Alpine collision (Marotta et al., 2002; Kaiser et al., 2005).

During and after the Cretaceous inversion phase, the compressional stress field in northern Germany was NE-SW and rotated counterclockwise from NE-SW to NW-SE in the Neogene (Kley & Voigt, 2008). From the Pleistocene onwards to the present day, the main factor that influenced the stress field was the postglacial rebound of Fennoscandia (Kaiser et al., 2005). The growth and decay of the Fennoscandian ice sheet induced a temporal stress field that matched the orientation of the palaeo-stress field in northern Germany. This NNE-SSW oriented major stress direction led to the reactivation of pre-existing mainly Mesozoic faults.

Knowledge of the southern extent of GIA processes caused by the Fennoscandian ice sheet in Germany is limited. Coulomb failure stress (CFS) modelling results show that GIA processes play a major role in the area between the Magdeburger Börde and the Sorgenfrei-Tornquist Zone (Figure 2), while the area south of the Thuringian Forest experienced minor influence by GIA processes (Figure 1D) (Brandes et al., 2015). However, GIA processes are also described for the Alps (e.g. Norton & Hampel, 2010; Mey et al., 2016), but it is difficult to clearly distinguish GIA fault activity in the foreland of the Alps due to the ongoing Alpine collision.

## Neotectonic Activity and Seismicity in Northern Germany

### Palaeoseismological Studies and GIA Induced Movements

Evidence of palaeo-earthquakes is shown by Brandes et al. (2012) and Brandes and Winsemann (2013) for the Osning Thrust. Hoffmann and Reicherter (2012) and Pisarska-Jamroży et al. (2018, 2019) found evidence of seismic activity in Pleistocene sediments along the south-western coast of the Baltic Sea in the area of Usedom and Rügen Island. In addition, studies by Hübscher et al. (2004), Lehné and Sirocko (2007, 2010), Brandes et al. (2011), Ludwig (2011), Brandes and Tanner (2012), Al Hseinat and Hübscher (2014), Brandes et al. (2015), Al Hseinat et al. (2016), Grützner et al. (2016), Al Hseinat and Hübscher (2017), Brandes et al. (2018a), Grube (2019a, b) and Huster et al. (2020) also point to higher GIA induced neotectonic activity in northern Germany than previously thought.

A palaeoseismological study in northwestern Germany was presented by Grützner et al. (2016) for the Rurrand Fault in the Lower Rhine Embayment, which is part of an intraplate rift system (Roer Valley Rift system). The Peel Boundary fault zone, located in the Netherlands and the Geelen Fault in Belgium are part of the rift system and were analysed by Vanneste et al. (2018) and van Balen et al. (2019). They found evidence of seismic fault activity in the Late Pleistocene (Vanneste et al., 2018; van Balen et al., 2019). Grützner et al. (2016) identified two surface rupturing events at the Rurrand Fault in Holocene sediments. Furthermore, historical earthquakes in this region occurred near Düren in 1755/1756, with epicentral intensities of IV–VI (6.5) (Leydecker, 2011). Grützner et al. (2016) mentioned that surface rupturing events can occur after peak deglaciation on locked faults. However, the fault is part of an intraplate rift system and GIA processes probably play a minor role in this area. Therefore, it is not yet clear if this is a GIF in the proper sense.

Evidence of neotectonic movements in eastern Germany in the Lausitz and Niederlausitz areas are described from several fault zones and graben structures. Above these deep-seated faults, sediment thickness anomalies, facies changes and displaced Pleistocene deposits have been mapped (e.g. Stackebrandt, 2008; Krentz et al., 2010; Kühner, 2010). At these structures repeated phases of reactivation are documented from Cretaceous until Middle Pleistocene times. Evidence of neotectonic activity during the Pleistocene were found at the Erpitzer Fault Zone (Kühner, 2010), the Stradow–Buckower Fault system, the Pritzen Fault (Kühner, 2010), and the Kauscher Graben (Krentz et al., 2010; Kühner, 2009, 2010). Furthermore, evidence was found at the Weisswasser Graben, the Nochtener Graben, the Graben of Calau and the Zinnitzer Graben (Krentz et al., 2010). Stackebrandt (2008) described that some of the NW-SE oriented graben structures displaced Pleistocene sediments and assumed GIA as a possible trigger. However, only one earthquake with local magnitude ( $M_L$ ) of 3.2 was registered in this area, in the year 1920 near Cottbus (Leydecker, 2011). The absence of Lateglacial and historical earthquakes in this area and the connection to long-lasting Late Mesozoic–Cenozoic extensional structures that were active for more than 65 Ma make a GIA-driven reactivation of the fault and graben structures unlikely. Therefore, the above-mentioned structures are not considered as GIFs and GIA may have played a subordinate role in their reactivation in Pleistocene times.

Evidence of palaeo-earthquakes is shown by Brandes et al. (2012) and Brandes and Winsemann (2013) for the Osning Thrust. Hoffmann and Reicherter (2012) and Pisarska-Jamroży et al. (2018, 2019) found evidence of seismic activity in Pleistocene sediments along the southwestern coast of the Baltic Sea in the area of Usedom and Rügen Island. In addition, studies by Hübscher et al. (2004), Lehné and Sirocko (2007, 2010), Brandes et al. (2011), Ludwig (2011), Brandes and

Tanner (2012), Al Hseinat and Hübscher (2014), Brandes et al. (2015), Al Hseinat et al. (2016), Grützner et al. (2016), Al Hseinat and Hübscher (2017), Brandes et al. (2018a) and Grube (2019a, b), also point to higher GIA-induced neotectonic activity in northern Germany than previously thought.

Evidence of neotectonic movements in the Glückstadt Graben, in the North German Basin, are indicated by two supra-salt faults that form a wide crestal-collapse graben and pierce Pleistocene sediments. Holocene growth strata within the graben indicate young tectonic activity (Al Hseinat et al., 2016). A clear relationship exists between the location of the faults and the location of the NNW-SSE-trending basement faults, implying that basement faults control salt tectonics. The recent salt tectonics and upward propagation of the faults may have resulted from differential ice-sheet loading (Al Hseinat et al., 2016).

In the Glückstadt Graben, recent activity due to halokinetic movements and tectonic activity was identified by Lehné and Sirocko (2007). At three locations, recent uplift and subsidence rates in areas with near-surface faults indicate tectonic activity. Possible trigger mechanisms are loading and unloading stresses caused by the Fennoscandian ice sheet or subsidence within the Glückstadt Graben.

Previous studies on palaeoseismicity and potential GIFs or GIA processes are largely based on soft-sediment deformation structures (SSDS) (Hoffmann & Reicherter, 2012; Brandes & Winsemann, 2013; Pisarska-Jamroży et al., 2018; Müller et al., 2021) and numerical simulations of fault reactivation potential (Brandes et al., 2012, 2015; Pisarska-Jamroży et al., 2019). Some palaeoseismological studies are based on SSDS and cannot be connected to a particular fault or fault systems (e.g. Ludwig, 2011; Hoffmann & Reicherter, 2012; Grube, 2019a, b). See Müller et al. (2021) for a review of the use of SSDS in palaeoseismology.

## **Recent Seismicity**

Knowledge of tectonic activity in northern Germany is incomplete, due to the rather infrequent earthquakes and the brief period of instrumental observation, which began around 1900. The work of Leydecker (2011) summarises historical earthquakes in Germany since 800 CE. Historical seismicity, probably connected with basement faults, is shown in Table 1.

In recent decades, more than 70 earthquakes (excluding quarry blasts) affected northern Germany. Some of these earthquakes are located near natural gas fields (Dahm et al., 2007, 2015; Müller et al. 2020a).

Two outstanding seismic events that were instrumentally recorded were the Soltau Earthquake, in 1977, with  $M_L$  4.0, and the Rotenburg Earthquake, in 2004, with a moment magnitude ( $M_w$ ) of 4.4 (Figure 1E) (Leydecker et al., 1980, 2011; Dahm et al., 2007, 2015; Uta et al., 2018). Due to their relatively high magnitude, the Soltau and Rotenburg earthquakes are key events that play a major role in the seismic hazard assessment of northern Germany. A clear classification (whether purely tectonic or triggered by gas recovery) of these earthquakes was investigated e.g. in Uta et al. (2018) or Müller et al. (2020a) but has not been possible until now.

In addition, there were also natural earthquakes, such as the Wittenburg 2000 event, with  $M_L$  3.3, the Rostock 2001 Earthquake, with  $M_L$  3.4, and two earthquakes in the Halle/Leipzig area, in 2015 and 2017, with  $M_w$  3.2 and 2.8, respectively (Leydecker, 2011; Dahm et al., 2018). From 2000 to

2018, seven deep earthquakes with hypocentre depths of 17.0 – 31.4 km were registered in northern Germany with  $M_L$  1.7 – 3.1 (Brandes et al., 2019).

Recent work has shown that northern Germany is a seismically active intraplate region (Brandes et al., 2015). Typical for earthquakes in intraplate areas are long intervals between the earthquakes (Gangopadhyay & Talwani, 2003) and wide spatial and temporal distribution. Seismic activity concentrates for a period of time on one fault and then shifts to the next fault (McKenna et al., 2007). Intraplate earthquakes can be thus characterised as episodic, clustered and migrating.

## Potential GIFs in Northern Germany

In northern Germany, the WNW-ESE-trending faults have the highest reactivation potential, because they trend parallel to the former ice margin (Figure 1E, Table 1) (Brandes et al., 2011, 2012, 2015). For these faults, the maximum horizontal components of the ice-sheet-induced stress are in-line with the palaeo-stress field (cf. Stewart et al., 2000).

Al Hseinat and Hübscher (2017) identified neotectonic movements along several faults in the south-western Baltic Sea, based on a dense grid of seismic reflection profiles. The Agricola Fault, Langeland Fault, Prerow Fault, Werre Fault and Wiek Fault (Figure 1E) cut through unconsolidated Pleistocene sediments and were most likely reactivated due to the combination of the present-day stress field and GIA-induced stress variations. Two historical earthquakes occurred in the years 1888 and 1905, with an epicentral intensity of III – IV in the Mecklenburg bay of the Baltic Sea (Figure 1E). In the area of Fehmarn Island, two earthquakes occurred in 1906 and 1907, with epicentral intensities of III – IV (Leydecker, 2011). Further, seven earthquakes with  $M_L$  2.3 – 3.1 were detected in the Baltic Sea and on Rügen Island (Leydecker, 2011; BGR, 2019).

Close to the Schaabe Fault, located near the sea cliff at Dwasieden, in the SW Baltic Sea (Rügen Island), Pisarska-Jamroży et al. (2018, 2019) found evidence of palaeo-earthquakes derived from SSDS in Weichselian sediments. The two deformed beds were deposited between 22.7 – 1.9 ka and 19.0 – 1.8 ka (Pisarska-Jamroży et al., 2018) and must have formed in front of the advancing Weichselian ice sheet before the LGM (Pisarska-Jamroży et al., 2019). CFS modelling results supported a glacially induced origin of the seismites in this time window. Pisarska-Jamroży et al. (2019) point to GIA-related fault activity at the nearby faults on Rügen Island, e.g. the Parchow, Lietow, Nord-Jasmund, Boldewitz and Wiek Faults. Two earthquakes with  $M_L$  2.3 – 2.6 were detected close to the Rügen Island (NW Baltic Sea) (Leydecker, 2011; BGR, 2019).

Evidence of neotectonic movements at the Aller Valley Fault are derived from analysis of normal-displaced, shear-deformation bands in Middle Pleistocene Saalian sediments that developed close to the fault and imply that the Aller Valley Fault was active since Saalian times and possibly in historical times. In the Magdeburg area, historical earthquakes occurred with epicentral intensities of IV – VI (Leydecker, 2011, Figure 1E). These events are probably related to the Aller Valley Fault. Recent earthquakes were detected in 1977 near Soltau, with  $M_L$  4.0, in 2004; near Rotenburg, with  $M_L$  4.4 (Dahm et al., 2007; Uta et al., 2018), in 2014, close to Walsrode, with  $M_L$  1.3 at a depth of 25.5 km; and in 2018, close to Rethem with  $M_L$  2.0 at a depth of 28.5 km (Figure 1E) (Brandes et al., 2019). However, some of these earthquakes are most likely too deep to be related to the Aller Valley Fault.

At the Halle Fault system, evidence of neotectonic movements is indicated by shear-deformation bands with normal displacement, above a blind fault, to the north of the Halle Fault. The neotectonic movements occurred in post Saalian times, because the sediments have a Middle Pleistocene Saalian age (Knoth, 1992). The Halle Fault and related faults were active since Middle Pleistocene Saalian times and in historical times. Historical earthquakes, with epicentral intensities of III (3.5) – IV (4.5) occurred near Merseburg, Halle and Halle/Weißenfels (Leydecker, 2011, Figure 1E). Recent earthquakes were detected in 1908 near Halle/Weißenfels, with an epicentral intensity of III; in 1987 near Gröbzig, with  $M_L$  2.4; in 2015 near Röglitz, with  $M_L$  3.2 and  $M_L$  2.0 (Dahm et al., 2018; BGR, 2019); and 2017 near Schkeuditz with  $M_L$  2.8 (Dahm et al., 2018; Figure 1E). Historical earthquakes with epicentral intensities of III – IV (4.5) and recent earthquakes with epicentral intensities of III – VI and magnitudes ( $M_i$ ) of 2.8 to 4.1 occurred near Leipzig but are most likely linked to the Leipzig fault system.

At the Harz Boundary Fault, evidence of neotectonic movements is indicated by a fault that is exposed in a nearby sinkhole (Franzke et al., 2015; Müller et al., 2020b). This fault shows a polyphase tectonic evolution with initial normal fault movements and a later reactivation as oblique reverse fault with strike-slip component. Luminescence dating of the surrounding deposits indicates that fault movement occurred after ~15 ka (Müller et al., 2020b). CFS modelling results support this reactivation time. A recent earthquake with an epicentral intensity of IV occurred near Quedlinburg, several kilometres north of the Harz Boundary Fault (Leydecker, 2011, Figure 1E).

At the Leine Valley Fault system, evidence of neotectonic movements are indicated by shear-deformation bands with normal displacement (Figure 1E). The shear-deformation bands were analysed using ground-penetrating radar profiles and can be connected to movement on one of the basement faults (Brandes & Tanner, 2012; Brandes et al., 2018a; Winsemann et al., 2018).

At the Osning Thrust evidence of neotectonic movements associated with palaeo-earthquakes was described by Brandes et al. (2012). Indicators are shear-deformation bands with normal displacement and SSDS that include clastic dykes and a sand volcano. The neotectonic movements occurred in the Lateglacial between 16 to 13 ka (Brandes et al., 2012; Brandes & Winsemann, 2013). CFS modelling results also support this reactivation time. Historical earthquakes occurred in the nearby area of Bielefeld and near Oerlinghausen, with an epicentral intensity of VI (Leydecker, 2011, Figure 1E). A recent earthquake was detected in 2019, NE of Paderborn, with  $M_L$  2.1 (BGR, 2019).

At the Steinhuder Meer Fault, evidence of neotectonic movements are indicated by shear-deformation bands with normal displacement (Figure 1E). Growth strata point to Saalian neotectonic movements.

Brandes et al. (2019) showed that the major faults of the Thor Suture are under reactivation, triggered by stress changes due to GIA processes (Figure 1E). Indicators are deep crustal earthquakes at a depth of 17.0 - 31.4 km.

At the Weser Valley Fault system, evidence of neotectonic movements are indicated by a fault system that developed within the glaciolacustrine Emme delta that can be connected to the Mesozoic basement fault (Figure 1E; Brandes et al., 2011; Winsemann et al., 2011). The fault system shows syn-sedimentary activity. According to Brandes et al. (2011) and Winsemann et al. (2011), these basement faults were reactivated during the Middle Pleistocene by the advancing Saalian ice sheet, water and sediment loading.



Table 1: Potential GIFs in northern Germany. Strike, fault type and earthquakes that were registered in the vicinity of the faults (~ 20 km) are listed. Note, the 2014 and 2018 earthquakes near Walsrode and Rethem were probably too deep to be related to the Aller Valley Fault.

GIFs	Strike	Fault type	Earthquakes in the vicinity (~20 km)	Reference
<b>Langeland Fault</b>	NNW-SEE	Normal	1888 I <sub>o</sub> IV Baltic Sea (Leydecker, 2011) 2011 M <sub>L</sub> 2.2 Baltic Sea (BGR, 2019)	Al Hseinat et al. (2017)
<b>Prerow Fault and Werre Fault</b>	NW-SE	Crestal Collapse Graben (Strike-slip?)	1997 M <sub>L</sub> 2.6 Zingst (BGR, 2019) 1998 M <sub>L</sub> 2.7 Baltic Sea (BGR, 2019)	Al Hseinat et al. (2017)
<b>Agricola Fault</b>	NNE-SSW	Normal	1981 M <sub>L</sub> 3.1 Baltic Sea (Leydecker, 2011) 1997 M <sub>L</sub> 2.6 Zingst (BGR, 2019) 1997 M <sub>L</sub> 2.8 Baltic Sea (BGR, 2019)	Al Hseinat et al. (2017)
<b>Wiek Fault</b>	WNW-ESE	Normal	1981 M <sub>L</sub> 3.1 Baltic Sea (Leydecker, 2011) 1990 M <sub>L</sub> 2.3 Binz (Leydecker, 2011) 1997 M <sub>L</sub> 2.8 Baltic Sea (BGR, 2019) 2000 M <sub>L</sub> 2.6 Hagen (BGR, 2019)	Al Hseinat et al. (2017)
<b>Schaabe Fault</b>	WNW-ESE	Normal, Strike-slip?	1990 M <sub>L</sub> 2.3 Binz (Leydecker, 2011) 2000 M <sub>L</sub> 2.6 Hagen (BGR, 2019)	Pisarska-Jamroży et al. (2018, 2019)
<b>Aller Valley Fault system</b>	NW-SE	Reverse, Normal, Strike-slip	997 I <sub>o</sub> VI Altmark (Leydecker, 2011) 1298 I <sub>o</sub> IV Magdeburg (Leydecker, 2011) 1409 I <sub>o</sub> VI Magdeburg (Leydecker, 2011) 1576 I <sub>o</sub> IV Magdeburg (questioned) (Leydecker, 2011) 1977 M <sub>L</sub> 4.0 Soltau (Dahm et al., 2007) 2004 M <sub>w</sub> 4.4 Rotenburg (Dahm et al., 2007; Uta et al., 2018) 2014 M <sub>L</sub> 1.3 Walsrode (Brandes et al., 2019) 2018 M <sub>L</sub> 2.0 Rethem (Brandes et al., 2019)	Winsemann et al. (2011)

<b>Halle Fault system</b>	NW-SE	Reverse	1536 I <sub>0</sub> III (3.5) Merseburg (Leydecker, 2011) 1578 I <sub>0</sub> III (3.5) Halle (Leydecker, 2011) 1642 I <sub>0</sub> III (3.5) Halle (Leydecker, 2011) 1645 I <sub>0</sub> IV Halle/Weißenfels (Leydecker, 2011) 1668 I <sub>0</sub> IV Halle/Weißenfels (Leydecker, 2011) 1670 I <sub>0</sub> IV Halle/Weißenfels (Leydecker, 2011) 1720 I <sub>0</sub> IV (4.5) Halle/Weißenfels (Leydecker, 2011) 1908 I <sub>0</sub> III Halle/Weißenfels (Leydecker, 2011) 1987 M <sub>L</sub> 2.4 Gröbzig (BGR, 2019) 2015 M <sub>w</sub> 3.2 Röglitz (Dahm et al., 2018) 2015 M <sub>L</sub> 2.0 Röglitz (BGR, 2019) 2017 M <sub>w</sub> 2.8 Schkeuditz (Dahm et al., 2018)	This study
<b>Harz Boundary Fault</b>	WNW-ESE	Reverse	1908 I <sub>0</sub> III Quedlinburg (Leydecker, 2011)	Müller et al. 2020b
<b>Leine Valley Fault system</b>	NNW-SSE	Normal/Reverse	none	Brandes et al. (2018a)
<b>Osning Thrust</b>	WNW-ESE	Reverse	1612 I <sub>0</sub> VI Bielefeld (Leydecker, 2011) 1767 I <sub>0</sub> VI Oerlinghausen (Leydecker, 2011) 2019 M <sub>L</sub> 2.1 NE of Paderborn (BGR, 2019)	Brandes et al. (2012) Brandes & Winsemann (2013)
<b>Weser Valley Fault system</b>	WNW-ESE	Reverse	none	Brandes et al. (2011)
<b>Thor Suture</b>	NW-SE	Reverse	2012 M <sub>L</sub> 2.0 Hitzacker (Brandes et al., 2019) 2014 M <sub>L</sub> 2.2 Rögnitz (Brandes et al., 2019)	Brandes et al. (2019)
<b>Steinhuder Meer Fault</b>	NNW-SSE	Reverse	none	This study

\*M<sub>w</sub> can be calculated using the equation  $M_w = 0.682 I_0 + 0.16$  according to Grünthal et al. (2009).

## Discussion

The neotectonic activity in northern Germany is a consequence of the regional lithospheric stress field, which is controlled by the push of the Mid-Atlantic Ridge and the ongoing Alpine Orogeny (Reicherter et al., 2005). The work of Brandes et al. (2011, 2012), Brandes and Winsemann (2013) and Brandes et al. (2015) have shown that additional stress field changes due to glacial isostatic adjustment may have induced the Pleistocene and historical seismicity. In northern Germany, the WNW-ESE-striking faults have the highest reactivation potential, because they trend parallel to the former ice-margin (Brandes et al., 2015). Glacially-induced fault reactivation is largely controlled by deglaciation processes in the Late Pleistocene. The best evidence available points to the decay of the Weichselian ice sheet as the reason for potential GIFs. However, studies of Brandes et al. (2011), Winsemann et al. (2011) and Pisarska-Jamrozý et al. (2018, 2019) also point to possible fault reactivation during the previous ice advances.

### Tectonic Structures and the Distribution of Fault Activity

The tectonic structure of northern Germany is the result of the Palaeozoic Caledonian and Variscan orogenies (Krawczyk et al., 2008), Late Palaeozoic to Mesozoic lithospheric extension (Betz et al., 1987) and a distinct Late Mesozoic to Palaeogene inversion phase (Kley & Voigt, 2008). Different studies have shown that the inherited structural grain is an important controlling factor for young tectonic activity (e.g. Sykes, 1978). Brandes et al. (2012) showed that neotectonic activity occurred at the Osning Thrust, and the study of Müller et al. (2020b) found evidence of neotectonic activity on the Harz Boundary Fault system. Both the Osning Thrust and the Harz Boundary Fault were active during the Late Cretaceous inversion phase. Historical seismicity with epicentral intensities of up to VI is also concentrated on Late Cretaceous reverse faults such as the Osning Thrust, the Gardelegen Fault and the Haldensleben Fault.

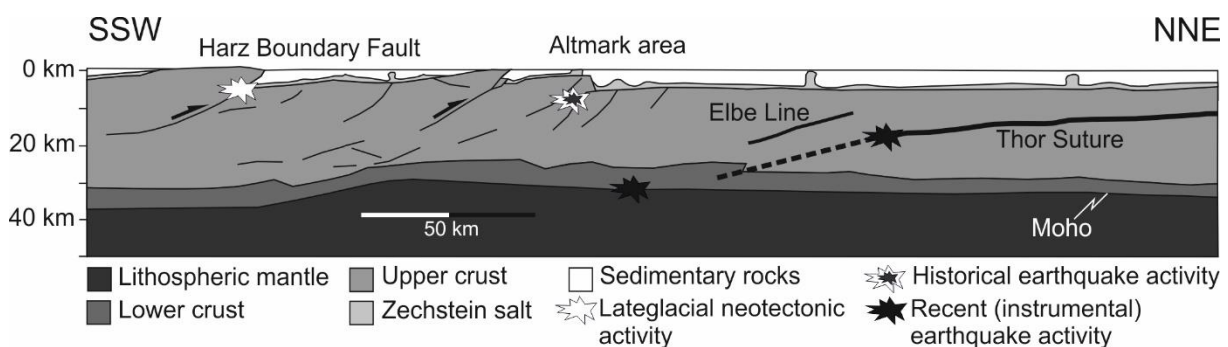


Figure 3: Tectonic activity in northern Germany. The cross-section shows Lateglacial neotectonic activity, historical earthquake activity and recent (instrumental) earthquake activity at several fault systems (based on Leydecker, 2011; Brandes et al., 2019; Müller et al., 2020b). Unlike the other faults, the Elbe Line and the Thor Suture are terrane boundaries. The dashed line represents the uncertain location of the Thor Suture. Cross-section is modified after Kley & Voigt (2008).

Recent natural earthquakes detected over the last 18 years point to deep-seated seismicity in northern Germany. These earthquakes reach a magnitude of 3.1 and are partly concentrated on the Thor Suture, which is the remnant of a Silurian subduction zone. Numerical simulations imply that GIA processes play a role in triggering these events (Brandes et al., 2019) and that reverse

faults in northern Germany have a high potential to be reactivated as GIFs. For these faults, the CFS became positive with increasing time since deglaciation (Brandes et al., 2015). Lehné and Sirocko (2007), Al Hseinat et al. (2016), Huster et al. (2020) and Christian Hübscher (personal communication, 2020) described evidence of neotectonic activity from the Glückstadt Graben. It is difficult to decide whether this activity is the result of GIA processes. Numerical simulations of GIA-related stress-field changes in the southern part of northern Germany imply that normal fault activity was possible in the last 25 ka, but the fact that the Coulomb stress has decreased over the last 20 ka implies that the likelihood of GIA related normal fault activity will decrease, whereas the likelihood for movements on reverse faults has increased over the last 15 Ma. Further deep earthquakes are located at the Moho at a depth of up to 30 km. This seismicity implies that the Moho may act as a regional detachment on which recent shortening could be compensated (Figure 3; Brandes et al., 2019).

## Conclusions

- Key parameters to classify faults in northern Germany as GIFs are the timing of reactivation, their orientation to the former ice margins and numerical simulations that show the increase of the CFS over the time since the onset of deglaciation.
- In the southwestern Baltic Sea, the Langeland Fault, the Prerow and Werre faults, the Agricola Fault and the Wiek Fault all show evidence of neotectonic activity induced by GIA processes.
- In the southwestern Baltic Sea at Rügen Island evidence of palaeo-earthquakes were found near the Schaabe Fault. The estimated age of the deformation and modelling results indicate that the reactivation of the fault is glacially induced.
- At the Osning Thrust evidence of palaeo-earthquakes occurs.
- The Thor Suture shows ongoing seismicity that might be related to GIA processes.
- At the Weser Valley Fault system, a fault system in the glaciolacustrine Emme delta, can be connected to Mesozoic basement faults. These basement faults were probably reactivated during the Middle Pleistocene by the advancing Saalian ice sheet and by water and sediment loading.
- At the Aller Valley Fault, the Halle Fault system, the Leine Valley Fault system and the Steinhuder Meer Fault, neotectonic movements are indicated by shear-deformation bands in Middle Pleistocene sediments, which developed in the process zone of the faults.
- Neotectonic activity occurred at the Harz Boundary Fault. Lateglacial fault activity (post 15 ka) corresponds with the timing of fault reactivation at the Osning Thrust and the Sorgenfrei–Tornquist Zone.
- At the Harz Boundary Fault, the Osning Thrust and Schaabe Fault, field evidence, modelling results and luminescence ages indicate that these faults were reactivated due to GIA-related stress field changes.
- Studies in the Lower Rhine Rift show a possible link between GIA processes and fault activity in this area.

The results support the interpretation that northern Germany is a tectonically active intraplate area, with clustered and migrating seismic activity that mainly occurred on major Late Cretaceous reverse faults. The timing of fault movements implies that the seismicity is most likely induced by varying lithospheric stress conditions related to GIA, and some faults are therefore classified as GIFs. This is supported by numerical simulations of GIA-related stress-field changes. Lateglacial, historical and recent earthquakes occurred in this region. Thus, GIA processes are also a likely driver for historical and parts of recent fault activity.

## **Acknowledgements**

We thank Christian Hübscher and Werner Stackebrandt for their constructive reviews, which helped to improve the manuscript. The work has been financially supported by project *Paläoseismische Untersuchung Norddeutschlands* from the BGR (No. 201-10079313). Reproduced with permission of The Licensor through PLSclear.

## References

- Al Hseinat, M., Hübscher, C. (2014). Ice-load induced tectonics-controlled tunnel valley evolution- instances from the southwestern Baltic Sea. *Quaternary Science Reviews*, 97,121-135.
- Al Hseinat, M., Hübscher, C., Lang, J., Lüdmann, T., Ott, I., Polom, U. (2016). Triassic to recent tectonic evolution of a crestal collapse graben above a salt-cored anticline in the Glückstadt Graben/North German Basin. *Tectonophysics*, 680,50-66.
- Al Hseinat, M., Hübscher, C. (2017). Late Cretaceous to recent tectonic evolution of the North German Basin and the transition zone to the Baltic Shield/southwest Baltic Sea. *Tectonophysics*, 708,28-55.
- Betz, D., Führer, F., Greiner, G., Plein, E. (1987). Evolution of the Lower Saxony Basin. *Tectonophysics*, 137,127-170.
- BGR (2019). Der Geodatendienst GERSEIS innerhalb der interaktiven Kartenanwendung Geoviewer der BGR. [https://geoviewer.bgr.de/mapapps4/resources/apps/geoviewer/index.html?lang=de&tab=geophysik&cover=geophysik\\_gerseis\\_ag\\_s\\_wms](https://geoviewer.bgr.de/mapapps4/resources/apps/geoviewer/index.html?lang=de&tab=geophysik&cover=geophysik_gerseis_ag_s_wms). Accessed,2019.
- Böse, M., Lüthgens, C., Lee, J.R., Rose, J. (2012). Quaternary glaciations of northern Europe. *Quaternary Science Reviews*, 44,1-25.
- Brandes, C., Polom, U., Winsemann, J. (2011). Reactivation of basement faults: interplay of ice-sheet advance, glacial lake formation and sediment loading. *Basin Research*, 23,53-64.
- Brandes, C., Tanner, D.C. (2012). Three-dimensional geometry and fabric of shear deformation-bands in unconsolidated Pleistocene sediments. *Tectonophysics*, 518,84-92.
- Brandes, C., Winsemann, J., Roskosch, J., Meinsen, J., Tanner, D.C., Frechen, M., Steffen, H., Wu, P. (2012). Activity along the Osning Thrust in Central Europe during the Lateglacial: ice-sheet and lithosphere interactions. *Quaternary Science Reviews*, 38,49-62.
- Brandes, C., Winsemann, J. (2013). Soft-sediment deformation structures in NW Germany caused by Late Pleistocene seismicity. *International Journal of Earth Sciences*, 102,2255-2274.
- Brandes, C., Steffen, H., Steffen, R., Wu, P. (2015). Intraplate seismicity in northern Central Europe is induced by the last glaciation. *Geology*, 43,611-614.
- Brandes, C., Igel, J., Loewer, M., Tanner, D.C., Lang, J., Müller, K., Winsemann, J. (2018a). Visualisation and analysis of shear-deformation bands in unconsolidated Pleistocene sand using ground-penetrating radar: Implications for paleoseismological studies. *Sedimentary Geology*, 367,135-145.
- Brandes, C., Steffen, H., Sandersen, P.B., Wu, P., Winsemann, J. (2018b). Glacially induced faulting along the NW segment of the Sorgenfrei-Tornquist Zone, northern Denmark: Implications for neotectonics and Lateglacial fault-bound basin formation. *Quaternary Science Reviews*, 189,149-168.
- Brandes, C., Plenefisch, T., Tanner, D.C., Gestermann, N., Steffen, H. (2019). Evaluation of deep crustal earthquakes in northern Germany-Possible tectonic causes. *Terra Nova*, 31,83-93.
- Dahm, T., Krüger, F., Stammler, K., Klinge, K., Kind, R., Wylegalla, K., Grasso, J.R. (2007). The 2004  $M_w$  4.4 Rotenburg, northern Germany, earthquake and its possible relationship with gas recovery. *Bulletin of the Seismological Society of America*, 97,691-704.
- Dahm, T., Cesca, S., Hainzl, S., Braun, T., Krüger, F. (2015). Discrimination between induced, triggered and natural earthquakes close to hydrocarbon reservoirs: A probabilistic approach based on the modeling of depletion-induced stress changes and seismological source parameters. *Journal of Geophysical Research*, 120,2491-2509.
- Dahm, T., Heimann, S., Funke, S., Wendt, S., Rappsilber, I., Bindi, D., Plenefisch, T., Cotton, F. (2018). Seismicity in the block mountains between Halle and Leipzig, Central Germany: centroid moment tensors, ground motion simulation, and felt intensities of two  $M \approx 3$  earthquakes in 2015 and 2017. *Journal of Seismology*, 22,985-1003.
- Ehlers, J., Grube, A., Stephan, H.J., Wansa, S. (2011). Pleistocene glaciations of North Germany-new results. In: Ehlers, J., Gibbard, P.L., Hughes, P.D. (Eds.), *Quaternary Glaciations: Extent and Chronology-A Closer Look: Developments in Quaternary Science*, 15,149-162.



- Eissmann, L. (2002). Quaternary geology of eastern Germany (Saxony, Saxon-Anhalt, south Brandenburg, Thuringia), type area of the Elsterian and Saalian stages in Europe. *Quaternary Science Reviews*, 21,1275-1346.
- Franke, W. (2000). The mid-European segment of the Variscides: tectonostratigraphic units, terrane boundaries and plate tectonic evolution. *Geological Society, London, Special Publications*, 179,35-61.
- Franke, W., Cocks, L.R.M., Torsvik, T.H. (2017). The Palaeozoic Variscan oceans revisited. *Gondwana Research*, 48,257-284.
- Franzke, H.J., Hauschke, N., Hellmund, M. (2015). Spätpleistozäne bis frühholozäne Tektonik in einem Karsttrichter im Bereich der Störungszone des Harznordrandes nahe Benzingerode (Sachsen-Anhalt). *Hallesches Jahrbuch für Geowissenschaften*, 37,1-10.
- Gangopadhyay, A., Talwani, P. (2003). Symptomatic features of intraplate earthquakes. *Seismological Research Letters*, 74,863-883.
- Gast, R., Gundlach, T. (2006). Permian strike slip and extensional tectonics in Lower Saxony, Germany. *Zeitschrift der Deutschen Gesellschaft für Geowissenschaften*, 157,41-56.
- Grollmund, B., Zoback, M.D. (2001). Did deglaciation trigger intraplate seismicity in the New Madrid Seismic Zone? *Geology*, 29,175-178.
- Grube, A. (2019a). Palaeoseismic structures in Quaternary sediments of Hamburg (NW Germany), earthquakes evidence during the younger Weichselian and Holocene. *International Journal of Earth Sciences*, 108,845-861.
- Grube, A. (2019b). Palaeoseismic structures in Quaternary sediments, related to an assumed fault zone north of the Permian Peissen-Gnutz salt structure (NW Germany)-Neotectonic activity and earthquakes from the Saalian to the Holocene. *Geomorphology*, 328,15-27.
- Grünthal, G., Mayer-Rosa, D., Lenhardt, W.A. (1998). Abschätzung der Erdbebengefährdung für die D-A-CH-Staaten-Deutschland, Österreich, Schweiz. *Bautechnik*, 75,753-767.
- Grünthal, G., Stromeyer, D., Wahlström, R. (2009). Harmonization check of  $M_w$  within the central, northern, and northwestern European earthquake catalogue (CENEC). *Journal of Seismology*, 13,613-632.
- Grützner, C., Fischer, P., Reicherter, K. (2016). Holocene surface ruptures of the Rurrand Fault, Germany-insights from palaeoseismology, remote sensing and shallow geophysics. *Geophysical Journal International*, 204,1662-1677.
- Hampel, A., Hetzel, R., Maniatis, G., Karow, T. (2009). Three-dimensional numerical modeling of slip rate variations on normal and thrust fault arrays during ice cap growth and melting. *Journal of Geophysical Research*, 114,B08406.
- Hardt, J., Lüthgens, C., Hebenstreit, R., Böse, M. (2016). Geochronological (OSL) and geomorphological investigations at the presumed Frankfurt ice-marginal position in northeast Germany. *Quaternary Science Reviews*, 154,85-99.
- Hardt, J., Böse, M. (2018). The timing of the Weichselian Pomeranian ice marginal position south of the Baltic Sea: a critical review of morphological and geochronological results. *Quaternary International*, 478,51-58.
- Heidbach, O., Rajabi, M., Reiter, K., Ziegler, M. (2016). World stress map 2016. *Science*, 277,1956-62.
- Hoffmann, G., Reicherter, K. (2012). Soft-sediment deformation of Late Pleistocene sediments along the southwestern coast of the Baltic Sea (NE Germany). *International Journal of Earth Sciences*, 101,351-363.
- Hughes, A.L.C., Gyllencreutz, R., Lohne, Ø.S., Mangerud, J., Svendsen, J.I. (2016). The last Eurasian ice sheets-a chronological database and time-slice reconstruction, DATED-1. *Boreas*, 45,1-45.
- Hübscher, C., Lykke-Andersen, H., Hansen, M.B., Reicherter, K. (2004). Investigating the structural evolution of the western Baltic. *Eos, Transactions American Geophysical Union*, 85,115-115.
- Huster, H., Hübscher, C., Seidel, E. (2020). Impact of Late Cretaceous to Neogene plate tectonics and Quaternary ice loads on supra-salt deposits at Eastern Glückstadt Graben, North German Basin. *International Journal of Earth Sciences*, 109, 1029-1050.

- Kaiser, A., Reicherter, K., Hübscher, C., Gajewski, D. (2005). Variation of the present-day stress field within the North German Basin - insights from thin shell FE modeling based on residual GPS velocities. *Tectonophysics*, 397,55-72.
- Kley, J., Voigt, T. (2008). Late Cretaceous intraplate thrusting in central Europe: effect of Africa-Iberia-Europe convergence, not Alpine collision. *Geology*, 36,839-842.
- Knoth, W. (1992). Geologische Übersichtskarte von Sachsen-Anhalt 1:400000, *Geologisches Landesamt Sachsen-Anhalt, 1. Edition, Halle/Saale*.
- Kockel, F. (2003). Inversion structures in Central Europe. Expressions and reasons, an open discussion. *Netherlands Journal of Geosciences*, 82,367-382.
- Kossmat, F. (1927). Gliederung des varistischen Gebirgsbaues. *Abhandlungen des Sächsischen Geologischen Landesamts*, 1,1-39.
- Krawczyk, C.M., McCann, T., Cocks, L.R.M., England, R.W., McBride, J.H., Wybraniec, S. (2008). Caledonian tectonics. In: *McCann, T. (Ed.), The Geology of Central Europe. Precambrian and Paleozoic, 1, Geological Society London, pp.303-381*.
- Krentz, O., Lapp, M., Seibel, B., Bahrt, W. (2010). Bruchtektonik. In: *Autorenkollektiv (Eds.), Die geologische Entwicklung der Lausitz. Vattenfall Europe Mining AG, Cottbus, pp.137-160*.
- Kujansuu, R. (1964). Nuorista siirroksista Lapissa. Summary: Recent faults in Finnish Lapland. *Geologi*, 16,30-36.
- Kühner, R. (2009). Neue Ergebnisse zum Nachweis neotektonischer Aktivitäten im Quartär des Tagebaus Welzow-Süd, Südbrandenburg. *Brandenburgische Geowissenschaftliche Beiträge*, 16,87-93.
- Kühner, R. (2010). Quartär. In: *Autorenkollektiv (Eds.), Die geologische Entwicklung der Lausitz. Vattenfall Europe Mining AG, Cottbus, pp.97-134*.
- Lang, J., Hampel, A., Brandes, C., Winsemann, J. (2014). Response of salt structures to ice-sheet loading: implications for ice-marginal and subglacial processes. *Quaternary Science Reviews*, 101,217-233.
- Lang, J., Lauer, T., Winsemann, J. (2018). New age constraints for the Saalian glaciation in northern central Europe: implications for the extent of ice sheets and related proglacial lake systems. *Quaternary Science Reviews*, 180,240-259.
- Lauer, T., Weiss, M. (2018). Timing of the Saalian-and Elsterian glacial cycles and the implications for Middle Pleistocene hominin presence in central Europe. *Scientific Reports*, 8,5111.
- Lehmkuhl, F., Zens, J., Krauß, L., Schulte, P., Kels, H. (2016). Loess-paleosol sequences at the northern European loess belt in Germany: distribution, geomorphology and stratigraphy. *Quaternary Science Reviews*, 153,11-30.
- Lehné, R.J., Sirocko, F. (2007). Rezente Bodenbewegungspotenziale in Schleswig-Holstein (Deutschland)-Ursachen und ihr Einfluss auf die Entwicklung der rezenten Topographie. *Zeitschrift der Deutschen Gesellschaft für Geowissenschaften*, 158,329-347.
- Lehné, R.J., Sirocko, F. (2010). Recent vertical crustal movements and resulting surface deformation within the North German Basin (Schleswig-Holstein) derived by GIS-based analysis of repeated precise leveling data. *Zeitschrift der Deutschen Gesellschaft für Geowissenschaften*, 161,175-188.
- Leydecker, G., Steinwachs, M., Seidl, D., Kind, R., Klusmann, J., Zerna, W. (1980). Das Erdbeben vom 2. Juni 1977 in der Norddeutschen Tiefebene bei Soltau. *Geologisches Jahrbuch Reihe E*, 18,3-18.
- Leydecker, G. (2011). Erdbebenkatalog für die Bundesrepublik Deutschland mit Randgebieten für die Jahre 800 bis 2008. *Geologisches Jahrbuch Reihe E*, 59, pp.1-198.
- Littke, R., Scheck-Wenderoth, M., Brix, M.R., Nelskamp, S. (2008). Subsidence, inversion and evolution of the thermal field. In: *Littke, R., Bayer, U., Gajewski, D., Nelskamp, S. (Eds.), Dynamics of Complex Intracontinental Basins-The Central European Basin System. Springer-Verlag, Berlin-Heidelberg, pp.125-141*.
- Ludwig, A.O. (2011). Zwei markante Stauchmoränen: Peski/Belorusland und Jasmund, Ostseeinsel Rügen/Nordostdeutschland-Gemeinsame Merkmale und Unterschiede. *E&G-Quaternary Science Journal*, 60,464-487.
- Lüthgens, C., Böse, M. (2011). Chronology of Weichselian main ice marginal positions in north-eastern Germany. *E&G-Quaternary Science Journal*, 60,236-247.

- Marotta, A.M., Bayer, U., Thybo, H. (2000). The legacy of the NE German Basin-Reactivation by compressional buckling. *Terra Nova*, 12,132-140.
- Marotta, A.M., Bayer, U., Thybo, H., Scheck, M. (2002). Origin of regional stress in the North German basin: Results from numerical modeling. *Tectonophysics*, 360,245-264.
- Marotta, A.M., Mitrovica, J.X., Sabadini, R., Milne, G. (2004). Combined effects of tectonics and glacial isostatic adjustment on intraplate deformation in central and northern Europe: applications to geodetic baseline analyses. *Journal of Geophysical Research*, 109,B01413.
- Mazur, S., Scheck-Wenderoth, M., Krzywiec, P. (2005). Different modes of the Late Cretaceous Early Tertiary inversion in the North German and Polish basins. *International Journal of Earth Sciences*, 94,782-798.
- McCann, T. (2008). Introduction and overview. In: McCann, T. (Ed.), *The Geology of Central Europe: Precambrian and palaeozoic*. The Geological Society of London, pp.1-20.
- McKenna, J., Stein, S., Stein, C.A. (2007). Is the New Madrid seismic zone hotter and weaker than its surroundings? In: Stein, S., Mazzotti, S. (Eds.), *Continental Intraplate Earthquakes: Science, Hazard, and Policy Issues: Geological Society of America, Special Paper 425*, pp.167-175.
- Meinsen, J., Winsemann, J., Roskosch, J., Brandes, C., Frechen, M., Dultz, S., Böttcher, J. (2014). Climate control on the evolution of Late Pleistocene alluvial-fan and aeolian sand-sheet systems in NW Germany. *Boreas*, 43,42-66.
- Meschede, M. (2015). *Geologie Deutschlands: Ein prozessorientierter Ansatz*. Springer, Berlin, Heidelberg, p.249.
- Mey, J., Scherler, D., Wickert, A. D., Egholm, D.L., Tesauero, M., Schildgen, T.F., Strecker, M. R. (2016). Glacial isostatic uplift of the European Alps. *Nature Communications*, 7, 13382.
- Mörner, N.A. (1978). Faulting, fracturing, and seismicity as functions of glacio-isostasy in Fennoscandia. *Geology*, 6,41-45.
- Müller, U., Obst, K. (2008). Junge halokinetische Bewegungen im Bereich der Salzkissen Schlieven und Marnitz in Südwest-Mecklenburg. *Brandenburgische Geowissenschaftliche Beiträge*, 15,147-154.
- Müller, B., Scheffzük, F., Schilling, M., Westerhaus, K., Zippelt, M., Wampach, T., Röckel, C., Lempp, C., Schöner, A. (2020a). Reservoir-Management and Seismicity - Strategies to Reduce Induces Seismicity.- DGMK-Research Report 776, ISBN 978-3-947716-09-8
- Müller, K., Polom, U., Winsemann, J., Steffen, H., Tsukamoto, S., Günther, T., Igel, J., Spies, T., Lege, T., Frechen, M., Franzke, H.-J., Brandes, C. (2020b). Structural style and neotectonic activity along the Harz Boundary Fault, northern Germany: A multimethod approach integrating geophysics, outcrop data and numerical simulations. *International Journal of Earth Sciences*.
- Müller, K., Winsemann, J., Pisarska-Jamroży, M., Lege, T., Spies T., Brandes, C. (2021). The challenge to distinguish soft-sediment deformation structures (SSDS) formed by glaciotectionic, periglacial and seismic processes in a formerly glaciated area: a review and synthesis In: Steffen, H., Olesen, O., Sutinen, R. (Eds.), *Glacially-Triggered Faulting*. Cambridge University Press.
- Norton, K.P., Hampel, A. (2010). Postglacial rebound promotes glacial re-advances—a case study from the European Alps. *Terra Nova*, 22,297-302.
- Pharaoh, T.C., Dugar, M., Geluk, M.C., Kockel, F., Krawczyk, C.M., Krzywiec, P., Scheck-Wenderoth, M., Thybo, H., Vejbæk, O.V., Van Wees, J.D. (2010). Tectonic evolution. In: Doornenbal, J.C., Stevenson, A.G. (Eds.), *Petroleum Geological Atlas of the Southern Permian Basin Area*. EAGE Publications, Houten, pp.25-57.
- Pisarska-Jamroży, M., Belzyt, S., Börner, A., Hoffmann, G., Hüneke, H., Kenzler, M., Obst, K., Rother, H., Van Loon, A.T. (2018). Evidence from seismites for glacio-isostatically induced crustal faulting in front of an advancing land-ice mass (Rügen Island, SW Baltic Sea). *Tectonophysics*, 745,338-348.
- Pisarska-Jamroży, M., Belzyt, S., Börner, A., Hoffmann, G., Hüneke, H., Kenzler, M., Obst, K., Rother, H., Steffen, H., Steffen, R., Van Loon, T. (2019). The sea cliff at Dwasieden: soft-sediment deformation structures triggered by glacial isostatic adjustment in front of the advancing Scandinavian ice-sheet. *DEUQUA, Special Publications*, 2,61-67.

- Reicherter, K., Kaiser, A., Stackebrandt, W. (2005). The Post-Glacial landscape evolution of the North German Basin: morphology, neotectonics and crustal deformation. *International Journal of Earth Science*, 94,1083-1093.
- Reinecker, J., Heidebach, O., Müller, B. (2004). World Stress Map (2004 release). *World Wide Web address: www.world-stress-map.org. Accessed 2019.*
- Roskosch, J., Winsemann, J., Polom, U., Brandes, C., Tsukamoto, S., Weitkamp, A., Bartholomäus, W.A., Henningsen, D., Frechen, M. (2015). Luminescence dating of ice-marginal deposits in northern Germany: evidence for repeated glaciations during the Middle Pleistocene (MIS 12 to MIS 6). *Boreas*, 44,103-126.
- Schulz, R., Suchi, E., Öhlschläger, D., Dittmann, J., Knopf, S., Müller, C. (2013). Geothermieatlas zur Darstellung möglicher Nutzungskonkurrenzen zwischen CCS und Tiefer Geothermie. *Leibniz-Institut für Angewandte Geophysik und Bundesanstalt für Geowissenschaften und Rohstoffe, Hannover, p.107.*
- Seidel, E., Meschede, M., Obst, K. (2018). The Wiek Fault System east of Rügen Island: origin, tectonic phases and its relationship to the Trans-European Suture Zone. *Geological Society, London, Special Publications*, 469,59-82.
- Stackebrandt, W. (2004). Zur Neotektonik in Norddeutschland. *Zeitschrift für geologische Wissenschaften*, 32,85-95.
- Stackebrandt, W. (2005). Neotektonische Aktivitätsgebiete in Brandenburg (Norddeutschland). *Brandenburgische Geowissenschaftliche Beiträge*, 12,165-172.
- Stackebrandt, W. (2008). Zur Neotektonik der Niederlausitz. *Zeitschrift der Deutschen Gesellschaft für Geowissenschaften*, 159,117-122.
- Stackebrandt, W. (2015) Neotektonische Beanspruchung. In: *Stackebrandt, W., Franke, D. (Eds.), Geologie von Brandenburg. Schweizerbart, Stuttgart, pp.480-487.*
- Stewart, I.S., Sauber, J., Rose, J. (2000). Glacio-seismotectonics: ice sheets, crustal deformation and seismicity. *Quaternary Science Reviews*, 19,1367-1389.
- Sykes, L.R. (1978). Intraplate seismicity, reactivation of pre-existing zones of weakness, alkaline magmatism, and other tectonism postdating continental fragmentation. *Reviews of Geophysics and Space Physics*, 16, pp.621-688.
- Torsvik, T.H., Cocks, L.R.M. (2017). The integration of palaeomagnetism, the geological record and mantle tomography in the location of ancient continents. *Geological Magazine*, 156,242-260.
- Uta, P., Brandes, C., Bönnemann, C., Gestermann, N., Kaiser, D., Plenefisch, T., Winsemann, J. (2018). Re-evaluation of the Rotenburg mainshock 2004; DGMK-Project 806, Final Report, p. 85.
- Van Balen, R.T., Bakker, M.A.J., Kasse, C., Wallinga, J., Woolderink, H.A.G. (2019). A Late Glacial surface rupturing earthquake at the Peel Boundary fault zone, Roer Valley Rift System, the Netherlands. *Quaternary Science Reviews*, 218,254-266.
- Vanneste, K., Camelbeeck, T., Verbeeck, K., Demoulin, A. (2018). Morphotectonics and past large earthquakes in Eastern Belgium. In: *Demoulin, A. (Ed.), Landscapes and Landforms of Belgium and Luxembourg, World Geomorphological Landscapes, Springer, Cham, pp.215-236.*
- Van Wees, J.D., Stephenson, R.A., Ziegler, P.A., Bayer, U., McCann, T., Dadlez, R., Gaupp, R., Narkiewicz, M., Bitzer, F., Scheck, M. (2000). On the origin of the southern Permian basin, central Europe. *Marine and Petroleum Geology*, 17,43-59.
- Winsemann, J., Brandes, C., Polom, U. (2011). Response of a proglacial delta to rapid high-amplitude lake-level change: an integration of outcrop data and high-resolution shear wave seismics. *Basin Research*, 23,22-52.
- Winsemann, J., Lang, J., Polom, U., Loewer, M., Igel, J., Pollok, L., Brandes, C. (2018). Ice-marginal forced regressive deltas in glacial lake basins: geomorphology, facies variability and large-scale depositional architecture. *Boreas*, 47,973-1002.
- Winsemann, J., Koopmann, H., Tanner, D.C., Lutz, R., Lang, J., Brandes, C., Gaedicke, C. (2020). Seismic interpretation and structural restoration of the Heligoland glaciotectionic thrust-fault complex: implications for multiple deformation during (pre-)Elsterian to Warthian ice advances into the southern North Sea Basin. *Quaternary Science Reviews*, 227,106068.

## Publication 3

This chapter has been published as Müller et al. 2021,  
In: Steffen H, Olesen O and Sutinen R (eds) Glacially-Triggered Faulting,  
Cambridge University Press

### **The challenge to distinguish soft-sediment deformation structures (SSDS) formed by glaciotectonic, periglacial and seismic processes in a formerly glaciated area: a review and synthesis**

Katharina Müller<sup>1</sup>, Jutta Winsemann<sup>1</sup>, Małgorzata Pisarska-Jamroży<sup>2</sup>, Thomas Lege<sup>3</sup>, Thomas Spies<sup>3</sup> and Christian Brandes<sup>1</sup>

<sup>1</sup>Institut für Geologie, Leibniz Universität Hannover, Callinstraße 30, 30167 Hannover, Germany

<sup>2</sup>Institute of Geology, Adam Mickiewicz University, Krygowskiego 12, 61-680 Poznań, Poland

<sup>3</sup>Bundesanstalt für Geowissenschaften und Rohstoffe (BGR), Stilleweg 2, 30655 Hannover, Germany

Corresponding Author: Katharina Müller, Institut für Geologie, Leibniz Universität Hannover, Callinstraße 30, 30167 Hannover, Germany

Email: [mueller@geowi.uni-hannover.de](mailto:mueller@geowi.uni-hannover.de)

## Abstract

This chapter gives an overview of the use of soft-sediment deformation structures (SSDS) as palaeo-earthquake indicators in formerly glaciated and periglacial areas. We review the most important processes of soft-sediment deformation and the different nomenclature used in the scientific communities.

Over the last years many studies focused on SSDS to identify past seismic events. So-called seismites are beds with SSDS that formed as a result of seismic shaking. However, in regions that were affected by glacial and periglacial processes, the use of SSDS as palaeo-earthquake indicator is challenging and the interpretation must be done with care. Earthquakes are only one trigger process of many that can cause liquefaction and/or fluidization of sediments, leading to the formation of SSDS such as load casts, flame structures, ball-and-pillow structures, convolute bedding, sand intrusions, dish-and-pillar structures, clastic dykes, sand volcanoes, craters/bowls, or gravity induced mass-flows. Ice-sheet loading, glaciotectonism and freeze and thaw processes in glacial and periglacial environments are also potential trigger processes that can cause the formation of similar types of SSDS, which can be easily mistaken for seismites. Therefore, it is important to use clear criteria to recognize seismites in the field. Characteristic features of seismically-induced SSDS are: 1) their occurrence close to major faults; 2) their presence in several outcrops in the same stratigraphic interval; 3) their large lateral extent, although high lateral variabilities of the deformation style, pattern, and bed thicknesses are possible, depending on the susceptibility of the sediments for liquefaction and/or fluidization and 4) the occurrence of deformation bands close to the tip line, where the fault displacement goes to zero.

The combination of deformation bands that occur in the vicinity of basement faults with carefully evaluated SSDS is a robust indicator for palaeo-earthquakes. The results presented in this chapter are transferable to other comparable, seismically active intraplate regions.

**Keywords:** Soft-sediment deformation structures, glaciotectonics, cryoturbation, earthquakes, deformation bands



## Introduction

Soft-sediment deformation structures (SSDS) are used as indicators for past seismic events (e.g. Montenat et al., 2007; Obermeier, 2009; Tuttle et al., 2019). However, in regions that were frequently affected by ice-sheet loading/unloading and periglacial processes, the use of SSDS for interpreting seismic events is challenging. In these regions glacial and periglacial processes affected the near-surface sediments and led to the formation of SSDS (e.g. Van Vliet-Lanoë et al., 2004; van Loon, 2009; Brandes & Winsemann, 2013; Gehrmann & Harding, 2018) similar to those caused by earthquakes. Also, depositional loading, gravity-induced sediment failure, storm or flood events in fluvial, lacustrine or shallow marine settings or salt tectonics may lead to the formation of SSDS (e.g. Li et al., 1996; Molina et al., 1998; Fossen, 2010; Vandekerkhove et al., 2020; van Loon et al., 2019) similar to those caused by earthquakes. It may therefore be difficult to distinguish the trigger process of the formation of SSDS. In addition, the use of different nomenclatures for similar SSDS (Figure 1) in the various scientific communities (e.g. seismology, sedimentology, Quaternary geology, civil engineering) may lead to confusion.

A detailed analysis of SSDS and the depositional environment in which they occur is thus important, and the use of SSDS as indicator for palaeo-earthquakes must be done with care to avoid misinterpretation. In this context, the formation and differentiation of SSDS and seismites were discussed in several studies (e.g. Van Vliet-Lanoë et al., 2004; Moretti & Sabato, 2007; Obermeier, 2009; van Loon, 2009; Shanmugam, 2016a; Tuttle et al., 2019).

Seismites are represented by beds or bed sets that contain seismically-induced SSDS (Moretti et al., 2016). The term 'seismites' was introduced by Seilacher (1969) and referred to sediment beds that were deformed by earthquake-related shaking. These deformed beds occur sandwiched between undeformed beds (e.g. van Loon et al., 2016). The deformation structures are caused by liquefaction and/or fluidization of the sediment, triggered by seismic waves (e.g. Moretti & Sabato, 2007), if the magnitude of an earthquake is high enough ( $M \geq 5.0$ ) (e.g. Atkinson et al., 1984; Rodríguez-Pascua et al., 2000; Obermeier, 2009). An earthquake with the intensity of V to VI can cause liquefaction and fluidization of sediments that occur at up to 40 km from the epicentre, depending on the nature of the sediments (Galli, 2000).

Pleistocene to Holocene seismites related to glacially-induced earthquakes are known from e.g. Belgium, Canada, Denmark, Finland, Germany, Latvia, Lithuania, the Netherlands, Poland, Russia, Scotland and the United States (e.g. Davenport et al., 1989; Ringrose, 1989; Hoffmann & Reicherter, 2012; Brandes & Winsemann, 2013; van Loon & Pisarska-Jamroży, 2014; van Loon et al., 2016; Druzhinina et al., 2017; Brandes et al., 2018a; Brooks, 2018; Ojala et al., 2018; Pisarska-Jamroży et al., 2018, 2019a,b; Woźniak & Pisarska-Jamroży, 2018; Grube, 2019a,b; Pisarska-Jamroży & Woźniak, 2019; Van Balen et al., 2019; Belzyt et al., 2021).

The most common SSDS triggered by seismic waves are load casts, flame structures, ball-and-pillow structures, convolute bedding and liquefaction spreads (Figure 1), which are mainly related to liquefaction (Rydelek & Tuttle, 2004; Obermeier, 2009; van Loon, 2009; van Loon & Pisarska-Jamroży, 2014; Sutinen et al., 2019a, b; Naik et al., 2020). Brittle deformation as well as water-escape structures (e.g. dish-and-pillar structures, clastic dykes, sand volcanoes, craters/bowls and hydrofractures) related to fluidization indicate higher pore-water pressure and often occur closer to the potential seismogenic fault (Brandes & Winsemann, 2013; Brandes et al. 2018a) and are caused by high magnitude earthquakes (e.g. Rydelek & Tuttle, 2004; Obermeier, 2009; Naik et al., 2020).

This chapter reviews the use of SSDS as palaeo-earthquake indicators in periglacial and glacial environments with a focus on northern central Europe. We describe the most important SSDS, their formation, different nomenclatures and potential trigger processes. Based on this review we deliver criteria to identify a neotectonically active fault based on SSDS. Our synthesis is transferable to other intraplate regions.

## **Formation Processes of SSDS**

Important factors that control SSDS formation are hydraulic gradient, grain size, permeability, tensile strength and flexural resistance of the sediments (e.g. Mörz et al., 2007; Obermeier, 2009; Giona Bucci et al., 2017, 2019; Pisarska-Jamrozý & Woźniak, 2019). Lowe (1975) identified two main processes of fluid escape referred to as liquefaction and fluidization that are responsible for soft-sediment deformation. The main characteristics of these processes are briefly summarised below.

### **Liquefaction**

Liquefaction is the loss of grain-to-grain contact, resulting from increased pore pressure of a static fluid (Frey et al., 2009). During liquefaction a rapid temporary increase in the porefluid pressure occurs, leading to a sudden loss of shearing resistance, which is associated with a grain framework collapse and the resulting mobilization and deformation of the liquefied bed. As fluid flow rapidly dissipates upwards, a grain-supported framework is re-established. Reversed density gradients in the liquefied sediments lead to the formation of SSDS (e.g. Lowe, 1975; Rodríguez et al., 2009; Ross et al., 2011). Liquefaction mostly develops in sediments that were buried at less than 5 m (Owen & Moretti, 2011), because higher vertical effective stress caused by the overlying sediment greatly increases the shearing and deformation resistance of the sediment (Obermeier, 2009).

Characteristic SSDS caused by liquefaction are load casts, flame structures, ball-and-pillow structures, convolute bedding (involutions), slides (liquefaction spreads) and slumps (e.g. Collinson et al., 2006; Obermeier, 2009; Sutinen et al., 2019a, b). Several processes can cause liquefaction. These include depositional loading or loading during advancing and/or overriding ice sheets, storm waves, flood events, seismic events and freeze and thaw processes in periglacial environments (e.g. Boulton & Caban, 1995; Li et al., 1996; Alfaro et al., 2002; Van Vliet-Lanoë et al., 2004; Brandes & Winsemann, 2013; van Loon et al., 2016; Bertran et al., 2019a).

### **Fluidization**

Fluidization is a process that requires pore fluid to move upwards with sufficient velocity to suspend or carry individual grains with it. Therefore, fluidization often needs an additional fluid source (Van Vliet-Lanoë et al., 2004; Shanmugam, 2016a).

The increased pore pressure leads to the expansion of the pore spaces until grain interaction is negligible and particles are free to move with the fluid (e.g. Lowe, 1975; Nichols et al., 1994; Frey et al., 2009). The fluid tends to follow preferred escape paths (e.g. faults, heterogeneities in sediment properties and layer thicknesses), while the surrounding sediment remains largely unfluidized (Mörz et al., 2007; Frey et al., 2009; Ross et al., 2011). The primary lamination is destroyed in fluidized zones, and fluid-escape structures develop that cross-cut the primary

bedding, accompanied by the injection of sand or mud into overlying layers (Lowe, 1975; Hurst & Cartwright, 2007; Frey et al., 2009; Hurst et al., 2011).

Characteristic SSDS that form due to fluidization are mud or sand intrusions, dish-and-pillar structures, clastic dykes, sand or mud volcanoes and craters/bowls (e.g. Collinson et al., 2006; Sutinen et al., 2019b). Sand volcanoes and craters in terrestrial sediments are commonly regarded as highly diagnostic features for palaeo-earthquakes (e.g. Obermeier, 2009; Sutinen et al., 2019b). However, fluidization can also be caused by different processes such as depositional loading, freeze and thaw cycles in periglacial environments (Lowe, 1975; Brandes & Winsemann, 2013; Vandenberghe, 2013; Bertran et al., 2019a), river floods or artesian groundwater rise (e.g. Deynoux et al., 1990; Li et al., 1996; Obermeier, 2009).







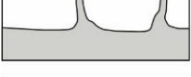


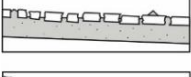





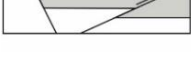
Sedimentary structures	Deformation process	Possible trigger
 load casts flame structures	liquefaction	<b>depositional loading</b> (Owen 2003); <b>storm wave loading</b> (Molina et al. 1998); <b>glacial loading</b> (Rijsdijk 2001); <b>freezing and thawing</b> (Bertran et al. 2019a); <b>seismic event</b> (Suter 2011)
 ball-and-pillow structures (pseudonodules)	liquefaction	<b>depositional loading</b> (Owen 2003; Owen & Moretti 2008); <b>storm wave loading</b> (Molina et al. 1998; Chen & Lee 2013); <b>glacial loading</b> (Rijsdijk 2001); <b>freezing and thawing</b> (Weise 1983; Bertran et al. 2019a); <b>seismic event</b> (Brandes & Winsemann 2013)
 convolute bedding (involutions)	liquefaction	<b>depositional loading</b> (Collinson et al. 2006); <b>freezing and thawing</b> (Weise 1983); <b>seismic event</b> (Chamley 1990)
 intrusions diapirs	liquefaction fluidization	<b>depositional loading</b> (Owen 2003; Suter et al. 2011); <b>seismic event</b> (Brandes & Winsemann 2013)
 dish-and-pillar structures	fluidization	<b>depositional loading</b> (Suter et al. 2011); <b>seismic event</b> (Suter et al. 2011)
 irregular branched and stepped dykes	fluidization	<b>depositional loading</b> (Alfaro et al. 2002); <b>seismic event</b> (Brandes & Winsemann 2013)
 clastic dykes (injectites)	fluidization	<b>depositional loading</b> (Alfaro et al. 2002; Hurst et al. 2003); <b>glacial loading</b> (Boulton & Caban 1995); <b>freezing and thawing</b> (Weise 1983; Bertran et al. 2019a); <b>seismic event</b> (Rodríguez-Pascua et al. 2000; Suter 2011; Brandes & Winsemann 2013)
 mud and sand volcanoes (sand blows, sand boils)	fluidization	<b>depositional loading</b> (Alfaro et al. 2002; Pisarska-Jamroży & Weckwerth 2013); <b>storm wave loading</b> (Chen & Lee 2013); <b>flood events</b> (Li et al. 1996); <b>glacial loading</b> (Benn & Evans 2013); <b>freezing and thawing</b> (Bertran et al. 2019a); <b>seismic event</b> (Rydelek & Tuttle 2004; Brandes & Winsemann 2013)
 craters (dry craters, liquefaction bowls)	fluidization	<b>freezing and thawing</b> (Buldovicz et al. 2018); <b>seismic event</b> (Rydelek & Tuttle 2004; Obermeier 2009; Sutinen et al. 2019a, b; Naik et al. 2020)
 slide blocks (liquefaction spreads, lateral spreads)	sliding (liquefaction)	<b>gravitational stress</b> (Owen 1991); <b>seismic event</b> (Obermeier 2009; Naik et al. 2020)
 folds and thrusts	slumping, creeping	<b>gravity-induced sediment failure</b> (Collinson et al. 2006; Pisarska-Jamroży 2013); <b>wetting and drying</b> (Owen 1991); <b>freezing and thawing</b> (Owen 1991; Bertran 1993); <b>seismic event</b> (Perucca et al. 2014)
 folds, thrusts and thrust-sheets	glacial stress	<b>proglacial compression</b> (Phillips et al. 2008; Brandes & Le Heron 2010; Pedersen 2014; Winsemann et al. 2020)
 kettle holes, kettle- hole fills (gravifossus)	gravitational stress	<b>thawing of (buried) ice blocks</b> (Maizels 1992; Gruszka & Van Loon 2011; Winsemann et al. 2016)
 iceberg scours (iceberg (gravity) craters, iceberg plough marks)	shearing and contractional stress	<b>iceberg ploughing</b> (Eden & Eyles 2001; Winsemann et al. 2003; Van Loon et al. 2019); <b>gravitational compression</b> (Longva & Bakkejord 1990)
 ice-wedge casts	thermal cracking	<b>freezing and thawing</b> (Weise 1983; Worsley 2014)
 deformation bands	tectonic or gravitational stress	<b>glacial loading</b> (Phillips et al. 2008); <b>proglacial compression</b> (Phillips et al. 2008); <b>freezing and thawing</b> (Bertran et al. 2019a); <b>fault movements</b> (Brandes et al. 2018a); <b>salt tectonics</b> (Fossen 2010)

Figure 1: SSDS induced by different trigger mechanisms. It has to be kept in mind that SSDS cannot be treated as equivalent to seismites. This figure shows a compilation of common SSDS and does not include all structures and trigger mechanisms that may induce SSDS. The definition of deformation mechanisms (fluidization, liquefaction) is based on Lowe (1975).

## Common Trigger Processes and Timing of SSDS Formation

As shown above, different processes can cause the formation of SSDS.

The timing of soft-sediment deformation provides an important criterion for the genetic interpretation of SSDS. Based on the style of faulting/folding or the style of truncation of bedding/lamination within the deformed sediment, 1) syndepositional, 2) metadepositional and 3) postdepositional deformation can be distinguished (Figure 2). Syndepositional soft-sediment deformation forms during the deposition of the sediment; metadepositional deformation occurs after deposition but before the overlying sediments were deposited; and postdepositional deformation takes place after the sediments have been deposited (e.g. Collinson et al., 2006; van Loon, 2009).

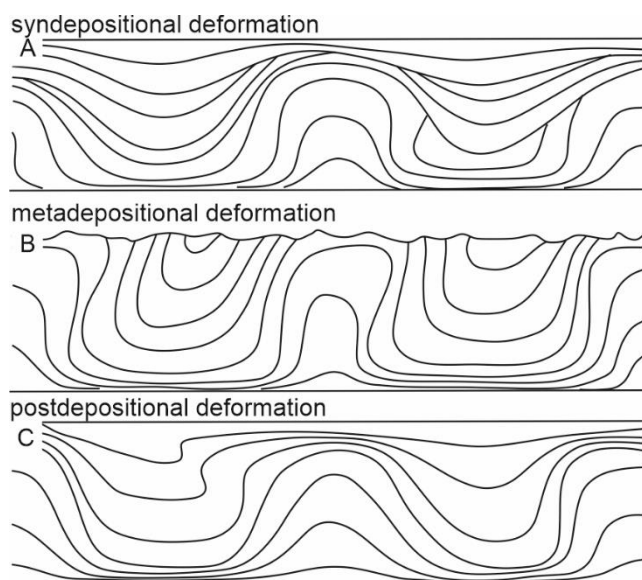


Figure 2: Based on the style of truncation of lamination within the deformed sediment (convolute bedding) the timing of soft-sediment deformation can be derived. (A) Syndepositional deformation occurs during the deposition of the sediment. (B) Metadepositional deformation occurs after deposition but before the overlying sediment was deposited. (C) Postdepositional deformation occurs after the sediments have been deposited (modified after Collinson et al., 2006).

## Earthquakes

Earthquakes can induce many different liquefaction and fluidization structures that vary in size, morphology and deformation style, depending on the earthquake magnitude and the strength of the sediment (e.g. Rodríguez-Pascua et al., 2000; Obermeier, 2009; Giona Bucci et al., 2017, 2019). In an ideal case, the formation of liquefaction or fluidization structures can be directly tied to earthquakes, as shown e.g. in the studies of Giona Bucci et al. (2017, 2019) for the 2010–12 Canterbury earthquake sequence ( $M_w$  5.8 to 7.1) and the 2016 Valentine earthquake ( $M_w$  5.7) in New Zealand.

During earthquakes the applied shear stress and accumulation of shear strain can cause a breakdown of the grain framework and an increase of the pore-water pressure, which results in liquefaction and/or fluidization of unconsolidated sediments (e.g. Obermeier et al., 2005; Obermeier, 2009). The sedimentary microfabric of SSDS is similar for different depositional environments (e.g. Giona Bucci et al., 2019).

Besides the standard SSDS that are described from outcrops and artificial trenches, seismic events can cause mass flows such as slides and slumps that may have a large lateral extent in the range of hundreds to thousands of metres. So-called liquefaction-induced lateral spreading (liquefaction spreads) occurs when unsaturated sediments slide as intact blocks over liquefied sediment. These

slide processes can occur on very gentle slopes or even relatively flat terrains (inclined as gently as 0.1–5 per cent) (Obermeier, 2009; Hungr et al., 2014; Sutinen, 2019a, b). The internal structures may include fissures, scarps and grabens. On steeper slopes, slumps and debris flows can develop, which may transition into turbidity currents in subaqueous settings (e.g. Shanmugam, 2016b; Vandekerkhove et al., 2020).

Brittle deformation and fluidization of sediment may occur in settings with higher porewater pressure and often indicate higher magnitude earthquakes and a closer location to the potential seismogenic fault (Rodríguez-Pascua et al., 2000; Brandes & Winsemann, 2013; Brandes et al., 2018a). However, these features may not always indicate a higher magnitude or a closer location to the earthquake epicentre and instead may also reflect a higher susceptibility of the sediment for deformation (Giona Bucci et al., 2017; Morsilli et al., 2020).

Longer-lived (glacial) lakes may provide excellent archives for reconstructing palaeo-earthquakes, based on well-dated flood or mass-failure events related to earthquakes that occur contemporaneously in different lakes (e.g. Monecke et al., 2006; Strasser et al., 2006; Vandekerkhove et al., 2020). Holocene earthquakes triggered by the glacial rebound of Fennoscandia are recorded in form of SSDS in varves that were deposited in a glacial lake in Finland (Ojala et al., 2018).

In recent years SSDS have been used to identify palaeo-earthquakes related to glacial isostatic adjustment (GIA). Hoffmann and Reicherter (2012) analysed SSDS in Late Pleistocene meltwater deposits, which are interpreted to have been induced by earthquakes at the southwest Baltic Sea coast in northwest Germany. Brandes et al. (2018a) reconstructed strong Lateglacial earthquakes along the northwest segment of the Sorgenfrei–Tornquist Zone in northern Denmark. Brandes et al. (2012) and Brandes and Winsemann (2013) found evidence for palaeo-earthquakes in Lateglacial sediments near the Osning Thrust, where a large variety of SSDS are developed in mixed alluvial-aeolian sediments (Meinsen et al., 2014). Several studies in the Lower Rhine Rift and the Roer Valley Rift present evidence of Pleistocene to Holocene palaeo-earthquakes and higher slip rates at several faults during the Quaternary, and they interpreted glacial rebound as possible trigger (e.g. Vanneste, 1999; Houtgast et al., 2005; Vanneste et al., 2018; Van Balen, 2019). Van Loon and Pisarska-Jamroży (2014), Pisarska-Jamroży and Woźniak (2019) reported evidence for palaeo-earthquakes in northwest and northern Poland, and van Loon et al. (2016) and Pisarska-Jamroży et al. (2019a) found evidence for palaeo-earthquakes in Latvia and Lithuania. However, more recently Pisarska-Jamroży et al. (2019a) stated that these structures alternatively may have formed by large-scale stick-slip processes during ice-sheet motion.

### **Depositional Loading**

The most common process that creates SSDS is depositional loading in water-saturated sediments, which is commonly related to high sedimentation rates (e.g. Lowe, 1975; Moretti et al., 2001; Oliveira et al., 2009). These sediments may include all styles of liquefaction and fluidization structures (Figure 1), if the overburden is thick enough. In (glacio-)lacustrine settings high sedimentation rates may cause the formation of Synsedimentary faults and liquefaction structures. Flood events, high-magnitude lake-level fluctuations or strong wave action may also generate mass-failure and liquefaction structures (Monecke et al., 2006; Vandekerkhove et al., 2020).

## **Gravity-driven sediment failure**

Gravity-driven sediment failure occurs on slopes and can be induced by different processes such as depositional loading, wetting and drying, freezing and thawing (Owen, 1991) or earthquakes (e.g. Monecke et al., 2006; Obermeier, 2009; Sutinen et al., 2019b). Climate, hydrology, vegetation, geology and topography define rates and types of the downslope displacement (Matsuoka, 2001).

Mass-flow processes include creeping, sliding and slumping and the resulting mass-flow deposits are distinguished by the degree of their internal deformation.

Creep is a granular flow with slow intergranular frictional sliding downslope with quasi-static grain contacts driven by gravity (Owen, 1991). In periglacial environments these downslope movements are referred to as solifluction or gelifluction and are caused mainly by freeze and thaw processes in the so-called active layer (e.g. French, 2017). Typical structures that develop due to these processes are thrusts and fold structures (e.g. Bertran, 1993).

Slides are translational or rotational coherent masses with a commonly planar glide plane and with minor or no internal deformation. Slumps often have concave glide planes and considerable internal deformation such as folds and thrusts (Owen, 1991; Shanmugam, 2016a). Slides and slumps may transform downslope into debris-flows, and in subaqueous settings they may transform further into turbidity currents (Shanmugam, 2016b).

## **Glaciotectonic Deformation**

Glaciotectonic deformation structures are induced by the advance of ice sheets (Figure 3A, B). During the last decades, the processes and products of glaciotectonic deformation have been studied in detail (e.g. Van der Wateren et al., 2000; Bennett et al., 2004; Phillips et al., 2008; Pedersen, 2014; Woronko et al., 2018; Winsemann et al., 2020). Glaciotectonic deformation includes: 1) proglacial contractional structures, formed at the margin of an ice sheet and 2) subglacial predominantly extensional and shearing related deformation beneath the ice sheet (Hart & Boulton, 1991). Different deformation structures commonly develop due to stress field variations caused by the advancing ice sheet. At the margin of large ice sheets, SSDS can develop due to high pore-water pressure in front or at the toe of the ice sheet (Boulton & Caban, 1995).

### ***Subglacial Deformation***

Subglacial deformation is highly variable in style and intensity and can often result in normal faulting and the formation of horst and graben structures (Figure 3A), heterogeneous folds and SSDS, which are associated with subglacial shear zones (e.g. Åmark, 1986; Piotrowski et al., 2004; Phillips et al., 2008). The initial water (or ice) content of the deformed sediments controls the pattern of deformation within the shear zone (Lee & Phillips, 2008; Phillips et al., 2008; Szuman et al., 2013; Kowalski et al., 2018). Subglacial deformation can also affect the bedrock, (e.g. Kenzler et al., 2010; Gehrmann & Harding, 2018; Winsemann et al., 2020).

### ***Proglacial Deformation***

Proglacial deformation leads to the formation of large-scale contractional structures such as folds, reverse and thrust faults (Figure 3B, C; Aber & Ber, 2007; Phillips et al., 2008; Pedersen, 2014;



Gehrmann & Harding, 2018). Depending on the rheology, competence, strain rate and strain history of the sediments and the behaviour of the ice sheet, folding (ductile deformation) or faulting (brittle deformation) may occur (Hart & Boulton, 1991; Brandes & Le Heron, 2010).

### ***Iceberg Scours, Iceberg Gravity Craters and Kettle Holes***

Iceberg scours, iceberg gravity craters and kettle holes are common features in proglacial areas. The keel of a floating iceberg creates a curvilinear scour by ploughing through the substrate. The plough mark is usually preserved as a furrow, bounded by normal faults, and a frontal ridge of scoured material on either side (Longva & Bakkejord, 1990; Eden & Eyles, 2001; Winsemann et al., 2003; van Loon et al., 2019). In cross-section the sheared scour fill may resemble sand volcanoes or clastic dykes (cf. Winsemann et al., 2003). Iceberg gravity craters form when icebergs strand and get stuck into the sediment. The resulting structures are semi-circular depressions, rimmed by low ridges (e.g. Longva & Bakkejord, 1990).

Kettle holes form by the melt-out of (buried) isolated blocks of glacier ice and commonly consist of near-circular depressions, which may be bounded by steep normal faults (Maizels, 1992). The kettle-hole fill may be characterised by a pronounced down warping of strata into the central depression, showing small scale deformation structures such as folds and faults (e.g. Gruszka & van Loon, 2011; Winsemann et al., 2016).

### **Periglacial Processes**

The periglacial environment is the marginal zone of an ice sheet that is not directly influenced by the glacier but characterised by permafrost conditions (Figure 3C–G; French, 2017). Cryoturbation is a widely used term for different deformation structures that develop in unconsolidated sediments under periglacial conditions. It is related to seasonal freeze and thaw processes in the so-called active layer (e.g. Dobiński, 2011; French, 2017).

Processes that produce cryoturbation structures are shrinkage, frost heave pressure or swelling and differential loading, which cause vertical grain movement or gravity-induced lateral mass movements (Bockheim & Tarnocai, 1998; Van Vliet-Lanoë et al., 2004; Ogino & Matsuoka, 2007). Buldovicz et al. (2018) and Bertran et al. (2019a) showed that SSDS may be caused by the formation of ground ice and a related pore-water overpressure in underlying or overlying sediments if water is available. Therefore, the most important controlling factors for the type and abundance of cryoturbation structures are moisture content, thermal gradient and grain size of the sediments (e.g. Van Vliet-Lanoë et al., 2004).

### ***Ice Wedges and Ice-Wedge Casts***

Ice wedges are wedge-shaped bodies with their apex pointing downwards; they are composed of foliated or vertically banded ice (Harry, 1988). Ice wedges develop in thermal contraction cracks, in which hoar frost forms and water from melting snow percolates into the near-surface sediments (Weise, 1983).

Repeated annual contraction cracking of the ice in the wedge, followed by freezing of water in the crack, leads to a gradual increase in the width and depth of the wedge and causes vertical banding of the ice mass (Harry, 1988; Collinson et al., 2006). The size of ice wedges typically ranges 1–3 m in width and 2–6 m in depth (Worsley, 2014).

An ice-wedge cast is the fill in the space formerly occupied by ice (Figure 3D–F). Ice-wedge casts are a widespread indicator of past periglacial conditions and permafrost.

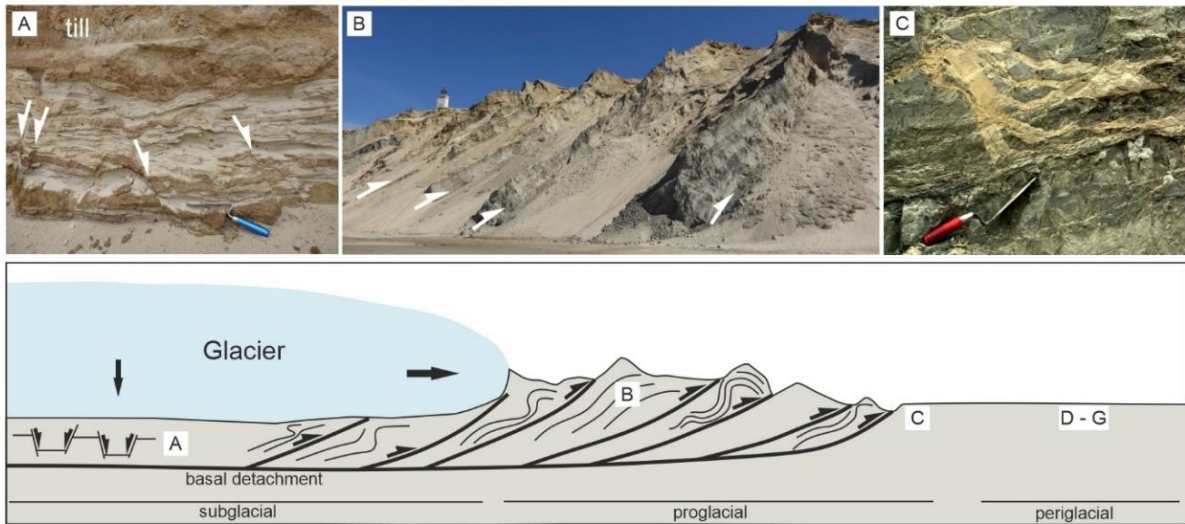
### ***Periglacial Involutions and craters***

Involutions and convolute bedding describe comparable structures, reported from past and present periglacial environments with permafrost or deep seasonal frost (Ogino & Matsuoka, 2007; Vandenberghe, 2013; Figure 3G). These deformation structures include folding of a pre-existing lamination, commonly into upright cusped forms with sharp anticlines and more gentle synclines (Collinson et al., 2006) or more swirl-like or tear-drop patterns (Bockheim & Tarnocai, 1998; Pisarska-Jamroży & Zieliński, 2012).

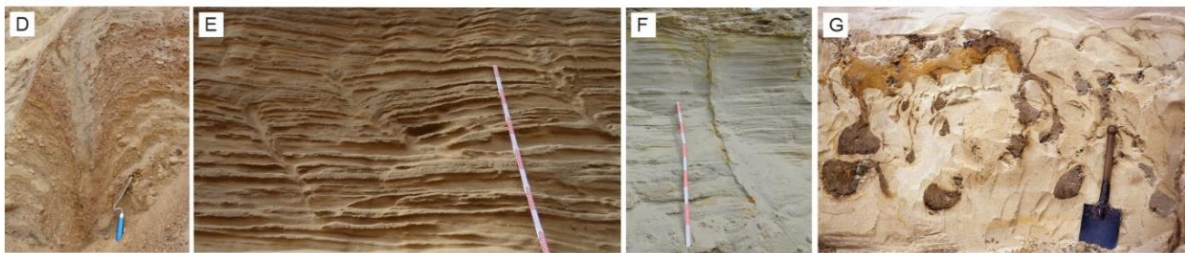
In the literature the term involution is connected with cryoturbation. Involutions that occur in seasonal frost regions show smaller vertical amplitudes (0.6 m) than involutions with up to 2-m amplitudes that developed in permafrost regions (Vandenberghe, 2013; French, 2017). However, the size of the involutions can also differ with the lithology and the forming process (Ogino and Matsuoka, 2007).

Craters may form by collapsing pingos, also referred to as cryovolcanism. In a recent study Buldovicz et al. (2018) showed that pingos in Siberia collapsed under cryogenic hydrostatic pressure build-up in the closed system of a freezing talik. This happened before the freezing was complete, when a core of wet sediment remained unfrozen and stored a large amount of carbon dioxide dissolved in pore water. When gas-phase saturation was reached, the resulting overpressure led to an explosion of the pingos.

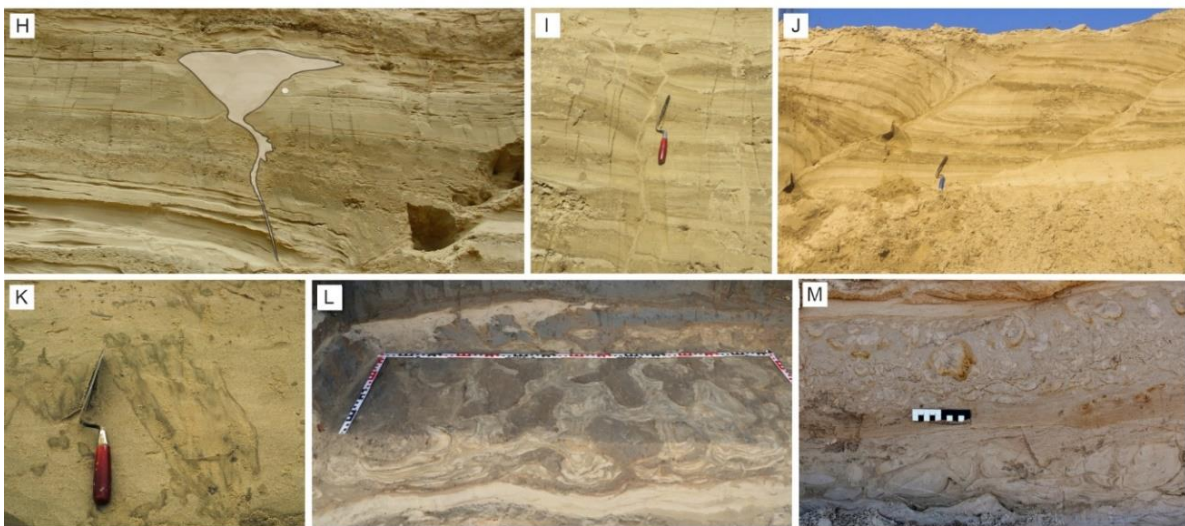
Glaciotectonic complex



Periglacial soft-sediment deformation structures



Earthquake-induced soft-sediment deformation structures



Deformation bands

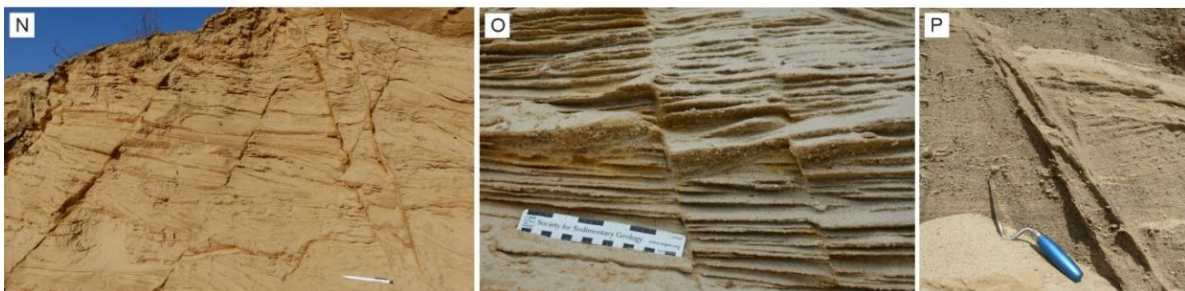


Figure 3: Typical SSDS that formed by glaciotectonics, periglacial processes and earthquakes. (A-C) Deformation structures related to glaciotectonic complexes (based on Aber & Ber, 2007). (A) Normal faults

in meltwater sand, overlain by till (Gardelegen, Germany). The faults formed by subglacial deformation. (B) Thrust-sheets in glaciolacustrine deposits (Lønstrup Klint, Denmark), formed by proglacial deformation. (C) Hydrofractures in silt. These structures were most probably caused by a high pore water pressure in front of an ice sheet (Lønstrup Klint, Denmark). (D-G) Cryoturbation features that formed by freeze and thaw processes in periglacial settings. (D) Ice-wedge cast in meltwater deposits (Bolsehle, Germany). (E) Three ice-wedge casts in alluvial-fan deposits (Dresden, Germany). (F) Thin ice-wedge cast in meltwater sand (Groß Eilstorf, Germany). (G) Involutions in meltwater deposits and till (Stukenbrock, Germany; by courtesy of K. Skupien). (H-M) Earthquake-induced SSDS. (H) Sand volcano in mixed alluvial-aeolian sediments (Oerlinghausen, Germany; Brandes and Winsemann, 2013). (I) Clastic dykes in mixed alluvial-aeolian sediments (Oerlinghausen, Germany; Brandes et al., 2012; Brandes & Winsemann, 2013). (J) Inversion structures with a typical harpoon shape in mixed alluvial-aeolian sediments (Oerlinghausen, Germany; Brandes and Winsemann, 2013). (K) Irregular branched and stepped dykes in mixed alluvial-aeolian sediments (Augustdorf, Germany; Brandes and Winsemann, 2013). (L) Load casts, pseudonodules, and flame structures in glaciolacustrine deposits (Dwasieden, Germany; Pisarska-Jamroży et al., 2018). (M) Load casts, flame structures and water escape-structures in glaciolacustrine deposits (Baltmuiža, Latvia; Belzyt et al., 2018). (N-P) Deformation bands. (N) Set of conjugate deformation bands with normal displacement in ice-marginal delta slope sediments deposits (Altenhagen, Germany). (O) Two thin deformation bands with normal displacement in meltwater sand (Groß Eilstorf, Germany). (P) Deformation bands in ice-marginal delta slope sediment (Freden, Germany).

## Limitation of SSDS to Identify Palaeo-Earthquakes

As shown above, SSDS can be used to indicate past seismic events, and in an ideal case they can directly indicate palaeo-earthquakes.

However, it must be kept in mind that SSDS can be also induced by a set of different non-seismic processes as discussed in Section *Common Trigger Processes and Timing of SSDS Formation*. (Figures 1, 3A-G), and it is often challenging to derive the related triggers, especially in areas that were affected by glacial and periglacial processes. Moreover, not all earthquakes trigger liquefaction and fluidization processes. SSDS are likely to be formed only in susceptible sediments, (Figure 3H-M). They often develop in fine- to medium-grained water-saturated sand with a loose grain packing (high porosity). Barriers, with low permeability such as mud laminae or matrix-rich impermeable beds that support the increase in pore-water pressure, must be present. The susceptibility of the sediment is therefore the most important requirement for the formation of seismically triggered liquefaction and/or fluidization features (Rodríguez-Pascua et al., 2000; Giona Bucci et al., 2017, 2019; Morsilli et al., 2020). Thus, the most distinct liquefaction and fluidization features may not necessarily be located close to the earthquake epicentre. Instead their distribution may reflect the grain size, sorting and cohesion of the sediments and the position of the groundwater table (Giona Bucci et al., 2017; Morsilli et al., 2020).

To ensure a careful application of SSDS in palaeoseismological studies, various criteria and schemes were proposed, which in general are quite similar (e.g. Wheeler 2002; Van Vliet-Lanoë et al., 2004, Obermeier, 2009; Owen & Moretti, 2011; van Loon et al., 2016; Morsilli et al., 2020).

To identify seismically-induced SSDS, Wheeler (2002) introduced a test scheme that involves the following criteria: 1) sudden formation, 2) synchronicity, 3) zoned distribution over several outcrops, 4) size, 5) tectonic setting and 6) depositional setting.

Owen and Moretti (2011) defined six criteria to ensure identification of seismites in the field: 1) large areal extent, 2) lateral continuity, 3) vertical repetition of beds with SSDS, 4) comparable morphology of SSDS with deformation structures described from earthquakes, 5) proximity to active faults and 6) complexity and frequency of SSDS as dependent on the distance to the triggering fault.

According to van Loon et al. (2016) the most important criterion for recognizing seismites is the vertical repetition of beds with SSDS. However, Morsilli et al. (2020) reported that the number of deformed beds and their main physical character (size of deformation, morphologies and thicknesses of the deformed intervals) may change laterally. So, many applied criteria are not diagnostic and do not rule out other trigger mechanisms (Owen & Moretti, 2011; Brandes & Winsemann, 2013). A vertical repetition of beds with SSDS in (glacial) lakes (e.g. Monecke et al., 2006), often regarded as diagnostic for seismic events, can be also the result of major (meltwater) flood events or retrogressive slides leading to the rapid deposition of thicker beds. In periglacial environments, for example, seasonal freeze and thaw cycles can lead to the formation of vertically stacked beds with SSDS, which are produced by loading or diapirism (Vandenberghe, 2013). In non-glacigenic settings, fast depositional loading of water-saturated sediments may lead to the formation of all styles of liquefaction and fluidization structures (Figure 1), if the overburden and pore pressure is high enough (Owen, 2003; Rodrigues et al., 2009). These SSDS may also appear in different stratigraphic levels but are not the result of an earthquake. However, many of the criteria described above are difficult to evaluate. It remains a challenge to identify a large areal extent of seismites, because outcrops are often isolated or restricted to sand and gravel pits.

The limitations in the use of SSDS as palaeo-earthquake indicators have been recognized by several authors. Montenat et al. (2007) pointed out that SSDS are not always univocal and their interpretation has to be placed in the geological context. Shanmugam (2016a) summarised that earthquakes are only one of the twenty-one mechanisms that can cause liquefaction and/or fluidization. Consequently, the use of SSDS as indicators for palaeoseismicity is controversial (e.g. Bertran et al., 2019b).

## **Deformation Bands as Indicators for Neotectonic Fault Activity**

The inconclusive nature of SSDS requires a more robust indicator for neotectonic activity. The work of Cashman et al. (2007), Brandes and Tanner (2012), Shipton et al. (2017) and Brandes et al. (2018a, b) showed that near-surface deformation bands in unconsolidated sediments are such an indicator for neotectonic activity at basement faults. Deformation bands are tabular zones of local deformation, which can occur in unconsolidated sandy sediments and sedimentary rocks (Ballas et al., 2015). They form in porous material (Figure 3N–P) and represent equivalents to faults that usually form in nonporous rocks. Recent studies show that near-surface deformation bands, which formed in unconsolidated sediments, can develop due to tectonic activity along large faults (Cashman et al., 2007; Brandes et al., 2018a, b). Especially, shear-deformation bands are a relevant tool in palaeoseismological and neotectonic studies and, if developed in young, unconsolidated sediments, can serve as a strong indicator for recently active faults. Deformation bands that formed in a glaciotectonic environment can show a spread in strike direction, whereas those formed by neotectonics follow the strike of the regional basement faults (Brandes et al., 2018a, b). In the latter case the deformation processes were caused by fault propagation and reflect the fault-related deformation above the tip line of reactivated basement faults (Brandes et al., 2018b). Deformation bands might also be formed by cryoturbation processes. In such a case they reflect the local near-surface extension and contraction of the sediments related to freeze and thaw processes (Bertran et al., 2019a).

Cataclastic deformation bands are an indicator for fault rupture processes (Cashman et al., 2007). The non-cataclastic deformation bands shown by Brandes and Tanner (2012) and Brandes et al. (2018b) are not indicators for palaeo-earthquakes. Nevertheless, their orientation follows the

strike of underlying basement faults, thus indicating a close relation. We argue that deformation bands in combination with (carefully evaluated) SSDS are the most reliable indicator for palaeo-earthquakes, if the deformation bands follow the strike of the nearby fault and the SSDS match the criteria of Wheeler (2002) and Owen and Moretti (2011). The deformation bands reflect the fault activity, and the SSDS indicate the passage of seismic waves.

## Conclusions

Different processes that include depositional loading, flood and storm events, glacial loading and proglacial compression, iceberg ploughing, freeze and thaw processes, mass failure and salt tectonics can produce SSDS that may be mistaken for earthquake-induced deformation structures. Therefore, the use of SSDS as indicators for palaeo-earthquakes in intraplate areas (characterised by rather low magnitudes and long earthquake recurrence intervals) that were affected by glaciotectonic deformation and periglacial processes is difficult and has to be done with care to ensure a correct application.

Nevertheless, SSDS can deliver valuable hints to palaeoseismology if they 1) are developed close to major faults; 2) are exposed in several outcrops in the same stratigraphic interval; 3) show a large lateral extent, although high lateral variabilities of the deformation style, pattern and bed thicknesses are possible, depending on the susceptibility of the sediments for liquefaction and/or fluidization; and 4) are associated with deformation bands that have the same strike direction as the regional faults.

## Acknowledgements

We thank Gösta Hoffmann and Ronald Van Balen for their constructive reviews, which helped to improve the manuscript. The work has been financially supported by the project *Paläoseismische Untersuchung Norddeutschlands* from the BGR (No. 201-10079313) and *GREBAL* from the National Science Centre Poland No. 2015/19/B/ST10/00661. Reproduced with permission of The Licensor through PLSclear.



## References

- Aber, J.S., Ber, A. (2007). *Glaciotectonism. Developments in Quaternary Science*, 6. Elsevier, Amsterdam, p.246.
- Alfaro, P., Delgado, J., Estévez, A., Molina, J., Moretti, M., Soria, J. (2002). Liquefaction and fluidization structures in Messinian storm deposits (Bajo Segura Basin, Betic Cordillera, southern Spain). *International Journal of Earth Sciences*, 91,505-513.
- Åmark, M. (1986). Clastic dikes formed beneath an active glacier. *Geologiska Föereningen i Stockholm Föerhandlingar*, 108,13-20.
- Ballas, G., Fossen, H., Soliva, R. (2015). Factors controlling permeability of cataclastic deformation bands and faults in porous sandstone reservoirs. *Journal of Structural Geology*, 76,1-21.
- Belzyt, S., Nartišs, M., Pisarska-Jamroży, M., Woronko, B., Bitinas, A. (2018). Large-scale glaciotectonically-deformed Pleistocene sediments with deformed layers sandwiched between undeformed layers, Baltmuiža site, Western Latvia. In: Pisarska-Jamroży, M., Bitinas, A. (Eds.), *Soft-sediment deformation structures and palaeoseismic phenomena in the South-eastern Baltic Region. Excursion guide of International Palaeoseismological Field Workshop*, 17-21st September 2018, Vilnius, Lithuania. Lithuanian Geological Survey, Lithuanian Geological Society, pp. 38-42
- Belzyt, S., Pisarska-Jamroży, M., Bitinas, A., Woronko, B., Phillips, E. R., Piotrowski, J. A. and Jusienė, A. (2021). Repetitive Late Pleistocene soft-sediment deformation by seismicity-induced liquefaction in north-western Lithuania. *Sedimentology*, doi: 10.1111/sed.12883.
- Bennett, M.R., Huddart, D., Waller, R.I., Midgley, N.G., Gonzalez, N., Tomio, N. (2004). Styles of ice-marginal deformation at Hagafellsjökull-Eystri, Iceland during the 1998/99 winter-spring surge. *Boreas*, 33,97-107.
- Bertran, P. (1993). Deformation-induced microstructures in soils affected by mass movements. *Earth Surface Processes and Landforms*, 18,645-660.
- Bertran, P., Font, M., Giret, A., Manchuel, K., Sicilia, D. (2019a). Experimental soft-sediment deformation caused by fluidization and intrusive ice melt in sand. *Sedimentology*, 66,1102-1117.
- Bertran, P., Manchuel, K., Sicilia, D. (2019b). Discussion on 'Palaeoseismic structures in Quaternary sediments, related to an assumed fault zone north of the Permian Peissen-Gnutz salt structure (NW Germany)-Neotectonic activity and earthquakes from the Saalian to the Holocene' (Grube, 2019). *Geomorphology*, 365,106704.
- Bockheim, J.G., Tarnocai, C. (1998). Recognition of cryoturbation for classifying permafrost-affected soils. *Geoderma*, 81,281-293.
- Boulton, G.S., Caban, P. (1995). Groundwater flow beneath ice sheets: part II-its impact on glacier tectonic structures and moraine formation. *Quaternary Science Reviews*, 14,563-587.
- Brandes, C., Le Heron, D.P. (2010). The glaciotectonic deformation of Quaternary sediments by fault-propagation folding. *Proceedings of the Geologists' Association*, 121,270-280.
- Brandes, C., Tanner, D.C. (2012). Three-dimensional geometry and fabric of shear deformation-bands in unconsolidated Pleistocene sediments. *Tectonophysics*, 518-521,84-92.
- Brandes, C., Winsemann, J., Roskosch, J., Meinsen, J., Tanner, D.C., Frechen, M., Steffen, H., Wu, P. (2012). Activity along the Osning Thrust in Central Europe during the Lateglacial: ice-sheet and lithosphere interactions. *Quaternary Science Reviews*, 38,49-62.
- Brandes, C., Winsemann, J. (2013). Soft-sediment deformation structures in NW Germany caused by Late Pleistocene seismicity. *International Journal of Earth Sciences*, 102,2255-2274.
- Brandes, C., Steffen, H., Sandersen, P.B.E., Wu, P., Winsemann, J. (2018a). Glacially induced faulting along the NW segment of the Sorgenfrei-Tornquist Zone, northern Denmark: Implications for neotectonics and Lateglacial fault-bound basin formation. *Quaternary Science Reviews*, 189,149-168.
- Brandes, C., Igel, J., Loewer, M., Tanner, D.C., Lang, J., Müller, K., Winsemann, J. (2018b). Visualisation and analysis of shear-deformation bands in unconsolidated Pleistocene sand using ground-penetrating radar: Implications for paleoseismological studies. *Sedimentary Geology*, 367,135-145.



- Brooks, G.R. (2018). Deglacial record of palaeoearthquakes interpreted from mass transport deposits at three lakes near Rouyn-Noranda, north-western Quebec, Canada. *Sedimentology*, 65,2439-2467.
- Buldovicz, S.N., Khilimonyuk, V.Z., Bychkov, A.Y., Ospennikov, E.N., Vorobyev, S.A., Gunar, A.Y., Gorshkov, E.I., Chuvilin, E.M., Cherbunina, M.Y., Kotov, P.I., Lubnina, N.V., Motenko, R.G., Amanzhurov, R.M. (2018). Cryovolcanism on the Earth: Origin of a spectacular crater in the Yamal peninsula (Russia). *Scientific Reports*, 8,1-6.
- Cashman, S.M., Baldwin, J.N., Cashman, K.V., Swanson, K., Crawford, R. (2007). Microstructures developed by coseismic and aseismic faulting in near-surface sediments, San Andreas fault, California. *Geology*, 35,611-614.
- Chen, J., Lee, H.S. (2013). Soft-sediment deformation structures in Cambrian siliciclastic and carbonate storm deposits (Shandong Province, China): Differential liquefaction and fluidization triggered by storm-wave loading. *Sedimentary Geology*, 288,81-94.
- Collinson, J.D., Mountney, N.P., Thompson, D.B. (2006). *Sedimentary Structures*. Terra Publishing, England, 3 edition, pp.292.
- Davenport, C.A., Ringrose, P.S., Becker, A., Hancock, P., Fenton, C. (1989). Geological investigations of late and post glacial earthquake activity in Scotland. In: Gregersen, S., Basham, P.W. (Eds.), *Earthquakes at North-Atlantic passive margins: neotectonics and postglacial rebound*. Springer, Dordrecht, pp.175-194.
- Deynoux, M., Proust, J.N., Durand, J., Merino, E. (1990). Water-transfer cylindrical structures in the Late Proterozoic eolian sandstones in the Taoudeni Basin, West Africa. *Sedimentary Geology*, 66,227-242.
- Dobiński, W. (2011). Permafrost. *Earth-Science Reviews*, 108,158-169.
- Druzhinina, O., Bitinas, A., Molodkov, A., Kolesnik, T. (2017). Palaeoseismic deformations in the Eastern Baltic region (Kaliningrad District of Russia). *Estonian Journal of Earth Sciences*, 66,119-129.
- Eden, D.J., Eyles, N. (2001). Description and numerical model of Pleistocene iceberg scours and ice-keel turbated facies at Toronto, Canada. *Sedimentology*, 48,1079-1102.
- Fossen, H. (2010). Deformation bands formed during soft-sediment deformation: observations from SE Utah. *Marine and Petroleum Geology*, 27,215-222.
- French, H.M. (2017). *The periglacial environment*. John Wiley and Sons. 4. edition, Chichester, p.544.
- Frey, S.E., Gingras, M.K., Dashtgard, S.E. (2009). Experimental studies of gas-escape and water-escape structures: mechanisms and morphologies. *Journal of Sedimentological Research*, 79,808-816.
- Galli, P. (2000). New empirical relationships between magnitude and distance for liquefaction. *Tectonophysics*, 324,169-187.
- Gehrmann, A., Harding, C. (2018). Geomorphological Mapping and Spatial Analyses of an Upper Weichselian Glacitectonic Complex Based on LiDAR Data, Jasmund Peninsula (NE Rügen), Germany. *Geosciences*, 8,208-232.
- Giona Bucci, M., Almond, P., Villamor, P., Ries, W., Smith, C., Tuttle, M.P. (2017). When the earth blisters: exploring recurrent liquefaction features in the coastal system of Christchurch, New Zealand. *Terra Nova*, 29,162-172.
- Giona Bucci, M., Smith, C.M., Almond, P.C., Villamor, P., Tuttle, M.P. (2019). Micromorphological analysis of liquefaction features in alluvial and coastal environments of Christchurch, New Zealand. *Sedimentology*, 66,963-982.
- Grube, A. (2019a). Palaeoseismic structures in Quaternary sediments of Hamburg (NW Germany), earthquakes evidence during the younger Weichselian and Holocene. *International Journal of Earth Sciences*, 108,845-861.
- Grube, A. (2019b). Palaeoseismic structures in Quaternary sediments, related to an assumed fault zone north of the Permian Peissen-Gnutz salt structure (NW Germany) – Neotectonic activity and earthquakes from the Saalian to the Holocene. *Geomorphology*, 328,15-27.
- Gruszka, B., Van Loon, A.J. (2011). Genesis of a giant gravity-induced depression (gravifossum) in the Enköping esker, S. Sweden. *Sedimentary Geology*, 235,304-313.

- Harry, D.G. (1988). Ground ice and permafrost. *Advances in Periglacial Geomorphology*. Wiley, Chichester, pp.113-149.
- Hart, J.K., Boulton, G.S. (1991). The interrelation of glaciotectonic and glacio-depositional processes within the glacial environment. *Quaternary Science Reviews*, 10, 335-350.
- Hoffmann, G., Reicherter, K. (2012). Soft-sediment deformation of Late Pleistocene sediments along the southwestern coast of the Baltic Sea (NE Germany). *International Journal of Earth Sciences*, 101,351-363.
- Houtgast, R.F., Van Balen, R.T., Kasse, C. (2005). Late Quaternary evolution of the Feldbiss Fault (Roer Valley Rift System, the Netherlands) based on trenching, and its potential relation to glacial unloading. *Quaternary Science Reviews*, 24,489-508.
- Hungr, O., Leroueil, S., Picarelli, L. (2014). The Varnes classification of landslide types, an update. *Landslides*, 11,167-194.
- Hurst, A., Cartwright, J., Duranti, D. (2003). Fluidization structures produced by upward injection of sand through a sealing lithology. Geological Society, London, Special Publications, 216,123-138.
- Hurst, A., Cartwright, J. (2007). Relevance of sand injectites to hydrocarbon exploration and production. In: Hurst A., Cartwright, J. (Eds.), *Sand injectites: implications for hydrocarbon exploration and production*, AAPG Memoir 87, Tulsa, pp. 1-19.
- Hurst, A., Scott, A., Vigorito, M. (2011). Physical characteristics of sand injectites. *Earth-Science Reviews*, 106,215-246.
- Kenzler, M., Obst, K., Hüneke, H., Schütze, K. (2010). Glazitektonische Deformation der kretazischen und pleistozänen Sedimente an der Steilküste von Jasmund nördlich des Königsstuhls (Rügen). *Brandenburger Geowissenschaftliche Beiträge*, 17,107-122.
- Kowalski, A., Makoś, M., Pitura, M. (2019). New insights into the glacial history of southwestern Poland based on large-scale glaciotectonic deformations-a case study from the Czaple II Gravel Pit (Western Sudetes). *Annales Societatis Geologorum Poloniae*, 88,341-359.
- Lee, J.R., Phillips, E.R. (2008). Progressive soft sediment deformation within a subglacial shear zone—a hybrid mosaic-pervasive deformation model for Middle Pleistocene glaciotectonised sediments from eastern England. *Quaternary Science Reviews*, 27,1350-1362.
- Li, Y., Craven, J., Schweig, E.S., Obermeier, S.F. (1996). Sand boils induced by the 1993 Mississippi River flood: Could they one day be misinterpreted as earthquake-induced liquefaction? *Geology*, 24,171-174.
- Longva, O., Bakkejord, K.J. (1990). Iceberg deformation and erosion in soft sediments, southeast Norway. *Marine Geology*, 92,87-104.
- Lowe, D.R. (1975). Water escape structures in coarse-grained sediments. *Sedimentology*, 22,157-204.
- Maizels, J.K. (1992). Boulder ring structures produced during jökulhaups flows: origin and hydraulic significance. *Geografiska Annaler*, 74A,21-33.
- Matsuoka, N. (2001). Solifluction rates, processes and landforms: a global review. *Earth-Science Reviews*, 55,107-134.
- Meinsen, J., Winsemann, J., Roskosch, J., Brandes, C., Frechen, M., Dultz, S., Böttcher, J. (2014). Climate control on the evolution of Late Pleistocene alluvial-fan and aeolian sand-sheet systems in NW Germany. *Boreas*, 43,42-66.
- Molina, J.M., Alfaro, P., Moretti, M., Soria, J.M. (1998). Soft-sediment deformation structures induced by cyclic stress of storm waves in tempestites (Miocene, Guadalquivir Basin, Spain). *Terra Nova*, 10,145-150.
- Monecke, K., Anselmetti, F.S., Becker, A., Schnellmann, M., Sturm, M., Giardini, D. (2006). Earthquake-induced deformation structures in lake deposits: A Late Pleistocene to Holocene paleoseismic record for Central Switzerland. *Eclogae Geologicae Helvetiae*, 99,343-362.
- Moretti, M., Miguel, J., Alfaro, P., Walsh, N. (2001). Asymmetrical soft-sediment deformation structures triggered by rapid sedimentation in turbiditic deposits (Late Miocene, Guadix Basin, Southern Spain). *Facies*, 44,283-294.

- Moretti, M., Sabato, L. (2007). Recognition of trigger mechanisms for soft-sediment deformation in the Pleistocene lacustrine deposits of the Sant'Arcangelo Basin (Southern Italy): seismic shock vs. overloading. *Sedimentary Geology*, 196,31-45.
- Moretti, M., Alfaro, P., Owen, G. (2016). The environmental significance of soft-sediment deformation structures: key signatures for sedimentary and tectonic processes. *Sedimentary Geology*, 344,1-4.
- Mörz, T., Karlik, E.A., Kreiter, S., Kopf, A. (2007). An experiment setup for fluid venting in unconsolidated sediments: new insights to fluid mechanics and structures. *Sedimentary Geology*, 196,251-267.
- Montenat, C., Barrier, P., d'Estevou, P.O., Hibsich, C. (2007). Seismites: an attempt at critical analysis and classification. *Sedimentary Geology*, 196,5-30.
- Morsilli, M., Bucci, M.G., Gliozzi, E., Lisco, S., Moretti, M. (2020). Sedimentary features influencing the occurrence and spatial variability of seismites (late Messinian, Gargano Promontory, southern Italy). *Sedimentary Geology*, 105628.
- Naik, S.P., Mohanty, A., Porfido, S., Tuttle, M., Gwon, O., Kim, Y.S. (2020). Intensity estimation for the 2001 Bhuj earthquake, India on ESI-07 scale and comparison with historical 16th June 1819 Allah Bund earthquake: A test of ESI-07 application for intraplate earthquakes. *Quaternary International*, 536,127-143.
- Nichols, R.J., Sparks, R.S.J., Wilson, C.J.N. (1994). Experimental studies of fluidization of layered sediments and the formation of fluid escape structures. *Sedimentology*, 41,233-253.
- Obermeier, S.F., Olson, S.M., Green, R.A. (2005). Field occurrences of liquefaction-induced features: a primer for engineering geologic analysis of paleoseismic shaking. *Engineering Geology*, 76,209-234.
- Obermeier, S.F. (2009) Using liquefaction-induced and other soft-sediment features for paleoseismic analysis. In: McCalpin J.P. (Ed.), *Paleoseismology*. International Geophysics Series, 95, Elsevier, Amsterdam, pp.497-564.
- Ogino, Y., Matsuoka, N. (2007). Involutions resulting from annual freeze - thaw cycles: a laboratory simulation based on observations in northeastern Japan. *Permafrost and Periglacial Processes*, 18,323-335.
- Ojala, A.E., Mattila, J., Virtasalo, J., Kuva, J., Luoto, T.P. (2018). Seismic deformation of varved sediments in southern Fennoscandia at 7400 cal BP. *Tectonophysics*, 744,58-71.
- Oliveira, C.M.M, Hodgson, D.M., Flint, S.S. (2009). Aseismic controls on in situ soft-sediment deformation processes and products in submarine slope deposits of the Karoo Basin, South Africa. *Sedimentology*, 56,1201-1225.
- Owen, L.A. (1991). Mass movement deposits in the Karakoram Mountains: their sedimentary characteristics, recognition and role in Karakoram landform evolution. *Zeitschrift für Geomorphologie*, 35,401-424.
- Owen, G. (2003). Load structures: gravity-driven sediment mobilization in the shallow subsurface. Geological Society, London, Special Publications, 216,21-34.
- Owen, G., Moretti, M. (2008). Determining the origin of soft-sediment deformation structures: a case study from Upper Carboniferous delta deposits in south-west Wales, UK. *Terra Nova*, 20,237-245.
- Owen, G., Moretti, M. (2011). Identifying triggers for liquefaction-induced soft-sediment deformation in sands. *Sedimentary Geology*, 235,141-147.
- Pedersen, S.A.S. (2014). Architecture of Glaciotectonic Complexes. *Geosciences*, 4,269-296.
- Perucca, L.P., Godoy, E., Pantano, A. (2014). Late Pleistocene-Holocene earthquake-induced slumps and soft-sediment deformation structures in the Acequion River valley, Central Precordillera, Argentina. *Geologos*, 20,147-156.
- Phillips, E.R., Lee, J.R., Burke, H. (2008). Progressive proglacial to subglacial deformation and syntectonic sedimentation at the margins of the Mid-Pleistocene British Ice Sheet: evidence from north Norfolk, UK. *Quaternary Science Reviews*, 27,1848-1871.
- Piotrowski, J.A., Larsen, N.K., Junge, F.W. (2004). Reflections on soft subglacial beds as a mosaic of deforming and stable spots. *Quaternary Science Reviews*, 23,993-1000.

- Pisarska-Jamroży, M., Zieliński, T. (2012). Specific erosional and depositional processes in a Pleistocene subglacial tunnel in the Wielkopolska region, Poland. *Geografiska Annaler*, 94A,429-443.
- Pisarska-Jamroży, M. (2013). Varves and megavarves in the Eberswalde Valley (NE Germany)-A key for the interpretation of glaciolimnic processes. *Sedimentary Geology*, 291,84-96.
- Pisarska-Jamroży, M., Weckwerth, P. (2013). Soft-sediment deformation structures in a Pleistocene glaciolacustrine delta and their implications for the recognition of sub-environments in delta deposits. *Sedimentology*, 60,637-665.
- Pisarska-Jamroży, M., Belzyt, S., Börner, A., Hoffmann, G., Hüneke, H., Kenzler, M., Obst, K., Rother, H., Van Loon, A.J. (2018). Evidence from seismites for glacio-isostatically induced crustal faulting in front of an advancing land-ice mass (Rügen Island, SW Baltic Sea). *Tectonophysics*, 745,338-348.
- Pisarska-Jamroży, M., Woźniak, P.P. (2019). Debris-flow and glacio isostatic-induced soft-sediment deformation structures in a Pleistocene glaciolacustrine fan: The southern Baltic Sea coast, Poland. *Geomorphology*, 326,225-238.
- Pisarska-Jamroży, M., Belzyt, S., Bitinas, A., Jusienė, A., Woronko, B. (2019a). Seismic shocks, periglacial conditions and glaciotectonics as causes of the deformation of a Pleistocene meandering river succession in central Lithuania. *Baltica*, 32,63-77.
- Pisarska-Jamroży, M., Belzyt, S., Börner, A., Hoffmann, G., Hüneke, H., Kenzler, M., Obst, K., Rother, H., Steffen, H., Steffen, R., Van Loon, A.J. (2019b). The sea cliff at Dwasieden: Soft-sediment deformation structures triggered by glacial isostatic adjustment in front of the advancing Scandinavian Ice Sheet. *DEUQUA Special Publication*, 2,61-67.
- Rijsdijk, K.F. (2001). Density-driven deformation structures in glacially consolidated diamicts: examples from Traeth Y Mwnt, Cardiganshire, Wales, UK. *Journal of Sedimentary Research*, 71,122-135.
- Ringrose, P.S. (1989). Palaeoseismic (?) liquefaction event in late Quaternary lake sediment at Glen Roy, Scotland. *Terra Nova*, 1,57-62.
- Rodríguez, N., Cobbold, P.R., Løseth, H. (2009). Physical modeling of sand injectites. *Tectonophysics* 474,610-632.
- Rodríguez-Pascua, M.A., Calvo, J.P., De Vicente, G., Gómez-Gras, D. (2000). Soft-sediment deformation structures interpreted as seismites in lacustrine sediments of the Prebetic Zone, SE Spain, and their potential use as indicators of earthquake magnitudes during the Late Miocene. *Sedimentary Geology*, 135,117-135.
- Ross, J.A., Peakall, J., Keevil, G.M. (2011). An integrated model of extrusive sand injectites in cohesionless sediments. *Sedimentology*, 58,1693-1715.
- Rydelek, P.A., Tuttle, M. (2004). Explosive craters and soil liquefaction. *Nature*, 427,115-116.
- Seilacher, A. (1969). Fault-graded beds interpreted as seismites. *Sedimentology*, 13,155-159.
- Shanmugam, G. (2016a). The seomite problem. *Journal of Palaeogeography*, 5,318-362.
- Shanmugam, G. (2016b). Submarine fans: a critical retrospective (1950–2015). *Journal of Palaeogeography*, 5,110-184.
- Shipton, Z.K., Meghraoui, M., Monroe, L. (2017). Seismic slip on the west flank of the Upper Rhine Graben (France-Germany): evidence from tectonic morphology and cataclastic deformation bands. In: Landgraf, A., Kuebler, S., Hintersberger, E., Stein, S. (Eds.), *Seismicity, Fault Rupture and Earthquake Hazards in Slowly Deforming Regions*. Geological Society, London, Special Publication 432,147-161.
- Strasser, M., Anselmetti, F.S., Fäh, D., Giardini, D., Schnellmann, M. (2006). Magnitudes and source areas of large prehistoric northern Alpine earthquakes revealed by slope failures in lakes. *Geology*, 34,1005-1008.
- Suter, F., Martínez, J.I., Vélez, M.I. (2011). Holocene soft-sediment deformation of the Santa Fe-Sopetrán Basin, northern Colombian Andes: Evidence for pre-Hispanic seismic activity? *Sedimentary Geology*, 235,188-199.
- Sutinen, R., Andreani, L., Middleton, M. (2019a). Post-Younger Dryas fault instability and deformations on ice lineations in Finnish Lapland. *Geomorphology*, 326,202-212.

- Sutinen, R., Hyvönen, E., Liwata-Kenttälä, P., Middleton, M., Ojala, A., Ruskeeniemi, T., Sutinen, A., Mattila, J. (2019b). Electrical-sedimentary anisotropy of landforms adjacent to postglacial faults in Lapland. *Geomorphology*, 326,213-224.
- Szuman, I., Ewertowski, M., Kasprzak, L. (2013). Thermo-mechanical facies representative of fast and slow flowing ice sheets: the Weichselian ice sheet, a central west Poland case study. *Proceedings of the Geologists' Association*, 124,818-833.
- Tuttle, M.P., Hartleb, R., Wolf, L., Mayne, P. W. (2019). Paleoliquefaction Studies and the Evaluation of Seismic Hazard. *Geosciences*, 9,311.
- Vandenbergh, J. (2013). Cryoturbation Structures. In: Elias, S.A. (Ed.), *The Encyclopedia of Quaternary Science*, 3, Elsevier, Amsterdam, pp.430-435.
- Vandekerckhove, E., Van Daele, M., Praet, N., Cnudde, V., Haeussler, P.J., De Batist, M. (2020). Flood-triggered versus earthquake-triggered turbidites: A sedimentological study in clastic lake sediments (Eklutna Lake, Alaska). *Sedimentology*, 67, 364-389, doi:10.1111/sed.12646.
- Van Balen, R.T., Bakker, M.A.J., Kasse, C., Wallinga, J., Woolderink, H.A.G. (2019). A Late Glacial surface rupturing earthquake at the Peel Boundary fault zone, Roer Valley Rift System, the Netherlands. *Quaternary Science Reviews*, 218,254-266.
- Van Vliet-Lanoë, B., Magyar, I.A., Meilliez, F. (2004). Distinguishing between tectonic and periglacial deformations of quaternary continental deposits in Europe. *Global and Planetary Change*, 43,103-127.
- Van der Wateren, F.M., Kluiving, S.J., Bartek, L.R. (2000). Kinematic indicators of subglacial shearing. In: Maltman, A.J., Hubbard, B., Hambrey, M.J. (Eds.), *Deformation of Glacial Materials*. Geological Society, London, Special Publications, 176,259-278.
- Van Loon, A.J.T. (2009). Soft-sediment deformation structures in siliciclastic sediments: an overview. *Geologos*, 15,3-55.
- Van Loon, A.J.T., Pisarska-Jamroży, M. (2014). Sedimentological evidence of Pleistocene earthquakes in NW Poland induced by glacio-isostatic rebound. *Sedimentary Geology*, 300,1-10.
- Van Loon, A.J.T., Pisarska-Jamroży, M., Nartišs, M., Krievāns, M., Soms, J. (2016). Seismites resulting from high-frequency, high-magnitude earthquakes in Latvia caused by Late Glacial glacio-isostatic uplift. *Journal of Palaeogeography*, 5,363-380.
- Van Loon, A.J.T., Soms, J., Nartišs, M., Krievāns, M., Pisarska-Jamroży, M. (2019). Sedimentological traces of ice-raft grounding in a Weichselian glacial lake near Dukuli (NE Latvia). *Baltica*, 32,170-181.
- Van Loon, A.J.T., Pisarska-Jamroży, M. and Woronko, B. (2020). Sedimentological distinction in glacial sediments between load casts induced by periglacial processes from those induced by seismic shocks. *Geological Quarterly*, 64, 626-640. dx.doi.org/10.7306/gq.1546
- Vanneste, K., Meghraoui, M., Camelbeeck, T. (1999). Late Quaternary earthquake-related soft-sediment deformation along the Belgian portion of the Feldbiss Fault, Lower Rhine Graben system. *Tectonophysics*, 309,57-79.
- Vanneste, K., Camelbeeck, T., Verbeeck, K., Demoulin, A. (2018). Morphotectonics and past large earthquakes in Eastern Belgium. In: Demoulin, A. (Ed.), *Landscapes and Landforms of Belgium and Luxembourg*, World Geomorphological Landscapes, Springer, Cham, pp.215-236.
- Wheeler, R.L., Etensohn, F.R., Rast, N., Brett, C.E. (2002). Distinguishing seismic from nonseismic soft-sediment structures: criteria from seismic-hazard analysis. *Geological Society of America*, Special paper,359,1-11.
- Weise, O.R. (1983). *Das Periglazial. Geomorphologie und Klima in gletscherfreien, kalten Regionen*. Gebrüder Bornstraeger, Berlin Stuttgart, p.199.
- Winsemann, J., Asprion, U., Meyer, T., Schultz, H., Victor, P. (2003). Evidence of iceberg ploughing in a subaqueous ice-contact fan, glacial Lake Rinteln, Northwest Germany. *Boreas*, 32,386-398.
- Winsemann, J., Alho, P., Laamanen, L., Goseberg, N., Lang, J., Klostermann, J. (2016). Flow dynamics, sedimentation and erosion of glacial lake outburst floods along the Middle Pleistocene Scandinavian ice sheet (northern Central Europe). *Boreas*, 45,260-283.

- Winsemann, J., Koopmann, H., Tanner, D., Lutz, R., Lang, J., Brandes, C., Gaedicke, C. (2020). Seismic interpretation and structural restoration of the Heligoland glaciotectionic thrust-fault complex: implications for multiple deformation during (pre-)Elsterian to Warthian ice advances into the southern North Sea Basin. *Quaternary Science Reviews*, 227,106068.
- Woronko, B., Belzyt, S., Bujak, Ł., Pisarska-Jamroży, M. (2018). Glaciotectionically deformed glaciofluvial sediments with ruptured pebbles (the Koczery study site, E Poland). *Bulletin of the Geological Society of Finland*, 90,145-159.
- Worsley, P. (2014). Ice-wedge growth and casting in a Late Pleistocene periglacial, fluvial succession at Baston, Lincolnshire. *Mercian Geologist*, 18,159-170.
- Woźniak, P.P., Pisarska-Jamroży, M. (2018). Debris flows with soft-sediment clasts in a Pleistocene glaciolacustrine fan (Gdańsk Bay, Poland). *Catena*, 165,178-191.

## Publication 4

This chapter has been submitted as Müller et al. (subm.),  
International Journal of Earth Sciences

### **Re-examination and neotectonic analysis of the N-S trending Regensburg-Leipzig-Rostock fault system between Leipzig and Cheb**

Katharina Müller<sup>1</sup>, Jutta Winsemann<sup>1</sup>, Diethelm Kaiser<sup>2</sup>, Thomas Spies<sup>2</sup>, Thomas Lege<sup>2</sup>, Christian Brandes<sup>1</sup>

<sup>1</sup>Institut für Geologie, Leibniz Universität Hannover, Callinstraße 30, 30167 Hannover, Germany

<sup>2</sup>Bundesanstalt für Geowissenschaften und Rohstoffe (BGR), Stilleweg 2, 30655 Hannover, Germany

Corresponding Author: Katharina Müller, Institut für Geologie, Leibniz Universität Hannover, Callinstraße 30, 30167 Hannover, Germany

Email: [mueller@geowi.uni-hannover.de](mailto:mueller@geowi.uni-hannover.de)



## Abstract

The major objective of this study is to re-examine the central part of the Regensburg-Leipzig-Rostock fault system between Leipzig and Cheb. The seismicity in this N-S trending zone is remarkable, however, the nature of the fault system is far from being understood. Here we present new evidence for neotectonic fault activity along this fault system and discuss the structural style and focal mechanisms. The palaeoseismological analysis is based on fieldwork, DEM lineament analysis, earthquake datasets, epicentre maps, fault maps and other published data from the literature.

At 5 locations, evidence for post-Palaeogene and Quaternary fault activity was found, indicated by the presence of deformation bands. The N-S trending Regensburg-Leipzig-Rostock fault system most likely represents a strike-slip system of en-échelon faults that is intersected by NW-SE and NE-SW oriented faults. The deformation bands developed above NW-SE and NNW-SSE striking faults, which intersect with NE-SW and NW-SE oriented ones. This underlines the importance of the distribution of seismicity along NW-SE oriented faults in the study area. Among the increased seismicity along the Regensburg-Leipzig-Rostock fault system, several prominent earthquakes like the 1872 Mid-German Earthquake (VII) near Gera, and the earthquakes in 2015, 2017 in the Halle/Leipzig area occurred at fault intersections of NW-SE and N-S trending faults. This matches with the hypothesis that fault intersections act as stress concentrators in the recent stress field, where seismic activity concentrates. Further potential trigger mechanisms for fault re-activation are glacial isostatic adjustment, the formation and drainage of large Pleistocene ice-dammed lakes, fluid emanations and magmatic activity. Our results show that the studied area of the Regensburg-Leipzig Rostock fault system can be separated into two seismogenic zones. The northern part (north of Zwickau) is characterised by deep single earthquakes, whereas the southern part is dominated by swarm earthquakes at shallower depth.

**Keywords:** Regensburg-Leipzig-Rostock (RLR) fault system, palaeoseismological analysis, lineament analysis, seismic activity, Finne-Gera-Jáchymov fault system, Lusatian Thrust

## Introduction

### Objectives

In the view of the search for a nuclear waste disposal in central Europe, and in the light of the recent earthquakes that occurred between Halle and Leipzig (Dahm et al. 2018), a re-evaluation of seismicity in the area of the Regensburg-Leipzig-Rostock (RLR) fault system is crucial.

The main objective of this study is to map fault systems with neotectonic activity that helps to re-examine the structural style of this fault system. We focus on the active central part of the RLR fault system (Fig. 1), which has been understudied in comparison to the Cheb Basin (Fig. 2). Based on palaeoseismological analysis and DEM based lineament analysis we present new evidence that point to neotectonic activity in the area between Leipzig and Aue and give new insights into the nature of the RLR fault system.

For a holistic view of the seismicity in this area the knowledge of palaeo-earthquakes and neotectonic activity is important. The palaeoseismological analysis helps to extend the time series of seismicity further into the past, which allows to better understand the tectonic history and the potential driver for seismicity. Furthermore, the analysis of the orientation of tectonically induced soft-sediment deformation structures, such as deformation bands, can help to detect active blind faults. This is particularly important for the northern part of the RLR fault system, where geological indicators for N-S trending structures are lacking because thick Cenozoic sediments cover the bedrock. To close this gap, a new palaeoseismological study in Palaeogene and Pleistocene deposits was carried out. We discuss whether the RLR fault system is a deep-seated active shear zone and evaluate the causes of increased seismic activity along this N-S trending zone.

### Background

The area around northwestern Bohemia, the Vogtland and Leipzig, is one of three areas in Germany and the Czech Republic with increased seismic activity (Grünthal et al. 1998a, 2018), characterised by single earthquakes and earthquake swarms (Grünthal et al. 1985, Grünthal 1992; Bankwitz et al. 1998; GERSEIS 2020). Historic seismicity with epicentral intensities above VII (EMS-98), as well as significant instrumentally observed earthquakes and earthquake swarms were detected over several centuries. An important observation is that the area of eastern Thuringia and northwestern Saxony shows different seismotectonic characteristics compared to the Vogtland and northwestern Bohemia (e.g., Neunhöfer et al. 1996; Fischer et al. 2014; Dahm et al. 2018).

Seismicity in these areas accumulates along a trans-regional N-S trending zone (e.g., Bankwitz et al. 1998; Korn et al. 2008; Neunhöfer 2009; Buchholz et al. 2016; Sonnabend 2019). Several regional studies (e.g., Siegert et al. 1901; Weise and Credner 1904; Weise et al. 1913; Gläßer and Wiefel 1999) mentioned distinct N-S oriented faults in the area between Altenburg and Plauen, besides E-W oriented faults that commonly show normal displacements (Bankwitz et al. 1995). Based on geomagnetic data, Lauterbach (1952) was the first who described a continuous N-S trending zone and called it Pritzwalk-Naab Line. Later studies concluded that the occurrence of N-S trending basement faults in this area is not validated and their interpretation based on lineament mapping on aerial photography is not sufficiently proven (e.g., Kämpf et al. 1991; Bram and Hirschmann 1992; Dahm et al. 2018). Bouguer gravity data image a N-S trending zone, bounded by a positive gravity anomaly in the west and a negative gravity anomaly in the east.

Bram and Hirschmann (1992) interpreted these gravity anomalies in Saxony and adjacent regions as deep-seated N-S and E-W striking structures. Behr et al. (2002) applied a linear filtering approach of the Bouguer gravity data that enables to derive tomography images of the Bouguer gravity field in selective depth levels. This study indicates that E-W striking structures occur in depth levels of 2.5-20.0 km, whereas the number of N-S striking structures increases with depth. At 20.0 km depth, distinct N-S oriented structures occur in the area of Saxony and eastern-Thuringia (Behr et al. 2002). However, Švancara et al. (2008) questioned the presence of these deep-seated N-S structures and presented new results based on the same dataset. They postulate that the so-called RLR fault system is not a deep-seated steep lineament, because it is not accompanied with a significant density contrast (Švancara et al. 2008). Pohl et al. (2006) extracted NW-SE, NE-SW and subordinated N-S striking lineaments in the study area by using remote sensing data. The N-S striking lineaments commonly appear as linking structures between the NW-SE and NE-SW oriented faults. N-S striking structures occur especially in the area between Gera and Plauen and were not investigated in the area of Leipzig, where thick Cenozoic sediments cover the bedrock. According to Pohl et al. (2006) no supra-regional system, like the postulated RLR fault system, occurs in the study area.

Recently, a continuous N-S trending shear zone from Kufstein in the south to Rostock at the Baltic Sea coast in the north was detected via satellite-based distance measurements, which is a new approach to detect small-scale horizontal velocities in intraplate settings (Dahm and Deng 2021). However, the new results of Dahm and Deng (2021) point to fault kinematics that are contrary to the generally expected sense of fault movement in the area of Leipzig and the Vogtland. Increased historic and recent seismicity is only observed between Cheb in the south and Leipzig in the north (Leydecker 2011; GERSEIS 2020). Conversely, the N-S trending high seismicity zone is partly located in the region with low deformation rates. Such a non-correlation is completely unexpected and requires explanation (Dahm and Deng 2021).

The controversial nature of the RLR fault system, that is far from being understood, and the strong evidence for significant seismic activity in this region (e.g., Neunhöfer et al. 1996; Hemmann et al. 2003; Korn et al. 2008; Dahm et al. 2018; GERSEIS 2020) fuels the demand of additional studies. Especially palaeoseismological investigations are necessary to extend the knowledge about past seismic activity in this region. Although the area was studied for more than 70 years, only a few structural studies focus on the RLR fault system. A key publication is Bankwitz et al. (2003a).

### ***Seismicity in the study area***

Several studies show the importance of the RLR fault system regarding the seismic activity in the study area (e.g., Bankwitz et al. 1998, 2003a; Grünthal et al. 1985; Grünthal 1992; Korn et al. 2008; Dahm et al. 2018; Sonnabend 2019). The central segment of the RLR fault system is the most seismically active zone with a length of ~ 150 km between Cheb (Czech Republic) and Leipzig (Germany) (Bankwitz et al. 2003a). As described above, the N-S oriented RLR fault system is crosscut by several NW-SE-oriented major faults and NE-SW oriented faults (Fig. 2) (e.g., Bankwitz et al. 1991; Leonhardt 1995; Wendt et al. 1996). At both, the N-S oriented and at the NW-SE-oriented faults, historic and instrumentally detected earthquakes are located (Fig. 2) (e.g., Wendt et al. 1996; Leydecker 2011; Grünthal and Wahlström 2012; Buchholz et al. 2011, 2013, 2016; GERSEIS 2020). Major seismotectonic structures comprise the Kyffhäuser-Crimmitschau Fault system, the Finne Fault, the Gera-Jáchymov Fault and the Bergen-Klingenthal fault system (Fig. 2) (Bankwitz et al. 2003a; Dahm et al. 2018; Sonnabend 2019) and the Lusatian Thrust.

The accuracy of the epicentre location has been rather imprecise in the past. Especially the reliability of the location of historic earthquakes before 1800 is weak and the intensities may be partly overestimated as common with historic earthquakes (e.g., Kracke et al. 2000).

Since 1994, 32.000 earthquakes with magnitudes  $M_L$  ranging from -0.5 to 4.2 were detected along the RLR fault system, between Leipzig and Regensburg (e.g., Sonnabend 2019). Earthquakes in the north of Plauen mostly appear as single events and of greater depths (Neunhöfer et al. 1996; Korn et al. 2008; Fischer et al. 2014; Dahm et al. 2018; Sonnabend 2019). Two prominent earthquakes took place in the Halle/Leipzig area. The first earthquake occurred in 2015 close to Gröbers with a magnitude  $M_w$  of 3.2 at a depth of 29 km and had one single aftershock with a magnitude  $M_w$  of 1.7 (Buchholz et al. 2016; Dahm et al. 2018). In 2017, an earthquake near Markenstädt with a magnitude of  $M_w$  2.8 at 26 km depth, was detected (Tables 3, 4) (Dahm et al. 2018).

In the area of Plauen and south, earthquake swarms occur frequently (e.g., Klinge et al. 2003; Fischer and Horálek 2003; Neunhöfer and Meier 2004). Periodic earthquake swarms are characteristic for the Vogtland and NW Bohemian region especially in the Nový Kostel area (Neunhöfer 1976, 2018; Neunhöfer and Meier 2004; Bräuer et al. 2009; Fischer et al. 2014). Strong earthquake swarms ( $M_L > 3$  to 4) were recorded in the years 1897, 1901, 1903, 1908, 1985/1986, 1997, 2000, 2008, 2011 and 2018 (e.g., Klinge et al. 2003; Fischer and Horálek 2003; Neunhöfer and Meier 2004; Wendt and Buchholz 2019). The northernmost location of earthquake swarms is the Werdau focal zone (Fig. 2), which is situated at the intersection of the RLR fault system with the Finne-Gera-Jáchymov fault system (e.g., Skamletz et al. 2000; Hemmann et al. 2003; Korn et al. 2008). Further earthquake swarms concentrate in the Bad Elster area, the Bad Brambach/Plešná area, the Nový Kostel area, and the Klingenthal area (Fig. 2).

### ***Palaeoseismological analysis***

Systematic studies of palaeo-earthquake activity along the RLR fault system were only carried out in the Cheb Basin (e.g., Bankwitz et al. 2003b; Štěpančíková et al. 2019). Until today, the database of neotectonic activity in the northern part of the study area is limited.

Commonly, evidence of palaeo-earthquakes and neotectonic activity are derived from seismites, which are produced by seismically triggered liquefaction and fluidization of sediments (e.g., Montenat et al. 2007; Obermeier 2009; Brandes and Winsemann 2013; Tuttle et al. 2019; Müller et al. 2021a). Recent studies show that an indicator for neotectonic activity are deformation bands that occur in the damage and process zone of large faults (e.g., Cashman et al. 2007; Brandes and Tanner 2012; Brandes et al. 2018a; Müller et al. 2021a). As demonstrated by Brandes et al. (2018b) deformation bands are excellent indicators for neotectonic activity along blind faults. However, the occurrence of deformation bands provides no indications whether a basement fault had ruptured and emitted seismic waves or if it was characterised by aseismic creep without emitting seismic waves.

### ***Geomorphological evidence for fault activity***

The recent seismicity in the study area of the RLR fault system is an indication of ongoing lithospheric processes. Stress variations were monitored based on geochemical and hydrological variations (e.g., Bräuer et al. 2009; Heinicke et al. 2018). This raises the question whether young and recent deformation processes can be also detected based on geomorphological indications.

To detect recent crustal deformation geodetic levelling was used in the past. Levelling is a geodetic standard approach with a high precision, which is state-of-the-art and frequently used to detect deformations of the Earth's surface. If levelling results are compared, which have been taken at various epochs covering a longer span, slight differences could be caused by different methods utilized in the data analysis. Principally, to verify the results of an older levelling survey and to evaluate its quality, the original datasets have to be re-examined, which is beyond the scope of this study. Nowadays, levelling surveys and modern satellite-based approaches should agree within the error bars of each method. Deviations of recent satellite results and older levelling results can have many causes including real geophysical processes as well as some inconsistencies in the data analysis (Feldmann-Westendorff 2016). For a comprehensive overview published geodetic data are summarised below.

Geodetic measurements along several faults (e.g., the Mulde Fault, Finne Fault, Kyffhäuser-Crimmitschau Fault, Weimar Fault) in the study area point to recent, slow activity. Ellenberg (1992) point out that the measured velocities are geodetically without any significance, but are important in the geological context. The movements along these faults are interpreted to represent creep processes (Ellenberg 1992). However, this needs further analysis. Ellenberg (1992) separated the investigated area into several blocks that are flanked by NW-SE oriented faults like e.g., the FGJ fault system. On average, the blocks are tilting. The NE-side subsided, whereas the SW-side was uplifted (Ellenberg 1992). Ellenberg (1992) measured activity in a range of  $\sim 0.11$  to  $0.18$  mm/a along the FGJ fault system. Geodetic profiles along the FGJ fault system were also measured by Bankwitz et al. (1993). They observed changes in elevation across the fault system at Roßleben, Crimmitschau and Tellerhäuser. The highest uplift rates are derived for the SW section of the FGJ fault system (Bankwitz et al. 1993).

GPS campaigns were carried out from 1994 to 2001 in the German part of the West Bohemia/Vogtland region and delivered evidence for significant relative displacements of up to 5 mm over the analysed time series (Wendt and Dietrich 2003). Comparable displacements of 4 - 6 mm/a were observed in the Nový Kostel area (Czech Republic) (Mrlina 2000).

Results of GPS surveys indicate that phases of relatively low seismic activity show a gradual build-up of tension in the N-S direction (Wendt 2002). Using geodetic approaches, Mrlina (2000) and Wendt and Dietrich (2003) show that the deformation processes in the Vogtland/NW Bohemia and the Nový Kostel area, correlate with the seismic activity and vary non-linearly with time. An example is the N-S striking Reichenbach-Schöneck-Erlbach Fault zone, which is a southern segment of the RLR fault system (Fig. 2). Precise GPS measurements were carried out along this fault that point to co-seismic surface deformation (Wendt and Dietrich 2003). The datasets show that the western block moves northward and the eastern block moves southwards (Krentz and Witthauer 2000; Forkmann et al. 2002), pointing to dextral strike-slip movements which does not concur with Bankwitz et al. (2003), who discussed sinistral strike-slip movements in this area.

However, these observations were investigated several decades ago. Recently, analyses of vertical motions (Jähne-Klingberg 2019) show minor changes over a long period of time. Via satellite-based distance measurements, which is a new approach to detect small-scale horizontal velocities in intraplate settings, shear deformation in the N-S trending zone was detected (Dahm and Deng 2021). Using GNSS network solutions in Vogtland region between 2000 and 2018 Deng and Dahm (2021) investigated transient signals (horizontal and vertical) and relate them to volcanic activity or aseismic creep in this region.

## Geological setting

### Geological development

The study area, with the distinct seismically active section of the RLR fault system comprises parts of southern Brandenburg, Saxony, Saxony-Anhalt, Thuringia, Northeast Bavaria and the north of the Czech Republic with the Eger Rift. It is defined by the coordinates 52°N 11°E, 52°N 13.5°E and 50°N 11°E, 50°N 13.5°E see Figs 1 and 2). This area belongs to the Mid-German Crystalline Zone, the Saxo-Thuringian zone and the Moldanubian zone with the Teplá-Barrandian zone of the central European Variscides (Fig. 1a), which developed in Palaeozoic times due to the collision of Gondwana and Laurussia (Kroner et al. 2007).

After the Variscan Orogeny in Late Carboniferous and Permian times, slab delamination led to a higher heat flow and a thermal thinning of the crust accompanied with strong volcanic activity. During the Permian, the lithospheric stress field changed to extension. Rift processes were caused by thermal contraction of the lithosphere (McCann 2008). Thermal subsidence occurred throughout the entire Mesozoic, which led to the development of different sedimentary basins. The extensional stress field changed to compression in the Late Cretaceous, caused by a rotation of the Iberian Peninsula (Kley and Voigt 2008). This inversion of the stress field led to the reactivation of several faults in central Europe e.g., the Harz Boundary Fault, the Osning Thrust, the Gardelegen Fault and the Lusatian Thrust (Franzke et al. 2004; Voigt et al. 2006) and initiated the formation of typical positive tectonic inversion structures (Kockel 2003).

During the Cenozoic, extension accompanied by alkaline magmatic activity led to the evolution of the Eger Rift (Prodehl et al. 1995). Bram and Hirschmann (1992) postulate that N-S and E-W striking fault systems in this area are products of late Variscan and Cenozoic strike-slip movements. Today the region is characterised by an extensional tectonic regime with magmatic activity, which causes the recent degassing of CO<sub>2</sub> (e.g., Dahm et al. 2013; Fischer et al. 2014).

### Pleistocene deposits as archives for neotectonic fault activity

The study area was transgressed by the Middle Pleistocene Elsterian and Saalian ice sheets (Fig. 1b) (Eissmann 2002; Ehlers et al. 2011; Lang et al. 2018). In the lowland area around Halle and Leipzig two Elsterian tills and three Saalian tills are vertically stacked (Eissmann 2002). They are separated by meltwater deposits, fluvial deposits, and loess (Eissmann 1994, 2002; Lang et al. 2018, 2019).

The maximum extent of the Elsterian ice sheets is recorded from Bad Schandau and represents the southernmost advance of the ice sheets during the Pleistocene (Eissmann 2002). In northern Germany, the Elsterian glaciations has been correlated with Marine Isotope Stage MIS 12 and MIS 10 (Lang et al. 2012; Roskosch et al. 2015; Lauer and Weiss 2018). Three major ice advances with several sub-phases occurred during the Saalian glaciation (Eissmann 2002; Ehlers et al. 2011; Lang et al. 2018, 2019). The maximum extent of the Saalian ice sheets reached the area around Meißen (Fig. 1b) (Eissmann 2002; Lang et al. 2018). These repeated ice advances are commonly correlated with MIS 6 and are referred to as Drenthe and Warthe ice advances (Ehlers et al. 2011; Lang et al. 2018). The middle and younger Saalian Warthe ice-advances did not reach the study area (Lang et al. 2018; Winsemann et al. 2020) and the Late Pleistocene Weichselian ice sheets did not cross the Elbe river (Lüthgens and Böse 2011; Hardt et al. 2016; Hardt and Böse 2018).

The blocking of the northwestern river drainage led to the repeated formation of numerous ice-dammed lakes along the southwestern margin of the Middle Pleistocene Elsterian and Saalian ice sheets (Fig. 1c, d) (Eissmann 2002; Junge 1998; Junge et al. 1999; Lang et al. 2018, 2019). Lake levels were controlled by the height of bedrock-overspill channels and commonly reached ~190 m to 200 m a.s.l. (Lang et al. 2018).

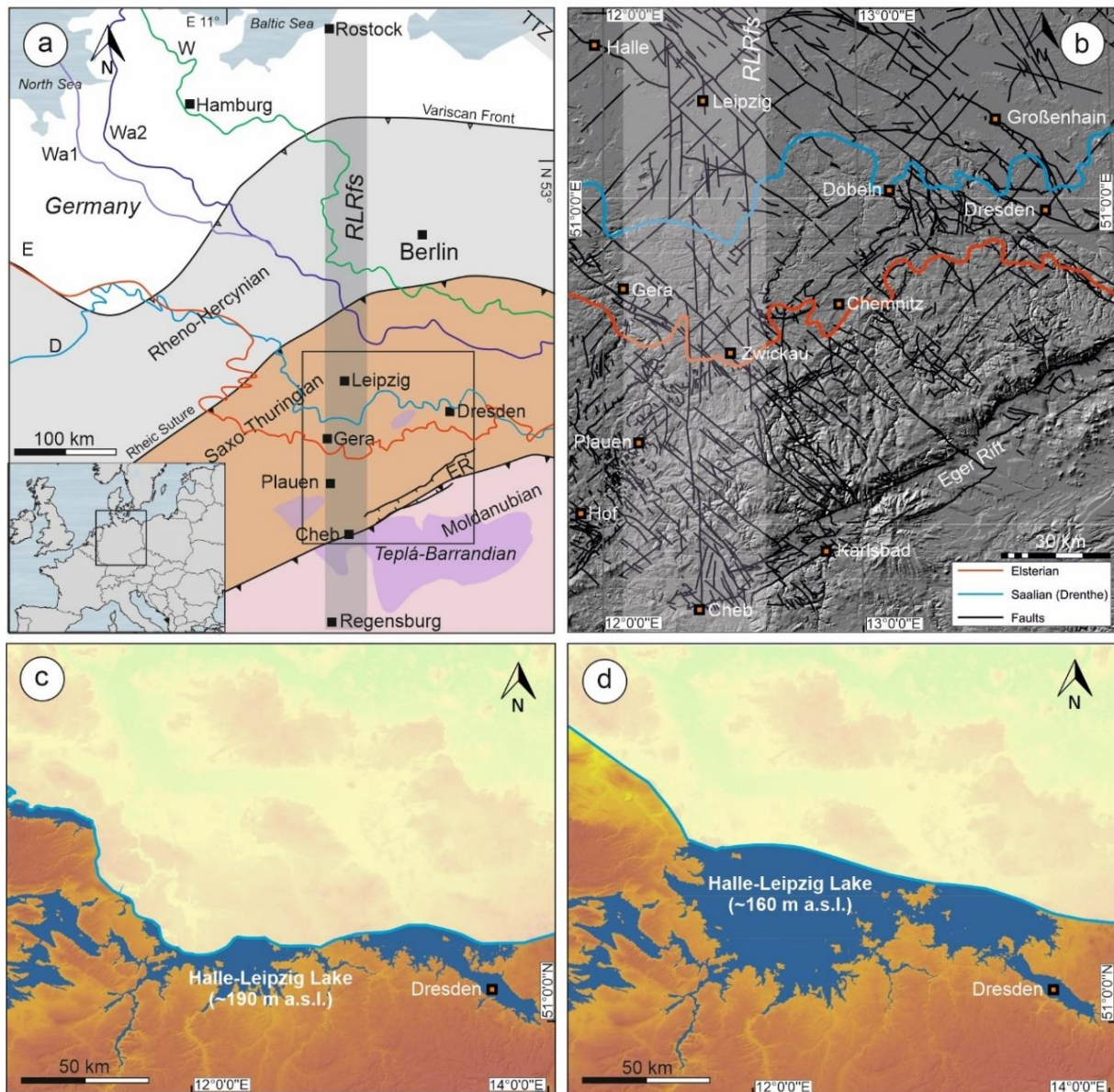


Figure 1: Location of the study area in Germany. a) Overview of the European Variscides subdivided into three zones: the Rheno-Hercynian, Saxo-Thuringian and Moldanubian zone with the location of the study area and the Regensburg-Leipzig-Rostock (RLR) fault system: RLRfs; Eger Rift: ER; Teisseyre-Tornquist Zone: TTZ (modified from McCann 2008) and the maximum extent of the Middle to Late Pleistocene (Elsterian (E), Saalian Drenthe (D), Warthe1 (Wa1), Warthe 2 (Wa2) and Weichselian (W)) ice sheets (modified after Lang et al. 2018; Winsemann et al. 2020); b) Investigated area with the RLR fault system and the maximum extent of the Middle Pleistocene (Elsterian, Saalian: Drenthe) ice sheets (modified after Ehlers et al. 2011; Lang et al. 2018), the black lines represent faults (Leonhardt 1995; Wendt et al. 1996); c- d) Palaeogeography of ice-dammed lakes during the older Saalian Drenthe glaciation. c) Maximum ice advance. The reconstructed volume is c. 117 km<sup>3</sup> with a lake level of > 190 m a.s.l.; d) During ice-sheet retreat the volume of the Halle-Leipzig Lake increased and reached c. 224 km<sup>3</sup> and the lake level fell to 160 m a.s.l. (from Lang et al. 2018). During further ice-margin retreat the glacial lakes completely drained.



The size and volume of Elsterian glacial lakes is not well constrained and potential lake sediments are poorly dated (Junge 1998; Eissmann 2002; Roskosch et al. 2015; Winsemann and Lang 2020). The best database exists for the ice-dammed lakes that formed along the older Saalian Drenthe ice sheet (Junge 1998; Junge et al. 1999; Eissmann 2002; Lang et al. 2018). These glaciolacustrine deposits are commonly well dated and comprise fine-grained lake-bottom sediments, subaqueous (ice-contact) fans and (ice-marginal) deltas. The successive opening of lake-overspill channels eventually led to the west-ward and north-westward drainage of the glacial lakes (Lang et al. 2018; Winsemann and Lang 2020). The drainage of the Middle Pleistocene Elsterian and Saalian ice-dammed lakes strongly modified the regional drainage network due to the incision of channels (e.g., Lang et al. 2019; Panin et al. 2020; Winsemann and Lang 2020).

### **The regional fault patterns**

Besides NE-SW oriented faults, the regional fault pattern in the study area is characterised by NW-SE oriented faults (Fig. 2) (e.g., Siegert et al. 1901; Dalmer and Credner 1901; Weise et al. 1913; Zimmermann and Liebe 1930; Picard et al. 1937; Gläßer et al. 1995; Gläßer and Wiefel 1999), including among others the distinct Lusatian Thrust, the Finne Fault, the Gera-Jáchymov Fault and the Bergen-Klingenthal fault system (Fig. 2). Furthermore, based on lineations derived from orthophotos, DEMs and the presence of gravity anomalies, N-S and E-W striking deep seated structures are interpreted (Grünthal et al. 1985; Kämpf et al. 1991; Bram and Hirschmann 1992; Bankwitz et al. 1998; Behr et al. 2002; Bankwitz et al. 2003a; Pohl et al. 2006). Many major faults intersect with the N-S trending zone in the area around Leipzig, Gera, Zwickau and in the Cheb Basin, which results in a complex subsurface structure (e.g., Skamletz et al. 2000) and fault pattern (Fig. 2).

### ***The Regensburg-Leipzig-Rostock (RLR) fault system***

In the literature, segments of the N-S striking zone with distinct seismicity were named the Pritzwalk-Naab Line, Naab-Pritzwalk-Lineament, the Naab-Pritzwalk-Rostock (NPR) Lineament, the Wismar-Leipzig-Regensburg Photolineament, the Plauen/Klingenthal-Altenburg/Gera-Leipzig/Halle-Dessau/Bernburg fault zone, Vogtland-Leipzig Zone (VLZ), the Regensburg-Leipzig-Rostock Zone (RLRZ), zone of Regensburg-Leipzig-Prignitz, and because of its most active middle part, the Regensburg-Leipzig Zone (Lauterbach 1952; Kämpf et al. 1991; Hemmann 2002; Hemmann and Kämpf 2002; Bankwitz et al. 2003a; Schneider 2004; Buchholz et al. 2016; Grünthal et al. 2018). In this paper the term Regensburg-Leipzig-Rostock (RLR) fault system is employed, because the term fault zone is used in the modern literature to describe the sum of all structural elements of a single fault (e.g., Chester and Logan 1986), whereas an array of faults like the RLR zone that shows a mechanical interaction is best described with the term fault system (see Brandes and Tanner, 2020 for a summary of the nomenclature).

Based on satellite images the RLR fault system was traced from the area of Regensburg passing through the Vogtland and the region of Leipzig further to the north up to the area of Rostock at the Baltic Sea coast (e.g., Grünthal et al. 1985; Kämpf et al. 1991; Kämpf et al. 1992; Bankwitz et al. 2003a).

The RLR fault system is commonly interpreted as a N-S trending sinistral shear zone (Bankwitz et al. 2003a; Schneider 2004; Neunhöfer 2009). It is a roughly ~ 700 km long and ~ 40 km wide

network of faults (Figs 1, 2) (Bankwitz et al. 2003a). The fault system consists of a set of N-S trending sub-parallel faults composed of en-échelon segments (Bram and Hirschmann 1992; Bankwitz et al. 2003a; Neunhöfer and Hemmann 2005). Because of the segmentation of several short lineaments, Pohl et al. (2006) excluded the possibility of a strike-slip zone and assumed normal fault kinematics with oblique components.

### ***The Lusatian Thrust***

The Lusatian Thrust is a NW-SE oriented major fault in the study area. It does not cross the RLR fault system, but nevertheless represents a key structure in central Germany (Fig. 2). The Lusatian Thrust is part of the Elbe Fault Zone, which showed repeated phases of activity since the Late Carboniferous (Scheck et al. 2002). It has a maximum vertical offset of 500 – 1000 m and is 80 – 100 km long (Krentz and Stanek 2015). The Lusatian Thrust is the boundary between the Lusatian Block and the Elbe Zone. In the NE of Dresden Klotzsche, the Elbe Zone is flanked by the Großenhainer Fault (Leonhard 1995; Wendt et al. 1996; Krentz et al. 2010). Near Dresden the position of the fault is not well constrained (e.g., cf. Bankwitz 1971; Voigt 2009; Krentz and Stanek 2015; Käßner et al. 2020). The Lusatian Thrust is regarded as one of the most important faults in central Europe and consists of several short segments that are offset by younger Cenozoic, NE-SW oriented faults (e.g., by the Borsberg Fault, Ebersbacher Fault, Hoyerswerder Fault, Stráž fault system) (Bankwitz 1971; Krentz 2008; Krentz and Stanek, 2015; Käßner et al. 2020). From SE to NW the fault characteristics (e.g., offset, dip of the fault) change, which causes a separation of the fault in different segments. All segments of the Lusatian Thrust show a different kinematic evolution and varying dip angles along the thrust, which significantly change along-strike (Coubal et al. 2014).

The curved geometry of the fault is interpreted to result from a multiphase tectonic evolution of these different fault segments (Käßner et al. 2020). The main phase of fault activity was in the Late Cretaceous to Palaeogene (Kley and Voigt 2008; Krentz 2008; Krentz and Stanek 2015). Since the Pliocene, uplift and subsidence took place along the Lusatian Thrust (Bankwitz 1977). Pleistocene activity was derived from the Sonnenberg Scoria Cone. Scoria cones are steep-sided volcanic cones that consist of loose pyroclastic fragments (e.g., Settle 1979). At the Sonnenberg Scoria Cone an unsteady state and disequilibrium between erosion and uplift close to the Lusatian Thrust was observed (Tietz et al. 2011). Furthermore, faults in Middle Pleistocene (Elsterian) deposits near Waltersdorf point to Pleistocene activity (Bankwitz et al. 1977).

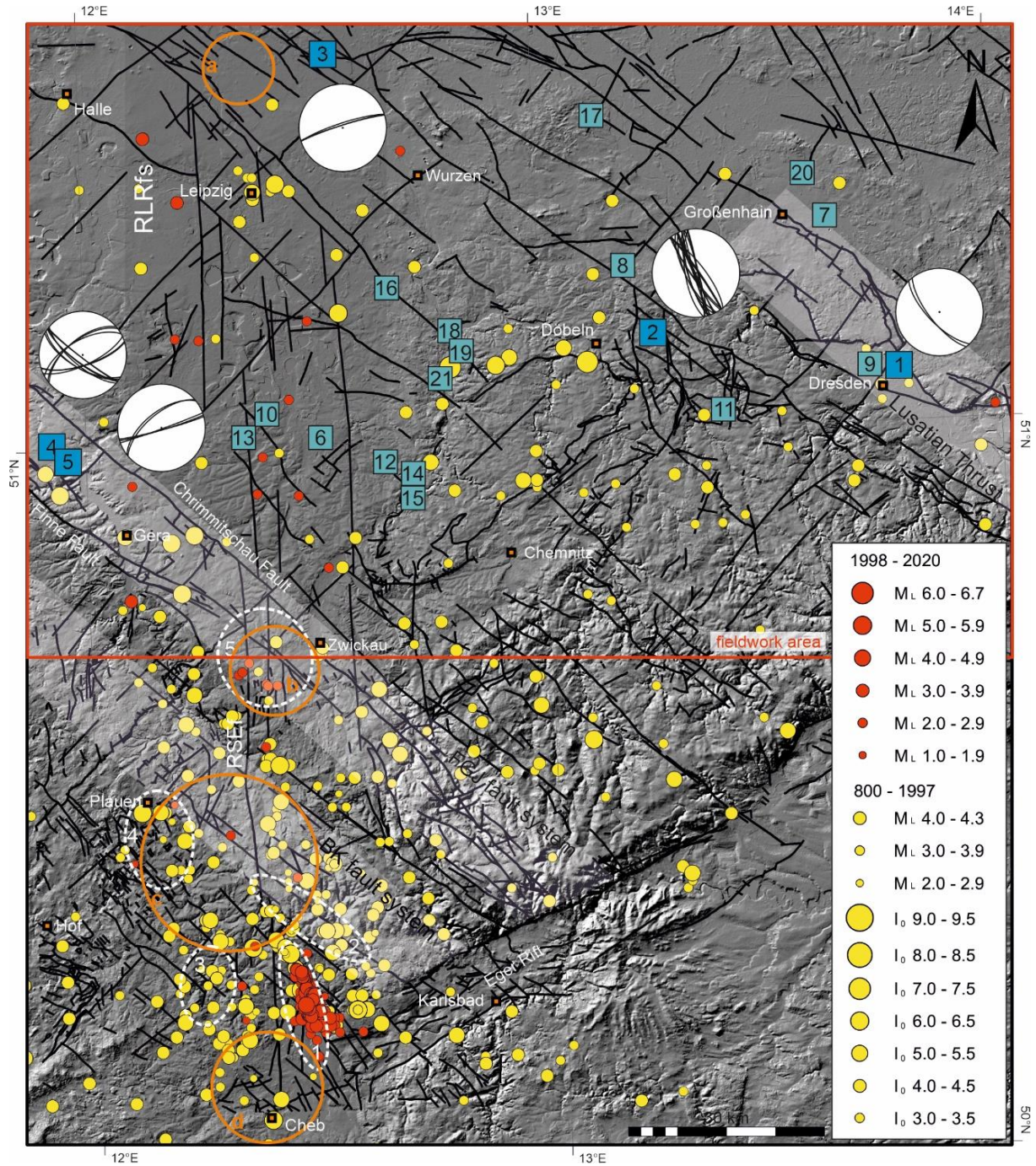


Figure 2: Seismicity in the study area with the main seismotectonic structures: Berge-Klingenthal fault system: BKfs; Finne-Gera-Jáchymov fault system: FGJfs; Lusatian Thrust and Regensburg-Leipzig-Rostock fault system: RLRfs; Reichenbach-Schöneck-Erlbach Fault: RSEf. Historic seismicity (years 800-1997) and earthquakes detected in 1998-2020 with magnitudes and epicentral intensities (GERSEIS, 2020). Faults are from Leonhardt (1995) and Wendt et al. (1996). The numbers (blue box) represent locations of identified neotectonic activity: 1: Dresden Klotzsche, 2: Churschütz, 3: Badrina, 4: Schkölen. 5: Hainchen with stereographic projections of the orientation of deformation bands. The numbers (green box) represent locations of identified deformation structures (Table 2). Dashed circles show earthquake-swarm areas: 1: Nový Kostel focal zone, 2: Klingenthal focal zone, 3: Bad Elster focal zone 4: Plauen focal zone 5: Werdau focal zone. Yellow circles represent volcanic fields in the study area: a: Delitzsch-Bitterfeld volcanic field with the Serbitz and Storkwitz Diatremes; b: Weißenbrunn Diatreme, Ebersbrunn Diatreme; 'Triassscholle' Greiz assumed Diatreme; c: Vogtland volcanic field; d: Hartoušov, Bublák, Devín, Mostek, Františkovy Lázně. The fieldwork area is outlined by a red box.

### ***Finne-Gera-Jáchymov fault system***

The Gera-Jáchymov fault system is a ~ 10 km wide tectonically significant fault array with several parallel fault segments. One of the most important fault segments is the Roter Kamm Fault. The Roter Kamm Fault is a normal fault with a throw of ~ 580 m (Hiller and Schuppan 2008; Berger et al. 2011). The polyphase evolution of the FGJ fault system started with the Variscan Orogeny (Bankwitz et al. 1993). The fault system incorporates the Kyffhäuser-Crimmitschau Fault in the NW, the Finne Fault in the SW and the Gera-Jáchymov Fault in the SE. Based on geophysical datasets (such as seismic, gravimetric and magnetic data) this zone is interpreted as a distinct deep-seated fault system between the Franconian Line in the south and the Elbe Line in the north (Bankwitz and Bankwitz 1991; Haupt and Conrad 1991). The N-S oriented RLR fault system intersects with the NW-SE oriented ~ 250 km long Finne-Gera-Jáchymov (FGJ) fault system near the city of Gera (Fig. 2).

### ***The Eger Rift***

The southern part the RLR fault system in the study area is intersected by the ENE-WSW oriented Eger Rift (Figs 1, 2). The Eger Rift is a ~300 km-long volcanotectonic zone that developed on Proterozoic crystalline basement rocks (Kasiński 1991). It is an element of the European Cenozoic Rift System (ECRIS) that evolved in late Eocene times (Ziegler 1992). The ECRIS is supposed to have developed as a result of the Alpine collision (e.g., Ziegler 1992; Dèzes et al. 2004). The Eger Graben, which is part of the Eger Rift, roughly trends parallel to the major crustal boundary between the Saxo-Thuringian and the Teplá-Barrandian zones of the Variscan orogenic belt (Ziegler 1992) (Fig. 1c). The Eger Rift is characterised by a high heat-flow and voluminous alkaline intraplate volcanism (Prodehl et al. 1995; Dèzes et al. 2004; Ulrych et al. 2013). Quaternary rift processes are characterised by CO<sub>2</sub> emanations, and earthquake-swarm activity in NW-Bohemia and the southern Vogtland and alkaline volcanic activity (Geissler 2005).

The Eger Graben in the east of the rift system is separated by the Marienbader Fault from the Cheb Basin that is located in the western part of the Eger Rift. The Cheb Basin is located at the intersection of the Eger Graben with the RLR fault system (Fig. 2).

### ***Cheb Basin with the Marienbader Fault and the Pocatky-Plesná Zone (PPZ)***

The formation of the Cheb Basin in late Oligocene to early Pliocene times (Peterek et al. 2011) was initiated by the reactivation of basement faults inherited from the Variscan Orogeny (Špičáková et al. 2000; Bankwitz et al. 2003a). The basin is situated at a junction of three Variscan structural units: the Saxo-Thuringian zone, the Moldanubian zone and the Teplá-Barrandian zone (Franke 2000). Seismic analyses of Babuška et al. (2007) and Babuška and Plomerová (2008) defined this area as a kind of triple junction of three microplates and thus three different mantle domains.

The NNE-SSW striking Marienbader Fault intersects the Pocatky-Plesná Zone (PPZ) with the Plesná Fault in the area of Nový Kostel (Fig. 2) (e.g., Štěpančíková et al. 2019). The PPZ is part of the main seismogenic zone and represents a southward prolongation of the RLR fault system (Bankwitz et al. 2003a, b; Schneider and Bankwitz 2003). The Cheb Basin represents the highest concentration of earthquakes swarm activity and CO<sub>2</sub> degassing in this area (Fischer et al. 2014).



## Database and Methods

Palaeoseismological analyses in Palaeogene and Pleistocene deposits were carried out in the seismically active part of the RLR fault system, between the cities of Leipzig and Aue (Fig. 2). This area was selected, because of the presence of thick Cenozoic sediments, which are susceptible to record neotectonic activity. The database includes own geological field data and DEM analysis combined with published fault maps and earthquake datasets.

### Field data

In total, 59 sand and gravel pits were investigated. Geological maps and satellite images were used for the selection process. In the vicinity of faults, outcrops of Cenozoic deposits in sand- and gravel pits were analysed to find indicators of neotectonic activity, including sedimentological descriptions and reconstructions of the depositional environment and the identification of structural elements and their orientation. Special emphasis was placed on the analysis of soft-sediment deformation structures. The orientation of tectonic fabrics is displayed as stereographic projections.

### Lineament analysis

To test, if there are N-S striking morphological features in the study area, which might be a hint of young fault activity, lineament analyses were carried out based on open-source DEMs (EU-DEM v1.1) with 30 m grid, vertical accuracy  $\pm 2$  m, provided by Copernicus and a high-resolution DEM (5 m grid, vertical accuracy  $\pm 0.15$  m) (Staatsbetrieb Geobasisinformation und Vermessung Sachsen (GeoBasis-DE/GeoSN, dl-de/by-2.0 2019) of the area around the Lusatian Thrust. The DEMs were analysed in a Geographic Information System (GIS), which is a well-established method that has been successfully applied in many other studies (e.g., Grohmann 2004; Abdullah et al. 2010; Zhumabek et al. 2017).

The advantage of digital elevation models to satellite data is that the azimuth and inclination of illumination can be adapted and changed during analyses. We created eight shaded relief maps with lighting  $20^\circ$  above the horizon at  $N000^\circ$   $N045^\circ$ ,  $N090^\circ$   $N135^\circ$ ,  $N180^\circ$   $N225^\circ$ ,  $N270^\circ$   $N315^\circ$ . To show all lineaments with different orientations in the study area, we used different directions of illumination as shown e.g., in Grohmann (2004).

Table 1: Input parameters used in the software PCI Geomatica.

Parameter (abbreviation)	Parameter	Values
RADI	Filter Radius	10
GTHR	Edge Gradient Threshold	100
LTHR	Curve Length Threshold	30
FTHR	Line Fitting Threshold	3
ATHR	Angular Difference Threshold	30
DTHR	Linking Distance Threshold	20

We used the LINE module of the software PCI Geomatica for automatic lineament extraction (PCI Geomatica 2020). This module extracts linear features from an image and transforms the polylines into vector segments by using six parameters. The parameters that are used by the

algorithm are listed in Table 1 (see Abdullah et al. 2010; Sedrette and Rebaï 2016; Zhumabek et al. 2017 for further details). The workflow of the software PCI Geomatica includes three steps: Edge detection, thresholding and curve extraction. The applied threshold values are shown in Table 1. The edge detection is based on the Canny edge detector algorithm, which is a multi-stage algorithm to detect a wide range of edges in images (Canny 1986). A binary image is generated in the second step, by a threshold processing of the before obtained image. In the last step of the PCI Geomatica algorithm, the curved lines are recovered from a byte grid. This step is divided into several sub-steps, which are described in detail by Zhumabek et al. (2017). The extracted shapefiles were loaded in ArcGIS for showing the results and for post-processing. Rose diagrams of the automatic extracted lineaments were generated to show the predominant direction of the lineaments in the study area.

## **Fault maps**

Specific, actualized fault maps of the study area are not published yet (pers. comm. LfULG: Engelhardt 2021). To create a basis for the analysis of the RLR fault system in the study area, a combination of deep-seated structural elements provided by geophysical analyses and remote-sensing techniques (e.g. Grünthal et al. 1985; Kämpf et al. 1991; Kämpf et al. 1992; Bram and Hirschmann 1992) with faults derived from geological mapping projects (e.g., Siegert et al. 1901; Weise and Credner 1904; Weise et al. 1913; Gläßer and Wiefel 1999) was used and is the best approach. We combined two established tectonic datasets derived from geological and geophysical maps (Leonhardt 1995; Wendt et al. 1996).

## **Earthquake database**

### ***Historic earthquakes***

Historic sources show that earthquakes were documented in the study area since 823 CE (Leydecker 2011; GERSEIS 2020). However, the strength, location and authenticity of most earthquakes of the medieval period is uncertain or doubtful. In the following, we use the term 'historic earthquakes' for those events that took place between 800 and 1997, because of the inaccuracy of the epicentre determination in this time.

The earthquakes shown in this study are compiled in the catalogue of Leydecker (2011), listed in GERSEIS (2020) and shown in Figures 2 and 6.

### ***Earthquake registration since 1902***

In 1900, the first seismometer was installed in Jena and further in 1902 in Leipzig and Göttingen (Mittag 2000; Neunhöfer 2009). In 1908, the first permanent seismic station was set up in Bohemia (Horálek et al. 2000). Intensive seismic monitoring started in 1962, after an earthquake swarm in the Vogtland area (Neunhöfer 1976). In the following years, the development of the 'Sachsennetz' (SXNET) (Leipzig University 2001), the 'Thüringer Seismologisches Netz' (TSN) (Jena 2009) and the 'Westböhmennetz' WEBNET (Institute of Geophysics 1991) provided improved quality in the registration and evaluation of earthquakes (e.g., Horálek et al. 2000; Neunhöfer 2009; Buchholz et al. 2016). The database of instrumentally detected earthquakes since 1998 are

from GERSEIS (2020) and the *Seismologie-Verbund zur Erdbebenbeobachtung in Mitteldeutschland* (TLUBN 2020).

## Results

In 21 pits, deformation structures were observed (Table 2). Deformation structures include periglacial features like ice-wedge casts, and involutions and glaciotectonic deformation structures like folds, sheared sediments, thrust sheets and ball-and-pillow structures (e.g., Müller et al. 2021a). In five sand and gravel pits deformation bands are exposed that show the same strike as the underlying basement faults.

Table 2: Investigated sand and gravel pits with deformation structures in the selected fieldwork area along the RLR fault system (see Fig. 2).

Outcrop	Cryoturbation features	Glaciotectonic features	Neotectonic features
1 Dresden Klotzsche			X
2 Churschütz	-	-	X
3 Badrina	-	-	X
4 Schkölen	-	-	X (tectonic)
5 Hainichen	-	-	X (tectonic)
6 Borgishain	X	-	-
7 Brockwitz	X	-	-
8 Casabra	-	X	-
9 Dresden Hellerberge	X	-	-
10 Heukendorf	X	X	-
11 Hirschfeld	X	X	-
12 Neuenmörbitz	-	X	-
13 Neuposa	-	X	-
14 Niedersteinbach 1	X	-	-
15 Niedersteinbach 2	-	X	-
16 Pomßen	X	-	-
17 Puschwitz	-	X	-
18 Sermuth 2	X	-	-
19 Sermuth 1	-	X	-
20 Strauch	X	X	-
21 Tierbaum	-	X	-

### Lusatian Thrust north of Dresden

In a sand pit (pit number 1) (Fig. 2) in the area of Dresden Klotzsche, which exposes Middle Pleistocene (Saalian) meltwater and Late Pleistocene (Weichselian) alluvial deposits (Steding et al. 1994; Trautmann et al. 1999; Alexowsky et al. 2001; Lange et al. 2016; Winsemann et al. in prep.) deformation bands with normal displacement occur. These deformation bands have a NW-SE orientation like the nearby Lusatian Thrust (Figs 2, 3a). The pit is located near the NW segment of the Lusatian Thrust, in a key position close to an intersection of a younger NE-SW oriented fault that offsets the Lusatian Thrust and leads to a pronounced segmentation (Krentz and Stanek 2015).

#### Interpretation

The presence of deformation bands with normal displacement in Middle Pleistocene Saalian meltwater deposits point to a post Middle Pleistocene (Saalian) reactivation of the fault under



different stress regimes. This observation is in line with the results of Coubal et al. (2015), who showed that the Lusatian Thrust has a complex kinematic history and is not exclusively characterised by thrusting, also indicated by the development of pull-apart basins in the southeastern part of the Lusatian Thrust (Krentz et al. 2000). The sand pit is located close to an intersection of the Lusatian Thrust and Hoyerswerder Fault (Fig. 2), which might have acted as stress concentrator and favoured seismic activity as described in the model of Talwani (1988). However, the relation of deformation bands with normal displacement at a thrust fault is not well understood. Although counter intuitive, similar observations, where extensional structures are developed at thrust faults, have been made in studies from the Osning Thrust and the Harz Boundary Fault (Brandes et al. 2012; Müller et al. 2020). A possible cause of this kinematic difference might be an effect of multiphase tectonic evolutions of the Lusatian Thrust.

Additionally, an unsteady state and disequilibrium between erosion and uplift rates supports the assumption that there is Pleistocene activity along the Lusatian Thrust (Tietz et al. 2011). Furthermore, changes in direction of river courses from N-S to NW-SE and the geometry of the river network points to ongoing neotectonic activity in the Lower Lusatian area (Stackebrandt 2008).

### **Faults west of Dresden**

Evidence of post Middle Pleistocene (Elsterian) fault activity was found in a sand pit in the area of the village Churschütz. In this sand pit (pit number 2) (Fig. 2) Middle Pleistocene (Elsterian) meltwater deposits (Steding et al. 1996) with conjugate sets of deformation bands with normal displacement are exposed (Fig. 3b, c). Besides the deformation bands, the succession is undisturbed. The pit is located above a small NNW-SSE striking basement fault that intersects with a NW-SE oriented basement fault (Fig. 2). The exposed deformation bands are vertically continuous, NNW-SSE oriented and match the strike of the underlying basement fault.

#### *Interpretation*

The presence of distinct deformation bands strongly points to fault activity, either related to seismic or aseismic neotectonic activity at an underlying basement fault (e.g., cf. Brandes and Tanner 2012; Brandes et al. 2018a; Müller et al. 2021b). This evidence for neotectonic activity might be supported by Eissmann (1975, 1987) who described steeply dipping deposits (*'untere Döbelner Schotter'*) in the area of Döbeln between the rivers Elbe and Mulde.

However, the area of Döbeln was repeatedly covered by ice-dammed lakes during the Middle Pleistocene (Fig. 1c, d; Lang et al. 2018) and a review of depositional systems in this area reveals that steeply dipping Pleistocene deposits commonly represent glaciolacustrine deltas and are not tilted by tectonic movements (e.g., Winsemann et al. 2018; Lang et al. 2018, 2019). A typical example are wedge-shaped, steeply dipping Middle Pleistocene delta deposits (25-36°) exposed in a sand pit near the village Piskowitz, approximately 20 km northeast of Döbeln, as well as steeply dipping delta deposits at Karsdorf, west of Leipzig (Lang et al. 2018) that were previously interpreted as fluvial terrace deposits (*'Unstrut Main Terrace'*), (Meng and Wansa 2008). This weakens Eissmann's (1975, 1987) arguments for tectonic activity in this region.

Nevertheless, with the investigation of deformation bands close to an intersection of distinct faults, tectonic activity in this area can be verified and the location can be narrowed down to the area of Churschütz. The observed deformation bands are likely formed in the process zone of a basement fault that was active in post Middle Pleistocene times.

### **Faults north of Leipzig and along the Finne-Gera-Jáchymov fault system**

In a sand pit (pit number 3) (Fig. 2) near the village Badrina deformation bands with normal displacement are exposed that are developed in an undisturbed Middle Pleistocene (Saalian) meltwater succession (Koch et al. 1996). The orientation of the observed deformation bands is ENE-WSW and closely matches with a nearby NE-SW trending fault (Figs 2, 3d).

Deformation bands with normal displacement and conjugate normal faults are also exposed in Palaeogene (Eocene-Oligocene) fluvial sand and gravel (Fig. 3e-h) (Seidel and Steinmüller 1994) near the villages Hainchen (pit number 5) and Schkölen (pit number 4). The sand pits are located close to the NW-SW oriented Finne-Gera-Jáchymov fault system (Fig. 2).

#### *Interpretation*

The intersection pattern of the basement faults and the match in orientation of the observed deformation bands implies a close connection of these structural elements. This points to potential neotectonic activity along the regional basement faults.

The presence of deformation bands in the pit near the village Badrina point to post Middle Pleistocene (Saalian) fault activity. Close to the sand pit near Badrina, the Mulde Fault is located (Fig. 2). The Mulde river follows the Mulde Fault between the villages of Bad Düben and Wurzen. In the area around this fault, Ellenberg (1992) found evidence for recent vertical ground motions by using geodetic methods.

In the pits along the Finne-Gera-Jáchymov fault system the host sediments have an Eocene-Oligocene age (Seidel and Steinmüller 1994) and therefore the tectonic movements could be potentially older than the Pleistocene. This delivers evidence for post-Palaeogene fault activity on faults in the RLR fault system.

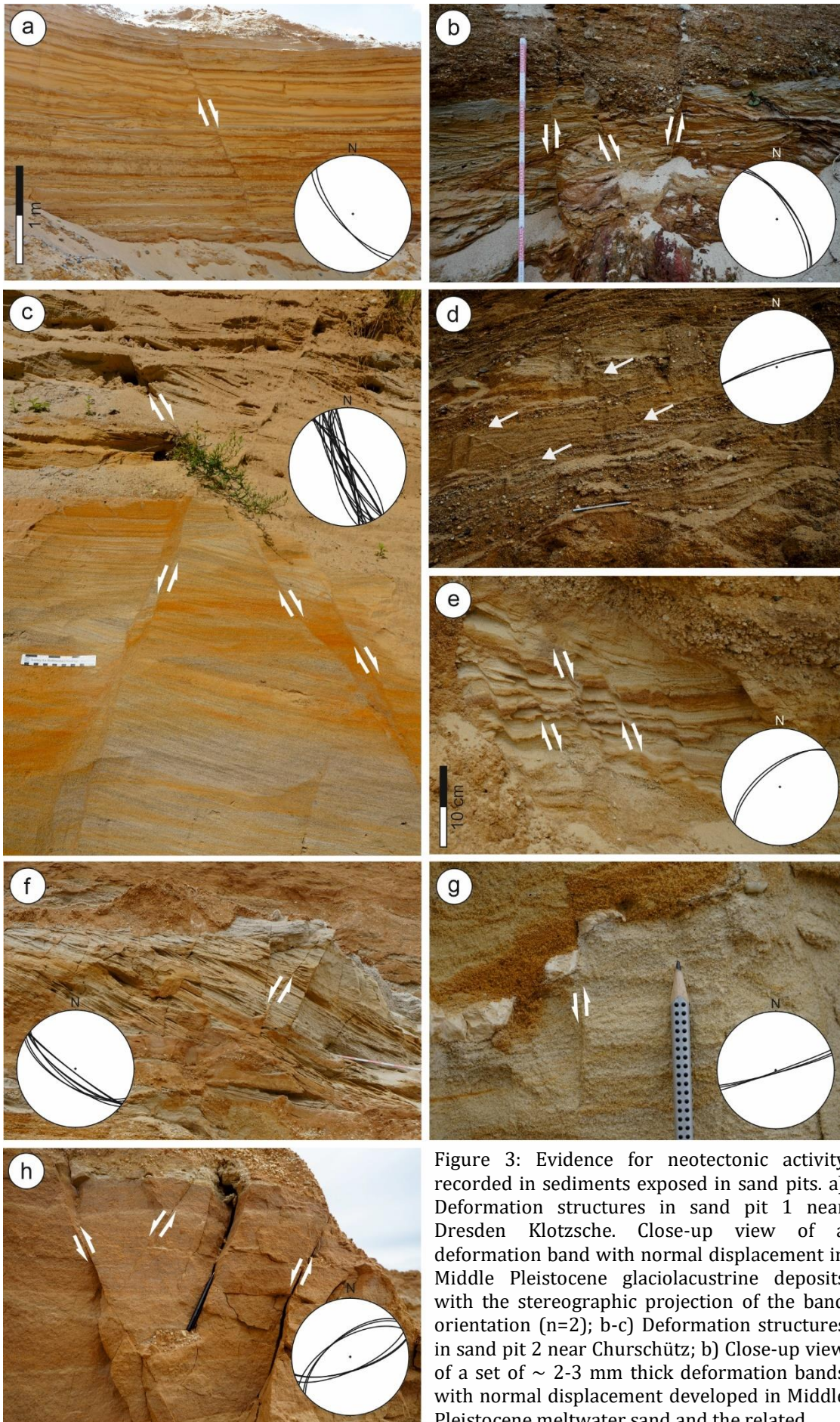


Figure 3: Evidence for neotectonic activity recorded in sediments exposed in sand pits. a) Deformation structures in sand pit 1 near Dresden Klotzsche. Close-up view of a deformation band with normal displacement in Middle Pleistocene glaciolacustrine deposits with the stereographic projection of the band orientation ( $n=2$ ); b-c) Deformation structures in sand pit 2 near Churschütz; b) Close-up view of a set of  $\sim 2$ -3 mm thick deformation bands with normal displacement developed in Middle Pleistocene meltwater sand and the related



stereographic projection of the orientation of the deformation bands (n= 3); c) Close-up view of Middle Pleistocene meltwater sand with a set of conjugate deformation bands with normal displacement and ~ 2-4 cm offset. Stereographic projection of the orientation of the deformation bands (n= 23); d) Deformation structures in sand pit 3 near Badrina. Close-up view of two deformation bands with normal displacement in Middle Pleistocene meltwater sand with the related stereographic projection of the band orientations (n=3), pen for scale; e-f) Deformation structures in Palaeogene fluvial sand and gravel in pit 5 near Hainchen. e) Close-up view of a set of deformation bands with normal displacement and 1-2 cm offset in fluvial sand and the related stereographic projection (n=2); f) Close-up view of normal faults with 3 cm offset in fluvial sand and the related stereographic projection (n=3); g-h) Deformation structures in Palaeogene fluvial sand and gravel in pit 4 Schkölen. g) Set of deformation bands with normal displacement (~ 3 cm thick) in fluvial sand and the related stereographic projection (n=7), pen for scale; h) Conjugate normal faults in compacted fluvial sand with the related stereographic projection (n=6), pen for scale.

## Lineament analysis

Traditionally, lineaments in the RLR fault system were analysed based on satellite images (e.g., Kämpf et al. 1991; Bram and Hirschmann 1992). However, a strong anthropological overprint of the area makes the usage of satellite data less appropriate. Thus, lineaments are obscured by artificial objects like roads and railroad tracks, settlement areas or boundaries of farmland. This makes photolineament interpretation in general difficult and the results are commonly not reliable (Van der Pluijm and Marshak 2004).

To overcome these limitations, we used digital elevation models (30 m and 5 m grids with vertical accuracy of  $\pm 2$  m and  $\pm 0.15$  m). The applied eight different directions of illumination (N000° N045°, N090° N135°, N180° N225°, N270° N315°) are shown in Figure 4 and for the Lusatian Thrust in Figure 5. The different illumination directions show lineaments at nearly similar positions and do not show significant variations in their pattern. For the Lusatian Thrust, which is a discrete structure that is also visible in Figure 4, a higher resolution (5 m grid, vertical accuracy of  $\pm 0.15$  m) DEM was used. We selected the area of the Lusatian Thrust, which is not part of the RLR fault system, for a more detailed lineament analysis, because of seismic and tectonic activity in this area (e.g., Stackebrandt 2008; Tietz et al. 2011) and new neotectonic evidence.

The results of the lineament analysis indicate a diffuse array of lineaments. In the northern part of the study area less lineaments are detected than in the southern area (Fig. 4a). No distinct N-S trending structures are visible. At some locations the accumulation of lineaments point to distinct NW-SE and NE-SW oriented structures (Fig. 4a). The rose diagram of all extracted lineaments (Fig. 4a) shows the predominance of NW-SE oriented structures. Figure 4b shows the illumination directions N045° and N225°, which images NW-SE striking structures very well and the illumination directions N090° and N270° (Fig. 4c) that images N-S striking structures. We have chosen these directions of illumination because N-S and NW-SE striking structures are the most relevant ones in the study area.

The results of the lineament analysis at the Lusatian Thrust show that most of the lineaments in this area strike NW-SE. Distinctive is the river Prießnitz north of the Lusatian Thrust (Fig. 5) that abruptly changes its course from SE-NW to NNE-SSW (Fig. 5). A waterfall is developed in the Prießnitz river (Fig. 5) that is a remarkable morphological feature.

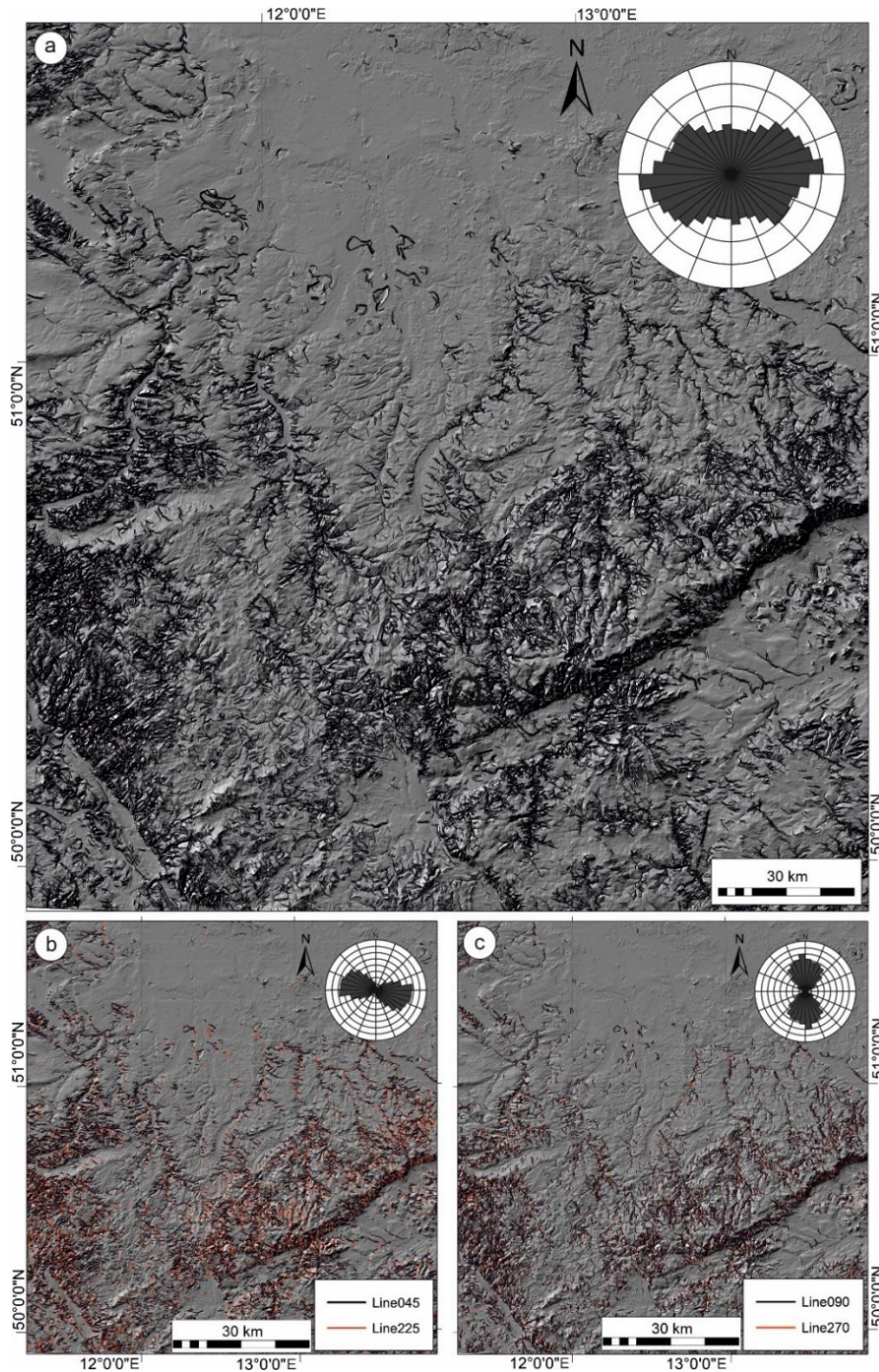


Figure 4: Lineament analysis in the study area. Inset rose diagrams illustrating the overall directions of lineaments; a) Overview image of the lineament analysis in the study area with eight illumination directions N000°, N045°, N090°, N135°, N180°, N225°, N270°, N315°; b) Lineament analysis of the study area using illumination direction N045°, N225°; c) Lineament analysis of the study area using illumination direction N090°, N270°.

### Interpretation

Prominent morphologic tectonic structures are the Lusatian Thrust with the Elbe Zone, the Eger Rift, the Franconian Line and the Finne Fault (Figs 4, 5). The Gera-Jáchymov Fault is not clearly imaged (Fig. 4). No lineaments were identified especially in the northern part of the area, which is covered by thick unconsolidated Middle to Late Pleistocene sediments (see Fig. 4). This can have two reasons. Firstly, the thick cover of unconsolidated sediments hampers the detection of lineaments and faults at the Earth's surface. With the increased thickness of Pleistocene deposits, the number of extracted lineaments decreases (Fig. 4). Secondly, it is possible that no faults are present that reach the Earth's surface. Only the Prießnitz river in the area of the Lusatian Thrust is an indicator for neotectonic activity in the study area. Near Dresden, the Prießnitz river flows

SE-NW and changes its course towards the NNE-SSW close to Dresden Klotzsche. The NNE-SSW flow direction of the Prießnitz river is parallel to the NE-SW striking Hoyerswerder Fault. At the Lusatian Thrust neotectonic activity was observed at the intersection with the Hoyerswerder Fault. A waterfall is developed at the Prießnitz river, which might have formed in response to young tectonic activity. Waterfalls are key features, as they represent knickpoints, which are localities where the slope of a river changes (e.g., Burband and Anderson 2001). In the case of the Prießnitz waterfall, the origin cannot be derived. According to geological maps (Siegert 1907; Alexowsky et al. 2001), the area is characterised by different granite types and by granites that are mechanically altered. This alteration is likely related to the activity along the Lusatian Thrust and the NE-SW oriented fault presumably represents the damage zone of these faults. The waterfall possible formed, where the mechanical resistivity of the rocks changes from intact granite to the fault damage zone. Another possibility is that the break-in-elevation represents a fault scarp that formed during an earthquake. However, it is also possible that the waterfall is simply the result of a lithological change of different granite types (Siegert 1907; Alexowsky et al. 2001).

Equally, no N-S trending lineaments were identified in the southern part of the study area. In contrast to previous studies (e.g., Kämpf et al. 1991; Bram and Hirschmann 1992) our lineament analysis indicates that the RLR fault system is not visible at the Earth's surface.

Distinct morphologic structures are commonly interpreted as evidence for strong tectonic activity. This could imply that strong tectonic activity is absent. Slow creep processes along faults are probably not producing distinct features at the surface, although possible as proposed by Ellenberg (1992). Although the seismic activity in the northern part of the study area around Leipzig is reduced in comparison to the southern area (Vogtland/Cheb) and focal mechanisms do not point to N-S striking structures.

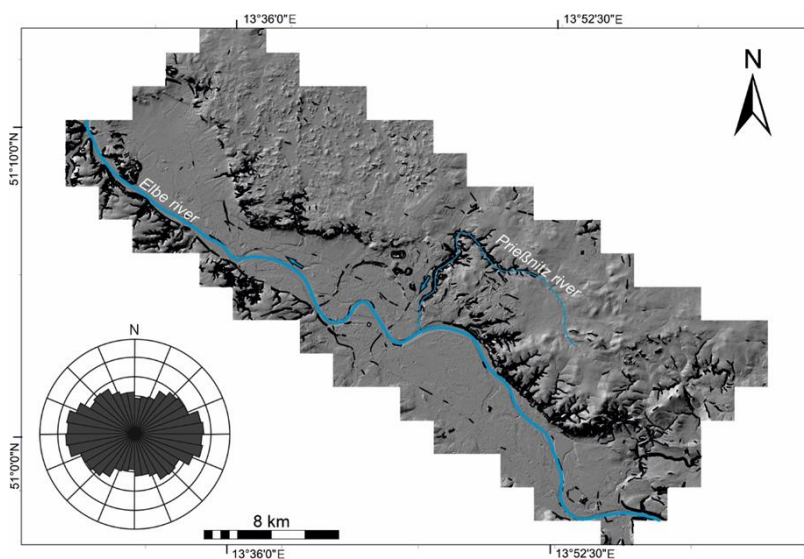


Figure 5: Overview image of the lineament analysis at the Lusatian Thrust with eight illumination directions N000°, N045°, N090°, N135°, N180°, N225°, N270°, N315°. Inset rose diagram illustrating the overall directions of lineaments. The prominent change of the course of the Prießnitz river from NW-SE towards NNE-SSW is probably related to the NE-SW striking Hoyerswerder Fault. A waterfall developed in approx. 500 m distance to the change in the course direction.

## Discussion

Many studies focus on single seismicity clusters along the RLR fault system like e.g., the Werdau and Nový Kostel focal zones or individual faults or fault systems like the Finne-Gera-Jáchymov fault system. There is no synthesis that combines the different results published yet and an overview of different seismotectonic characteristics is lacking. The recent study of Dahm et al. (2018) and Dahm and Deng (2021) raises the question about the presence of different seismotectonic zones along the RLR fault system, because focal mechanisms show that the earthquakes are related to deep NW-SE oriented faults, whereas earthquakes in the southern part of the study area are commonly related to N-S trending faults and the shear sense derived from geodetic analysis did not match with focal mechanisms of N-S trending faults and previous geodetic measurements in this region (e.g., Korn et al. 2008; Wendt and Buchholz et al. 2019; Dahm and Deng 2021).

### Tectonic stress and focal mechanisms

Important driver for the neotectonic activity and the recent seismicity in central Europe is the lithospheric stress field caused by the Alpine collision and the Atlantic ridge push (Marotta et al. 2001; Kaiser et al. 2005). Local variations in the stress field are caused by rheology and crustal structures.

The recent stress field in the area of the Ore Mountains is NW-SE oriented (Heidbach et al. 2016). Korn et al. (2008) also point out that the maximum horizontal compression ( $S_{Hmax}$ ) in the region between Leipzig and the Vogtland is NW-SE oriented, like the general stress field in Western Europe. Grünthal and Stromeyer (1994) show that the Bohemian Massif deflects the regional stress field and  $S_{Hmax}$  changes from a NW-SE orientation in the south to a NE-SW orientation in the north. Similar observations were made by Roth and Fleckenstein (2001) and Heidbach et al. (2016). Tectonic stress, derived from focal mechanisms in the Vogtland/NW Bohemia, show a NW-SE oriented  $S_{Hmax}$  in a strike-slip regime (Klinge and Plenefisch 2001; Ibs-von Seht et al. 2006). Ibs-von Seht et al. (2006) analysed focal mechanisms of earthquakes and earthquake swarms between 1999 and 2002 in the area of NW Bohemia and proposed two different stress models for this area. The first model implies a strike-slip regime with  $S_{Hmax}$  striking into a NW-SE direction and a clockwise rotation of nearly 30° for sigma  $\sigma_1$  and  $\sigma_3$  from the Vogtland to NE Bavaria (KTB drill). The second model suggests a thrust-fault regime with  $S_{Hmax}$  striking in N-S direction and has two different stress orientations developing at different depth levels.

Focal mechanisms for several earthquakes in the Nový Kostel focal zone exist (e.g., Klinge and Plenefisch 2001; Ibs-von Seht et al. 2008; Dahm et al. 2013; Fischer et al. 2014; Čermáková and Horálek 2015), whereas focal mechanisms for earthquakes in the northern part of the RLR fault system are rare (e.g., Neunhöfer et al. 1996; Dahm et al. 2018). Korn et al. (2008) analysed available data of fault plane solutions from online stations, obtained between 2002 and 2007. They deduce that a N-S strike predominates in the dataset and tectonic activity seems to be coupled to the RLR fault system (see Fig. 6, Table 3).



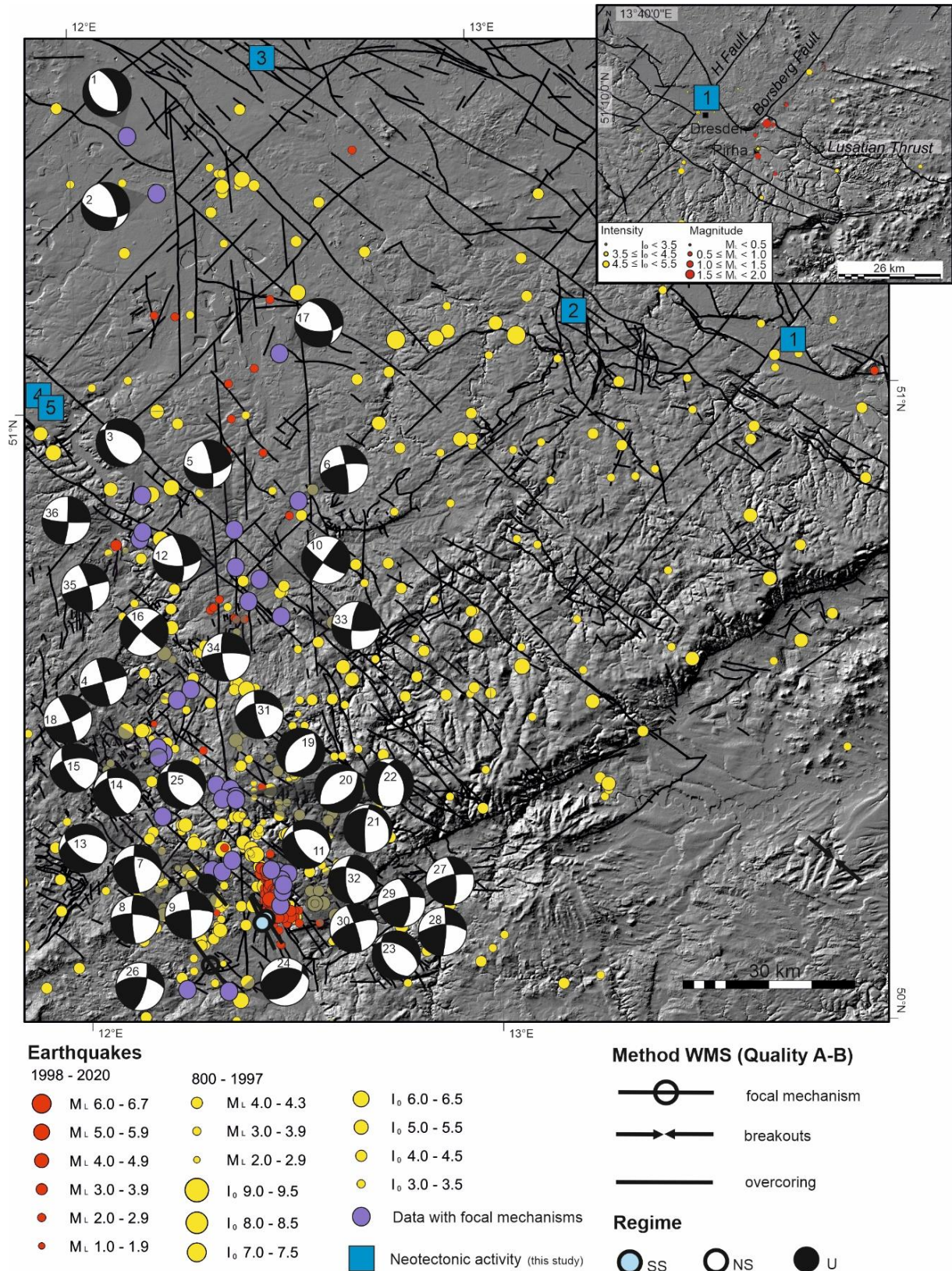


Figure 6: Seismic activity in the study area with focal mechanisms (purple dots) (from Neunhöfer et al. 1996; Korn et al. 2008; Dahm et al. 2018) and the recent stress field from WSM (Heidbach et al. 2016). Source parameters of events are listed in Table 3. Further seismic data are from GERSEIS (2020). The cut-out shows the Lusatian Thrust with the Hoyerwerder Fault (H Fault) and the Borsberg Fault. Seismic data are from TLUBN (2020).

In the southern part of the analysed section of the RLR fault system, fault plane solutions from the Nový Kostel focal zone show that the seismic activity is represented by local earthquake swarms with hypocentre depths of up to ~12 km, with normal fault, oblique-normal and strike-slip mechanisms, and less frequently oblique-thrust mechanisms that are mostly related to N-S and NNW-SSE trending faults (Klinge and Plenefisch 2001; Dahm et al. 2013; Fischer et al. 2014; Čermáková and Horálek 2015), although focal mechanisms during earthquake swarms can change (e.g., Plenefisch and Klinge 2003). The focal mechanisms imply that the seismic activity is most likely related to the Počátky-Plesná-Zone and the Marienbader Fault, which intersect in the Nový Kostel area (Bankwitz et al. 2003b). North of Colditz, an earthquake ( $M_L$  2.1) with a hypocentre depth of 15.4 km occurred along a potential WNW-ESE or NW-SE striking source fault (Korn et al. 2008). Further to the north in the Leipzig area, earthquakes were detected in 2015 and 2017 with magnitudes of  $M_w$  3.2 and 2.8, of much greater depths of 29 km and 26 km, respectively, which are both probably related to the Halle Fault or a fault that runs parallel to it (Dahm et al. 2018; Rappsilber and Funke 2019). Neotectonic activity along the Halle Fault system was already observed by Müller et al. (2021b). Thus, the depth of the earthquake hypocentres increases to the north of the RLR fault system and the observed recent seismic activity in this area is clearly related to NW-SE striking faults. Consequently, the earthquake distribution in the northern part of the RLR fault system up to a latitude of 50.5° (e.g., Sonnabend 2019) is comparable to northern Germany, where several deep events (17.0 – 31.4 km) occurred over the last 20 years (Brandes et al. 2019) and where WNW-ESE striking faults are the source for one of the recent deep earthquakes (Brandes et al. 2019) and also for many historic events (Brandes et al. 2015). However, the database is limited in the northern part of the RLR fault system and the apparent northward increasing earthquake focal depths can be an effect of the dominant shallow earthquake swarms in the south that lack in the northern area, where only deeper events were recently detected.

The results of the palaeoseismological analysis in the area around the seismically active section (Leipzig – Cheb) of the RLR fault systems, indicate that fault intersections are an important trigger for tectonic activity. We did not find N-S striking structures, however, we observed fault activity along smaller NW-SE, NNE-SSW and NE-SW striking faults in the vicinity to fault intersections, based on deformation bands.

The lineament analyses in the study area give no new indications for N-S trending structures. Only distinct morphological features like the Lusatian Thrust with the Elbe Zone, the Eger Rift, the Franconian Line and the Finne Fault were imaged. These structures expose bedrock and do not necessarily represent faults that are neotectonically active. Blind faults were not directly imaged. A shaded relief map of horizontal gravity contrasts indicates three major regional structural trends: a NW-SE, which is the most prominent one, a NNE-SSW and an ENE-WSW direction (Švancara et al. 2008). The N-S trend of the RLR fault system is not directly reflected by this dataset which is in line with our lineament analyses. Only isolated N-S trending structures between Altenburg and Nový Kostel were imaged (Švancara et al. 2008). In this section of the RLR fault system, focal mechanisms show nodal planes that strike in N-S direction (e.g., Plenefisch and Klinge 2003; Korn et al. 2008) and geological maps indicate N-S striking faults (e.g., Leonhardt 1995). We cannot verify these results with lineament mapping.

Table 3: Source parameters of earthquakes from 2002 to 2017 with fault plane solutions imaged in Fig. 6. M = Magnitude.

No.	Date	Coordinates	Depth [km]	M	Nodal Plane 1			Nodal Plane 2			Reference
					strike	dip	rake	strike	dip	rake	
1	2015	51.42 12.13	29.0	M <sub>w</sub> 3.2	330	040	-076	132	051	-101	Dahm et al. 2018
2	2017	51.34 12.21	26.0	M <sub>w</sub> 2.8	338	043	-042	101	063	-125	Dahm et al. 2018
3	1993	50.87 12.12	16.1	M <sub>L</sub> 2.5	153	044	-060	295	053	-115	Neunhöfer et al. 1996
4	2002	50.55 12.19	2.9	M <sub>L</sub> 1.3	343	089	-001	074	089	-179	Korn et al. 2008
5	2002	50.81 12.35	10.8	M <sub>L</sub> 1.2	342	067	-044	093	050	-149	Korn et al. 2008
6	2002	50.86 12.51	14.0	M <sub>L</sub> 2.0	351	082	018	258	072	171	Korn et al. 2008
7	2002	50.29 12.31	16.6	M <sub>L</sub> 1.3	174	079	-045	275	046	-164	Korn et al. 2008
8	2002	50.27 12.28	14.7	M <sub>L</sub> 2.0	178	081	-020	271	070	-171	Korn et al. 2008
9	2002	50.27 12.27	14.6	M <sub>L</sub> 1.5	355	085	017	264	073	175	Korn et al. 2008
10	2002	50.72 12.40	17.4	M <sub>L</sub> 1.4	218	088	013	128	077	178	Korn et al. 2008
11	2002	50.24 12.43	7.3	M <sub>L</sub> 1.3	154	046	-059	293	052	-119	Korn et al. 2008
12	2002	50.75 12.35	17.2	M <sub>L</sub> 2.0	350	071	-029	090	063	-159	Korn et al. 2008
13	2002	50.37 12.15	15.3	M <sub>L</sub> 1.4	130	060	-057	258	043	-134	Korn et al. 2008
14	2003	50.47 12.15	14.8	M <sub>L</sub> 1.6	157	070	-056	274	039	-147	Korn et al. 2008
15	2003	50.47 12.14	14.0	M <sub>L</sub> 1.6	151	064	-037	260	057	-149	Korn et al. 2008
16	2003	50.56 12.23	8.2	M <sub>L</sub> 1.6	223	082	005	132	086	172	Korn et al. 2008
17	2003	51.09 12.49	15.4	M <sub>L</sub> 2.1	334	052	-043	094	057	-133	Korn et al. 2008
18	2003	50.47 12.15	12.8	M <sub>L</sub> 1.4	338	084	-011	069	080	-174	Korn et al. 2008
19	2003	50.41 12.31	6.2	M <sub>L</sub> 1.4	217	050	-085	029	040	-096	Korn et al. 2008
20	2003	50.40 12.31	5.9	M <sub>L</sub> 1.5	053	049	-085	225	041	-096	Korn et al. 2008
21	2004	50.40 12.31	6.3	M <sub>L</sub> 1.4	185	079	-068	300	025	-153	Korn et al. 2008
22	2004	50.40 12.31	7.2	M <sub>L</sub> 1.8	200	054	-059	333	046	-126	Korn et al. 2008
23	2004	50.25 12.43	13.9	M <sub>L</sub> 1.5	151	045	-064	296	050	-114	Korn et al. 2008
24	2004	50.10 12.30	14.3	M <sub>L</sub> 1.4	046	053	065	264	044	120	Korn et al. 2008
25	2004	50.40 12.30	16.8	M <sub>L</sub> 1.4	146	063	-063	278	038	-132	Korn et al. 2008
26	2004	50.09 12.19	11.0	M <sub>L</sub> 1.3	350	078	017	256	073	167	Korn et al. 2008
27	2005	50.26 12.42	9.2	M <sub>L</sub> 1.0	352	070	017	256	074	159	Korn et al. 2008
28	2005	50.26 12.43	8.7	M <sub>L</sub> 0.4	360	078	019	266	072	167	Korn et al. 2008
29	2005	50.25 12.43	9.0	M <sub>L</sub> 0.9	358	061	019	259	074	150	Korn et al. 2008
30	2005	50.26 12.42	9.2	M <sub>L</sub> 1.0	342	083	019	250	072	172	Korn et al. 2008
31	2005	50.41 12.28	6.1	M <sub>L</sub> 1.0	166	081	-039	263	051	-169	Korn et al. 2008
32	2006	50.22 12.42	10.2	M <sub>L</sub> 1.5	178	065	-041	288	054	-148	Korn et al. 2008
33	2006	50.67 12.46	7.2	M <sub>L</sub> 1.5	188	077	017	094	074	166	Korn et al. 2008
34	2006	50.69 12.38	4.8	M <sub>L</sub> 2.1	174	076	-014	268	076	-165	Korn et al. 2008
35	2007	50.80 12.12	6.9	M <sub>L</sub> 2.8	344	078	003	254	087	168	Korn et al. 2008
36	2007	50.81 12.13	5.6	M <sub>L</sub> 1.0	004	083	-007	095	083	-173	Korn et al. 2008

### Seismicity close to faults with neotectonic activity

Neotectonic activity derived from geological indicators like deformation bands, is combined with an earthquake dataset which underpins the tectonic activity at some faults (Figs 2, 6, Tables 3, 4). Each location, where neotectonic activity has been detected, can be correlated to historic and instrumentally recorded earthquakes in 20 km distance (Figs 2, 6). The epicentral intensities of historic earthquakes range between III and V (5.5) (Leydecker 2011), with one of the strongest earthquakes occurring close to the village of Churschütz in 1568 with an epicentral intensity of V (5.5) (pit number 2) (Leydecker 2011) for further earthquakes see Table 4. The strongest historic earthquakes are located in an area, where a significant number of deformation bands occur that point to Pleistocene neotectonic activity.

Furthermore, near the pits close to the villages Hainchen (pit number 5) and Schkölen (pit number 4), which are located along the Finne-Gera-Jáchymov fault system, several earthquakes with epicentral intensities above V occurred (Fig. 2). The strongest instrumentally detected event

in the study area, occurred in 1926 with an epicentral intensity of VI and was located along the Finne-Gera-Jáchymov fault system, (Leydecker 2011) which underlines the seismotectonic importance of this fault system and supports the evidence of fault activity.

Neotectonic activity at the intersection of the Lusatian Thrust and the Hoyerswerder Fault that was recorded in Middle Pleistocene Saalian sediments, is supported by a recent seismotectonic analysis. Approximately 30 earthquakes that occurred since 2013 NE of Pirna are interpreted to be related to the Lusatian Thrust (Buchholz et al. 2016). Further micro-earthquakes were detected in 2016 and 2018 along the Lusatian Thrust (Funke and Hänel 2019). In 2013 to 2018, several seismic events were detected along the NE-SW oriented Borsberg Fault SW of Dresden close to Pirna (Fig. 2; TLUBN 2020). The earthquakes have magnitudes ranging from  $M_L$  0.3 to 2.0 and focal depths between 10.1 and 12.5 km (Table 4) (TLUBN 2020). The earthquakes along the NE-SW Borsberg Fault show NE-ward migrating hypocentres. The younger Borsberg Fault intersects with the Lusatian Thrust close to the village Dürrröhrsdorf-Dittersbach and may represent a fault parallel to the Hoyerswerder Fault or an en-échelon segment of this fault. Bouguer gravity data image linear structures, which are interpreted as fault (Krentz and Stanek 2015). At the Borsberg Fault horizontal slickensides show small strike-slip offsets, but geodetic measurements across the fault point to normal fault movements (Bankwitz 1968).

Table 4: Historic (800- 1997) and instrumentally detected (1998- 2020) earthquakes that are located in a 20 km radius of the sites with observed neotectonic activity (Fig. 2). The magnitude  $M_w$  was calculated using the equation  $M_w=0.682 I_0 + 0.16$  according to Grünthal et al. (2009b).

Year	Coordinates	Epicentral Intensity	Magnitude	Depth (km)	Reference
<b>1 Dresden Klotzsche</b>					
1574	51,05; 13,74	4.0	2.9 ( $M_w$ )	-	Leydecker 2011
1756	51,05; 13,74	3.5	2.6 ( $M_w$ )	-	Leydecker 2011
1901	51,96; 13,95	4.5	3.3 ( $M_w$ )	-	Leydecker 2011
1901	51,96; 13,95	4.0	2.9 ( $M_w$ )	-	Leydecker 2011
1902	51,05; 13,74	3.0	2.2 ( $M_w$ )	-	Leydecker 2011
1905	51,05; 13,80	3.0	2.2 ( $M_w$ )	-	Leydecker 2011
1908	51,10; 13,89	3.0	2.2 ( $M_w$ )	-	Leydecker 2011
1908	51,05; 13,74	3.0	2.2 ( $M_w$ )	-	Leydecker 2011
1908	51,05; 13,74	3.0	2.2 ( $M_w$ )	-	Leydecker 2011
1908	51,05; 13,74	3.5	2.6 ( $M_w$ )	-	Leydecker 2011
1908	51,05; 13,74	3.0	2.2 ( $M_w$ )	-	Leydecker 2011
1908	51,05; 13,74	3.0	2.2 ( $M_w$ )	-	Leydecker 2011
1908	51,05; 13,74	4.0	2.9 ( $M_w$ )	-	Leydecker 2011
1908	51,02; 13,52	3.0	2.2 ( $M_w$ )	-	Leydecker 2011
1909	51,05; 13,74	3.0	2.2 ( $M_w$ )	-	Leydecker 2011
1909	51,02; 13,52	3.0	2.2 ( $M_w$ )	-	Leydecker 2011
1909	51,02; 13,52	3.0	2.2 ( $M_w$ )	-	Leydecker 2011
1910	51,10; 13,71	3.0	2.2 ( $M_w$ )	-	Leydecker 2011
1910	51,10; 13,71	3.0	2.2 ( $M_w$ )	-	Leydecker 2011
1915	51,03; 13,74	3.0	2.2 ( $M_w$ )	-	Leydecker 2011
1949	50,94; 13,68	4.0	2.9 ( $M_w$ )	-	Leydecker 2011
1986	51,13; 13,82	-	3.2 ( $M_L$ )	-	Leydecker 2011
2013	51,02; 13,99	-	2.0 ( $M_L$ )	12.1	TLUBN 2020
2013	51,01; 14,01	-	0.8 ( $M_L$ )	12.5	TLUBN 2020
2013	50,99; 13,94	-	0.7 ( $M_L$ )	10.1	TLUBN 2020
2016	51,06; 14,06	-	0.6 ( $M_L$ )	12.1	TLUBN 2020
<b>2 Churschütz</b>					
1513	51,16; 13,47	3.0	2.2 ( $M_w$ )	-	Leydecker 2011
1568	51,12; 13,05	5.5	4.0 ( $M_w$ )	-	Grünthal & Wahlström 2012
1784	51,16; 13,47	3.5	2.6 ( $M_w$ )	-	Leydecker 2011
1828	51,32; 13,17	4.5	3.3 ( $M_w$ )	-	Leydecker 2011



1830	51,07; 13,03	3.0	2.2 (M <sub>w</sub> )	-	Leydecker 2011
1903	51,16; 13,13	4.0	2.9 (M <sub>w</sub> )	-	Leydecker 2011
1908	51,22; 13,12	3.0	2.2 (M <sub>w</sub> )	-	Leydecker 2011
1908	51,22; 13,12	3.0	2.2 (M <sub>w</sub> )	-	Leydecker 2011
1908	51,22; 13,12	4.0	2.9 (M <sub>w</sub> )	-	Leydecker 2011
1908	51,06; 13,20	3.0	2.2 (M <sub>w</sub> )	-	Leydecker 2011
1908	51,02; 13,55	4.0	2.9 (M <sub>w</sub> )	-	Leydecker 2011
1911	51,15; 13,47	3.0	2.2 (M <sub>w</sub> )	-	Leydecker 2011
2012	51,00; 13,14	-	1.0 (M <sub>L</sub> )	25.0	TLUBN 2020
<b>3 Badrina</b>					
1819	51,47; 12,43	4.5	3.3 (M <sub>w</sub> )	-	Leydecker 2011
2013	51,59; 12,45	-	1.3 (M <sub>L</sub> )	-	TLUBN 2020
2015	51,43; 12,61	-	0.9 (M <sub>L</sub> )	19.6	TLUBN 2020
2015	51,46; 12,29	-	1.3 (M <sub>L</sub> )	16.3	TLUBN 2020
2016	51,59; 12,45	-	1.2 (M <sub>L</sub> )	13.1	TLUBN 2020
2016	51,40; 12,70	-	2.0 (M <sub>L</sub> )	20.4	TLUBN 2020
2016	51,38; 12,59	-	0.9 (M <sub>L</sub> )	19.0	TLUBN 2020
2018	51,39; 12,41	-	1.1 (M <sub>L</sub> )	18.6	TLUBN 2020
<b>4, 5 Hainchen, Schkölen</b>					
1690	50,97; 11,91	5.0	3.4 (M <sub>w</sub> )	-	Leydecker 2011
1695	50,97; 11,91	5.5	4.0 (M <sub>w</sub> )	-	Grünthal & Wahlström 2012
1830	51,10; 11,62	4.0	2.9 (M <sub>w</sub> )	-	Leydecker 2011
1884	51,04; 12,04	3.5	2.6 (M <sub>w</sub> )	-	Leydecker 2011
1926	50,94; 11,94	4.0	2.9 (M <sub>w</sub> )	-	Leydecker 2011
1926	50,94; 11,94	3.5	2.6 (M <sub>w</sub> )	-	Leydecker 2011
1926	50,94; 11,94	6.0	4.3 (M <sub>w</sub> )	-	Leydecker 2011
1926	50,94; 11,94	3.5	2.6 (M <sub>w</sub> )	-	Leydecker 2011
1926	50,94; 11,94	3.0	2.2 (M <sub>w</sub> )	-	Leydecker 2011
1926	50,94; 11,94	3.5	2.6 (M <sub>w</sub> )	-	Leydecker 2011
1926	50,94; 11,94	3.5	2.6 (M <sub>w</sub> )	-	Leydecker 2011
1926	50,94; 11,94	3.5	2.6 (M <sub>w</sub> )	-	Leydecker 2011
1926	50,94; 11,94	3.0	2.2 (M <sub>w</sub> )	-	Leydecker 2011
1926	50,94; 11,94	3.0	2.2 (M <sub>w</sub> )	-	Leydecker 2011
2009	51,07; 12,06	-	1.3 (M <sub>L</sub> )	14.0	TLUBN 2020
2011	51,10; 12,08	-	1.8 (M <sub>L</sub> )	12.7	TLUBN 2020
2011	51,00; 12,02	-	0.4 (M <sub>L</sub> )	16.4	TLUBN 2020
2012	51,09; 12,08	-	0.2 (M <sub>L</sub> )	18.3	TLUBN 2020
2015	51,08; 12,09	-	0.3 (M <sub>L</sub> )	11.5	TLUBN 2020
2016	51,04; 12,02	-	0.7 (M <sub>L</sub> )	13.4	TLUBN 2020
2020	50,98; 12,00	-	1.1 (M <sub>L</sub> )	18.3	TLUBN 2020

### The structural style of the RLR fault system

The RLR fault system is regarded as a deep-seated system of faults (e.g., Behr et al. 2002; Korn et al. 2008). According to Bankwitz et al. (2003a), the RLR fault system is interpreted as a horizontal shear zone. The term shear zone was adopted in some publications (e.g., Schneider 2004; Meschede 2015).

In the international literature the term shear zone is used for a wide zone of deformation dominated by simple shear that is present when a discrete fault passes the brittle-ductile transition (Vauchez et al. 2012; Brandes and Tanner 2020). Shear zones are less commonly exposed at the Earth's surface, because they generally form in the ductile mid-to-lower crust (Wrona et al. 2020). Therefore, it is questionable if the RLR fault system is a shear zone in the proper sense or if it more likely represents an array of strike-slip faults (e.g., Krentz and Witthauer 2000; Forkmann et al. 2002), which might pass downwards into a deep vertical shear zone.

An important question is whether there are deep-seated N-S trending faults in the northern study area around Leipzig. The surface conditions in the northern part make the detection of small earthquakes difficult (Buchholz et al. 2011). Many small earthquakes that might be located at greater depth are not registered. Švancara et al. (2008) questioned that the RLR system is a deep-seated system of faults. Bram and Hirschmann (1992) discussed the occurrence of N-S trending structures not only in the deep crust but show that N-S trending structures also occur in the near surface. The absence of geological evidence makes this questionable.

The results of the palaeoseismological analysis in the area around the RLR fault system indicate neotectonic activity that can be related to approximately NW-SE, NE-SW and NNW-SSE striking faults. The occurrence of major N-S trending structures in the northern section around the city of Leipzig cannot be verified by our analyses, because there are no new geological indicators for those structures. The N-S striking faults only imply a minor neotectonic activity. However, the results indicate that intersecting faults may play a major role in triggering earthquakes in this area.

### **Age of the RLR fault system**

The age of the RLR fault system is a key question for understanding its evolution. Knowledge about the timing of fault activity can help to better understand the geodynamic drivers for the development of the fault system and is important for estimating the recurrence of fault activity. According to Grünthal et al. (2009a) the Leipzig-Regensburg Zone might represent a failed rift system.

Nickschick (2017) analysed the palaeo-volcanic situation along the RLR fault system. The Delitzsch complex (Delitzsch-Bitterfeld volcanic field) is the northernmost volcanic field with ultramafic rocks in the NW of Leipzig (Fig. 2) (Seifert et al. 2000). The dolomite-carbonatite diatremes Serbitz and Storkwitz are located nearby (Seifert et al. 2000; Nickschick et al. 2014; Nickschick 2017). In the area of Werdau, which is the northernmost location of earthquake swarms, a second volcanic field is marked by the Weißenbrunn diatreme, Ebersbrunn diatreme and a potential diatreme near Waldhaus-Greiz, the so-called 'Triasscholle' that is located in the intersection zone of the RLR fault system and the FGJ fault system (Schmidt et al. 2013; Nickschick 2017). These diatremes are assumed to be Tertiary or Cretaceous in age (Seifert et al. 2000; Schmidt et al. 2013; Nickschick 2017). A third volcanic field is the Vogtland volcanic field that is Oligocene to Miocene in age (Nickschick 2017). In the study area, the southernmost volcanic field is located in the area where the Eger Rift intersects with the RLR fault system. Several Cenozoic diatremes, maar structures and scoria cones occur (Mrlina et al. 2007, 2009; Rohrmüller et al. 2017). This time shift from Cretaceous volcanic activity in the north of the RLR fault system to Oligocene and Miocene activity in the Vogtland area and finally to Cenozoic volcanic activity in the southernmost study area points to a repeated magmatic activity (Nickschick 2017). Thus, the N-S striking zone of crustal weakness may likely be older than the Cretaceous.

The Roter Kamm Fault as part of the Gera-Jáchymov Fault evolved during the Variscan Orogeny (Berger et al. 2011) and matches to the NNW-SSE striking Elbe Fault system that originated from late Variscan wrench movements (Scheck et al. 2002). This shows that many of the NW-SE oriented faults are potentially Late Palaeozoic in age and underwent a reactivation during the Mesozoic (Kley et al. 2008). The N-S structures are also interpreted to be related to the Variscan Orogeny (Meschede 2015). Therefore, both elements, the N-S and the NW-SE structures, likely evolved in Palaeozoic times and their reactivation potential in younger periods of the Earth

history depends on the regional stress field. Thus, the RLR fault system is prone to future activity under the current stress field.

### **Seismotectonic zones**

Grünthal et al. (2009a) divides the study area into three seismic regions based on their tectonic characteristics and independent from spatial distribution of seismicity: the Vogtland Leipzig Zone, the Saxonian Block, and the Eger Graben. They analysed the overall tectonic regime in these areas and concluded that strike-slip faulting is the dominating kinematic followed by normal faulting (Grünthal et al. 2009a). Later they added the Vogtland Cheb Basin as a magmatic terrane (Grünthal et al. 2016).

The nature of seismicity in the study area changes along the RLR fault system from swarm earthquakes in the south (Cheb) to deep single earthquakes in the north (Leipzig) (Leydecker 2011; Fischer et al. 2014; Dahm et al. 2018; Sonnabend 2019). The increase of focal depth, seismic energy release and the magnitudes of earthquakes towards the northern part (e.g., Korn et al. 2008; Dahm et al. 2018) and decrease in the southern part of the RLR fault system (Vogtland/NW Bohemia, Nový Kostel) (e.g., Fischer et al. 2014), implies clear spatial differences in the seismotectonic regime of these areas.

These differences likely reflect lateral variations in the seismogenic rupture processes driven by different earthquake trigger mechanisms, the different crustal structures of the central European Variscides (e.g., Franke 2000) and crustal conditions (e.g., material properties, stress state and fluid pressure).

Also, based on the number of extracted lineaments along the RLR fault system in the study area, the RLR fault system can be separated in two zones. In the northern section from Leipzig to Zwickau the number of lineaments decreased in comparison to the southern section from Zwickau to Cheb. This might be caused by thick Cenozoic cover beds in the northern section and the presence of bedrock at the Earth's surface in the southern section of the RLR fault system. However, no N-S trending lineaments were extracted in the northern and also in the southern section of the RLR fault system in the studied area (Fig 4).

Therefore, based on the current dataset, the RLR fault system in the study area can be separated in two seismotectonic zones: a northern zone from Leipzig to Zwickau, and a southern zone from Zwickau to Cheb.

### **Earthquake trigger mechanisms in the two seismotectonic zones of the RLR fault system**

In contrast to the earthquake swarms in the Vogtland and NW Bohemia, the earthquakes located in the area around Halle, Leipzig, Dresden, and Gera occur almost always as single events (Neunhöfer et al. 1996; Buchholz et al. 2016; Dahm et al. 2018) and thus may have different trigger mechanisms than the earthquake swarms. Korn et al. (2008) discussed different trigger mechanisms of the earthquakes in the northern and southern part of the study area. They suggested that the deeper earthquakes in the north near Leipzig are caused by tectonic movements along deep reaching faults of the RLR fault system, whereas earthquakes at shallower depth, like in the southern part Vogtland up to Cheb are controlled by fault intersections. These observations and interpretations require a more detailed analysis of the earthquakes along the



RLR fault system, to derive their potential trigger mechanism. The trigger mechanisms of earthquakes in this area are diverse and not conclusively clarified.

### ***Glacial isostatic adjustment (GIA) and glacial lake formation/drainage as potential trigger for seismic activity***

Lithospheric stress field changes can be controlled by loading and unloading applied to the Earth's surface (Nakiboglu and Lambeck 1982; Peltier et al. 2002). This has a fundamental effect on the rate of strain accumulation on normal faults (Hetzl and Hampel 2005). Ice sheet loading and unloading as well as (glacial) lake formation and drainage changes the lithospheric stress field (Hampel et al. 2010) and are possible triggers for fault activity.

The northern part of the study area was repeatedly covered by large ice-dammed lakes during the Middle Pleistocene (Eissmann, 2002; Lang et al. 2018) (Fig. 1c-d). In the Halle Leipzig lowland area, the Halle-Leipzig Lake formed. The reconstructed lake level highstand of  $\geq 190$  m a.s.l. was reached during the maximum ice advance (Lang et al. 2018) (Fig. 1c). Delta deposits in the area of Döbeln at an altitude of 227 m a.s.l. indicate a lake level of up to 230 m a.s.l. Catastrophic lake drainage due to the opening of lake overflows may have led to a reactivation of pre-existing faults controlled by variations in water load and water pressure (e.g., Brandes et al. 2011; Winsemann et al. 2011). Lithospheric rebound effects after lake drainage and deglaciation can probably lead to a stress field change and thus reactivate locked faults (cf. Hetzel and Hampel 2005; Hampel et al. 2010). Glacial lake formation and subsequent catastrophic drainage may therefore have led to partial loading/unloading stresses on the footwall of the Lusatian Thrust, which could have caused a reactivation of this fault.

In northern Germany, WNW-ESE trending faults run almost parallel to the margin of the former Fennoscandian ice sheets and thus have a high GIA induced reactivation potential, because in such a case the GIA induced stress-field matches with the palaeo-stress field under which the faults formed (Brandes et al. 2015).

In the study area, several WNW-ESE and NW-SE trending faults occur that partly have a high reactivation potential due to GIA. The Middle Pleistocene Elsterian and Saalian ice advances reached the northern part of the RLR fault system (Eissmann 2002) and the Elsterian ice sheet had a thickness of more than 400 m in the Lusatian area (Lange et al. 2009). DEM-based geomorphic analyses show an incision of rivers at the eastern tip of the Ore Mountains, which is related to recent topographic uplift along the Lusatian Thrust (Andreani et al. 2014). According to the world stress map that shows a NW-SE oriented stress field (Heidbach et al. 2016) and focal mechanisms that point to NW-SE compression and NE-SW extension in the study area (e.g., Fischer et al. 2014), reverse fault movements along the Lusatian Thrust are unlikely and the observed uplift (Bankwitz 1968; Andreani et al. 2014) may have different causes. Some studies (e.g., Stackebrandt 2008; Coubal et al. 2015) interpreted Pleistocene uplift processes in the Lusatian area as a result of glacial rebound. This points to GIA-related processes that might act as potential driver for the seismic activity in the study area. Modelling results of Coulomb-failure stress variations for the Late Pleistocene Weichselian ice sheet imply an influence of GIA as far south as the Thuringian Forest, (Brandes et al. 2015). However, modelling results of Coulomb-failure stress variations do not exist for the Middle Pleistocene glaciations, which extended further southwards. Therefore, GIA processes induced by the Late Pleistocene Weichselian ice sheet most probably only play a minor role in triggering earthquakes and fault movements in the southern part of the study area. It remains to be analysed and discussed whether GIA effects in the northern part can be the trigger for deep earthquakes in the area around Leipzig. Earthquakes in northern

Germany that may have been triggered by GIA, occurred as single event without significant aftershocks (e.g., Brandes et al. 2019), similar to those in the northern part of the study area near Leipzig (e.g., Buchholz et al. 2016; Dahm et al. 2018). In the southern part of the study area in the Vogtland, swarm-like earthquakes are frequent and GIA processes related to the Weichselian glaciations that far south are rather unlikely (Brandes et al. 2015).

### ***Distribution of seismicity along the RLR fault system controlled by fault intersections***

Even though the RLR fault system was interpreted as an active sinistral shear zone (Bankwitz et al. 2003a) the postulated northern lineaments, which are not geologically mapped until now, behave overall rather passively without measurable activity (Hemmann 2002). The earthquake activity is accumulated within the N-S trending RLR fault system which is intersected by major faults and fault systems like the Marienbader Fault, faults of the Eger Rift, the BK fault system, the FGJ fault system and the Halle Fault. These intersecting faults are characteristic for the study area (Fig. 2). Kracke et al. (2000) analysed the seismic energy release of historic earthquakes in the study area. They used the earthquake catalogue of Neunhöfer (1998) and Leydecker (1999) and the catalogue of Grünthal et al. (1998b). The highest seismic energy release was estimated for NW Bohemia where faults intersect and the area of Gera, where the Finne-Gera-Jáchymov fault system intersects with the RLR fault system. The seismic energy release of earthquakes in the north around Leipzig is higher than the seismic energy release of the swarm earthquakes in the Vogtland area, but the highest seismic energy is released in NW-Bohemia (Wendt and Buchholz 2019). Fault intersections are well known to act as stress concentrators that control seismicity in their vicinity (Talwani 1988, 2014). Gravity anomalies in the study area at intersecting faults and plutons show the pre-existing zones of weakness very well (Švancara et al. 2008). The intersection model of Talwani (1988) states that the mainshock of intersection-related earthquakes occurs away from the intersection points, and intense seismicity is commonly accompanied by uplift that occurs near the intersecting faults. An optimal location of stress accumulation are faults that are oriented  $45^\circ \pm 15^\circ$  relative to  $S_{Hmax}$  and faults that intersect at angles of  $90^\circ \pm 35^\circ$  (Gangopadhyay and Talwani 2007). In this area we assumed an NW-SE oriented  $S_{Hmax}$  (Heidbach et al. 2016) and thus optimal oriented faults for stress accumulation that trend  $\sim$ N-S and WNW-ESE.

Many earthquakes in the study area are located in areas where faults intersect. This can be clearly derived from the combination of the geological and seismological map of Saxony (cf. Leonhardt 1995; Wendt et al. 1996). The prominent Mid-German Earthquake that occurred 1872 close to Gera had a magnitude of  $M_w$  5.2. The 1993 earthquake with a magnitude of  $M_L$  2.55 were located at the intersection of the Finne-Gera-Jáchymov fault system and the RLR fault system. Two more recent earthquake swarms (in 1997/98 and 2006) also occurred in this area (Skamletz et al. 2000, Hemmann et al. 2003; Korn et al. 2008). Further south of the RLR fault system, in the area south of Plauen, a large number of NW-SE oriented faults are mapped that cross the N-S trending zone (Fig. 2). In this area many swarm-like earthquakes occurred in the past (e.g., Klinge and Plenefisch 2001; Dahm et al. 2013; Fischer et al. 2014; Čermáková and Horálek 2015). Triggers for these earthquake swarms are in discussion. A key controlling factor is most likely fluid migration in the crust (e.g., Špičák et al. 1999; Bräuer et al. 2009). At fault intersections, a higher fracture density (Talwani 1988 and references therein) can cause enhanced fluid flow with increased fluid pressure that leads to lower normal stress and subsequent higher seismic activity. Increased fluid-flow at intersecting faults and resulting earthquake swarm activity is also mentioned by Hemmann (2002). Evidence of neotectonic activity can also be observed at intersection points of fault systems (Fig. 2). An example for a linkage of fault intersections and the concentration of

seismic activity can be found at the Lusatian Thrust. The Lusatian Thrust is intersected by the seismically active Borsberg Fault and a second parallel fault (Hoyerswerder Fault). The Hoyerswerder Fault indicates a significant neotectonic activity. Similar observations were made at different locations, like the western Swabian Alb where ENE-WSW and NW-SE trending fault zone intersections control the location of Miocene volcanic centres (Reicherter et al. 2008).

Applying the model of Gangopadhyay and Talwani (2007), the faults of the study area have an optimal orientation for stress accumulation. In the vicinity of these intersections, historic and recent seismicity was detected (Fig. 2). The observed deformation bands provide information about neotectonic activity at the prominent fault intersection points.

Grünthal et al. (1990) deliver a seismotectonic model of fault intersections for the strong earthquake swarm ( $M_L$  4.6) in 1985/86, which was located in the area of Nový Kostel. According to Grünthal et al. (1990), the Marienbader Fault only provides a location (zone of weakness) for the foci, but the faulting process mainly occurred on secondary faults in this area. The Marienbader Fault shows a splay-like fault that is crossed by a bundle of N-S directed faults that Grünthal et al. (1990) called 'lamellar fault splits', where strain can accumulate.

### ***Fluid emanations and magmatic activity***

Trigger mechanisms for earthquake swarms in the Vogtland and NW Bohemia are still in debate, including e.g., hydraulically induced pore pressure perturbations (Heinicke et al. 2018) or intruding fluids and gases related to magmatic activity (e.g., Špičák et al. 1999; Bräuer et al. 2009; Fischer et al. 2014). According to Neunhöfer and Meier (2004), earthquake swarms may be triggered by fluids at deep reaching faults, which increase the Coulomb failure stress. The general assumption is that earthquake swarms are driven by fluid migration in the crust. Seismic rupture processes are triggered by fluid migration and overall are controlled by the regional stress field. At the intersection of the Eger Rift and the RLR fault system the crustal thickness decreases to 26-27 km from  $\sim$  31 km in the surroundings, and a local updoming of the Mohorovičić discontinuity was observed (Geissler 2005; Geissler et al. 2005; Heuer et al. 2006). The updoming of the Mohorovičić discontinuity matches with locations of carbon dioxide emanation and the occurrence of four Quaternary volcanoes (Mrlina et al. 2007, 2009; Rohrmüller et al. 2017). The combination of seismic and isotopic studies in this area point to local-scale magmatic emplacement (magmatic underplating) at the base of the continental crust beneath the Cheb Basin (Hrubcová et al. 2017), which might be the cause for the high carbon dioxide emanation in this area (Heuer et al. 2006).

In the Vogtland/NW-Bohemian region there is a higher fluid flow in the crust due to magmatic processes (Bräuer et al. 2008). The lack of an enhanced crustal fluid flow in the northern section of the RLR fault system, increases the locking along the fault planes. Thus, earthquake swarms in the northern part of the study area are uncommon.

### **Increasing hypocentre depths towards the north of the RLR fault system**

The available earthquake data of the RLR fault system in the study area point to deep-seated earthquakes rather than shallower events (e.g., Korn et al. 2008). Thus, for the re-evaluation of the seismotectonic situation an inside into the deep seismogenic zone is important. Frictional deformation mechanisms dominate the upper part of the crust, where most of the seismicity nucleates (cf. Scholz 1988, 2002). The deformation behaviour is strongly controlled by the strain

rate, temperature and rock type, which means that brittle deformation can even occur at great depths (e.g., Chen and Molnar 1983; Frost et al. 2011).

In the northern part of the RLR fault system, a lower heat flow than in the southern part of the RLR fault system is observed, which may lead to an increase of the brittle-ductile transition towards the south, leading to the southward-decrease in hypocentre depths (e.g., Förster and Förster 2000). The northernmost earthquakes in 2015 and 2017 occurred close to the Mohorovičić discontinuity of depth of 31 km (Dahm et al. 2018), like deep-seated earthquakes observed in northern Germany (Brandes et al. 2019). In the southern section of the RLR fault system, at the intersection with the Eger Rift, an updoming of the Mohorovičić discontinuity was observed (Geissler 2005; Geissler et al. 2005; Heuer et al. 2006) responsible for the depth decrease of the seismogenic brittle zone in this area. The lower crust of NW Bohemia and the Vogtland shows increased seismic reflectivity (Behr et al. 1994; Geissler et al. 2005 and references therein). Geissler et al. (2005) interpreted the increased seismic reflectivity as low-angle shear zones that are partly filled with fluids, magmatic intrusions, or partial melting.

## Conclusions

The RLR fault system, especially in the study area, is a complex structural feature that shows significant along-strike variations. Recent earthquake cluster can be observed in this N-S trending zone, whereas epicentre locations of historic earthquakes are distributed over the entire study area, and do not follow the pronounced N-S zone.

Recent earthquake activity is not exclusively related to the N-S trending RLR fault system, but also occurs at the intersection of major faults and fault systems like the Marienbader Fault, the faults of the Eger Rift, the BK fault system, the FGJ fault system, the Halle Fault system and the Lusatian Thrust.

Geological maps and focal mechanisms point to N-S trending faults in the southern part. They verify the occurrence of rather deep faults. However, in the northern part (north of Plauen) no geological evidence for the occurrence of N-S trending structures could be observed. Furthermore, no focal mechanisms verify the presence of this postulated N-S trending structures and lineament analyses does not allow to verify these faults, because of the Cenozoic cover beds.

Based on the characteristics of the earthquakes, the RLR fault system can be separated into two seismotectonic zones. The northern zone (area of Leipzig – Zwickau) shows rare single earthquakes at greater depth and the southern zone (area of Zwickau – Cheb) with frequent earthquake swarms at shallower depth. These differences are likely caused by the lithospheric fluid flow and temperature distribution. In the southern zone, an updoming of the Mohorovičić discontinuity leads to fluid migrations, a shift of the brittle-ductile transition into shallower depth, and a reduced locking of faults. This is also visible in the seismic energy that is released during earthquakes.

Seismic energy release of earthquakes in the north (Leipzig) is higher than the energy release of the earthquakes that occur in swarms in the Vogtland area. Furthermore, fault creep is observed especially in the northern zone of the study area. Creep processes along many faults may reduce seismic activity along these faults. Our evidence for neotectonic activity supports the previous assumption of active faults in this area.

Important controlling factors for the distribution of the seismicity are fault intersections. At intersecting faults, stress concentrations occur, which lead to earthquakes. Focal mechanisms in the north (Leipzig) show a clear correlation to NW-SE striking intersecting faults and in the south

(Vogtland/Cheb) also to N-S striking faults. Evidence of neotectonic activity was observed in the vicinity of intersecting faults.

Deformation bands as indicators for neotectonic activity are exposed in several sand and gravel pits close to approximately NW-SE, NNW-SSE and NE-SW oriented basement faults that intersect with the RLR fault system or smaller faults in the vicinity of it.

The neotectonic activity is very likely related to these basement faults. This points to fault movements in post-Palaeogene and Pleistocene to post-Pleistocene times. The N-S striking faults only show a minor neotectonic activity.

Many earthquake swarms in the southern section (south of Plauen) can also be correlated with intersection points of N-S, NW-SE and NNW-SSE oriented faults, which underlines their importance.

The accumulation of seismicity in the N-S trending zone is obvious and NW-SE oriented faults are major faults in the study area. Our analysis points out that the strain rates in this intracontinental area are too low to show lineaments in areas with a high cover of unconsolidated sediments. The results of the palaeoseismological analysis show the importance of fault intersections for the distribution of intraplate seismicity. We postulate that N-S trending structures also occur in the area around Leipzig but they might act rather passive and NW-SE crossing faults and fault systems are the seismically active or at least creeping major faults and that activity concentrates at intersection points.

Different triggers can be assumed for the earthquakes along the RLR fault system such as fluid and gas flow in the south and probably processes related to GIA and/or glacial lake formation in the north. These different trigger mechanisms and the difference of the Mohorovičić discontinuity depth (updoming of the Mohorovičić discontinuity in the south and deeper flat the Mohorovičić discontinuity in the north) are likely the controlling factors for the contrasting seismic characteristics (shallow seismicity and earthquake swarms in the south compared to deep single events in the north).

The northern part of the study area shares more characteristics with northern Germany that shows deep earthquakes, neotectonic activity at NW-SE oriented faults, whereas the southern part of the study area, with shallow earthquakes, is influenced by the magmatic activity of the region.

## **Acknowledgements**

We thank Runa Fälber for supporting the fieldwork campaign and the lineament analysis, Prof. Dr. J. Müller for discussion and Dr. Yvonne Therese Spychala for editing the text. The owners of the sand and gravel pits are thanked for the permission to work on their properties. The hill-shaded relief maps were produced using Copernicus data and information funded by the European Union (EU-DEM layers). The *'Staatsbetrieb Geobasisinformation und Vermessung Sachsen'* kindly provided the 5-m digital elevation model of the Saxony portion of the Lusatian Thrust (Elbe Zone) (GeoSN, dl-de/by-2.0 2019). Financial support by Bundesanstalt für Geowissenschaften und Rohstoffe (BGR No. 200-4500117863) is highly appreciated.

## References

- Abdullah A, Akhir JM, Abdullah I (2010) Automatic mapping of lineaments using shaded relief images derived from digital elevation model (DEMs) in the Maran - Sungai Lembing area, Malaysia. *Electron J Geotech Eng* 15:949-958
- Alexowsky W, Schneider JW, Tröger KA, Wolf L, Hoffmann U, Horna F, Huhle K, Kardel K, Kulikov S, Lapp K, Palme G, Pohlenz R, Schauer M, Symmangk R, Voigt S, Witthauer B (2001) Geologische Karte des Freistaates Sachsen 1:25 000, Blatt 4948 Dresden, 4 Edition, Sächsisches Landesamt für Umwelt, Landwirtschaft und Geologie, Freiberg
- Andreani L, Stanek KP, Gloaguen R, Krentz O, Domínguez-González L (2014) DEM-based analysis of interactions between tectonics and landscapes in the Ore Mountains and Eger Rift (East Germany and NW Czech Republic). *Remote Sens* 6:7971-8001,
- Babuška V, Plomerová J, Fischer T (2007) Intraplate seismicity in the western Bohemian Massif (central Europe): a possible correlation with a paleoplate junction. *J Geodyn* 44:149-159, <https://doi.org/10.1016/j.jog.2007.02.004>
- Babuška V, Plomerová J (2008) Control of paths of quaternary volcanic products in western Bohemian Massif by rejuvenated Variscan triple junction of ancient microplates. *Studia Geophys et Geod* 52:607-630, <https://doi.org/10.1007/s11200-008-0040-0>
- Bankwitz P (1968) Stellungnahme zu rezenten horizontalen Krustenbewegungen und zur Geologie in einem Abschnitt der Elbelinie. *Geod Geophys Veröff R III* 11:27-59
- Bankwitz P (1971) Geologische Auswertung von geodätisch ermittelten rezenten Krustenbewegungen im Gebiet der DDR. *Petermanns Geogr Mitt* 115:130-140
- Bankwitz P (1977) Rezente Bewegungen im Südteil der DDR und ihre Beziehungen zu geologischen Vorgängen. Bratislava
- Bankwitz P, Bankwitz E (1991) Tektonische Aspekte der Erdkrustenentwicklung im Raum Erzgebirge-Vogtland. In: Kurzfassungen der Vorträge und Poster, Geologisch-Tektonischer Bau der Gera-Jáchymov Störungzone und die daran gebundenen Uranlagerstätten, Stratigraphie, Tektonik, Metallogenie, Umweltengineering. Gera/Thüringen. Kurzfassungen der Vorträge und Poster, p 1
- Bankwitz P, Bankwitz E, Gottesmann B, Kämpf H, Kramer W, Wasternack J (1991) Struktur- und regionalgeologisches E-W-Profil im Gebiet Westerzgebirge-Vogtland. In: Bankwitz P (ed) *Exkursionsführer*, pp 31-53
- Bankwitz P, Grossand U, Bankwitz E (1993) Krustendeformation im Bereich der Finne-Kyffhäuser-Gera-Jáchymov-Zone. *Z Geol Wiss* 21:3-20
- Bankwitz P, Bankwitz E, Franzke H-J, Rauche H (1995) In-situ Spannungsermittlung in Thüringen und Sachsen. DFG-Ergebnisbericht Teil II, Geoforschungszentrum Potsdam, p 31, <https://doi.org/10.2312/GFZ.b103-95040>
- Bankwitz P, Wetzel HU, Kämpf H (1998) Fototektonische Interpretation des Schwarmbeben- und Quellengebietes am NW-Rand des Böhmisches Massivs. *Publ Deutsch Ges Photogrammetrie und Fernerkundung* 6:95-102
- Bankwitz P, Schneider G, Kämpf H, Bankwitz E (2003a) Structural characteristics of epicentral areas in Central Europe: study case Cheb Basin (Czech Republic). *J Geodyn* 35:5-32, [https://doi.org/10.1016/S0264-3707\(02\)00051-0](https://doi.org/10.1016/S0264-3707(02)00051-0)
- Bankwitz P, Bankwitz E, Bräuer K, Kämpf H, Störr M (2003b) Deformation structures in Plio- and Pleistocene sediments (NW Bohemia, Central Europe). In: Van Rensberger P, Hillis RR, Maltman AJ, Morley CK (eds) *Subsurface Sediment Mobilization*. *Geol Soc Lond Spec Publ* 216:73-93, <https://doi.org/10.1144/GSL.SP.2003.216.01.06>
- Behr HJ, Dorbaum H-J, Bankwitz P (1994) Crustal structure of the Saxothuringian Zone: Results of the deep seismic profile MVE-90 (East). *Z Geol Wiss* 22:647-769
- Behr HJ, Conrad W, Muller A, Trzebski R (2002) Compilation, Linsser filtering and interpretation of the gravity map of Germany and adjacent regions at a scale of 1: 1,000,000. *Z Geol Wiss* 30:385-402
- Berger HJ, Felix M, Görne S, Koch E, Krentz E, Förster A, Förster HJ, Konietzky H, Lunow C, Walter K, Schütz H, Stanek K, Wagner S (2011) Tiefengeothermie Sachsen. Landesamt für Umwelt,

- Landwirtschaft und Geologie, Dresden, 9:108, <https://nbn-resolving.org/urn:nbn:de:bsz:14-qucosa-68815>
- Bram K, Hirschmann G (1992) Ergebnisse geowissenschaftlicher Umfelduntersuchungen - KTB Report 92-3, Schweizerbartsche Vertragsbuchhandlung, Hannover, p 260, <https://doi.org/10.2312/ktb.92-3>
- Brandes C, Polom U, Winsemann J (2011) Reactivation of basement faults: interplay of ice-sheet advance, glacial lake formation and sediment loading. *Basin Res* 23:53-64,
- Brandes C, Winsemann J, Roskosch J, Meinsen J, Tsukamoto S, Frechen M, Tanner DC, Steffen H, Wu P (2012) Activity along the Osning Thrust in Central Europe during the Late glacial: ice-sheet and lithosphere interactions. *Quat Sci Rev* 38:49-62,
- Brandes C, Tanner DC (2012) Three-dimensional geometry and fabric of shear deformation-bands in unconsolidated Pleistocene sediments. *Tectonophysics* 518:84-92
- Brandes C, Winsemann J (2013) Soft sediment deformation structures in NW Germany caused by Late Pleistocene seismicity. *Int J Earth Sci* 102:2255-2274
- Brandes C, Steffen H, Steffen R, Wu P (2015) Intraplate seismicity in northern Central Europe is induced by the last glaciation. *Geology* 43:611-614, <https://doi.org/10.1130/G36710.1>
- Brandes C, Igel J, Loewer M, Tanner DC, Lang J, Müller K, Winsemann J (2018a) Visualisation and analysis of shear-deformation bands in unconsolidated Pleistocene sand using ground-penetrating radar: Implications for paleoseismological studies. *Sediment Geol* 367:35-145, <https://doi.org/10.1016/j.sedgeo.2018.02.005>
- Brandes C, Steffen H, Sandersen PB, Wu P, Winsemann J (2018b) Glacially induced faulting along the NW segment of the Sorgenfrei-Tornquist Zone, northern Denmark: Implications for neotectonics and Lateglacial fault-bound basin formation. *Quat Sci Rev* 189:149-168, <https://doi.org/10.1016/j.quascirev.2018.03.036>
- Brandes C, Plenefisch T, Tanner DC, Gestermann N, Steffen H (2019) Evaluation of deep crustal earthquakes in northern Germany–Possible tectonic causes. *Terra Nova* 31:83-93, <https://doi.org/10.1111/ter.12372>
- Brandes C, Tanner DC (2020) Fault mechanics and earthquakes. In: Tanner DC, Brandes C (eds) *Understanding Faults - Detection, Dating and Modeling*. Elsevier, Amsterdam, pp 11-80, <https://doi.org/10.1016/B978-0-12-815985-9.00002-3>
- Bräuer K, Kämpf H, Niedermann S, Strauch G, Tesar J (2008) Natural laboratory NW Bohemia: Comprehensive fluid studies between 1992 and 2005 used to trace geodynamic processes. *Geochem Geophys Geosy* 9:Q04018, <https://doi.org/10.1029/2007GC001921>
- Bräuer K, Kämpf H, Strauch G (2009) Earthquake swarms in non-volcanic regions: What fluids have to say. *Geophys Res Lett* 36:L17309, doi:10.1029/2009GL039615
- Buchholz P, Wendt S, Mittag R, Novak E, Burghardt T, Rappsilber I, Witthauer B (2011) Seismische Aktivität in Sachsen und angrenzenden Gebieten. In: Autorenkollektiv (eds) *Erdbebenbeobachtung im Freistaat Sachsen - Dreijahresbericht 2007-2009*. Sächsisches Landesamt für Umwelt und Geologie, Dresden, pp 4-21, <https://publikationen.sachsen.de/bdb/artikel/11958>
- Buchholz P, Funke S, Korn M, Wendt S, Hänel F, Mittag R, Novak E, Rappsilber I, Burghardt T, Burghardt T, Schönwald D, Pustal J, Koch U, Krentz O, Witthauer B (2013) *Erdbebenbeobachtung im Freistaat Sachsen - Dreijahresbericht 2010-2012*. Sächsisches Landesamt für Umwelt und Geologie, Dresden, p 48, <https://publikationen.sachsen.de/bdb/artikel/21134>
- Buchholz P, Funke S, Wendt S, Hänel F, Mittag R, Novak E, Rappsilber I, Burghardt T, Schönwald D, Pustal I, Busch P, Eberlein L, Horwath M, Schröder L, Krentz O, Witthauer B (2016) *Erdbebenbeobachtung in Mitteldeutschland. Dreijahresbericht 2013-2015*. Landesamt für Umwelt, Landwirtschaft und Geologie, Dresden, p 60, <https://publikationen.sachsen.de/bdb/artikel/28150>
- Burbank DW, Anderson R (2001) Holocene Deformation and Landscape Response. In: Burbank DW, Anderson R (eds) *Tectonic Geomorphology*, Blackwell, Oxford, pp 159-174
- Canny J (1986) A computational approach to edge detection. *IEEE Trans Pattern Anal Mach Intell* 6:679-698, 10.1109/TPAMI.1986.4767851



- Cashman SM, Baldwin JN, Cashman KV, Swanson K, Crawford R (2007) Microstructures developed by coseismic and aseismic faulting in near-surface sediments, San Andreas fault, California. *Geology* 35:611-614, <https://doi.org/10.1130/G23545A.1>
- Čermáková H, Horálek J (2015) The 2011 West Bohemia (Central Europe) earthquake swarm compared with the previous swarms of 2000 and 2008. *J Seismol* 19:899-913, <https://doi.org/10.1007/s10950-015-9502-3>
- Chen WP, Molnar P (1983) Focal depths of intracontinental and intraplate earthquakes and their implications for the thermal and mechanical properties of the lithosphere. *J Geophys Res* 88:4183-4214, <https://doi.org/10.1029/JB088iB05p04183>
- Chester FM, Logan JM (1986) Implications for mechanical properties of brittle faults from observations of the Punchbowl fault zone, California. *Pure Appl Geophys* 124:79-106
- Coubal M, Adamovic J, Malek J, Prouza V (2014) Architecture of thrust faults with alongstrike variations in fault-plane dip: anatomy of the Lusatian Fault, Bohemian Massif. *J Geosci* 59:183-208, doi: 10.3190/jgeosci.174
- Coubal M, Málek J, Adamovič J, Štěpančíková P (2015) Late Cretaceous and Cenozoic dynamics of the Bohemian Massif inferred from the paleostress history of the Lusatian Fault Belt. *J Geodyn* 87:26-49, <https://doi.org/10.1016/j.jog.2015.02.006>
- Dahm T, Hrubcová P, Fischer T, Horálek J, Korn M, Buske S, Wagner D (2013) Eger Rift ICDP: an observatory for study of non-volcanic, mid-crustal earthquake swarms and accompanying phenomena. *Sci Drill* 16:93-99, doi:10.5194/sd-16-93-2013
- Dahm T, Heimann S, Funke S, Wendt S, Rappsilber I, Bindi D, Plenefisch T, Cotton F (2018) Seismicity in the block mountains between Halle and Leipzig, Central Germany: centroid moment tensors, ground motion simulation, and felt intensities of two  $M \approx 3$  earthquakes in 2015 and 2017. *J of Seismol* 22:985-1003, <https://doi.org/10.1007/s10950-018-9746-9>
- Dahm T, Deng Z (2021) Die ungewöhnliche Intraplattenrotation in Deutschland und ihre mögliche Rolle zur Quantifizierung der seismischen Gefährdungszonen. Tagungsband, *Geophys Ges*, 81 p 288
- Dalmer K, Credner H (1901) Erläuterungen zur geologischen Spezialkarte des Königreichs Sachsen. Blatt 5341 Wilkau-Haßlau. 2 Edition, Königliches Finanzministerium, Leipzig, p 79
- Deng Z, Dahm D (2021) Intraplate deformation from dense GNSS network. Helmholtz-Zentrum Potsdam Deutsches GeoForschungsZentrum (GFZ). Präsentation EGU General Assembly
- Dèzes P, Schmid SM, Ziegler PA. (2004) Evolution of the Cenozoic Rift System: Interaction of the Alpine and Pyrenean orogens with their foreland lithosphere. *Tectonophysics* 389:1-33, <https://doi.org/10.1016/j.tecto.2004.06.011>
- Ehlers J, Grube A, Stephan HJ, Wansa S (2011) Pleistocene glaciations of North Germany – new results. In: Ehlers J, Gibbard PL, Hughes PD (eds) *Quaternary Glaciations: Extent and Chronology - A Closer Look: Developments in Quaternary Science* 15:149-162, <https://doi.org/10.1016/B978-0-444-53447-7.00013-1>
- Eissmann L (1975) Das Quartär der Leipziger Tieflandsbucht und angrenzender Gebiete um Saale und Elbe - Modell einer Landschaftsentwicklung am Rand der europäischen Kontinentalvereisung. *Schriftenr Geol Wiss* 2:1-263
- Eissmann L (1987) Lagerungsstörungen im Lockergebirge. Exogene und endogene Tektonik im Lockergebirge des nördlichen Mitteleuropas. *Geophys Veröff KMU Leipzig* 3:7-77
- Eissmann L (1994) Grundzüge der Quartärgeologie Mitteldeutschlands. *Altenburger Naturwisse Forsch* 7:55-136
- Eissmann L (2002) Quaternary geology of eastern Germany (Saxony, Saxony-Anhalt, south Brandenburg, Thuringia), type area of the Elsterian and Saalian stages in Europe. *Quat Sci Rev* 21:1275-1346, [https://doi.org/10.1016/S0277-3791\(01\)00075-0](https://doi.org/10.1016/S0277-3791(01)00075-0)
- Ellenberg J (1992) Recent fault tectonics and their relations to the seismicity of East Germany. *Tectonophysics* 202:117-121, [https://doi.org/10.1016/0040-1951\(92\)90089-0](https://doi.org/10.1016/0040-1951(92)90089-0)
- Feldmann-Westendorff U, Liebsch G, Sacher M, Müller J, Jahn C-H, Klein W, Liebig A, Westphal K (2016) Das Projekt zur Erneuerung des DHHN: Ein Meilenstein zur Realisierung des integrierten Raumbezugs in Deutschland. In: *Zeitschrift für Geodäsie, Geoinformation und Landmanagement* 141:354–367. DOI: 10.12902/zfv-0140-2016

- Fischer T, Horálek J (2003) Space-time distribution of earthquake swarms in the principal focal zone of the NW Bohemia/Vogtland seismoactive region: period 1985-2001. *J Geodyn* 35:125-144, [https://doi.org/10.1016/S0264-3707\(02\)00058-3](https://doi.org/10.1016/S0264-3707(02)00058-3)
- Fischer T, Horálek J, Hrubcová P, Vavryčuk V, Bräuer K, Kämpf H (2014) Intra-continental earthquake swarms in West-Bohemia and Vogtland: a review. *Tectonophysics* 611:1-27, <https://doi.org/10.1016/j.tecto.2013.11.001>
- Forkmann B, Docekal A, Donner F (2002) Projekt „Seismologisches Monitoring Westsachsen“. In: Witthauer B, Krentz O (eds) *Erdbebenbeobachtung im Freistaat Sachsen Zweijahresbericht 2000–2001*. Sächsisches Landesamt für Umwelt und Geologie, Dresden, pp 14-24
- Förster A, Förster HJ (2000) Crustal composition and mantle heat flow: Implications from surface heat flow and radiogenic heat production in the Variscan Erzgebirge (Germany). *J Geophys Res* 105: 27917-27938, <https://doi.org/10.1029/2000JB900279>
- Franke W (2000) The mid-European segment of the Variscides: tectonostratigraphic units, terrane boundaries and plate tectonic evolution. *Geol Soc Lond Spec Publ* 179:35-61, <https://doi.org/10.1144/GSL.SP.2000.179.01.05>
- Franzke H-J, Voigt T, von Eynatten H, Brix MR, Burmester G (2004). Geometrie und Kinematik der Harznordrandstörung, erläutert an Profilen aus dem Gebiet von Blankenburg. *Geowiss Mitt Thüringen* 11:39-62
- Frost E, Dolan J, Ratschbacher L, Hacker B, Seward G (2011) Direct observation of fault zone structure at the brittle-ductile transition along the Salzach-Ennstal-Mariazell-Puchberg fault system, Austrian Alps. *J Geophys Res* 116:B02411, <https://doi.org/10.1029/2010JB007719>
- Funke S, Hänel F (2019) Seismologische Netze in Mitteldeutschland. In: Autorenkollektiv (eds) *Erdbebenbeobachtung in Mitteldeutschland - Dreijahresbericht 2016-2018*. Landesamt für Umwelt, Landwirtschaft und Geologie, Dresden, pp 29-39, <https://publikationen.sachsen.de/bdb/artikel/28150>
- Gangopadhyay A, Talwani P (2007) Two-dimensional numerical modeling suggests preferred geometry of intersecting faults. In: Stein S, Mazzotti S (eds) *Continental intraplate earthquakes; science, hazard and policy issues*. *Geol Soc Am Spec Pap* 425:87-99; doi:10.1130/2007.2425(07)
- Geissler WH (2005) Seismic and petrological investigations of the lithosphere in the swarm-earthquake and CO<sub>2</sub> Degassing Region Vogtland/NW-Bohemia. Dissertation, GeoForschungsZentrum Potsdam, p 126
- Geissler WH, Kämpf H, Kind R, Bräuer K, Klinge K, Plenefisch T, Horálek J, Zedník J, Nehybka V (2005) Seismic structure and location of a CO<sub>2</sub> source in the upper mantle of the western Eger (Ohře) Rift, central Europe. *Tectonics* 24:TC5001,
- GERSEIS (2020) Geodatendienst für Erdbeben in Deutschland. URL: [https://www.bgr.bund.de/DE/Themen/Erdbeben-Gefahrdungsanalysen/Seismologie/Seismologie/Seis-Online/gerseis\\_node.html](https://www.bgr.bund.de/DE/Themen/Erdbeben-Gefahrdungsanalysen/Seismologie/Seismologie/Seis-Online/gerseis_node.html). Accessed 16 December 2020
- Gläßer W, Hänel M, Hecht G, Hiller W, Katzschmann L, Mädler J, Michel C, Pustal I, Seidel G, Wiefel H (1995) Erläuterungen zur geologischen Karte 1:25000 von Thüringen. Blatt 5040 Altenburg. 2 Edition, Thüringer Landesanstalt für Geologie, Weimar, p 288
- Gläßer W, Wiefel H (1999) Erläuterungen zur geologischen Karte 1:25000 von Thüringen. Blatt 5041 Langenleuba-Niederhain. 2 Edition, Thüringer Landesanstalt für Geologie, Weimar, p 212
- Grohmann CH (2004) Morphometric analysis in Geographic Information Systems: applications of free software GRASS and R. *Comput Geosci* 30:1055-1067
- Grünthal G, Bankwitz P, Bankwitz E, Bednarek J, Guterch B, Schenk V, Schenková Z, Zeman A (1985) Seismicity and geological features of the eastern part of the West European Platform. *Gerlands Beitr Geophys* 94:276-289
- Grünthal G, Schenk V, Zeman A, Schenková Z (1990) Seismotectonic model for the earthquake swarm of 1985–1986 in the Vogtland/West Bohemia focal area. *Tectonophysics* 174:369-383, [https://doi.org/10.1016/0040-1951\(90\)90332-3](https://doi.org/10.1016/0040-1951(90)90332-3)

- Grünthal G (1992) The Central German Earthquake of March 6, 1872. In: Gutdeutsch R, Grünthal G, Musson RMW (eds) *Historical Earthquakes in Central Europe: Monographs 1*, Geologische Bundesanstalt, Hannover 48:51-109
- Grünthal G, Stromeyer D (1994) The recent crustal stress field in Central Europe sensu lato and its quantitative modelling. *Neth J Geosci* 73:173-180
- Grünthal G, Mayer-Rosa D, Lenhardt WA (1998a) Abschätzung der Erdbebengefährdung für die D-A-CH-Staaten-Deutschland, Österreich, Schweiz. *Bautechnik* 75:753-767, <https://doi.org/10.1002/bate.199805380>
- Grünthal G, Musson RMW, Schwarz J, Stucchi M (1998b) European Macroseismic Scale 1998 (EMS-98). *Cahiers du Centre Européen de Géodynamique et de Séismologie* 15. Centre Européen de Géodynamique et de Séismologie, Luxembourg, p 99
- Grünthal G, Bosse C, Stromeyer D (2009a) Die neue Generation der probabilistischen seismischen Gefährdungseinschätzung der Bundesrepublik Deutschland. *Sci Technical Report STR 09/07*. doi:10.2312/GFZ.b103-09076
- Grünthal G, Wahlström R, Stromeyer D (2009b) The unified catalogue of earthquakes in central, northern, and northwestern Europe (CENEC)—updated and expanded to the last millennium. *J Seismol* 13:517-541, <https://doi.org/10.1007/s10950-008-9144-9>
- Grünthal G, Wahlström R (2012) The European-Mediterranean earthquake catalogue (EMEC) for the last millennium. *J Seismol* 16:535-570, <https://doi.org/10.1007/s10950-012-9302-y>
- Grünthal G, Stromeyer D, Bosse C, Cotton F, Bindi D (2018) The probabilistic seismic hazard assessment of Germany-version 2016, considering the range of epistemic uncertainties and aleatory variability. *Bull Earthq Eng* 16:4339-4395, <https://doi.org/10.1007/s10518-018-0315-y>
- Hampel A, Karow T, Maniatis G, Hetzel R (2010) Slip rate variations on faults during glacial loading and post-glacial unloading: implications for the viscosity structure of the lithosphere. *J Geol Soc* 167:385-399
- Hardt J, Lüthgens C, Hebenstreit R, Böse M (2016) Geochronological (OSL) and geomorphological investigations at the presumed Frankfurt ice marginal position in northeast Germany. *Quat Sci Rev* 154:85-99, <https://doi.org/10.1016/j.quascirev.2016.10.015>
- Hardt J, Böse M (2018) The timing of the Weichselian Pomeranian ice marginal position south of the Baltic Sea: a critical review of morphological and geochronological results. *Quat Int* 478:51-58, <https://doi.org/10.1016/j.quaint.2016.07.044>
- Haupt M, Conrad W (1991) Die Störungszone von Gera-Jáchymov aus Sicht der Potentialfelder. In: *Kurzfassungen der Vorträge und Poster, Geologisch-Tektonischer Bau der Gera-Jáchymov Störungszone und die daran gebundenen Uranlagerstätten, Stratigraphie, Tektonik, Metallogenie, Umweltengineering. Gera/Thüringen. Kurzfassungen der Vorträge und Poster*, p 11-12
- Heidbach O, Rajabi M, Reiter K, Ziegler M, WSM Team (2016) World Stress Map Database Release 2016. V. 1.1. GFZ Data Services. <https://doi.org/10.5880/WSM.2016.001>
- Heinicke J, Woith H, Alexandrakis C, Buske S, Telesca L (2018) Can hydroseismicity explain recurring earthquake swarms in NW-Bohemia? *Geophys J Int* 212:211-228, <https://doi.org/10.1093/gji/ggx412>
- Hemmann A (2002) *Relativrelokalisierung von Erdbebenschwärmen in der Saxothüringischen Seismotektonischen Provinz*. Dissertation, Friedrich-Schiller-Universität Jena, p 221
- Hemmann A, Kämpf H (2002) Seismicity in the central part of the Naab-Pritzwalk-Rostock lineament, related to mantle fluid activity? *EGSGA*:5193
- Hemmann A, Meier T, Jentzsch G, Ziegert A (2003) Similarity of waveforms and relative relocalisation of the earthquake swarm 1997/1998 near Werdau. *J Geodyn* 35:191-208, [https://doi.org/10.1016/S0264-3707\(02\)00062-5](https://doi.org/10.1016/S0264-3707(02)00062-5)
- Hetzel R, Hampel A (2005) Slip rate variations on normal faults during glacial–interglacial changes in surface loads. *Nature* 435:81-84, <https://doi.org/10.1038/nature03562>
- Heuer B, Geissler WH, Kind R, Kämpf H (2006) Seismic evidence for asthenospheric updoming beneath the western Bohemian Massif, central Europe. *Geophys Res Lett* 33:L05311, <https://doi.org/10.1029/2005GL025158>

- Hiller A, Schuppan W (2008) Geologie und Uranbergbau im Revier Schlema-Alberoda. Bergbau in Sachsen, Sächsisches Landesamt für Umwelt und Geologie 14, p 171
- Horálek J, Fischer T, Boušková A, Jedlička P (2000) The Western Bohemia/Vogtland region in the light of the WEBNET network. *Studia Geophys et Geod* 44:107-125, <https://doi.org/10.1023/A:1022198406514>
- Hrubcová P, Geissler WH, Bräuer K, Vavryčuk V, Tomek Č, Kämpf H (2017) Active magmatic underplating in western Eger rift, central Europe. *Tectonics* 36:2846-2862, <https://doi.org/10.1002/2017TC004710>
- Ibs-von Seht M, Plenefisch T, Schmedes E (2006) Faulting style and stress field investigations for swarm earthquakes in NE Bavaria/Germany—the transition between Vogtland/NW-Bohemia and the KTB-site. *J Seismol* 10:197-211, <https://doi.org/10.1007/s10950-005-9008-5>
- Ibs-von Seht M, Plenefisch T, Klinge K (2008) Earthquake swarms in continental rifts-A comparison of selected cases in America, Africa and Europe. *Tectonophysics* 452:66-77, <https://doi.org/10.1016/j.tecto.2008.02.008>
- Institute of Geophysics A, O, S, O, T, C, R (1991) West Bohemia Local Seismic Network. International Federation of Digital Seismograph Networks. <https://doi.org/10.7914/SN/WB>
- Jähne-Klingberg F, Stück H, Bebiolka A, Bense F, Stark L (2019) Prognosemöglichkeiten von großräumigen Vertikalbewegungen in Deutschland (9S2018100000). Bundesanstalt für Geowissenschaften und Rohstoffe. Hannover, Oktober 2019. [https://www.bgr.bund.de/DE/Themen/Endlagerung/Projekte/Standortauswahl/abgeschlossen/prognose\\_von\\_hebungen.html](https://www.bgr.bund.de/DE/Themen/Endlagerung/Projekte/Standortauswahl/abgeschlossen/prognose_von_hebungen.html), Accessed 1.06.2021
- Jena FSU (2009) Thüringer Seismologisches Netz (TSN). International Federation of Digital Seismograph Networks. <https://doi.org/10.7914/SN/TH>
- Junge FW (1998) Die Bändertone Mitteldeutschlands und angrenzender Gebiete. *Altenbg Naturwiss Forsch* 9:1-210
- Junge FW, Böttger T, Siegert C (1999) Die Stauseesedimente des Bruckdorfer Horizontes: Ergebnis der Eisrandoszillation des saaleglazialen skandinavischen Inlandeises in Mitteldeutschland. *Mauritiana* 17:257-276
- Kaiser A, Reicherter K, Hübscher C, Gajewski D (2005) Variation of the present-day stress field within the North German Basin - insights from thin shell FE modeling based on residual GPS velocities. *Tectonophysics* 397:55-72, <https://doi.org/10.1016/j.tecto.2004.10.009>
- Kasinski JR (1991) Tertiary lignite-bearing lacustrine facies of the Zittau Basin: Ohre rift system (Poland, Germany and Czechoslovakia). *Spec Publ Int Ass Sediment* 13:93-107, <https://doi.org/10.1002/9781444303919.ch5>
- Kämpf H, Franzke H-J, Neunhöfer H, Märtens P, Röllig G, Schauer M (1991) Zur strukturellen Bedeutung der Nord-Süd-Bruchstörungszone Plauen/Klingenthal - Altenberg/Gera - Leipzig/Halle - Dessau/Bernburg. In: *Geologisch-tektonischer Bau der Gera-Jachymov (Joachimsthal)-Störungszone und die daran gebundenen Uranlagerstätten - Kurzfassungen der Vorträge und Poster*, pp 12-13
- Kämpf H, Bräuer K, Koch H, Malkovský M, Strauch G, Weinlich FH, Weise S (1992) Vulkanismus-Mineralwässer-Seismizität im Bereich der Marienbaden Störungszone. Münchberger Gneismasse und ihr geologischer Rahmen. In: *Exkursionsführer zur 1. Jahrestagung der Gesellschaft für Geowissenschaften e.V. (i.G.), Falkenstein/Vogtland*, pp 129-155
- Käßner A, Stanek KP, Lapp M (2020) Post-Variscan tectonic and landscape evolution of the Elbe Fault Zone and the Lusatian Block based on apatite fission-track data and geomorphologic constraints. *Geomorphology* 355:106860
- Kley J, Franzke HJ, Jähne F, Krawczyk C, Lohr T, Reicherter K, Scheck-Wenderoth M, Sippel J, Tanner D, Van Gent H (2008) Strain and stress. In: Littke R, Bayer U, Gajewski D, Nelskamp S (eds) *Dynamics of complex intracontinental basins: The Central European Basin System*. Springer, Berlin, Heidelberg, pp 97-124
- Kley J, Voigt T (2008) Late Cretaceous intraplate thrusting in central Europe: Effect of Africa-Iberia-Europe convergence, not Alpine collision. *Geology* 36:839-842, <https://doi.org/10.1130/G24930A.1>

- Klinge K, Plenefisch T (2001) Der Erdbebenschwarm 2000 in der Region Vogtland/NW-Böhmen. *Mitt Geophys Ges* 2:11-21
- Klinge K, Plenefisch T, Stammeler K (2003) The earthquake swarm 2000 in the region Vogtland/NW-Bohemia-Earthquake recording at German stations and temporal distribution of events. *J Geod* 35:83-96, [https://doi.org/10.1016/S0264-3707\(02\)00055-8](https://doi.org/10.1016/S0264-3707(02)00055-8)
- Koch E, Geissler E, Eilers H, Fritzsche H (1996) Geologische Karte der eiszeitlich bedeckten Gebiete von Sachsen, 1:50000, Blatt 2465 Bitterfeld, 1 Edition, Sächsisches Landesamt für Umwelt und Geologie, Freiberg
- Kockel F (2003) Inversion structures in Central Europe-Expressions and reasons, an open discussion. *Neth J Geosci* 82:351-366
- Korn M, Funke S, Wendt S (2008) Seismicity and seismotectonics of West Saxony, Germany-new insights from recent seismicity observed with the Saxonian seismic network. *Studia Geophys et Geod* 52:479-492
- Kracke D, Heinrich R, Jentzsch G, Kaiser D (2000) Seismic hazard assessment of the East Thuringian region/Germany-Case study. *Stud Geophys et Geod* 44:537-548, <https://doi.org/10.1023/A:1021815701661>
- Krentz O, Witthauer B (2000) Geodätische Untersuchungen im Vogtländischen Bebengebiet. In: Autorenkollektiv (eds) Erdbebenbeobachtung im Freistaat Sachsen Zweijahresbericht 1998-1999 Sächsisches Landesamt für Umwelt und Geologie, Dresden, p 13-17
- Krentz O (2008) Postvariszische tektonische Entwicklung. In: Pälcher W, Walter H (eds) Geologie von Sachsen - Geologischer Bau und Entwicklungsgeschichte, Schweizenbart, Stuttgart, pp 472-478
- Krentz O, Lapp M, Seibel B, Bahrt W (2010) Bruchtektonik. In: Autorenkollektiv (eds) Die geologische Entwicklung der Lausitz. Vattenfall Europe Mining AG, Cottbus, pp 137-160
- Krentz O, Stanek K (2015) Die Lausitzer Überschiebung zwischen Meißen und Jeschken – neue Aspekte. *Ber Naturforsch Ges Oberlausitz* 23:123-137
- Kroner U, Hahn T, Romer RL, Linnemann U (2007) The Variscan orogeny in the Saxo-Thuringian zone - heterogenous overprint of Cadomian/Paleozoic Peri-Gondwana crust. *Geol Soc Am Spec Pap* 423:153-172, doi: 10.1130.2007.2423(06)
- Lang J, Winsemann J, Steinmetz D, Polom U, Pollok L, Böhner U, Serangeli J, Brandes C, Hampel A, Winghart S (2012) The Pleistocene of Schöningen, Germany: a complex tunnel valley fill revealed from 3D subsurface modelling and shear wave seismics. *Quat Sci Rev* 39:86-105, <https://doi.org/10.1016/j.quascirev.2012.02.009>
- Lang J, Lauer T, Winsemann J (2018) New age constraints for the Saalian glaciation in northern central Europe: Implications for the extent of ice sheets and related proglacial lake systems. *Quat Sci Rev* 180:240-259, <https://doi.org/10.1016/j.quascirev.2017.11.029>
- Lang J, Alho P, Kasvi E, Goseberg N, Winsemann J (2019) Impact of Middle Pleistocene (Saalian) glacial lake-outburst floods on the meltwater-drainage pathways in northern central Europe: Insights from 2D numerical flood simulation. *Quat Sci Rev* 209:82-99, <https://doi.org/10.1016/j.quascirev.2019.02.018>
- Lange JM, Alexowsky W, Horna F (2009) Neogen und Quartär im Elbtal und in der Westlausitz. *GeoDresden2009. Geologie der Böhmisches Masse. Reg Angew Geowiss Mitteleuropa* 161:151-164
- Lange JM, Alexowsky W, Haubold F (2016) Die Entwicklung der Elbe und ihr Einfluss auf die quartäre Landschaftsformung in der Umgebung von Dresden. In: Faust D, Heller K (eds) Erkundungen in Sachsen und Schlesien. Quartäre Sedimente im landschaftsgenetischen Kontext. Exkursionsführer DEUQUA-Tagung Dresden, Geozon Science Media, Berlin, p 13-30
- Lauterbach R (1952) Beiträge zur tektonischen Deutung der geomagnetischen Übersichtskarte der Deutschen Demokratischen Republik. *Wiss Z Karl-Marx-Univ Leipzig*, 3:271-279
- Lauer T, Weiss M (2018) Timing of the Saalian-and Elsterian glacial cycles and the implications for Middle Pleistocene hominin presence in central Europe. *Sci Rep* 8:5111, <https://doi.org/10.1038/s41598-018-23541-w>
- Leipzig University (2001) SXNET Saxon Seismic Network. International Federation of Digital Seismograph Networks. <https://doi.org/10.7914/SN/SX>

- Leonhardt D (1995) Geologische Übersichtskarte des Freistaates Sachsen 1:400 000, Karte ohne Känozoische Sedimente. Sächsisches Landesamt für Umwelt und Geologie, Freiberg
- Leydecker G (1999) Earthquake Catalogue for the Federal Republic of Germany and Adjacent Areas for the Years 800-1994 (for Damaging Earthquakes till 1998). Datafile. Federal Institute for Geosciences and Natural Resources, Hannover
- Leydecker G (2011) Erdbebenkatalog für die Bundesrepublik Deutschland mit Randgebieten für die Jahre 800 bis 2008. *Geol Jb E* 59, pp 1-198
- Lüthgens C, Böse M (2011) Chronology of Weichselian main ice marginal positions in north-eastern Germany. *E & G - Quaternary Sci J* 60:236-247, <https://doi.org/10.3285/eg.60.2-3.02>
- Marotta AM, Bayer U, Scheck M, Thybo H (2001) The stress field below the NE German Basin: effects induced by the Alpine collision. *Geophys J Int* 144:F8-F12, <https://doi.org/10.1046/j.1365-246x.2001.00373.x>
- McCann T (2008) Introduction and overview. In: McCann T (ed) *The Geology of Central Europe. Volume I: Precambrian and Palaeozoic*, The Geological Society, London, pp 1-20
- Meng S, Wansa S (2008) Sedimente und Prozesse am Außenrand der Saale-Vereisung südwestlich Halle (Saale). *Z Dtsch Ges Geowiss* 159:205-220
- Meschede M (2015) *Geologie Deutschlands – Ein prozessorientierter Ansatz*. Springer, Berlin Heidelberg, p 249
- Mittag R (2000) Stationsnetz, Datenerfassung und seismisch aktive Gebiete in Sachsen. In: Autorenkollektiv (eds), *Erdbebenbeobachtung im Freistaat Sachsen Zweijahresbericht 1998-1999*, Sächsisches Landesamt für Umwelt und Geologie, Dresden, p 8-13
- Montenat C, Barrier P, d'Estevou PO, Hibschi C (2007) Seismites: an attempt at critical analysis and classification. *Sediment Geol* 196:5-30, <https://doi.org/10.1016/j.sedgeo.2006.08.004>
- Mrlina J (2000) Vertical displacements in the Nový Kostel seismoactive area. *Studia Geophys et Geod* 44:336-345, <https://doi.org/10.1023/A:1022179329713>
- Mrlina J, Kämpf H, Geissler W, Van den Bogaard P (2007) Assumed quaternary maar structure at the Czech/German border between Mytina and Neualbenreuth (western Eger rift, Central Europe): geophysical, petrochemical and geochronological indications. *Z Geol Wiss* 35:213-230
- Mrlina J, Kämpf H, Kroner C, Mingram J, Stebich M, Brauer A, Geissler WH, Kallmeyer J, Matthes H, Seidl M (2009) Discovery of the first Quaternary maar in the Bohemian Massif, Central Europe, based on combined geophysical and geological surveys. *J Volcanol Geotherm Res* 182:97-112, <https://doi.org/10.1016/j.jvolgeores.2009.01.027>
- Müller K, Polom U, Winsemann J, Steffen H, Tsukamoto S, Günther T, Igel J, Spies T, Lege T, Frechen M, Franzke H-J, Brandes C (2020) Structural style and neotectonic activity along the Harz Boundary Fault, northern Germany: A multimethod approach integrating geophysics, outcrop data and numerical simulations. *Int J Earth Sci* 109:1811-1835, <https://doi.org/10.1007/s00531-020-01874-0>
- Müller K, Winsemann J, Pisarska-Jamrozý M, Lege T, Spies T, Brandes C (2021a) The challenge to distinguish soft-sediment deformation structures formed by glaciotectonic, periglacial and seismic processes in a formerly glaciated area: a review and synthesis. In: Steffen H, Olesen O, Sutinen R (eds) *Glacially-Triggered Faulting*, Cambridge University Press
- Müller K, Winsemann J, Tanner DC, Lege T, Spies T, Brandes C (2021b) Glacially-Induced Faults in Germany. In: Steffen H, Olesen O and Sutinen R (eds) *Glacially-Triggered Faulting*, Cambridge University Press
- Nakiboglu SM, Lambeck K (1982) A study of the Earth's response to surface loading with application to Lake Bonneville. *Geophys J Int* 70:577-620, <https://doi.org/10.1111/j.1365-246X.1982.tb05975.x>
- Neunhöfer H (1976) Ergebnisse der instrumentellen Aufzeichnung von Mikrobeben im Vogtland nach 1962. *Z Geol Wiss* 4:1617-1629
- Neunhöfer H, Studinger M, Tittel B (1996) Erdbeben entlang der Finne- und Gera-Jáchymov-Störung in Thüringen und Sachsen, Fallbeispiel: Das Beben am 18.09.1993 bei Gera. *Z angew Geol* 42:57-61

- Neunhöfer H (1998) Das Bulletin der lokalen Erdbeben im Vogtland, 1962- 1997, Mitt Dtsch Geophys Ges 4:2-7
- Neunhöfer H, Meier T (2004) Seismicity in the Vogtland/Western Bohemia earthquake region between 1962 and 1998. *Studia Geophys et Geod* 48:539-562, <https://doi.org/10.1023/B:SGEG.0000037471.18297.07>
- Neunhöfer H, Hemmann A (2005) Earthquake swarms in the Vogtland/Western Bohemia region: spatial distribution and magnitude-frequency distribution as an indication of the genesis of swarms? *J Geodyn* 39:361-385, <https://doi.org/10.1016/j.jog.2005.01.004>
- Neunhöfer H (2009) Erdbeben in Thüringen, eine Bestandsaufnahme. *Z Geol Wiss* 37:1-14
- Neunhöfer H (2018) Die makroseismisch dokumentierten historischen Erdbeben in Thüringen und Nordwestsachsen. Friedrich - Schiller - Universität Jena, Jena, p 175 <https://doi.org/10.22032/dbt.35217>
- Nickschick T, Kämpf H, Jahr T (2014) The “Triasscholle” near Greiz, Germany-a volcanic origin? *Bull Volcanol* 76:1-20, <https://doi.org/10.1007/s00445-014-0806-x>
- Nickschick T (2017) Palaeovolcanic and present magmatic structures along the NS trending Regensburg-Leipzig-Rostock-zone. Dissertation, Friedrich-Schiller-Universität Jena, p 147
- Obermeier SF (2009) Using liquefaction-induced and other soft-sediment features for paleoseismic analysis. In: McCalpin JP (ed) *Paleoseismology*. International Geophysics Series, 95, Elsevier, Amsterdam, pp 497-564
- Panin A, Astakhov V, Komatsu G, Lotsari E, Lang J, Winsemann J (2020) Middle and Late Quaternary glacial lake-outburst floods, drainage diversions and reorganization of fluvial systems in northwestern Eurasia. *Earth-Sci Rev* 201:103069, <https://doi.org/10.1016/j.earscirev.2019.103069>
- Peltier WR (2002) On eustatic sea level history: Last Glacial Maximum to Holocene. *Quat Sci Rev* 21:377-396, [https://doi.org/10.1016/S0277-3791\(01\)00084-1](https://doi.org/10.1016/S0277-3791(01)00084-1)
- Peterek A, Reuther CD, Schunk R (2011) Neotectonic evolution of the Cheb Basin (Northwestern Bohemia, Czech Republic) and its implications for the late Pliocene to Recent crustal deformation in the western part of the Eger Rift. *Z Geol Wiss* 39:335-365
- Picard E, Naumann E, Ihnen K (1937) Erläuterungen zur geologischen Karte von Preussen und benachbarten deutschen Ländern. Blatt 4439 Brehna. 2 Edition, Preussische geologische Landesanstalt, Berlin, p 78
- Plenefisch T, Klinge K (2003) Temporal variations of focal mechanisms in the Novy Kostel focal zone (Vogtland/NW-Bohemia)-comparison of the swarms of 1994, 1997 and 2000. *J Geodyn* 35:145-156, [https://doi.org/10.1016/S0264-3707\(02\)00059-5](https://doi.org/10.1016/S0264-3707(02)00059-5)
- Pohl D, Wetzel H-U, Grünthal G (2006): Tektonische Untersuchungen im Raum Vogtland-Leipzig mit Hilfe von Fernerkundung. - In: Seyfert E (ed) *Geoinformatik und Erdbeobachtung: Vorträge; 26. Wissenschaftlich-Technische Jahrestagung der DGPF, 11. - 13.09.2006 in Berlin*, (Publikationen der Deutschen Gesellschaft für Photogrammetrie, Fernerkundung und Geoinformation e. V.; 15: 277-286
- Prodehl C, Mueller S, Haak V (1995) The European Cenozoic rift system. In: Olsen KH (ed) *Continental Rifts: Evolution, Structure, Tectonics*. Elsevier, Amsterdam, pp 133-212, [https://doi.org/10.1016/S0419-0254\(06\)80012-1](https://doi.org/10.1016/S0419-0254(06)80012-1)
- Rappsilber I, Funke S (2019) Erdbeben vom 29. April 2017 bei Markranstädt. In: Autorenkollektiv (eds) *Erdbebenbeobachtung in Mitteldeutschland - Dreijahresbericht 2016-2018*. Landesamt für Umwelt, Landwirtschaft und Geologie, Dresden, pp 45-48
- Reicherter K, Froitzheim N, Jarosinski M, Badura J, Franzke H-J, Hansen M, Hübscher C, Müller R, Poprawa P, Reinecker J, Stackebrandt W, Voigt T, von Eynatten H, Zuchiewicz W (2008) Alpine tectonics north of the Alps. In: McCann (ed) *The geology of Central Europe – Mesozoic and Cenozoic* 2:1233-1285
- Rohrmüller J, Kämpf H, Geiß E, Großmann J, Grun I, Mingram J, Mrlina J, Plessen B, Stebich M, Veress C, Wendt A, Nowaczyk N (2018) Reconnaissance study of an inferred Quaternary maar structure in the western part of the Bohemian Massif near Neualbenreuth, NE-Bavaria (Germany). *Int J Earth Sci* 107:1381-1405, <https://doi.org/10.1007/s00531-017-1543-0>
- Roskosch J, Winsemann J, Polom U, Brandes C, Tsukamoto S, Weitkamp A, Bartholomäus WA, Henningsen D, Frechen M (2015) Luminescence dating of ice-marginal deposits in northern



- Germany: evidence for repeated glaciations during the Middle Pleistocene (MIS 12 to MIS 6). *Boreas* 44:103-126, <https://doi.org/10.1111/bor.12083>
- Roth F, Fleckenstein P (2001) Stress orientations found in north-east Germany differ from the West European trend. *Terra Nova* 13:289-296, <https://doi.org/10.1046/j.1365-3121.2001.00357.x>
- Scheck M, Bayer U, Otto V, Lamarche J, Banka D, Pharaoh T (2002) The Elbe Fault System in North Central Europe—a basement-controlled zone of crustal weakness. *Tectonophysics* 360:281-299, [https://doi.org/10.1016/S0040-1951\(02\)00357-8](https://doi.org/10.1016/S0040-1951(02)00357-8)
- Schmidt A, Nowaczyk N, Kämpf H, Schüller I, Flechsig C, Jahr T (2013) Origin of magnetic anomalies in the large Ebersbrunn diatreme, W Saxony, Germany. *Bull Volcanol* 75:1-18, <https://doi.org/10.1007/s00445-013-0766-6>
- Schneider G, Bankwitz P (2003) Neotektonische Krustenaktivität im Schwarmbebengebiet Vogtland/NW-Böhmen. Abschlussbericht DFG-Projekt, Stuttgart/Potsdam, p 117
- Schneider G (2004) Erdbeben. Eine Einführung für Geowissenschaftler und Bauingenieure. Spektrum Akademischer Verlag, München, p 246
- Scholz CH (1988) The brittle-plastic transition and the depth of seismic faulting. *Geol Rundsch* 77:319-328, <https://doi.org/10.1007/BF01848693>
- Scholz CH (2002) The mechanics of earthquakes and faulting. 2 Edition, Cambridge University Press, United Kingdom, p 471
- Sedrette S, Rebaï N (2016) Automatic extraction of lineaments from Landsat Etm+ images and their structural interpretation: Case study in Nefza region (North West of Tunisia). *J Res Environ Earth Sci* 4:139-145
- Seidel G, Steinmüller A (1994) Geologische Karte von Thüringen. 1:25000, Blatt 4936 Camburg, 3 Edition, Thüringer Landesanstalt für Bodenforschung, Weimar
- Seifert W, Kämpf H, Wasternack J (2000) Compositional variation in apatite, phlogopite and other accessory minerals of the ultramafic Delitzsch complex, Germany: implication for cooling history of carbonatites. *Lithos* 53:81-100, [https://doi.org/10.1016/S0024-4937\(00\)00010-4](https://doi.org/10.1016/S0024-4937(00)00010-4)
- Settle M (1979) The structure and emplacement of cinder cone fields. *Am J Sci* 279:1089-1107, <https://doi.org/10.2475/ajs.279.10.1089>
- Siegert T, Sterzel T, Credner H (1901) Erläuterungen zur geologischen Spezialkarte des Königreichs Sachsen. Blatt 5240 Zwickau-Werdau. 2. Edition, Königliches Finanzministerium, Leipzig, p 142
- Siegert T, Hazard J, Credner H (1907) Geologische Spezialkarte des Königreichs Sachsen. 1:25000, Blatt 4848 Moritzburg-Klotzsche, 2. Edition, Königliches Finanzministerium, Leipzig
- Skamletz J, Korn M, Forkmann B, Göthe W (2000) A temporary network for seismological monitoring in West-Saxony: first results. *Studia Geophys et Geod* 44:142-157, <https://doi.org/10.1023/A:1022102607423>
- Sonnabend L (2019) Leipzig-Regensburg-Zone. In: Autorenkollektiv (eds), Erdbebenbeobachtung in Mitteldeutschland - Dreijahresbericht 2016-2018. Landesamt für Umwelt, Landwirtschaft und Geologie, Dresden, pp 55-59, <https://publikationen.sachsen.de/bdb/artikel/36630>
- Špičáková L, Uličný D, Koudelková G (2000) Tectonosedimentary evolution of the Cheb Basin (NW Bohemia, Czech Republic) between late Oligocene and Pliocene: a preliminary note. *Studia Geophys et Geod* 44:556-580, <https://doi.org/10.1023/A:1021819802569>
- Špičák A, Horálek J, Boušková A, Tomek Č, Vaněk J (1999) Magma intrusions and earthquake swarm occurrence in the western part of the Bohemian Massif. *Studia Geophys et Geod* 43:87-106, <https://doi.org/10.1023/A:1023366210017>
- Stackebrandt W (2008) Zur Neotektonik der Niederlausitz, Ostdeutschland. *Z Dtsch Geol Ges* 159:117-122, doi: 10.1127/1860-1804/2008/0159-0117
- Štěpančíková P, Fischer T, Stemberk JJ, Nováková L, Hartvich F, Figueiredo PM (2019) Active tectonics in the Cheb Basin: youngest documented Holocene surface faulting in Central Europe? *Geomorphology* 327:472-488, <https://doi.org/10.1016/j.geomorph.2018.11.007>

- Steding D, Horth K, Eilers H, Eilers G (1994) Geologische Karte der eiszeitlich bedeckten Gebiete von Sachsen, 1:50000, Blatt 2668 Dresden, 1 Edition, Sächsisches Landesamt für Umwelt und Geologie, Freiberg
- Steding D, Geissler H, Eilers H, Fritzsche H (1996) Geologische Karte der eiszeitlich bedeckten Gebiete von Sachsen, 1:50000, Blatt 2667 Meißen, 1 Edition, Sächsisches Landesamt für Umwelt und Geologie, Freiberg
- Švancara J, Havří J, Conrad W (2008) Derived gravity field of the seismogenic upper crust of SE Germany and West Bohemia and its comparison with seismicity. *Studia Geophys et Geod* 52:567-588, <https://doi.org/10.1007/s11200-008-0038-7>
- Talwani P (1988) The intersection model for intraplate earthquakes. *Seismol Res Lett* 59:305-310, <https://doi.org/10.1785/gssrl.59.4.305>
- Talwani P (2014) Unified model for intraplate earthquakes. In: Talwani P (ed) *Intraplate earthquakes*, Cambridge University Press, New York, pp 275-302
- Tietz O, Gärtner A, Büchner J (2011) The monogenetic Sonnenberg scoria cone-implications for volcanic development and landscape evolution in the Zittauer Gebirge Mountains since the Paleogene. *Z Geol Wiss* 39:311-334
- TLUBN (2020) Kartendienst Seismologie in Mitteldeutschland. URL: <http://www.tlug-jena.de/erdbeben>, (Accessed 1 November 2020).
- Trautmann T, Krbetschek MR, Dietrich A, Stolz W (1999) Feldspar radioluminescence: a new dating method and its physical background. *J Lumin* 85:45-58, [https://doi.org/10.1016/S0022-2313\(99\)00152-0](https://doi.org/10.1016/S0022-2313(99)00152-0)
- Tuttle MP, Hartleb R, Wolf L, Mayne PW (2019) Paleoliquefaction Studies and the Evaluation of Seismic Hazard. *Geosci* 9:311 <https://doi.org/10.3390/geosciences9070311>
- Ulrych J, Ackerman L, Balogh K, Hegner E, Jelínek E, Pécskay Z, Foltýnová R (2013) Plio-Pleistocene basanitic and melilititic series of the Bohemian Massif: K-Ar ages, major/trace element and Sr-Nd isotopic data. *Chem Erde* 73:429-450
- Van der Pluijm BA, Marshak S (2004) *Earth Structures. An introduction to structural geology and tectonics*, 2 Edition, Norton & Company, New York, p 656
- Vauchez A, Tommasi A, Mainprice D (2012) Faults (shear zones) in the Earth's mantle. *Tectonophysics* 558:1-27, <https://doi.org/10.1016/j.tecto.2012.06.006>
- Voigt T, Wiese F, von Eynatten H, Franzke H, Gaupp R (2006) Facies evolution of syntectonic Upper Cretaceous deposits in the Subhercynian Cretaceous Basin and adjoining areas (Germany). *Z Dtsch Ges Geowiss* 157:203-244, doi: 10.1127/1860-1804/2006/0157-0203
- Voigt T (2009) Die Lausitz-Riesengebirgs-Antiklinalzone als kreidezeitliche Inversionsstruktur: Geologische Hinweise aus den umgebenden Kreidebecken. *Z Geol Wiss* 37:15-39
- Weise E, Credner H (1904) *Erläuterungen zur geologischen Spezialkarte des Königreichs Sachsen. Blatt 5438 Plauen-Pausa*. 1 Edition, Königliches Finanzministerium, Leipzig, p 71
- Weise W, Uhlemann A, Dalmer K, Credner H (1913) *Erläuterungen zur geologischen Spezialkarte des Königreichs Sachsen. Blatt 5439 Treuen-Herlasgrün*. 2 Edition, Königliches Finanzministerium, Leipzig, p 58
- Wendt S, Mittag R, Forkmann B, Berger H-J, Krentz O, Witthauer B, Eilers H, Neumann E (1996) *Seismologische Übersichtskarte des Freistaates Sachsen. 1: 400 000*, 1 Edition, Sächsisches Landesamt für Umwelt und Geologie, Freiberg
- Wendt J (2002) Geodätische Untersuchungen im vogtländischen Bebengebiet. In: Autorenkollektiv (eds) *Erdbebenbeobachtung im Freistaat Sachsen Zweijahresbericht 2000-2001*. Landesamt für Umwelt und Geologie, Freiberg, pp 25-34
- Wendt J, Dietrich R (2003) Determination of recent crustal deformations based on precise GPS measurements in the Vogtland earthquake area. *J Geodyn* 35:235-246,
- Wendt S, Buchholz P (2019) Seismische Aktivität in Mitteldeutschland (Sachsen, Sachsen-Anhalt und Thüringen) und im regionalen Umfeld. In: Autorenkollektiv (eds) *Erdbebenbeobachtung in Mitteldeutschland - Dreijahresbericht 2016-2018*. Landesamt für Umwelt, Landwirtschaft und Geologie, Dresden, pp 6-25, <https://publikationen.sachsen.de/bdb/artikel/36630>

- Winsemann J, Brandes C, Polom U (2011) Response of a proglacial delta to rapid high-magnitude lake-level change: an integration of outcrop data and shear-wave seismics. *Basin Res* 23:22-52. Doi: 10.1111/j.1365-2117.2010.00468.x.
- Winsemann J, Lang J, Polom U, Loewer M, Igel J, Pollok L, Brandes C (2018) Ice-marginal forced regressive deltas in glacial lake basins: geomorphology, facies variability and large-scale depositional architecture. *Boreas* 47:973-1002, <https://doi.org/10.1111/bor.12317>
- Winsemann J, Lang J (2020) Flooding Northern Germany: Impacts and Magnitudes of Middle Pleistocene Glacial Lake-Outburst Floods. In: Herget J, Fontana A (eds) *Palaeohydrology. Geography of the Physical Environment*. Springer, Cham pp 29-47
- Wrona T, Fossen H, Lecomte I, Eide CH, Gawthorpe RL (2020) Seismic expression of shear zones: Insights from 2-D point-spread-function based convolution modelling. *J Struct Geol* 140:104121, <https://doi.org/10.1016/j.jsg.2020.104121>
- Ziegler PA (1992) European Cenozoic rift system. In: Ziegler PA (ed) *Geodynamics of Rifting, Volume I. Case History Studies on Rifts: Europe and Asia*. *Tectonophysics* 208:91-111, [https://doi.org/10.1016/0040-1951\(92\)90338-7](https://doi.org/10.1016/0040-1951(92)90338-7)
- Zimmermann E, Liebe KT (1930) *Erläuterungen zur geologischen Karte von Preußen und benachbarten deutschen Ländern*. Blatt 5138 Gera. 3 Edition, Preußisch geologische Landesanstalt, Berlin, p 80
- Zhumabek Z, Assylkhan B, Alexandr F, Dinara T, Altynay K (2017) Automated lineament analysis to assess the geodynamic activity areas. *Procedia Comput Sci* 121:699-706

## 6. Synthesis and Discussion

The objective of this thesis was to analyse major faults and fault systems in northern and central Germany in order to derive evidence of neotectonic activity with the aim to extend the pre-historic seismic record into the past and to identify potentially active faults. The publications (1-4) presented in this dissertation address the challenges of SSDS as palaeo-earthquake indicators in formerly glaciated and periglacial areas. Major faults and fault systems with evidence for post-Pleistocene neotectonic fault activity, which are potentially GIFs, were investigated. A detailed analysis of a neotectonic active fault (Harz Boundary Fault) is shown using a multimethod approach that combines luminescence dating, shear-wave seismic surveys, ERT profiles and numerical simulations. In comparison to palaeoseismological analysis in the seismically calm area of northern Germany, a seismically more active region in central Germany was investigated using palaeoseismological and DEM lineament analysis. The following chapter discusses the major findings and summarises the results.

### 6.1 Neotectonic fault activity in northern and central Germany

The documented historic and instrumentally detected earthquakes since 800 CE (Leydecker 2011; GERSEIS 2020) and recent work have shown that besides central Germany, northern Germany is a seismically active intraplate region, too. In northern Germany NW-SE and WNW-ESE oriented major faults with a high reactivation potential due to stress field changes caused by GIA processes were analysed. In central Germany palaeoseismological analyses were conducted independently from the fault pattern. Major faults and fault systems in this area are the RLR fault system, the Lusatian Thrust and the FGJ fault system.

Based on this study, the existing palaeoseismic and neotectonic record of northern and central Germany (e.g. Hübscher et al. 2004; Stackebrandt 2008; Ludwig 2011; Brandes et al. 2011, 2012, 2018a, b; Brandes and Tanner 2012; Hoffmann and Reicherter 2012; Brandes and Winsemann 2013; Hürtgen 2017; Pisarska-Jamroży et al. 2018, 2019; Grube 2019a, b; Huster et al. 2020) can be extended with additional evidence for neotectonic activity at major basement faults.

Evidence of neotectonic fault activity was observed in nine sand and gravel pits exposing mainly Middle to Late Pleistocene sediments and one sinkhole that are located along deep-seated major fault systems: the Aller Fault, the FGJ fault system, the Halle Fault, the Harz Boundary Fault, the Lusatian Thrust, the Osning Thrust and the Steinhuder Meer Fault as well as close to NW-SE and NNW-SSE oriented faults, which are intersected by smaller NE-SW or N-S oriented faults in the vicinity of Dresden and Leipzig (Publications 1, 2, 4) (Fig. 19). The results show that evidence for neotectonic fault activity was mainly found at NW-SE and WNW-ESE oriented faults (Publications 1, 2, 4). Especially in the study area of central Germany it is obvious that tectonically induced deformation bands occur in the vicinity of fault intersections (Publication 4). Fault intersections act as stress concentrators that cause a localization of the seismicity (e.g. Talwani 1988, 2014).

Some of these faults are interesting targets for trench studies. Specifically, the Aller Fault represents a key structure for further analysis, because deformation bands exposed in Middle Pleistocene deposits near Eitze (pit 42) are likely to be formed as a consequence of neotectonic movements at the blind segment of the Aller Fault (Publication 2).

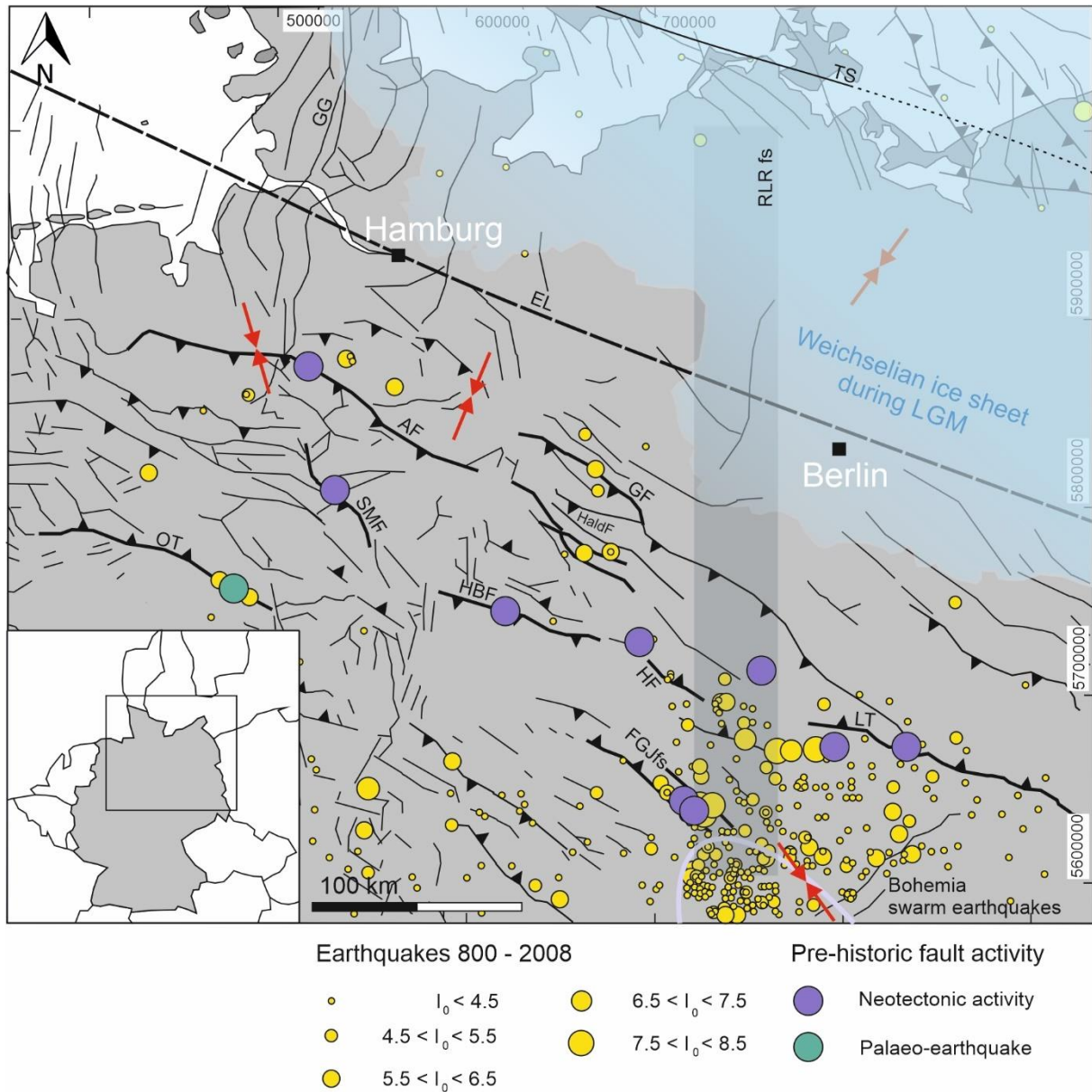


Figure 19: Palaeoseismological and neotectonic evidence combined with seismicity observed between 800 – 2008 in the study area of northern and central Germany. Aller Fault: AT; Elbe Lineament: EL; Finne-Gera-Jáchymov fault system: FGJfs; Gardelegen Fault: GF; Glückstadt Graben: GG; Haldensleben Fault: Haldf; Halle Fault: HF; Harz Boundary Fault: HBF; Lusatian Thrust: LT; Osning Thrust: OT; Regensburg-Leipzig-Rostock fault system: RLRfs; Steinhuder Meer Fault: SMF; Thor Suture: TS. Red arrows show the recent stress field orientation based on Marotta et al. (2000, 2002), Reicherter et al. (2005) and Heidbach et al. (2016). (Map is modified after Leydecker 2011; Brandes et al. 2015).

Summarising the neotectonic activity and the earthquake activity along the NW-SE and WNW-ESE oriented faults establishes a comprehensive view of the intraplate seismicity in northern and central Germany.

Neotectonic activity at Late Cretaceous reverse faults was observed along the Osning Thrust (Brandes et al. 2012), the Harz Boundary Fault (Publication 1) and the Lusatian Thrust (Publication 4) (Fig. 19) as well as at the Aller Fault, the Elbe Lineament, the Halle Fault, the Steinhuder Meer fault and the FGJ fault system. The historic earthquake record shows seismic activity along the Aller Fault, the Halle Fault, Thor Suture, the Osning Thrust, the Gardelegen Fault, the Haldensleben Fault and the Lusatian Thrust (Table 1; Fig. 19) (Publication 2; Leydecker 2011;

GERSEIS 2020). Recently, natural tectonic earthquakes were detected along the Osning Thrust (GERSEIS 2020), the Halle Fault and probably the Aller Fault (Figs 2, 19) (Dahm et al. 2018). Deep earthquakes along the Thor Suture were also detected in the last years (Brandes et al. 2019).

This repeated tectonic activity matches with the hypothesis that the loci of the epicentres of intraplate earthquakes may migrate between the individual fault systems in northern and central Germany (Fig. 19) (cf. Li et al. 2009; Liu et al. 2011; Talwani 2017). Without significant tectonic loading, earthquakes can occur repeatedly on a weakened fault zone (Li et al. 2009) controlled by a complex system of interacting faults that spread over a wide area (Stein et al. 2015). This is likely to be the case in northern and central Germany (Publication 2) (Fig. 3).

The results of the palaeoseismological analyses underline the importance of NW-SE oriented faults in regard to the seismicity and fault activity in the recent stress field (e.g. Heidbach et al. 2016). It must be kept in mind that NW-SE oriented faults were in the primary research focus. Nevertheless, Al Hseinat and Hübscher (2017) also identified neotectonic movements along NW-SE striking faults like the Langeland Fault, Prerow Fault, Werre Fault and Wiek Fault. Pisarska-Jamrozny et al. (2018, 2019) found seismically induced SSDS along the WNW-ESE oriented Schaabe Fault. Furthermore, at the WNW-ESE striking Weser Valley and the NW-SE striking Leine Valley Fault evidence for neotectonic fault activity was also found (Brandes et al. 2011; Winsemann et al. 2011, 2018; Brandes and Tanner 2012; Brandes et al. 2018a). This requires a more comprehensive treatment of the interplay of fault orientation and reactivation potential. In the future the analysis of faults that are not optimally oriented to the former ice sheet like NE-SW oriented faults might be an interesting task for palaeoseismological analysis in the area of northern and central Germany.

## 6.2 Timing of fault activity

In northern and central Germany fault activity and the timing of deformation could be estimated using luminescence dating at two major basement faults: the Harz Boundary Fault and the Steinhuder Meer Fault (Fig. 20). At the Steinhuder Meer Fault the estimated IRSL ages ( $189 \pm 5$  ka to  $158 \pm 4$  ka; Table A5) indicate Middle Pleistocene Saalian fault activity. This implies that the deformation bands have most likely developed during the Middle Pleistocene Saalian glaciations. At the Harz Boundary Fault, the estimated luminescence ages range in age from  $15.2 \pm 0.8$  ka (quartz) to  $14.2 \pm 0.8$  ka (polymineral, feldspar) that indicate fault movements after  $\sim 15$  ka. For the Osning Thrust luminescence dating was estimated in a previous study indicating that the neotectonic movements occurred in the Lateglacial between 16 to 13 ka (Brandes et al. 2012; Brandes and Winsemann 2013). This matches the data from the Harz Boundary Fault and supports the idea of widespread fault reactivation in the Late Pleniglacial to Lateglacial due to GIA processes.

In further sand and gravel pits with evidence of neotectonic fault activity, luminescence dating could not be applied, as undeformed cover beds were missing. However, the age of the sediments in which deformation structures are developed deliver the timing of fault activity after the sediment deposition. At the FGJ fault system deformation bands developed in Palaeogene sediments, pointing to post-Palaeogene fault activity (Publication 4) (Fig. 20). In the west of Dresden deformation bands developed in Middle Pleistocene Elsterian deposits in the vicinity to intersecting minor faults. This points to post-Elsterian fault movements along the underlying faults (Publication 4). At the Aller Fault, the Halle Fault, the Lusatian Thrust and minor faults in

the north of Leipzig, deformation bands developed in Middle Pleistocene Saalian sediments, which point to post-Saalian fault movements (Publications 2 and 4) (Fig. 20).

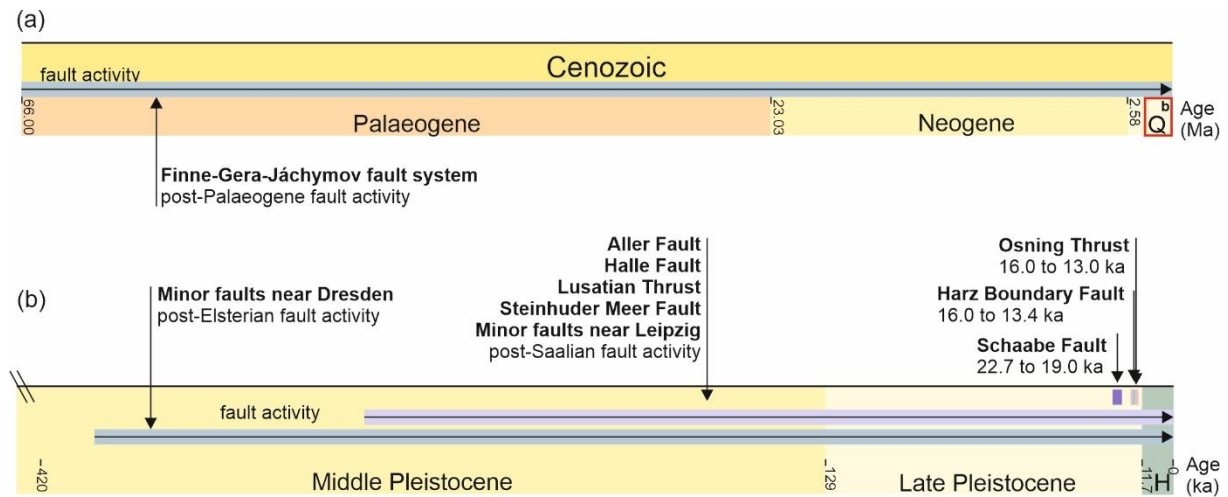


Figure 20: Timeline of the estimated neotectonic fault activity along the analysed faults in northern and central Germany. (a) Overview of the Cenozoic. At the FGJ fault system evidence of post-Palaeogene fault activity is observed. (b) Timing of Middle Pleistocene post-Elsterian neotectonic fault activity at minor faults near Dresden; Middle Pleistocene post-Saalian neotectonic activity at the Aller Fault, the Halle Fault, the Lusatian Thrust and minor faults near Leipzig; Middle Pleistocene Saalian neotectonic activity at the Steinhuder Meer Fault (194.0 to 154.0 ka), Late Pleniglacial to Lateglacial neotectonic activity at the Schaabe Fault (22.7 to 19.0 ka) (Pisarska-Jamroży et al. 2019), the Osning Thrust (16.0 to 13.0 ka) (Brandes et al. 2012) and the Harz Boundary Fault (16.0 to 13.4 ka) (Publication 1). Timeline is based on Cohen et al. (2013 updated 2021) and Cohen and Gibbard (2020).

The neotectonic activity in northern and central Germany is a consequence of the regional lithospheric stress field, which is governed by the push of the mid-Atlantic ridge and the continuing Alpine orogeny. The work of Brandes et al. (2011, 2012, 2015), Brandes and Winsemann (2013) and Diercks et al. (2021) has shown that additional stress field changes due to GIA might have induced Middle Pleistocene to Lateglacial and historic seismicity and neotectonic activity. Large parts of the study area were also affected by these stress field changes. WNW-ESE trending faults in northern Germany have the highest reactivation potential because they are trending parallel to the former Late Pleistocene Weichselian ice margin (Brandes et al. 2015). Thus, the maximum horizontal components of the ice sheet-induced stress for these faults are in line with the palaeo-stress field (Stewart et al. 2000).

In this study, the timing of fault movements implies that the seismicity in northern and parts of central Germany is likely induced by varying lithospheric stress conditions related to GIA and the faults can thus be classified as GIFs (Publication 2). For the Osning Thrust, the Schaabe Fault and the Harz Boundary Fault this is supported by numerical simulation of GIA-related stress field changes (Brandes et al. 2012; Pisarska-Jamroży et al. 2019; Publication 1; e. g. Munier et al. 2020). Geomorphological analyses of the Harz Mountains support GIA-induced neotectonic activity (Diercks et al. 2021). All of these faults, which show post-Pleistocene neotectonic activity, can be classified as potential GIFs. Potential GIFs that were investigated in this study are: the Aller Fault, the Halle Fault, the Lusatian Thrust and the Steinhuder Meer Fault (Publications 2 and 4).

The influence of GIA was estimated using modelling results of Coulomb-failure stress variations for the Late Pleistocene Weichselian ice sheet that imply an influence of GIA as far south as the



Thuringian Forest (Brandes et al. 2015). However, modelling results of Coulomb-failure stress variations do not exist for the Middle Pleistocene glaciations, which extended further southwards and might be more important for the triggering of faults along the N-S trending RLR fault system that is intersected by several NW-SE and NE-SW oriented faults.

### 6.3 Challenges and geological indicators of young fault activity at blind faults

In northern and central Germany deformation structures have been found in 68 of the 156 pits analysed. These structures mostly comprise glaciotectonically and periglacially-induced structures like folds, thrust-sheets, faults with reverse and normal displacement, deformation bands, ice-wedge casts and involutions (e.g. cf. Péwé 1973; Hart and Boulton 1991; Phillips et al. 2008; Lee and Phillips 2008; Vandenberghe 2013; Worsley 2014). In nine sand and gravel pits and one sinkhole, robust indicators for neotectonic activity were observed comprising deformation bands and faults (Publications 1, 2, 4 and cf. Publication 3). This underlines the importance of deep major tectonic basement faults (often NW-SE and WNW-ESE oriented) for the distribution of the seismicity in the intraplate area of northern and central Germany.

By comparing the seismically calmer area of northern Germany (Publication 2) to the seismically active area of central Germany (Publication 4), no further differences in the recording of neotectonic activity or palaeoseismic events were investigated. In all pits with neotectonic evidence, deformation bands close to the tip point of faults are developed (Fig. 21).

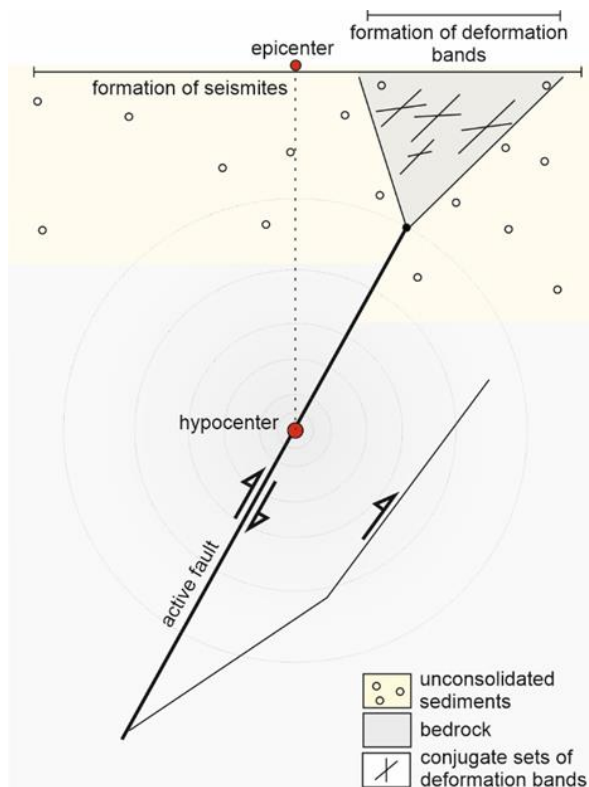


Figure 21: Schematic model of the formation and distribution of deformation bands and seismites at an active reverse fault (based on Ballas et al. 2015).

In greater distance to the major basement faults, no evidence for palaeoseismic or neotectonic events was observed in the Pleistocene deposits in the study area. Several reasons are possible. This might be due to the absent occurrence of palaeoseismic events since the Middle Pleistocene. However, historic as well as instrumentally detected earthquakes were recorded in the study area since 800 CE (Leydecker 2011; GERSEIS 2020; TLUBN 2020), especially in the area of central Germany (Fig. 2). The release of strain in continental interiors happens faster than the strain accumulation (e.g. Calais and Stein 2009). This indicates that fault activity is caused by pre-stored strain in the crust (Stein et al. 2015). This process is different to interplate earthquakes. Despite the nature of intraplate earthquakes with long intervals and a spatial and temporal distribution between individual events (Gangopadhyay and Talwani 2003; Li et al. 2009; Liu et al. 2011), it is unlikely that no earthquakes occurred since the Middle Pleistocene.

Another reason may be the recorded low magnitudes in northern and central Germany of up to  $M_L$  3.4 and  $M_L$  4.2 and maximum epicentral intensities of VI - (6.5) and VII - (7.5) (GERSEIS 2020). In the literature a magnitude of  $M \geq 5.0$  is assumed to produce seismites (e.g. Atkinson et al. 1984; Rodríguez-Pascua et al. 2000; Obermeier 2009; Publication 3). Such magnitudes are rare in Germany (GERSEIS 2020).

Large basement faults are necessary to produce earthquakes with magnitudes greater than 5. This is supported by the study of Wells and Coppersmith (1994) who correlate the magnitude of an earthquake with the fault rupture length. Only large faults with a rupture length of at least 10 km can produce earthquakes of magnitude 6 (cf. Wells and Coppersmith 1994). In northern and central Germany, potential faults of this size are the Harz Boundary Fault, the Aller Fault, the Elbe Lineament, the FGJ fault system, the RLR fault system and the Lusatian Thrust. However, some of these faults are segmented or represent parallel and overlapping faults. The Aller Fault system is composed of overlapping faults that range several hundred metres (e.g. Baldschuhn et al. 1996). This limitation is also present at the segmented Lusatian Thrust, the FGJ fault system and the RLR fault system which are composed of en-échelon faults (Bankwitz et al. 1993, 2003; Krentz and Stanek 2015).

Fault segments can act as barriers for fault rupture (e.g. McCalpin 2009) which was observed at the Wasatch fault zone (Utah) (Schwartz and Coppersmith 1984; Scholz 2002). Wesnousky (2006) showed that about two-thirds of the endpoints of fault ruptures along strike-slip faults are associated with fault steps or endpoints of active fault traces. A limiting dimension of fault steps (3 - 4 km) exists above which earthquake ruptures do not propagate and below which rupture propagation ceases in about 40 per cent of the time (Wesnousky 2006). However, during the Landers earthquake in 1992 (USA), rupture propagation across segment boundaries was observed (Sieh et al. 1993). DuRoss et al. (2016) present a new concept for the segmented Wasatch fault zone and describe complex ruptures, which are shorter or longer than the primary segment lengths thus pointing to fault interactions already described in a model of Scholz and Gupta (2000). With the increase of stress interaction between fault segments, rupture can propagate from one fault to another (Scholz and Gupta 2000). Thus, strain accumulation along segmented faults and fault systems and the subsequent failure of several fault segments may lead to higher magnitudes than expected.

A further reason for the rare recognition of seismites that point to earthquake activity in northern and central Germany are the properties of the investigated Middle to Late Pleistocene sediments. At the Harz Boundary Fault, the exposed sediments are often unsuitable to serve as archives for seismically triggered SSDS. The deposits comprise Middle to Late Pleistocene fluvial coarse-grained sand and gravel as well as coarse-grained meltwater deposits partly covered by loess (Schröder et al. 1927, 1931; Weymann 2004). In contrast, at the Osning Thrust Late Pleistocene fine-grained alluvial and aeolian, mixed alluvial-aeolian and meltwater deposits are exposed (Keilhack et al. 1917; Haack et al. 1930; Meinsen et al. 2014). These fine-grained deposits at the Osning Thrust are prone for seismically triggered SSDS as observed by Brandes and Winsemann (2013) who investigated SSDS in mixed alluvial-aeolian Late Pleniglacial deposits. At the Elbe Lineament, Steinhuder Meer Fault, Gardelegen Fault and Aller Fault mainly Middle to Late Pleistocene meltwater deposits are exposed. The meltwater deposits are partly overlain by till and paraglacial deposits (Tables A6-A12). In the area around the RLR fault system the deposits mainly comprise Middle to Late Pleistocene meltwater deposits and coarse-grained fluvial deposits (Table A13). Besides the coarse-grained fluvial deposits, the exposed meltwater sediments are mostly prone for the development of seismically triggered SSDS.

Nevertheless, seismically triggered SSDS in Pleistocene deposits of northern Germany were described in several studies (e.g. Hoffmann and Reicherter 2012; Brandes and Winsemann 2013; Pisarska-Jamroży et al. 2018), which point to earthquakes with higher magnitudes in prehistoric times in comparison to recently detected earthquakes. Due to the very long recurrence intervals in low strain intraplate areas, like Germany, it is possible that the recently recorded seismicity, represents after-shock sequences of unknown large earthquakes as described by Stein et al. (2015) for the intraplate area of Europe.

## 7. Conclusions

1. Five of the seven investigated major basement faults in northern Germany (Aller Fault, Harz Boundary Fault, Halle Fault, Osning Thrust and Steinhuder Meer Fault) reveal evidence of neotectonic activity.
2. The Osning Thrust is the only fault with clear evidence of palaeo-earthquakes.
3. Deformation bands in Middle Pleistocene sediments indicate neotectonic movement at the Aller Fault, Halle Fault and Steinhuder Meer Fault, which developed in the process zone of the faults. Both, seismic and aseismic creep, may have occurred along these faults.
4. A fault with a young polyphase evolution (normal and reverse fault movement) exposed in a sinkhole close to the Harz Boundary Fault indicates neotectonic activity at this location. The timing of the fault activity (Lateglacial) confirms observations made at the Osning Thrust and Sorgenfrei-Tornquist Zone by Brandes et al. (2012), Brandes and Winsemann (2013) and Brandes et al. (2018b).
5. In the area around the RLR fault system in central Germany, deformation bands in Eocene-Oligocene and Middle Pleistocene sediments indicate neotectonic movements at the FGJ fault system, the Lusatian Thrust and minor faults close to Leipzig and Dresden. Seismic rupture processes and aseismic creep, both may have occurred along these faults.
6. In central Germany neotectonic evidence point out that fault intersections play a major role for the distribution of seismicity and neotectonic fault activity, because they act as stress concentrators as shown by Talwani (1988).
7. The seismicity in northern Germany is most likely induced by varying lithospheric stress conditions related to GIA, with an influence reaching far south as the Thuringian Forest (Brandes et al. 2015). Late Pleniglacial to Lateglacial, historic and recent earthquakes have occurred in this region. Thus, the most likely driver for fault activity since the Middle Pleistocene is GIA.
8. The Harz Boundary Fault and the Osning Thrust can be classified as GIFs, because of the timing of reactivation, their orientation to the former ice margins and numerical simulations that show the increase of the CFS over the time since the onset of deglaciation.
9. Northern and central Germany were repeatedly overridden by ice sheets. This strongly limits the standard use of SSDS to determine palaeoseismic activity because many of these structures are likely to be the result of glaciotectonics.

10. Deformation bands potentially are a good indicator for neotectonic fault activity but they cannot provide any clear evidence of earthquakes. However, SSDS in combination with deformation bands indicate that the neotectonic activity was accompanied by earthquakes.

11. In the recent stress field NW-SE and WNW-ESE oriented faults may be active and play a major role for the localization of the seismicity in northern and central Germany.

## 8. References

- Alexowsky W, Schneider JW, Tröger KA, Wolf L, Hoffmann U, Horna F, Huhle K, Kardel K, Kulikov S, Lapp K, Palme G, Pohlenz R, Schauer M, Symmangk R, Voigt S, Witthauer B (2001) Geologische Karte des Freistaates Sachsen 1:25000, Blatt 4948 Dresden, 4. Edition, Sächsisches Landesamt für Umwelt, Landwirtschaft und Geologie, Freiberg
- Al Hseinat M, Hübscher C (2017) Late Cretaceous to recent tectonic evolution of the North German Basin and the transition zone to the Baltic Shield/southwest Baltic Sea. *Tectonophysics* 708:28-55
- Antares.Thuringen (2019) Digitale Geologische Karte des Freistaats Thüringen. URL: <http://antares.thuringen.de/cadenza/pages/map/default/index.xhtml?jsessionid=D2D84CB9DCA0E6FB3A288201150E7B57> (Accessed 06.08.2019)
- Atkinson GM, Finn WL, Charlwood RG (1984) Simple computation of liquefaction probability for seismic hazard applications. *Earthq Spectra* 1:107-123
- Baldschuhn R, Binot F, Fleig S, Kockel F (1996) Geotektonischer Atlas von Nordwest-Deutschland und dem deutschen Nordsee-Sektor. *Geol Jb A* 153:3-95
- Ballas G, Fossen H, Soliva R (2015) Factors controlling permeability of cataclastic deformation bands and faults in porous sandstone reservoirs. *J Struct Geol* 76:1-21
- Bankwitz P, Grossand U, Bankwitz E (1993) Krustendeformation im Bereich der Finne-Kyffhäuser-Gera-Jáchymov-Zone. *Z Geol Wiss* 21:3-20
- Bankwitz P, Schneider G, Kämpf H, Bankwitz E (2003) Structural characteristics of epicentral areas in Central Europe: study case Cheb Basin (Czech Republic). *J Geodyn* 35:5-32
- Beck R, Credner H (1889) Geologische Spezialkarte des Königreichs Sachsen. 1:250000, Blatt 5049 Pirna, 1. Edition, Königliches Finanzministerium, Leipzig
- BGR Geoviewer (2019) Karte zur Geologie Deutschlands URL: <https://geoviewer.bgr.de/mapapps4/resources/apps/geoviewer/index.html?lang=de> (Accessed 2019)
- Bode A, Schröder H (1926) Erläuterungen zu Blatt 4028 Goslar, Geologische Karte von Preußen und benachbarten deutschen Ländern 1:25000. Preußische Geologische Landesanstalt, Berlin, p107
- Brandes C, Polom U, Winsemann J (2011) Reactivation of basement faults: interplay of ice sheet advance, glacial lake formation and sediment loading. *Basin Res* 23:53-64
- Brandes C, Tanner DC (2012) Three-dimensional geometry and fabric of shear deformation bands in unconsolidated Pleistocene sediments. *Tectonophysics* 518:84-92
- Brandes C, Winsemann J, Roskosch J, Meinsen J, Tanner DC, Frechen M, Steffen H, Wu P (2012) Activity along the Osning Thrust in Central Europe during the Lateglacial: ice sheet and lithosphere interactions. *Quat Sci Rev* 38:49-62
- Brandes C, Winsemann J (2013) Soft-sediment deformation structures in NW Germany caused by Late Pleistocene seismicity. *Int J Earth Sci* 102:2255-2274
- Brandes C, Steffen H, Steffen R, Wu P (2015) Intraplate seismicity in northern Central Europe is induced by the last glaciation. *Geology* 43:611-614
- Brandes C, Igel J, Loewer M, Tanner DC, Lang J, Müller K, Winsemann J (2018a) Visualization and analysis of shear deformation bands in unconsolidated Pleistocene sand using ground-penetrating radar: Implications for paleoseismological studies. *Sediment Geol* 367:135-145
- Brandes C, Steffen H, Sandersen PBE, Wu P, Winsemann J (2018b) Glacially induced faulting along the NW segment of the Sorgenfrei-Tornquist Zone, northern Denmark: implications for neotectonics and Lateglacial fault-bound basin formation. *Quat Sci Rev* 189:149-168
- Brandes C, Plenefisch T, Tanner DC, Gestermann N, Steffen H (2019) Evaluation of deep crustal earthquakes in northern Germany - Possible tectonic causes. *Terra Nova* 31:83-93
- Buchholz P, Funke S, Wendt S, Hänel F, Mittag R, Novak E, Rappsilber I, Burghardt T, Schönwald D, Pustal I, Busch P, Eberlein L, Horwath M, Schröder L, Krentz O, Witthauer B (2016) Erdbebenbeobachtung in Mitteldeutschland. Dreijahresbericht 2013-2015. Landesamt für Umwelt, Landwirtschaft und Geologie, Dresden, p 60
- Calais E, Stein S (2009) Time-variable deformation in the New Madrid seismic zone. *Science* 323:1442-1442

- Cohen KM, Finney SC, Gibbard PL, Fan J-X (2013 updated 2021) The ICS International Chronostratigraphic Chart. *Episodes* 36:199-204
- Cohen KM, Gibbard PL (2020) Global chronostratigraphical correlation table for the last 2.7 million years v. 2019, V3, doi: 10.17632/dtsn3xn3n6.3
- Dahm T, Heimann S, Funke S, Wendt S, Rappsilber I, Bindi D, Plenefisch T, Cotton F (2018) Seismicity in the block mountains between Halle and Leipzig, Central Germany: centroid moment tensors, ground motion simulation, and felt intensities of two  $M \approx 3$  earthquakes in 2015 and 2017. *J Seismol* 22:985-1003
- Dalmer K, Rothpletz A, Lechmann J, Credner H (1879) Geologische Spezialkarte des Königreichs Sachsen. Blatt 5041 Langenleuba-Niedershain (vormals Blatt: Langenleuba), 1 Edition, Königliches Finanzministerium, Leipzig
- Dames W (1875) Geologische Spezialkarte von Preußen und den Thüringischen Staaten. 1:25000, Blatt 4734 Wiehe, 1 Edition, Königliche Geologische Landesanstalt, Berlin
- Danzig E, Sauer A, Credner H (1905) Geologische Spezialkarte des Königreichs Sachsen. 1:25000, Blatt 4741 Naunhof-Otterwisch, 2 Edition, Königliches Finanzministerium, Leipzig
- Dathe E, Rothpletz A, Credner H (1876) Geologische Spezialkarte des Königreichs Sachsen. 1:25000, Blatt 4942 Rochlitz, 1 Edition, Königliches Finanzministerium, Leipzig
- Dathe E, Credner H (1879) Geologische Spezialkarte des Königreichs Sachsen. 1:25000, Blatt 4844 Döbeln, 1 Edition, Königliches Finanzministerium, Leipzig
- Diercks ML, Stanek K, Domínguez-Gonzalez L, Ehling B (2021) Quaternary landscape evolution and tectonics in Central Germany – A case study of the Harz. *Geomorphology* 388:107794
- DuRoss CB, Personius SF, Crone AJ, Olig SS, Hylland MD, Lund WR, Schwartz DP (2016) Fault segmentation: New concepts from the Wasatch fault zone, Utah, USA. *J Geophys Res Solid Earth* 121:1131-1157
- Franzke HJ, Hauschke N, Hellmund M (2015) Spät Pleistozäne bis früh Holozäne Tektonik in einem Karsttrichter im Bereich der Störungzone des Harznordrandes nahe Benzingerode (Sachsen-Anhalt). *Hall JB Geowiss* 37:1-10
- Gagel C, Schlunck J (1911) Erläuterungen zu Blatt 2528 Geesthacht (Hamwarde), Geologische Karte von Preußen und benachbarten Bundesstaaten, 1:25000. Königliche Preußische Geologische Landesanstalt, Berlin, p 46
- Gagel C, Schlunck J (1914) Erläuterungen zu Blatt 2529/2530 Büchen (Pötrau-Gresse), Geologische Karten von Preußen und benachbarten Bundesstaaten, 1:25000. Königliche Preußische Geologische Landesanstalt, Berlin, p 62
- Gangopadhyay A, Talwani P (2003) Symptomatic features of intraplate earthquakes. *Seismol Res Lett* 74:863-883
- Geo.Brandenburg (2019) Karten des Landesamts für Bergbau, Geologie und Rohstoffe (LBGR) Land Brandenburg. URL: <http://www.geo.brandenburg.de/lbgr/bergbau>. (Accessed 06.08.2019)
- Geowiewer.Sachsen (2019) Geoportal Sachsen. URL: [https://geowiewer.sachsen.de/mapviewer2/index.html?lang=de&service=https://geodienst.sachsen.de/wms\\_smi\\_lep2013\\_Verkehr/guest](https://geowiewer.sachsen.de/mapviewer2/index.html?lang=de&service=https://geodienst.sachsen.de/wms_smi_lep2013_Verkehr/guest) (Accessed 06.08.2019)
- GERSEIS (2020) Geodatendienst für Erdbeben in Deutschland. URL: [https://www.bgr.bund.de/DE/Themen/Erdbeben-Gefahrdungsanalysen/Seismologie/Seismologie/Seis-Online/gerseis\\_node.html](https://www.bgr.bund.de/DE/Themen/Erdbeben-Gefahrdungsanalysen/Seismologie/Seismologie/Seis-Online/gerseis_node.html) (Accessed 16.12.2020)
- Gläßer W, Wiefel H (1999) Erläuterungen zur Geologischen Karte 1:25000 von Thüringen. Blatt 5041 Langenleuba-Niederhain, 2 Edition, Thüringer Landesanstalt für Geologie, Weimar, p 212
- Grahmann R, Kossmat F (1925) Geologische Karte von Sachsen. 1:25000, Blatt 4643 Dahlen, 2 Edition, Finanzministerium, Leipzig
- Grahmann R, Picard B, Kossmat F (1930) Geologische Karte von Sachsen. 1:25000, Blatt 4542 Thallwitz-Strelln, 2 Edition, Geologisches Landesamt, Finanzministerium, Leipzig
- Grube A (2019a) Palaeoseismic structures in Quaternary sediments of Hamburg (NW Germany), earthquakes evidence during the younger Weichselian and Holocene. *Int J Earth Sci* 108:845-861

- Grube A (2019b) Palaeoseismic structures in Quaternary sediments, related to an assumed fault zone north of the Permian Peissen-Gnutz salt structure (NW Germany) – Neotectonic activity and earthquakes from the Saalian to the Holocene. *Geomorphology* 328:15-27
- Grunder H (1896) Erläuterungen zu Blatt 3038 Glöwen, Geologische Spezialkarte von Preußen und den Thürngischen Staaten 1:25000. Königliche Preußische Geologische Landesanstalt, Berlin, p 63
- Guérin G, Mercier N, Adamiec G (2011) Dose-rate conversion factors: update. *Anc TL* 29:5-8
- Haack W, Görz G (1930) Erläuterungen zu Blatt 3814 Bad Iburg, Geologische Karte von Preußen und benachbarten deutschen Ländern 1:25000. Preußische Geologische Landesanstalt, Berlin, p93
- Harbort E, Monke H, Schucht F (1916a) Erläuterungen zu Blatt 3326 Celle, Geologische Karte von Preußen und benachbarten Bundesstaaten 1:25000. Königliche Preußische Geologische Landesanstalt, Berlin, p 56
- Harbort E, Monke H, Stoller J (1916b) Erläuterungen zu Blatt 3427 Wienhausen, Geologische Karte von Preußen und benachbarten Bundesstaaten 1:25000. Königliche Preußische Geologische Landesanstalt, Berlin, p 52
- Harbort E, Stoller J (1916c) Erläuterungen zu Blatt 3327 Lachendorf, Geologische Karte von Preußen und benachbarten Bundesstaaten 1:25000. Königliche Preußische Geologische Landesanstalt, Berlin, p 69
- Hart JK, Boulton GS (1991) The interrelation of glaciotectonic and glacio-depositional processes within the glacial environment. *Quat Sci Rev* 10:335-350
- Härtel F, Kossmat F (1931) Geologische Karte von Sachsen. 1:25000, Blatt 4845 Lommatzsch (alt: Lommatzsch-Leuben), 2 Edition, Finanzministerium
- Hazard J (1924) Erläuterungen zu Blatt 4739 Zwenkau, Geologische Karte von Sachsen 1:25000. Finanzministerium, Leipzig, p 44
- Heidbach O, Rajabi M, Reiter K, Ziegler M (2016) World stress map 2016. *Science* 277:1956-62
- Hellwig D, Müller A (1998) Geologische Karte der eiszeitlich bedeckten Gebiete von Sachsen, 1:50000, Blatt 2467 Bad Liebenwerda, 1 Edition, Sächsisches Landesamt für Umwelt und Geologie, Freiberg
- Herrmann O, Credner H (1886) Geologische Spezialkarte des Königreichs Sachsen. 1:25000, Blatt 4648 Ortrand (vormals Blatt: Schönfeld Ortrand), 1 Edition, Königliches Finanzministerium, Leipzig
- Hess von Wichdorff H (1927) Geologische Karte von Preußen und benachbarten deutschen Ländern. 1:25000, Blatt 4448 Lauchhammer-Grünwalde, (vormals Blatt: Klein-Leipisch), 1 Edition, Preußische Geologische Landesanstalt, Berlin
- Hoffmann G, Reicherter K (2012) Soft-sediment deformation of Late Pleistocene sediments along the southwestern coast of the Baltic Sea (NE Germany). *Int J Earth Sci* 101:351-363
- Höfle HC, Deichmüller J, Hofmann W, Irrlitz W, Komodromos A, Preuss H, Tüxen J, Mengeling H, Meyer KD, Schlenker B (1976) Erläuterungen zu Blatt 2717 Schwanewede, Geologische Karte von Niedersachsen 1:25000. Niedersächsisches Landesamt für Bodenforschung, Hannover, p 72
- Höfle HC (1977) Manuskriptkarte und Legende zur geologischen Übersichtskartierung von Niedersachsen 2831 Göhrde 1:25000, Niedersächsisches Landesamt für Bodenforschung, Hannover
- Hübscher C, Lykke-Andersen H, Hansen MB, Reicherter K (2004) Investigating the structural evolution of the western Baltic. *Eos Trans Am Geophys Union* 85:115-115
- Huntley DJ, Lamothe M (2001) Ubiquity of anomalous fading in K-feldspars and the measurement and correction for it in optical dating. *Can J Earth Sci* 38:1093-1106
- Hürtgen J (2017) The First Paleoseismic Database of Germany and Adjacent Regions PalSeisDB v1.0, Dissertation, Rheinisch-Westfälischen Technischen Hochschule Aachen, p 478
- Huster H, Hübscher C, Seidel E (2020) Impact of Late Cretaceous to Neogene plate tectonics and Quaternary ice loads on supra-salt deposits at Eastern Glückstadt Graben, North German Basin. *Int J Earth Sci* 109:1029-1050



- Jordan H, Besenecker H, Cosack E, Dahms E, Fauth H, Gramann F, Heinemann B, Hofmeister E, Kosmahl W, Merkt J, Schneekloth H, Tüxen J (1979) Erläuterungen zu Blatt 3521 Rehburg, Geologische Karte von Niedersachsen 1:25000. Niedersächsisches Landesamt für Bodenforschung, Hannover, p 134
- Jordan H, Cosack E, Dahms E, Eckelmann W, Groba E, Irrlitz W, Kockel F, Schneekloth H, Tüxen J (1980) Erläuterungen zu Blatt 3422 Neustadt am Rübenberge, Geologische Karten von Niedersachsen 1:25000. Niedersächsisches Landesamt für Bodenforschung, Hannover, p 88
- Keilhack K, Kraiss A, Renner O, Harbort E, Stoller J (1917) Erläuterungen zum Blatt 4018 Lage, Geologische Karte von Preußen und benachbarten Bundesstaaten 1:25000. Königliche Preußische Geologische Landesamt, Berlin, p 55
- Klemm G, Credner H (1886) Geologische Spezialkarte des Königreichs Sachsen. 1:25000, Blatt 4647 Hirschfeld (vormals Blatt: Grossenhain-Skässchen), 1 Edition, Königliches Finanzministerium, Leipzig
- Knoth W (1992) Geologische Übersichtskarte von Sachsen-Anhalt 1:400000, Geologisches Landesamt Sachsen-Anhalt, Halle/Saale, 1 Edition, Halle
- Koch E, Geissler E, Eilers H, Fritzsche H (1996a) Geologische Karte der eiszeitlich bedeckten Gebiete von Sachsen, 1:50000, Blatt 2465 Bitterfeld, 1 Edition, Sächsisches Landesamt für Umwelt und Geologie, Freiberg
- Koch E, Geissler E, Eilers H, Fritzsche H (1996b) Geologische Karte der eiszeitlich bedeckten Gebiete von Sachsen, 1:50000, Blatt 2666 Mittweida, 1 Edition, Sächsisches Landesamt für Umwelt und Geologie, Freiberg
- Koch E, Geissler E, Eilers H, Fritzsche H (1996c) Geologische Karte der eiszeitlich bedeckten Gebiete von Sachsen, 1:50000, Blatt 2665 Zeitz, 1 Edition, Sächsisches Landesamt für Umwelt und Geologie, Freiberg
- Koert W, Dienemann W (1927) Erläuterungen zu Blatt 3832 Welfensleben (Hötensleben), Geologische Karte von Preußen und benachbarten deutschen Ländern 1:25000. Preußische Geologische Landesanstalt, Berlin, p 88
- Korn J, Stoller J, Zimmermann IE (1923) Erläuterungen zu Blatt 3736 Zielitz (Niegripp), Geologische Karte von Preußen und benachbarten Bundesstaaten 1:25000. Preußische Geologische Landesanstalt, Berlin, p 55
- Kraiß A, Picard E (1922) Erläuterungen zu Blatt 4437 Halle an der Saale (Nord), Geologische Karte von Preußen und benachbarten Bundesstaaten 1:25000. Preußische Geologische Landesanstalt, Berlin, p 86
- Krentz O, Stanek K (2015) Die Lausitzer Überschiebung zwischen Meißen und Jeschken – neue Aspekte. *Ber Naturforsch Ges Oberlausitz* 23:123-137
- Krienke H-D, Nagel D, Bremer F, Heck H-L, Müller U, Schulz W (2001) Geologische Karte von Mecklenburg-Vorpommern 1:200000, Geologisches Landesamt Mecklenburg-Vorpommern, Güstrow
- Kunert R, Altermann M, Schmidt B, Schmidt E (1963) Erläuterungen zu Blatt 4336 Könnern, Geologische Spezialkarte der Deutschen Demokratischen Republik 1:25000. Zentrales Geologisches Institut, Berlin, p 205
- Kühn B, Dammer B (1901/02) Geologische Karte 1:25000, Blatt 4940 Altenburg Nord (vormals Blatt: Windischleuba (Regis), 1 Edition, Königliche Preußische Geologische Landesanstalt, Berlin
- Kühn B (1906a) Geologische Karte 1:25000, Blatt 4939 Meuselwitz, 1 Edition, Königliche Preußische Geologische Landesanstalt, Berlin
- Kühn B (1906b) Erläuterungen zur Geologischen Karte 1:25000 von Preußen und benachbarten Bundesstaaten, Blatt 4939 Meuselwitz. Königliche Preußische Geologische Landesanstalt, Berlin, p 67
- Lang HD, Anrich H, Baldschuhn R, Heine HW, Heinemann B, Irrlitz W, Resch M, Schneekloth H (1980) Erläuterungen zu Blatt 3224 Westenholz, Geologische Karte von Niedersachsen 1:25000. Niedersächsisches Landesamt für Bodenforschung, Hannover, p 98
- Lang J, Lauer T, Winsemann J (2018) New age constraints for the Saalian glaciation in northern central Europe: implications for the extent of ice sheets and related proglacial lake systems. *Quat Sci Rev* 180:240-259

- Lange JM, Alexowsky W, Haubold F (2016) Die Entwicklung der Elbe und ihr Einfluss auf die quartäre Landschaftsformung in der Umgebung von Dresden. In: Faust D, Heller K (eds), Erkundungen in Sachsen und Schlesien. Quartäre Sedimente im landschaftsgenetischen Kontext. Exkursionsführer DEUQUA-Tagung, Dresden, Geozon Science Media, Berlin, p 13-30
- Lee JR, Phillips ER (2008) Progressive soft-sediment deformation within a subglacial shear zone – a hybrid mosaic-pervasive deformation model for Middle Pleistocene glaciotectonised sediments from eastern England. *Quat Sci Rev* 27:1350-1362
- Lepper J, Tüxen J (1975) Geologische Übersichtskartierung 2932 Dannenberg (Elbe) Süd 1:25000. Niedersächsisches Landesverwaltungsamt, 8 Edition, Hannover
- Leydecker G (2011) Erdbebenkatalog für die Bundesrepublik Deutschland mit Randgebieten für die Jahre 800 bis 2008. *Geol Jb E* 59, Hannover, p 198
- Li Q, Liu M, Stein S (2009) Spatiotemporal complexity of continental intraplate seismicity: insights from geodynamic modeling and implications for seismic hazard estimation. *Bull Seismol Soc Am* 99:52-60
- Liebe KT (1878) Geologische Karte 1:25000, Blatt 5039 Kayna (vormals Blatt: Grossenstein), 1 Edition; Königliches Finanzministerium, Leipzig
- von Linstow O, Beyschlag F (1913) Geologische Karte von Preußen und benachbarten Bundesstaaten. 1:25000, Blatt 4339 Bitterfeld (West), 1 Edition, Königliche Preußische Geologische Landesanstalt, Berlin
- Liu M, Stein S, Wang H (2011) 2000 years of migrating earthquakes in North China: How earthquakes in midcontinents differ from those at plate boundaries. *Lithosphere* 3:128-132
- Lorenz W (2000) Geologische Karte der eiszeitlich bedeckten Gebiete von Sachsen, 1:50000, Blatt 2669 Bautzen, 1 Edition, Sächsisches Landesamt für Umwelt und Geologie, Freiberg
- Ludwig AO (2011) Zwei markante Stauchmoränen: Peski/Belarusland und Jasmund, Ostseeinsel Rügen/Nordostdeutschland - Gemeinsame Merkmale und Unterschiede. *E & G - Quat Sci J* 60:464-487
- McCalpin, JP (2009) Paleoseismology, 2 Edition, *Int Geophys Ser* pp 95:613
- Meinsen J, Winsemann J, Roskosch J, Brandes C, Frechen M, Dultz S, Böttcher J (2014) Climate control on the evolution of Late Pleistocene alluvial-fan and aeolian sand-sheet systems in NW Germany. *Boreas* 43:42-66
- Mejdahl V (1979) Thermoluminescence dating: Beta-dose attenuation in quartz grains. *Archaeometry* 21:61-72
- Mestwerdt A (1914) Erläuterungen zu Blatt 3631 Groß-Twülpstedt, Geologische Karte von Preußen und benachbarten Bundesstaaten 1:25000. Königliche Preußische Geologische Landesanstalt, Berlin, p 56
- Meyer KD, Boess J, Grimmelmann W, Kuster H, Resch M, Röhling H-G, Tüxen J (2004) Erläuterungen zu Blatt 2730 Bleckede, Geologische Karte von Niedersachsen 1:250000. Niedersächsisches Landesamt für Bodenforschung, Hannover, p 136
- Mietzsch H, Credner H (1875) Geologische Spezialkarte des Königreichs Sachsen. 1:25000, Blatt 5241 Zwickau Ost (vormals Blatt Lichtenstein), 1 Edition, Königliches Finanzministerium, Leipzig
- Müller A, Walther S, Geissler E, Eilers H, Baumgarten G (1995a) Geologische Karte der eiszeitlich bedeckten Gebiete von Sachsen, 1:50000, Blatt 2466 Eilenburg, 1 Edition, Sächsisches Landesamt für Umwelt und Geologie, Freiberg
- Müller A, Walther S, Geissler E, Eilers H, Eilers G (1995b) Geologische Karte der eiszeitlich bedeckten Gebiete von Sachsen. 1:50000, Blatt 2566 Wurzen, 1 Edition, Sächsisches Landesamt für Umwelt und Geologie, Freiberg
- Müller K, Polom U, Winsemann J, Steffen H, Tsukamoto S, Günther T, Igel J, Spies T, Lege T, Frechen M, Franzke H-J, Brandes C (2020) Structural style and neotectonic activity along the Harz Boundary Fault, northern Germany: A multimethod approach integrating geophysics, outcrop data and numerical simulations. *Int J Earth Sci* 109:1811-1835
- Munier R, Adams J, Brandes C, Brooks G, Dehls J, Gibbons SJ, Hjartardóttir ÁR, Hogaas F, Johansen TA, Kvaerna T, Mattila J, Mikko H, Müller K, Nikolaeva SB, Ojala A, Olesen O, Olsen L, Palmu J-P, Ruskeeniemi T, Ruud BO, Sandersen PBE, Shvarev SV, Smith CA, Steffen H, Steffen R,

- Sutinen R, Tassis G (2020) International database of Glacially Induced Faults. Pangaea, <https://doi.pangaea.de/10.1594/PANGAEA.922705>
- Murray AS, Wintle AG (2000) Luminescence dating of quartz using an improved single-aliquot regenerative-dose protocol. *Radiat Meas* 32:57-73
- Nibis Kartenserver (2018) Karten und Daten des Niedersächsischen Bodeninformationssystems NIBIS. URL: <http://nibis.lbeg.de/cardomap3/> (Accessed 26.02.2018)
- Obermeier SF (2009) Using liquefaction-induced and other soft-sediment features for paleoseismic analysis. In: McCalpin JP (ed), *Paleoseismology*. Int Geophys Ser 95, Elsevier, Amsterdam, pp 497-564
- Péwé TL (1973) Ice wedge casts and past permafrost distribution in North America. *Geoforum* 4:15-26
- Phillips ER, Lee JR, Burk, H (2008) Progressive proglacial to subglacial deformation and syntectonic sedimentation at the margins of the Mid-Pleistocene British Ice Sheet: evidence from north Norfolk, UK. *Quat Sci Rev* 27:1848-1871
- Picard E, Wieggers F (1908) Erläuterungen zu Blatt 3634 Bülstringen (Uthmöden), Geologische Karte von Preußen und benachbarten Bundesstaaten 1:25000. Königliche Preußische Geologische Landesanstalt, Berlin, p 22
- Picard E, Beyschlag F (1922) Geologische Karte von Preußen und benachbarten Bundesstaaten. 1:25000, Blatt 4440 Delitzsch, 1 Edition, Preußische Geologische Landesanstalt, Berlin
- Picard E (1930) Geologische Karte von Preußen und benachbarten deutschen Ländern. 1:25000, Blatt 4544 Belgern, 1 Edition, Preußische Geologische Landesanstalt, Berlin
- Pietzsch K (1913) Geologische Spezialkarte von Sachsen 1:25000, Blatt 5049 Pirna, 2 Edition, Finanzministerium, Leipzig
- Pietzsch K, Kossmat F (1914/16) Geologische Karte von Sachsen 1:25000, Blatt 4946 Mohorn (vormals Blatt: Tanneberg-Deutschenbora), 2 Edition, Finanzministerium Leipzig
- Pisarska-Jamrózy M, Belzyt S, Börner A, Hoffmann G, Hüneke H, Kenzler M, Obst K, Rother H, Van Loon AT (2018) Evidence from seismites for glacio-isostatically induced crustal faulting in front of an advancing land-ice mass (Rügen Island, SW Baltic Sea). *Tectonophysics* 745:338-348
- Pisarska-Jamrózy M, Belzyt S, Börner A, Hoffmann G, Hüneke H, Kenzler M, Obst K, Rother H, Steffen H, Steffen R, Van Loon AT (2019) The sea cliff at Dwasieden: soft-sediment deformation structures triggered by glacial isostatic adjustment in front of the advancing Scandinavian ice-sheet. *DEUQUASP* 2:61-67
- Prescott JR, Hutton JT (1994) Cosmic ray contributions to dose rates for luminescence and ESR dating: large depths and long-term time variations. *Radiat Meas* 23:497-500
- Radzinski K-H, Hoyningen-Huene E, Kriebel U, Schulze G (1962) Erläuterungen zum Blatt 4536 Teutschenthal, Geologische Spezialkarte der Deutschen Demokratischen Republik 1:25000, Halle, p 287
- Rees-Jones J (1995) Optical dating of young sediments using fine-grain quartz. *Anc TL* 13:9-14
- Reuter G (1975a) Manuskriptkarte zur geologischen Übersichtskartierung auf 2832 Dannenberg (Elbe) 1:25000, Niedersächsisches Landesverwaltungsamt, Hannover
- Reuter G (1975b) Manuskriptkarte zur geologischen Übersichtskartierung auf 2933 Gusborn 1:25000, Niedersächsisches Landesverwaltungsamt, Hannover
- Rodríguez-Pascua MA, Calvo JP, De Vicente G, Gómez-Gras D (2000) Soft-sediment deformation structures interpreted as seismites in lacustrine sediments of the Prebetic Zone, SE Spain, and their potential use as indicators of earthquake magnitudes during the Late Miocene. *Sediment Geol* 135:117-135
- Sauer A, Credner H (1880) Geologische Spezialkarte des Königreichs Sachsen 1:25000, Blatt 4741 Naunhof, 1 Edition, Königliches Finanzministerium, Leipzig
- Schalch F, Credner H (1881) Geologische Spezialkarte des Königreichs Sachsen 1:25000, Blatt 4641 Taucha (vormals Blatt: Brandis), 1 Edition, Königliches Finanzministerium, Leipzig
- Schmid EE (1875) Geologische Spezialkarte des Königreichs Sachsen 1:25000, Blatt 4937 Osterfeld, 1 Edition, Königliche Geologische Landesanstalt, Berlin

- Scholz M (1887a) Erläuterungen zu Blatt 3434 Gardelegen, Geologische Spezialkarte von Preußen und den Thüringischen Staaten 1:25000. Königliche Preußische Geologische Landesanstalt, Berlin, p 31
- Scholz M (1887b) Erläuterungen zu Blatt 3435 Lindstedt (Uchtspringe), Geologische Spezialkarte von Preußen und den Thüringischen Staaten 1:25000. Königliche Preußische Geologische Landesanstalt, Berlin, p 33
- Scholz CH, Gupta A (2000) Fault interactions and seismic hazard. *J Geodyn* 29:459-467
- Scholz CH (2002) *The mechanics of earthquakes and faulting*. 2 Edition, Cambridge University Press, p 471
- Schröder H, Dahlgrün F, Görz G (1927) Erläuterungen zu Blatt 4131 Derenburg, Geologische Karte von Preußen und benachbarten deutschen Ländern 1:25000, Berlin, p 80
- Schröder H, Behrend F, Fulda E (1929a) Erläuterungen zu Blatt 4032 Schwanebeck, Geologische Karte von Preußen und benachbarten deutschen Ländern 1:250000. Preußische Geologische Landesanstalt, Berlin, p 32
- Schröder H, Behrend F, Fulda E (1929b) Erläuterungen zu Blatt 4031 Dingelstedt am Huy, Geologische Karte von Preußen und benachbarten deutschen Ländern 1:25000. Preußische Geologische Landesanstalt, Berlin, p 49
- Schröder H, Behrend F, Fulda E (1931) Erläuterungen zu Blatt 4029 Vienenburg, Geologische Karte von Preußen und benachbarten Ländern 1:25000. Königliche Preußische Geologische Landesanstalt, Berlin, p 104
- Schwartz DP, Coppersmith KJ (1984) Fault behavior and characteristic earthquakes: Examples from the Wasatch and San Andreas fault zones. *J Geophys Res* 89:5681-5698
- Seidel G, Steinmüller A (1994) Geologische Karte von Thüringen. 1:25000, Blatt 4936 Camburg, 3 Edition, Thüringer Landesanstalt für Bodenforschung, Weimar
- Siebert T, Credner H (1881) Geologische Karte des Königreichs Sachsen 1:25000, Blatt 5140 Meerane-Crimmitschau (vormals Blatt: Meerane), 1 Edition, Königliches Finanzministerium, Leipzig
- Siebert T, Credner H (1884) Geologische Spezialkarte des Königreichs Sachsen 1:25000, Blatt 4744 Oschatz (vormals Blatt: Oschatz-Mügeln), 1 Edition, Königliches Finanzministerium, Leipzig
- Siebert L, Penck A, Credner H (1900) Geologische Spezialkarte des Königreichs Sachsen 1:25000, Blatt 4842 Colditz (vormals Blatt: Colditz-Grossbothen), 2 Edition, Königliches Finanzministerium, Leipzig
- Siebert T, Schalch F, Credner H (1903) Geologische Spezialkarte des Königreichs Sachsen 1:25000, Blatt 4641 Brandis Borsdorf (vormals Blatt: Taucha), 2 Edition, Königliches Finanzministerium, Leipzig
- Siebert T, Credner H (1904) Geologische Spezialkarte des Königreichs Sachsen 1:25000, Blatt 5140 Meerane-Crimmitschau, 2 Edition, Königliches Finanzministerium, Leipzig
- Siebert T, Credner H (1906) Geologische Spezialkarte des Königreichs Sachsen 1:25000, Blatt 4744 Oschatz (vormals Blatt: Oschatz-Mügeln), 2 Edition, Königliches Finanzministerium, Leipzig
- Siebert L, Bärtling R (1909) Erläuterungen zu Blatt 4638 Merseburg Ost (Leuna), Geologische Karten von Preußen und benachbarten Bundesstaaten 1:25000. Königliche Preußische Geologische Landesanstalt, Berlin, p 67
- Siebert L (1909) Erläuterungen zu Blatt 4738 Lützen (Bad Dürrenberg), Geologische Karte von Preußen und benachbarten Bundesstaaten 1:25000. Königliche Preußische Geologische Landesanstalt, Berlin, p 75
- Sieh K, Jones L, Hauksson E, Hudnut K, Eberhart-Phillips D, Heaton T, Hough S, Hutton K, Kanamori H, Lilje A, Lindvall S, McGill SF, Mori J, Rubin C, Spotila JA, Stock J, Thio HK, Treiman J, Wernicke B, Zachariasen J (1993) Near-field investigations of the Landers earthquake sequence, April to July 1992. *Science* 260:171-176
- Speyer O (1875/76) Geologische Spezialkarte von Preußen und den Thüringischen Staaten 1:25000, Blatt 4535 Schraplau, 1 Edition, Königliche Geologische Landesanstalt, Berlin
- Stackebrandt W (2008) Zur Neotektonik der Niederlausitz. *Z Dtsch Ges Geowiss* 159:117-122

- Steding D, Horth K, Eilers H, Eilers G (1994) Geologische Karte der eiszeitlich bedeckten Gebiete von Sachsen 1:50000, Blatt 2668 Dresden, 1 Edition, Sächsisches Landesamt für Umwelt und Geologie, Freiberg
- Steding D, Geissler H, Eilers H, Eilers G (1995) Geologische Karte der eiszeitlich bedeckten Gebiete von Sachsen 1:50000, Blatt 2568 Großenhain, 1 Edition, Sächsisches Landesamt für Umwelt und Geologie, Freiberg
- Steding D, Geissler H, Eilers H, Eilers G (1996a) Geologische Karte der eiszeitlich bedeckten Gebiete von Sachsen 1:50000, Blatt 2567 Riesa, 1 Edition, Sächsisches Landesamt für Umwelt und Geologie, Freiberg
- Steding D, Geissler H, Eilers H, Fritzsche H (1996b) Geologische Karte der eiszeitlich bedeckten Gebiete von Sachsen 1:50000, Blatt 2667 Meißen, 1 Edition, Sächsisches Landesamt für Umwelt und Geologie, Freiberg
- Stein S, Liu M, Camelbeeck T, Merino M, Landgraf A, Hintersberger E, Kübler S (2015) Challenges in assessing seismic hazard in intraplate Europe. *Geol Soc Lon Spec Publ* 432:13-28
- Steinmüller A (1993) Geologische Karte von Thüringen 1:25000, Blatt 4937 Osterfeld, 2 Edition, Thüringer Landesanstalt für Bodenforschung, Weimar
- Stewart IS, Sauber J, Rose J (2000) Glacio-seismotectonics: ice sheets, crustal deformation and seismicity. *Quat Sci Rev* 19:1367-1389
- Stoller J (1915) Erläuterungen zu Blatt 3227 Eschede, Geologische Karte von Preußen und benachbarten Bundesstaaten 1:25000. Königliche Preußische Geologische Landesanstalt, Berlin, p 54
- Talwani P (1988) The intersection model for intraplate earthquakes. *Seismol Res Lett* 59:305-310
- Talwani P (2014) *Intraplate earthquakes*. Cambridge University Press, New York, pp 338
- Talwani P (2017) On the nature of intraplate earthquakes. *J Seismol* 21:47-68
- TLUBN (2020) Kartendienst Seismologie in Mitteldeutschland. URL: <http://www.tlug-jena.de/erdbeben> (Accessed 1.11.2020)
- Trautmann T, Krbetschek MR, Dietrich A, Stolz W (1999) Feldspar radioluminescence: a new dating method and its physical background. *J Lumin* 85:45-58
- Vandenbergh J (2013) Cryoturbation Structures. In: Elias SA (ed), *The Encyclopedia of Quaternary Science*, 3, Elsevier, Amsterdam, pp 430-435
- Voss HH, Bauer G, Dahms E, Gramann F, Heine HW, Hofmeister E, Irrlitz W, Mayrhofer H, Merkt J, Scherler PC, Schneekloth H, Tüxen J (1979) Erläuterungen zu Blatt 3522 Wunstorf, Geologische Karte von Niedersachsen 1:25000. Niedersächsisches Landesamt für Bodenforschung, Hannover, p 102
- Voss HH, Fansa M, Gramann F, Hedemann HA, Irrlitz W, Jaritz W, Kosmahl W, Plaumann S, Roeschmann G, Scherler PC, Schütte H (1982) Erläuterungen zu Blatt 3421 Husum, Geologische Karte von Niedersachsen 1:25000. Niedersächsisches Landesamt für Bodenforschung, Hannover, p 130
- Wansa S, Radzinski KH, Berger C, Blumenstengel H, Friedel CH, Hartmann KJ, Herold U, Karpe P, Kater R, Müller DW, Rappsilber I, Schroeter A, Schumann G, Sommerwerk K, Thomae M (2004) Erläuterungen zu Blatt 4636 Müncheln, Geologische Karte von Sachsen-Anhalt 1:25000. Landesamt für Geologie und Bergwesen Sachsen-Anhalt, Halle p 143
- Weissermel W (1901) Erläuterungen zu Blatt 2935 Schnackenburg, Geologische Karte von Preußen und den Thüringischen Staaten 1:25000. Königliche Preußische Geologische Landesanstalt, Berlin, p 19
- Weissermel W, Picard E, Quitzow W, Kühn B, Dammer B (1909) Erläuterungen zu Blatt 4438 Landsberg, Geologische Karte von Preußen und benachbarten Bundesstaaten 1:25000. Königliche Preußische Geologische Landesanstalt, Berlin, p 17
- Weissermel W, Dahlgrün F (1926) Erläuterungen zu Blatt 4233 Ballenstedt, Geologische Karte von Preußen und benachbarten Ländern 1:25000. Preußische Geologische Landesanstalt, Berlin, p 78
- Wells DL, Coppersmith KJ (1994) New empirical relationships among magnitude, rupture length, rupture width, rupture area, and surface displacement. *Bull Seismol Soc Am* 84:974-1002
- Wesnousky SG (2006) Predicting the endpoints of earthquake ruptures. *Nature* 444:358-360

- Weymann HJ (2004) Die mittelpleistozäne Flußentwicklung im nord-östlichen Harzvorland. Petrographie, Terrassenstratigraphie. Geol Beitr Hann 6:3-116
- Wieggers F (1914) Erläuterungen zu Blatt 3535 Dolle, Geologische Karte von Preußen und benachbarten Bundesstaaten 1:25000. Berlin, p 27
- Williams GD, Powell CM, Cooper MA (1989) Geometry and kinematics of inversion tectonics. In: Cooper MA, Williams GD (eds), Inversion Tectonics. Geol Soc Spec Publ, London, 44, pp 3-15
- Winsemann J, Brandes C, Polom U (2011) Response of a proglacial delta to rapid high-amplitude lake-level change: an integration of outcrop data and high-resolution shear wave seismics. Basin Res 23:22-52
- Winsemann J, Lang J, Polom U, Loewer M, Igel J, Pollok L, Brandes C (2018) Ice-marginal forced regressive deltas in glacial lake basins: geomorphology, facies variability and large-scale depositional architecture. Boreas 47:973-1002
- Wintle AG (1973) Anomalous fading of thermo-luminescence in mineral samples. Nature 245:143-144
- Wintle AG, Murray AS (2006) A review of quartz optically stimulated luminescence characteristics and their relevance in single-aliquot regeneration dating protocols. Radiat Meas 41:369-391
- Wolf L, Berger HJ, Leonhard D (1998) Geologische Karte der eiszeitlich bedeckten Gebiete von Sachsen, 1:50000, Blatt 2766 Chemnitz, 1 Edition, Sächsisches Landesamt für Umwelt und Geologie, Freiberg
- Woltstedt P, Görz G (1929) Erläuterungen zu Blatt 3530 Wolfsburg, Geologische Karte von Preußen und benachbarten deutschen Ländern 1:25000. Preußische Geologische Landesanstalt, Berlin, p 71
- Worsley P (2014) Ice-wedge growth and casting in a Late Pleistocene periglacial, fluvial succession at Baston, Lincolnshire. Mercian Geol 18:159-170

## 9. Appendix

### 9.1 Supplementary data to luminescence dating (Steinhuder Meer Fault)

A growth-strata package indicative of sedimentation during deformation, has developed at one deformation band with a large offset. Luminescence dating of the growth-strata package was carried out to estimate the timing of fault movement. Coarse-grained samples were taken close to the Steinhuder Meer Fault in a sand pit near Altenhagen (pit 89) and measured using the IRSL method.

#### *Dose rate determination*

The radionuclide concentrations of uranium (U), thorium (Th), and potassium (K) were measured using high-resolution gamma spectrometry. 700 g of the sediment surrounding each sample were dried (130 °C) homogenized and packed into so-called Marinelli-beakers. To achieve an equilibrium between radon and its daughter nuclides, the samples were stored for at least six weeks before measuring. The radiation dose rates were calculated by using the conversion factors of Guérin et al. (2011) and the beta attenuation factors of Mejdahl (1979). An  $a$ -value of  $0.09 \pm 0.02$  for feldspar was used (Rees-Jones 1995). The in-situ water content of all samples was measured and used for the calculation of the attenuation caused by the contained water and for the correction of the  $\alpha$ -,  $\beta$ - and  $\gamma$ -dose rates. The cosmic dose rate was calculated taking into account altitude, geomagnetic latitude and sediment thickness according to Prescott and Hutton (1994). The results of the dose rate determination are listed in Table A3.

#### *Sample preparation*

The preparation of the samples for luminescence measurements was carried out under subdued red light in the luminescence laboratory. The outer ends (2 cm) of the undisturbed material in cylinders were removed to exclude any sediment that was exposed to light. For the luminescence measurement 50 - 100 g of the sample material was dried at  $\leq 50$  °C and chemically treated with 10% hydrochloric acid (HCl) until the reaction stopped. Afterwards, 200 ml disodium oxalate ( $\text{Na}_2\text{C}_2\text{O}_4$ ) was added for 2 hours and 30% hydrogen peroxide ( $\text{H}_2\text{O}_2$ ) was added for 12 hours to dissolve carbonates, break up aggregates and to eliminate the organic matter. Coarse-grained samples were sieved before they were chemically treated to obtain the following fractions:  $>250$   $\mu\text{m}$ , 200 - 250  $\mu\text{m}$ , 150 - 200  $\mu\text{m}$ , 100 - 150  $\mu\text{m}$ ,  $<100$   $\mu\text{m}$ . The fraction 150 - 200  $\mu\text{m}$  was chosen for further analysis. A separation of feldspar and quartz minerals was implemented by using sodium polytungstate ( $2.62 \text{ g cm}^{-3}$ ). This procedure was implemented twice more with densities of  $2.58 \text{ g cm}^{-3}$  and  $2.70 \text{ g cm}^{-3}$ . Sodium polytungstate with a density of  $2.58 \text{ g cm}^{-3}$  was used for the separation of potassium feldspar and plagioclase and a density of  $2.70 \text{ g cm}^{-3}$  was used for the separation of quartz and heavy minerals. For the quartz aliquots, a part of the sample was treated with 40% hexafluorosilicic acid ( $\text{H}_2\text{SiF}_6$ ) to remove the outer layers of the minerals affected by  $\alpha$  radiation. Finally, the feldspar aliquots were mounted on stainless steel discs using silicone to measure the luminescence signal.



## 9. Appendix

Table A3: Dosimetry results and dose rates for the samples from Altenhagen (pit 89). An a-value of  $0.09 \pm 0.02$  was used for the feldspar samples.

Sample	Water content (%)	Depth (m)	Radionuclide concentrations			Dose rate				
			Potassium (%)	Thorium (ppm)	Uranium (ppm)	$D_\alpha$ ( $\text{mGy a}^{-1}$ )	$D_\beta$ ( $\text{mGy a}^{-1}$ )	$D_\gamma$ ( $\text{mGy a}^{-1}$ )	$D_{\text{cosmic}}$ ( $\text{mGy a}^{-1}$ )	Feldspar ( $\text{mGy a}^{-1}$ )
Alt-1	3±1	2.4	1.03±0.01	1.46±0.02	0.46±0.01	0.16±0.02	0.36±0.09	1.43±0.0	0.21±0.2	1.53±0.3
Alt-2	3±1	2	1.00±0.01	1.50±0.02	0.46±0.01	0.16±0.02	1.64±0.12	0.35±0.0	0.21±0.2	1.50±0.3

### ***Luminescence measurements***

Feldspar luminescence signals were measured with one automated Risø TL/OSL reader (DA-20) with calibrated  $^{90}\text{Sr}/^{90}\text{Y}$  beta source (1.48 GBq = 40 mCi). The quartz signal was stimulated by blue LED diodes, emitting at 470 nm and detected through a Hoya U-340 filter. A single aliquot regenerative dose (SAR) protocol (Murray and Wintle 2000) was applied for equivalent dose ( $D_e$ ) determination.

Sample Alt-1 provided reliable luminescence ages. The dose recovery ratios Alt-1  $0.81 \pm 0.01$  for the pulsed IR<sub>50</sub> signal and for sample Alt-2  $0.84 \pm 0.02$  confirm that the applied SAR protocol (Table A4) was suitable for the  $D_e$  measurements. However, the value 0.9 - 1.1 (Wintle and Murray 2006) was not achieved. Further analysis represented nearly the same dose recovery ratio.

The pulsed IR<sub>50</sub> signal of the fine grain fraction yielded a recycling ratio of  $1.01 \pm 0.03$ . This value is within 10% of unity (cf. Wintle and Murray, 2006) and confirms that the SAR protocol corrected sensitivity changes successfully during the measurements.

Table A4: SAR protocol used for equivalent dose determination of feldspar samples taken at the Steinhuder Meer Fault.

Step	Treatment	Observed
	Feldspar IRSL (polym mineral)	
1	Give dose	
2	Preheat, 250°C, 60 s	
3	Pulsed IRSL, 50°C, 500 s <sub>a</sub>	Lx
4	Test dose	
5	Preheat, 250°C, 60 s	
6	Pulsed IRSL, 50°C, 500 s <sub>a</sub>	Tx
7	Return to step 1	

(a) 100 ms on and 400 ms off.

### ***Fading test and age calculation***

The fading test gave a mean g-value of  $2.82 \pm 0.19$  %. The pulsed IR<sub>50</sub> ages (Alt-1  $118 \pm 1.5$  ka) and (Alt-2  $141 \pm 1.5$  ka) was fading corrected using the R-software (R version 3.3.2.) based on Huntley and Lamothe (2001).

The estimated dosimetry results and dose rates from the samples from Altenhagen (pit 89) are listed in Table A3. The OSL ages were calculated by dividing the  $D_e$  by the total  $D_R$ . The estimated luminescence ages are  $158 \pm 4$  for Alt-1 and  $189 \pm 5$  ka for Alt-2. The fading corrected feldspar ages are listed in Table A5.

The estimated IRSL ages ( $189 \pm 5$  ka to  $158 \pm 4$  ka; Table A5) indicate Middle Pleistocene Saalian fault activity. This implies that the shear-deformation bands most likely developed during the Middle Pleistocene Saalian glaciations.

Table A5: Feldspar luminescence ages from Altenhagen (pit 89).

Sample	feldspar	uncorr.	corr.
	$D_e$ (Gy)	Age (ka)	Age (ka) corr
Alt-1	$180.37 \pm 4.34$	$118 \pm 1.5$	$158 \pm 4$
Alt-2	$211.07 \pm 15$	$141 \pm 1.5$	$189 \pm 5$

## 9.2 Outcrop locations

Table A6: Sand and gravel pits and one sinkhole along the Harz Boundary Fault in the Subhercynian Basin.

No	Locality	Coordinates	Geological map 1:25000	Geological map 1:50000	Deposits	References	Deformation structures	References
1	Abbenrode	51°56'21.77"N 10°37'6.96"E	4029 Vienenburg	L4128 Goslar	Fluvial gravel overlain by meltwater deposits	Weymann 2004; Field observations	Glaciotectonic features: normal faults	Weymann 2004; Field observations
2	Aschersleben 1	51°45'56.83"N 11°25'30.48"E	4234 Aschersleben	L4334 Aschersleben	Meltwater deposits overlain by fluvial sand and gravel and loess	Weymann 2004; Field observations	Cryoturbation features: convolute bedding	Field observations
3	Aschersleben 2	51°46'32.72"N 11°24'34.09"E	4234 Aschersleben	L4334 Aschersleben	Boulder clay overlain by meltwater deposits, fluvial sand and gravel and loess	Weymann 2004; Field observations	Glaciotectonic features	Weymann 2004
4	Badeborn	51°45'55.94"N 11°16'23.59"E	4233 Ballenstedt	L4332 Quedlinburg	Loess	Weissermel et al. 1926		
5	Benzingerode	51°49'33.02"N 10°52'33.01"E	4131 Derenburg	L4130 Werningerode	Debris flow deposits	Schröder et al. 1927; Field observations	Neotectonic feature: sinkholes with normal and reverse fault	Franzke et al. 2015; Müller et al. 2020; Field observations
6	Beuchte	51°59'11.92"N 10°30'35.01"E	4029 Vienenburg	L4128 Goslar	Fluvial gravel	Schröder et al. 1931; Field observations	Cryoturbation features	Field observations
7	Halberstadt	51°54'25.00"N 11° 5'29.35"E	4032 Schwanebeck	L4132 Halberstadt	Meltwater deposits overlain by loess	Schröder et al. 1929a Field observations		
8	Hoym	51°46'48.30"N 11°20'20.25"E	4234 Aschersleben	L4334 Aschersleben	Meltwater deposits overlain by fluvial sand and gravel, till and loess	Weymann 2004	Glaciotectonic features: recumbent fold	Field observations
9	Lengde	51°59'31.54"N 10°32'56.42"E	4029 Vienenburg	L4128 Goslar	Fluvial gravel	Schröder et al. 1931		
10	Palandsmühle	51°57'42.89"N 10°21'9.40"E	4028 Goslar	L4128 Goslar	Fluvial gravel	Bode et al. 1926		
11	Quedlinburg	51°47'8.52"N 11°10'35.85"E	4232 Quedlinburg	L4332 Quedlinburg	Fluvial gravel overlain by loess	Weymann 2004; Field observations	Cryoturbation features: ice-wedge casts, convolute bedding	Field observations
12	Reinstedt	51°45'53.97"N 11°21'49.91"E	4234 Aschersleben	L4334 Aschersleben	Fluvial gravel overlain by loess	Weymann 2004		
13	Ströbeck	51°54'46.04"N 10°57'25.75"E	4031 Dingelstedt am Huy	L4130 Werningerode	Meltwater deposits overlain by fluvial sand and gravel, till and loess	Schröder et al. 1929b		
14	Suderode	51°58'53.25"N 10°37'40.86"E	4029 Vienenburg	L4128 Goslar	Fluvial gravel overlain by loess	Weymann 2004; Field observations		
15	Warnstedt	51°47'6.07"N 11° 2'5.24"E	4232 Quedlinburg	L4332 Quedlinburg	Meltwater deposits	Weymann 2004; Field observations	Glaciotectonic features: conjugate normal faults, deformation bands, open fold	Weymann 2004; Field observations
16	Westdorf	51°43'48.54"N 11°25'45.69"E	4234 Aschersleben	L4334 Aschersleben	Meltwater deposits overlain by fluvial gravel	Weymann 2004; Field observations	Cryoturbation features	Weymann 2004
17	Wiedelah	51°58'20.93"N 10°34'46.28"E	4029 Vienenburg	L4128 Goslar	Fluvial gravel overlain by loess	Schröder et al. 1931; Field observations	Cryoturbation features: convolute bedding	Field observations

## 9. Appendix

Table A7: Sand pits along the Osning Thrust.

No	Locality	Coordinates	Geological map 1:25000	Geological map 1:50000	Deposits	References	Deformation structures	References
18	Am Ellenberg	52°11'17.47"N 8° 0'0.93"E	3814 Bad Iburg	L3914 Bad Iburg	Meltwater deposits	Haack et al. 1930		
19	Augustdorf 1	51°55'12.72"N 8°44'38.43"E	4018 Lage	L4118 Detmold	Alluvial-fan deposits overlain by mixed alluvial-aeolian and aeolian sand-sheet deposits	Meinsen et al. 2014	Neotectonic and cryoturbation features: irregular branched and stepped dikes, normal faults/joints, deformation bands: normal displacement;	Brandes & Winsemann 2013; Field observations
20	Augustdorf 2	51°54'49.13"N 8°42'55.69"E	4018 Lage	L4118 Detmold	Aeolian dune sand	Keilhack et al. 1917		
21	Müssen	51°57'22.31"N 8°46'52.64"E	4018 Lage	L4118 Detmold	Meltwater deposits overlain by subglacial till	Keilhack et al. 1917		
22	Oerlinghausen	51°56'30.14"N 8°40'25.64"E	4018 Lage	L4118 Detmold	Alluvial -fan deposits, overlain by mixed alluvial-aeolian and aeolian sand-sheet deposits	Meinsen et al. 2014	Neotectonic and cryoturbation features: Sand volcano, sharp-sided dikes, intrusive sedimentary bodies, flame structures, ball-and-pillow structures, small-scale inversion structures;	Brandes & Winsemann 2013; Field observations

Table A8: Sand and gravel pits along the Halle Fault.

No	Locality	Coordinates	Geological map 1:25000	Geological map 1:50000	Deposits	References	Deformation structures	References
23	Gutenberg	51°33'2.04"N 12° 0'10.63"E	4438 Landsberg	L4538 Landsberg	Meltwater deposits	Weissermel et al. 1909; Field observations	Glaciotectonic features: thrust-sheets, reverse faults, folds	Field observations
24	Köchstedt	51°28'29.42"N 11°47'39.24"E	4536 Teutschenthal	L4536 Halle (Saale)	Fluvial deposits	Radzinski et al. 1962; Field observations	Cryoturbation features: ice-wedge casts	Field observations
25	Könnern	51°41'0.52"N 11°44'31.18"E	4336 Könnern	L4226 Bernburg (Saale)	Glaciolacustrine subaqueous fan and glaciofluvial delta deposits overlain by loess	Kunert et al. 1963; Knoth 1992; Field observations	Neotectonic features: deformation bands	Field observations
26	Landsberg	51°30'48.67"N 12° 8'21.54"E	4438 Landsberg	L4538 Landsberg	Meltwater deposits	Weissermel et al. 1909; Field observations		
27	Morl	51°32'43.00"N 11°54'12.05"E	4437 Halle (Saale) Nord	L4536 Halle (Saale)	Palaeogene deposits overlain by Pleistocene deposits	Kraiß et al. 1922; Field observations	Neotectonic features?: deformation bands	Field observation
28	Nehlitz	51°34'40.38"N 11°58'25.50"E	4437 Halle (Saale) Nord	L4536 Halle (Saale)	Meltwater deposits and loess	Kraiß et al. 1922; Field observations		
29	Nellschütz 1	51°12'53.47"N 12° 1'10.28"E	4738 Bad Dürrenberg	L4738 Leipzig West	Fluvial deposits	Siegert 1909; Knoth 1992; Field observations	Cryoturbation features: ball-and-pillow structures, ice-wedge casts	Field observation
30	Nellschütz 2	51°12'40.60"N 12° 2'34.36"E	4738 Bad Dürrenberg	L4738 Leipzig West	Fluvial deposits	Siegert 1909; Knoth 1992; Field observations		

## 9. Appendix

31	Niederwünsch	51°21'32.26"N 11°48'8.70"E	4636 Müncheln	L4736 Merseburg	Glaciofluvial Gilbert-typ delta overlain by subglacial till	Wansa et al. 2004	Cryoturbation features: normal faults, folds	Wansa et al. 2004
32	Schkeitbar	51°14'53.44"N 12°13'9.17"E	4739 Zwenkau	L4738 Leipzig West	Terminal moraine deposits overlain by paraglacial deposits	Hazard 1924; Knoth 1992; Field observations		
33	Schladebach 1	51°18'27.01"N 12° 6'23.52"E	4638 Leuna	L4738 Leipzig West	Fluvial deposits	Siegert et al. 1909; Field observations		
34	Schladebach 2	51°19'38.10"N 12° 5'55.43"E	4638 Leuna	L4738 Leipzig West	Fluvial deposits	Siegert et al. 1909; Field observations	Glaciotectonic features: reverse faults Cryoturbation features: ice- wedge casts	Field observations

Table A9: Sand pits along the Aller Fault.

No	Locality	Coordinates	Geological map 1:25000	Geological map 1:50000	Deposits	References	Deformation structures	References
35	Am Aschenberg 1	52°42'14.82"N 10°15'45.77"E	3227 Eschede	L3326 Celle	Meltwater deposits overlain by paraglacial deposits (Geschiebedecksand)	Stoller et al. 1915	Glaciotectonic features: deformation bands with reverse displacement; fault- propagation fold	Field observations
36	Am Aschenberg 2	52°41'44.79"N 10°16'40.61"E	3327 Lachendorf	L3326 Celle	Meltwater deposits overlain by paraglacial deposits (Geschiebedecksand)	Harbort et al. 1916b		
37	Bahrdorf 1	52°23'23.81"N 10°59'14.76"E	3631 Groß Twülpstedt	L3730 Königslutter am Elm	Meltwater deposits	Mestwerdt et al. 1914		
38	Bahrdorf 2	52°23'26.55"N 10°59'31.64"E	3631 Groß Twülpstedt	L3730 Königslutter am Elm	Meltwater deposits	Mestwerdt et al. 1914	Glaciotectonic features: deformation- and compaction bands; cryoturbation features: ice-wedge casts	Field observations
39	Bissen	53° 3'35.90"N 8°32'55.97"E	2917 Delmenhorst	L2916 Delmenhorst	Meltwater deposits overlain by paraglacial deposits (Geschiebedecksand)	Mestwerdt et al. 1914	Cryoturbation features: ice-wedge casts	Field observations
40	Celle	52°37'4.70"N 10° 2'20.44"E	3326 Celle	L3326 Celle	Meltwater deposits	Field observations		
41	Eggstedt	53°14'8.67"N 8°37'38.96"E	2717 Schwanewede	L2716 Brake (Unterweser)	Glaciolacustrine sand overlain by paraglacial deposits (Geschiebedecksand)	Höfle et al. 1976	Glaciotectonic features: deformation bands with normal displacement; cryoturbation features	Höfle et al. 1976; Field observations
42	Eitze	52°54'27.62"N 9°18'10.45"E	3021 Verden (Aller)	L3120 Verden (Aller)	Meltwater deposits	NiBis Kartenserver 2018	Neotectonic features: deformation bands with normal displacement, conjugate systems	Field observations
43	Fallersleben- Sülfeld	52°25'38.53"N 10°43'4.06"E	3530 Wolfsburg	L3530 Wolfsburg	Fluvial sand	Woldstedt et al. 1929		
44	Filterberg	52°29'50.02"N 10°38'25.72"E	3529 Gifhorn	L3528 Gifhorn	Meltwater deposits	NiBis Kartenserver 2018	Glaciotectonic features: deformation bands with normal and reverse displacement	Field observations

## 9. Appendix

45	Garßen	52°41'27.86"N 10° 8'59.95"E	3326 Celle	L3326 Celle	Meltwater deposits overlain by paraglacial deposits (Geschiebedecksand)	Harbort et al. 1916a	Cryoturbation features: convolute bedding	Field observations
46	Giersberg	53° 0'19.39"N 9° 6'35.93"E	2920 Achim	L2920 Achim	Meltwater deposits overlain by aeolian sand	NiBis Kartenserver 2018		
47	Groß Eicklingen	52°33'34.26"N 10°11'45.61"E	3427 Wienhausen	L3526 Burgdorf	Aeolian dune sand	Harbort et al. 1916c		
48	Groß Eilstorf	52°49'36.11"N 9°26'16.27"E	3122 Häuslingen	L3122 Walsrode	Till overlain by paraglacial deposits (Geschiebedecksand)	NiBis Kartenserver 2018	Glaciotectonic features: deformation bands with normal and reverse displacement; cryoturbation features: ice-wedge casts, folds, remnants of sand volcanoes	Field observations
49	Groß Hehlen	52°39'50.75"N 10° 2'10.84"E	3326 Celle	L3326 Celle	Meltwater deposits overlain by paraglacial deposits (Geschiebedecksand)	Harbort et al. 1916a	Glaciotectonic features: deformation bands with normal displacement, fault-propagation fold	Field observations
50	Hassel	52°47'46.52"N 9°13'29.59"E	3221 Eystrup	L3320 Nienburg (Weser)	Aeolian dune sand	NiBis Kartenserver 2018		
51	Hinter dem Forde	52°58'43.31"N 8° 3'26.42"E	3014 Garrel	L3114 Cloppenburg	Fluvial sand	NiBis Kartenserver 2018		
52	Hinter dem Horn	53°15'42.09"N 8°42'2.56"E	2718 Osterholz-Scharmbeck	L2718 Osterholz-Scharmbeck	Meltwater deposits	NiBis Kartenserver 2018	Glaciotectonic features: folds	Field observations
53	Hohnsleben	52° 9'41.35"N 11° 3'54.89"E	3832 Welfensleben	L3932 Oschersleben (Bode)	Meltwater deposits	Koert et al. 1927		
54	Hülseberg	53°16'27.87"N 8°44'46.09"E	2718 Osterholz-Scharmbeck	L2718 Osterholz-Scharmbeck	Meltwater deposits overlain by paraglacial deposits (Geschiebedecksand)	NiBis Kartenserver 2018	Glaciotectonic features: deformation bands; Cryoturbation features: convolute bedding	Field observations
55	Kästorf	52°32'22.50"N 10°29'51.19"E	3428 Müden/3429 Wesendorf	L3528 Gifhorn	Meltwater deposits overlain by paraglacial deposits (Geschiebedecksand)	NiBis Kartenserver 2018		
56	Kreienmoor	53°12'50.84"N 8°36'8.10"E	2717 Schwanewede	L2716 Brake (Unterweser)	Glaciolacustrine sand overlain by paraglacial deposits (Geschiebedecksand)	Höfle et al. 1976	Cryoturbation features: deformation bands	Höfle et al. 1976
57	Langwedelermoor	52°59'59.59"N 9°10'17.23"E	2921 Ahausen	L2920 Achim	Meltwater deposits	NiBis Kartenserver 2018	Glaciotectonic features: deformation bands with normal displacement, conjugate systems, thrust sheets	Field observations
58	Lunsen	52°58'6.60"N 9° 3'48.79"E	3020 Thedinghausen	L3120 Verden (Aller)	Fluvial sand overlain by floodplain deposits	NiBis Kartenserver 2018		
59	Meinkot	52°23'13.34"N 10°58'23.37"E	3631 Groß Twülpstedt	L3730 Königslutter am Elm	Meltwater deposits	Mestwerdt et al. 1914	Cryoturbation features: ice-wedge casts	Field observations
60	Meißendorf	52°45'10.03"N 9°48'11.43"E	3224 Westenholz	L3324 Wietze	Meltwater deposits overlain by paraglacial deposits (Geschiebedecksand)	Lang et al. 1980		
61	Nordkampen	52°51'44.05"N 9°24'48.82"E	3122 Häuslingen	L3122 Walsrode	Meltwater deposits	NiBis Kartenserver 2018		
62	Ostenholz	52°46'0.90"N 9°43'38.07"E	3224 Westenholz	L3324 Wietze	Meltwater deposits overlain by paraglacial deposits (Geschiebedecksand)	Lang et al. 1980		

## 9. Appendix

63	Sassenburg	52°30'58.13"N 10°38'42.05"E	3429 Wesendorf	L3528 Gifhorn	Meltwater deposits overlain by paraglacial deposits (Geschiebedecksand)	NiBis Kartenserver 2018	Cryoturbation features: ice-wedge casts, deformation bands	Field observations
64	Scheuen	52°40'18.21"N 10° 3'55.91"E	3326 Celle	L3326 Celle	Meltwater deposits overlain by paraglacial deposits (Geschiebedecksand)	Harbort et al. 1916a	Glaciotectonic features: deformation bands with normal displacement, thrust sheets	Field observations
65	Schmede	53° 1'53.31"N 8°23'23.50"E	2916 Hatten	L2916 Delmenhorst	Till overlain by aeolian sand	NiBis Kartenserver 2018	Glaciotectonic features: deformation bands with normal displacement, thrusts, folds; cryoturbation features: convolute bedding	Field observations
66	Tappenbeck	52°28'16.07"N 10°43'18.78"E	3530 Wolfsburg	L3520 Wolfsburg	Meltwater deposits overlain by paraglacial deposits (Geschiebedecksand)	Woldstedt et al. 1929		
67	Walle	52°44'36.01"N 9°54'50.06"E	3225 Offen	L3324 Wietze	Meltwater deposits	Lang et al. 1983		
68	Wesendorf	52°35'26.95"N 10°30'58.82"E	3429 Wesendorf	L3528 Gifhorn	Meltwater deposits overlain by paraglacial deposits (Geschiebedecksand)	NiBis Kartenserver 2018	Cryoturbation features: ice-wedge casts	Field observations
69	Westenholz	52°46'12.35"N 9°42'25.21"E	3224 Westenholz	L3324 Wietze	Meltwater deposits overlain by paraglacial deposits (Geschiebedecksand)	Lang et al. 1980		
70	Wilsche	52°31'41.73"N 10°28'29.73"E	3428 Müden (Aller)	L3528 Gifhorn	Meltwater deposits overlain by paraglacial deposits (Geschiebedecksand)	NiBis Kartenserver 2018		

Table A10: Sand and gravel pits along the Gardelegen Fault.

No	Locality	Coordinates	Geological map 1:25000	Geological map 1:50000	Deposits	References	Deformation structures	References
71	Born	52°22'33.18"N 11°27'28.02"E	3634 Bülstringen	L3734 Haldensleben	Meltwater deposits	Picard et al. 1908		
72	Dolle	52°23'57.24"N 11°37'45.89"E	3535 Dolle	L3534 Hansestadt Gardelegen	Meltwater deposits and till	Wiegiers 1914; Field observations	Glaciotectonic features: normal faults, reverse faults, folds	Field observations
73	Gardelegen	52°32'35.43"N 11°25'9.19"E	3434 Gardelegen	L3534 Hansestadt Gardelegen	Meltwater deposits	Scholz 1887a	Glaciotectonic features: deformation bands	Field observations
74	Hottendorf	52°32'2.49"N 11°32'42.23"E	3435 Lindstedt (Uchtspringe)	L3534 Hansestadt Gardelegen	Meltwater deposits overlain by till	Scholz 1887b	Glaciotectonic features: normal faults	Field observations
75	Niegripp	52°15'20.76"N 11°46'6.60"E	3736 Zielitz	L3736 Burg	Fluvial deposits	Korn et al. 1923		



## 9. Appendix

Table A11: Sand pits along the Elbe Lineament.

No	Locality	Coordinates	Geological map 1:25000	Geological map 1:50000	Deposits	References	Deformation structures	References
76	Alt Garge	53°15'9.36"N 10°48'14.25"E	2730 Bleckede	L2730 Boizenburg (Elbe)	Meltwater deposits overlain by paraglacial deposits (Geschiebedecksand)	Meyer et al. 2004	Glaciotectonic features: deformation bands: normal displacement, folds	Field observations
77	Bendelin	52°54'33.14"N 12° 7'48.09"E	3038 Glöwen	L3138 Havelberg	Meltwater deposits overlain by till	Grunder 1896	Glaciotectonic features: deformation bands: normal displacement	Field observations
78	Boizenburg	53°22'33.20"N 10°40'34.08"E	2630 Boizenburg (Elbe)	L2730 Boizenburg (Elbe)	Aeolian dune sand	Krienke et al. 2001		
79	Breetze	53°15'48.27"N 10°43'24.24"E	2730 Bleckede	L2730 Boizenburg (Elbe)	Meltwater deposits overlain by paraglacial deposits (Geschiebedecksand)	Meyer et al. 2004		
80	Ferbitz	53° 5'17.09"N 11°34'37.74"E	2935 Schnackenburg	L2943 Lenzen (Elbe)	Meltwater deposits	Weissermel 1901	Glaciotectonic features: folds	Field observations
81	Gusborn	53° 5'15.08"N 11°13'5.86"E	2933 Gusborn	L2932 Dannenberg (Elbe)	Meltwater deposits	Reuter 1975b	Glaciotectonic features: deformation bands: normal displacement	Field observations
82	Meudelfitz	53° 9'46.30"N 11° 0'40.06"E	2832 Dannenberg Elbe/Nord	L2932 Dannenberg (Elbe)	Meltwater deposits	Reuter 1975a	Glaciotectonic features: deformation bands: normal displacement	Field observations
83	Niendorf	53°15'59.31"N 10°43'52.48"E	2730 Bleckede	L2730 Boizenburg (Elbe)	Meltwater deposits overlain by paraglacial deposits (Geschiebedecksand)	Meyer et al. 2004		
84	Riskau	53° 5'58.53"N 11° 2'2.23"E	2932 Dannenberg Elbe/Süd	L2932 Dannenberg (Elbe)	Meltwater deposits	Lepper & Tüxen 1975		
85	Tießau	53°11'27.30"N 10°58'12.12"E	2831 Görhde	L2930 Dahlenburg	Meltwater deposits	Höfle 1977		
86	Tramm	53° 3'29.69"N 11° 4'5.85"E	2932 Dannenberg Elbe/Süd	L2932 Dannenberg (Elbe)	Meltwater deposits	Lepper & Tüxen 1975		
87	Wiershop	53°26'2.14"N 10°26'6.24"E	2528 Geesthacht	L2528 Geesthacht	Meltwater deposits overlain by till	Gagel et al. 1911		
88	Zweedorf	53°26'29.00"N 10°38'43.38"E	2529 Büchen	L2528 Geesthacht	Meltwater deposits	Gagel et al. 1914		

## 9. Appendix

Table A12: Sand and gravel pits along the Steinhuder Meer Fault.

No	Locality	Coordinates	Geological map 1:25000	Geological map 1:50000	Deposits	References	Deformation structures	References
89	Altenhagen	52°26'3.31"N 9°22'50.82"E	3522 Wunstorf	L3522 Garbsen	Meltwater deposits overlain by loess and paraglacial deposits	Voss et al. 1979	Neotectonic features: (conjugate) normal faults, reverse faults	Field observations
90	Bolsehle	52°33'52.58"N 9°17'42.03"E	3421 Husum	L3520 Rehburg- Loccum	Meltwater deposits	Voss et al. 1982	Neotectonic features?: normal faults; cryoturbation features: ice-wedge casts	Field observations
91	Eilvese	52°32'27.86"N 9°23'19.38"E	3422 Neustadt am Rübenberge	L3522 Garbsen	Meltwater deposits overlain by paraglacial deposits (Geschiebedecksand)	Jordan et al. 1980	Glaciotectonic features: conjugate normal faults; cryoturbation features: ice- wedge casts	Field observations
92	Poggenhagen	52°27'50.71"N 9°26'36.39"E	3522 Wunstorf	L3522 Garbsen	Meltwater deposits	Voss et al. 1979		
93	Rehburg	52°29'22.68"N 9°14'4.07"E	3521 Rehburg	L3520 Rehburg- Loccum	Meltwater deposits overlain by paraglacial deposits (Geschiebedecksand)	Jordan et al. 1979	Cryoturbation features: ice- wedge casts	Field observations
94	Schneeren 1	52°31'9.21"N 9°19'33.95"E	3421 Husum	L3520 Rehburg- Loccum	Meltwater deposits	Voss et al. 1982		
95	Schneeren 2	52°32'45.43"N 9°20'29.12"E	3422 Neustadt am Rübenberge	L3522 Garbsen	Meltwater deposits overlain by paraglacial deposits (Geschiebedecksand)	Jordan et al. 1980	Glaciotectonic features: normal faults	Field observations
96	Schneeren 3	52°33'18.91"N 9°20'50.42"E	3422 Neustadt am Rübenberge	L3522 Garbsen	Meltwater deposits overlain by paraglacial deposits (Grundmoräne)	Jordan et al. 1980		
97	Vehrenheide	52°29'31.34"N 9°14'45.99"E	3521 Rehburg	L3520 Rehburg- Loccum	Meltwater deposits overlain by paraglacial deposits (Geschiebedecksand)	Jordan et al. 1979		

Table A13: Sand and gravel pits of the selected section of the Regensburg-Leipzig-Rostock fault system.

No	Locality	Coordinates	Geological map 1:25000	Geological map 1:50000	Deposits	References	Deformation structures	References
98	Dresden Klotzsche	51°5'27.22"N 13°46'40.72"E	4948 Dresden	2668 Dresden	Saalian meltwater sand overlain by Weichselian alluvial and aeolian sand	Steding et al. 1994; Lange et al. 2016; Alexowsky et al. 2001; Field observations	Neotectonic features: deformation bands	Field observations
99	Auerbach	50°43'55.95"N 12°32'14.87"E	5241 Zwickau Ost		Rotliegend rocks overlain by till	Mietzsch & Credner 1875; BGR Geoviewer 2019		
100	Badrina	51°32'22.53"N 12°31'36.25"E	4441 Dübren	2465 Bitterfeld	Saalian meltwater deposits	BGR Geoviewer 2019, Koch et al. 1996a	Neotectonic features: deformation bands	Field observations
101	Benndorf	51°33'35.09"N 12°20'47.66"E	4440 Delitzsch	2465 Bitterfeld	Saalian fluvial gravel and sand	Picard & Beyschlag 1922; Koch et al. 1996a		
102	Böhlitz 1	51°2'18.41"N 11°53'14.94"E	4937 Osterfeld		Eocene-Oligocene fluvial sand and gravel overlain by Weichselian loess	Schmid 1875; Steinmüller 1993; Antares.Thueringen 2019		

## 9. Appendix

<b>103</b>	Böhlitz 2	51°2'23.74"N 11°54'34.51"E	4937 Osterfeld		Eocene-Oligocene fluvial sand and gravel overlain by Weichselian loess	Schmid 1875; Steinmüller 1993; Antares.Thueringen 2019		
<b>104</b>	Borgishain	51°1'7.31"N 12°27'37.15"E	4940 Altenburg Nord	2665 Zeitz	Pleistocene fluvial sand overlain by Weichselian loess	Kühn & Dammer 1901/02; Koch et al. 1996c; Antares.Thueringen 2019; Field observations	Cryoturbation features: ball- and-pillow structures, flame structures, ice-wedge casts, frost cracks	Field observations
<b>105</b>	Brockwitz	51°18'38.13"N 13°37'24.14"E	4647 Grossenhain- Skässchen	2568 Großenhain	Saalian meltwater deposits	Klemm & Credner 1886; Steding et al. 1995; Geoviewer.Sachsen 2019	Cryoturbation features: ice- wedge casts	Field observations
<b>106</b>	Casabra	51°14'58.66"N 13°9'34.87"E	4744 Oschatz	2567 Riesa	Saalian meltwater deposits	Siegert & Credner 1884; Siegert & Credner 1906; Steding et al. 1996a; Geoviewer.Sachsen 2019	Glaciotectonic features: deformation bands	Field observations
<b>107</b>	Churschütz 1	51°10'12.87"N 13°14'27.46"E	4845 Lommatzsch	2667 Meißen	Elsterian meltwater deposits overlain by Weichselian loess	Härtel & Kossmat 1931; Steding et al. 1996b		
<b>108</b>	Churschütz 2	51°9'59.73"N 13°15'10.43"E	4845 Lommatzsch	2667 Meißen	Elsterian meltwater deposits	Steding et al. 1996b	Neotectonic features: deformation bands	Field observations
<b>109</b>	Doberschütz	51°29'23.37"N 12°45'2.23"E	4542 Thallwitz- Strelln	2466 Eilenburg	Elsterian meltwater deposits	Grahmann et al. 1930; Müller et al. 1995a		
<b>110</b>	Farnstädt1	51°25'25.13"N 11°35'51.05"E	4535 Schraplau		Muschelkalk rocks	Speyer 1875 and 1876; BGR Geoviewer 2019; Field observations		
<b>111</b>	Farnstädt2	51°25'46.87"N 11°35'47.09"E	4535 Schraplau		Muschelkalk rocks	Speyer 1875 and 1876; BGR Geoviewer 2019; Field observations		
<b>112</b>	Frohnsdorf	50°56'9.34"N 12°35'50.46"E	5041 Langenleuba- Niedershain	2766 Chemnitz	Elsterian meltwater deposits overlain by Weichselian loess	Dalmer et al. 1879; Wolf et al. 1998; Antares.Thueringen 2019		
<b>113</b>	Gähnsnitz	50°54'44.79"N 12°32'42.12"E	5041 Langenleuba- Niedershain	2766 Chemnitz	Eocene-Oligocene fluvial deposits overlain by Weichselian loess	Dalmer et al. 1879; Wolf et al. 1998; Gläßer & Wiefel 1999; Field observations		
<b>114</b>	Grethen	51°14'27.18"N 12°45'2.23"E	4741 Naunhof Otterwisch	2566 Wurzen	Saalian meltwater deposits (glacifluvial delta)	Sauer & Credner 1880; Danzig et al. 1905; Müller et al. 1995b; Lang et al. 2018; Geoviewer.Sachsen 2019		
<b>115</b>	Großthiemig	51°22'31.20"N 13°40'50.15"E	4648 Schönfeld Ortrand	2568 Großenhain	Elsterian meltwater deposits	Herrmann & Credner 1886; Steding et al. 1995; Geo.Brandenburg 2019		
<b>116</b>	Hainchen	51°1'40.95"N 11°49'49.35"E	4936 Camburg		Eocene-Oligocene fluvial sand and gravel	Seidel & Steinmüller 1994; Antares.Thueringen 2019; Field observations	Neotectonic features: deformation bands	Field observations
<b>117</b>	Dresden Hellerberge	51°6'6.95"N 12°45'2.23"E	4948 Dresden	2668 Dresden	Weichselian alluvial and aeolian sand	Steding et al. 1994; Lange et al. 2016; Field observations	Cryoturbation features: ice- wedge casts	Field observations
<b>118</b>	Heukendorf	51°2'32.63"N 12°20'0.77"E	4939 Meuselwitz	2665 Zeitz	Pleistocene fluvial deposits overlain by meltwater deposits and Weichselian loess	Kühn 1906a, b; Koch et al. 1996c; Field observations	Cryoturbation features; Glaciotectonic features: deformation bands	Field observations
<b>119</b>	Hirschfeld	51°2'37.35"N 13°22'44.23"E	4946 Tanneberg- Deutschenbo ra	2667 Meißen	Elsterian meltwater deposits	Pietzsch & Kossmat 1914/16; Steding et al. 1996b; Geoviewer.Sachsen 2019	Cryoturbation features: ice- wedge casts; Glaciotectonic features: reverse faults	Field observations

## 9. Appendix

120	Holzweißig	51°35'53.44"N 12°17'17.32"E	4339 Bitterfeld (West)	2465 Bitterfeld	Saalian meltwater deposits	von Linstow & Beyschlag 1913; Koch et al. 1996a		
121	Jagsal	51°40'35.14"N 13°20'31.71"E	4346 Schilda		Saalian meltwater deposits	Geo.Brandenburg 2019		
122	Kleinaga	50°58'6.44"N 12° 6'44.38"E	5038 Gera (Nord)		Weichselian loess	Antares.Thueringen 2019		
123	Köckern	51°36'39.36"N 12°12'16.53"E	4339 Bitterfeld (West)	2465 Bitterfeld	Saalian meltwater deposits overlain by Weichselian loess	von Linstow & Beyschlag 1913; Koch et al. 1996a		
124	Lichterfeld	51°35'20.11"N 13°45'33.66"E	4448 Lauchhammer- Grünwalde		Saalian meltwater deposits	Hess von Wichdorff 1927; Geo.Brandenburg 2019		
125	Lichterfeld 2	51°35'23.01"N 13°44'19.89"E	4448 Lauchhammer- Grünwalde		Saalian meltwater deposits	Hess von Wichdorff 1927; Geo.Brandenburg 2019		
126	Merlach	50°51'57.76"N 12°26'34.96"E	5140 Meerane- Crimmitschau		Elsterian meltwater deposits overlain by Weichselian loess	Siegert 1881; Siegert & Credner 1904; BGR Geoviewer 2019		
127	Mischütz	51°9'10.70"N 13° 9'0.95"E	4844 Döbeln	2667 Meißen	Elsterian meltwater deposits overlain by Weichselian loess	Dathe & Credner 1879; Steding et al. 1996b		
128	Münchhausen-Ossak	51°38'52.54"N 13°38'45.09"E	4347 Doberlug- Kirchhain		Saalian meltwater deposits	Geo.Brandenburg 2019		
129	Nepperwitz	51°22'38.87"N 12°39'13.92"E	4641 Brandis- Borsdorf	2566 Wurzen	Saalian sandy till	Schalch & Credner 1881; Siegert & Credner 1903; Müller et al. 1995b; Geoviewer.Sachsen 2019		
130	Neuenmörbitz	50°58'29.35"N 12°36'42.25"E	5041 Langenleuba- Niedershain	2766 Chemnitz	Elsterian meltwater deposits overlain by Weichselian loess	Dalmer et al. 1879; Wolf et al. 1998; Gläßer & Wiefel 1999; Field observations	Glaciotectonic features: deformation bands, folds	Field observations
131	Neuposa	51°0'48.21"N 12°17'39.24"E	4939 Meuselwitz	2665 Zeitz	Elsterian meltwater deposits overlain by till	Kühn 1906a; Koch et al. 1996c; Antares.Thueringen 2019	Glaciotectonic features: recumbent fold, faults	Field observations
132(1)	Niedersteinbach	50°57'19.37"N 12°38'53.47"E	5041 Langenleuba- Niedershain	2766 Chemnitz	Elsterian meltwater deposits overlain by Weichselian loess	Dalmer et al. 1879; Wolf et al. 1998; Gläßer & Wiefel 1999; Field observations	Glaciotectonic features: ball- and pillow structures, folds, diapir like structures	Field observations
132(2)	Niedersteinbach	50°57'4.53"N 12°39'4.27"E	5041 Langenleuba- Niedershain	2766 Chemnitz	Elsterian meltwater deposits overlain by Weichselian loess	Dalmer et al. 1879; Wolf et al. 1998; Gläßer & Wiefel 1999; Field observations	Glaciotectonic features: folds, faults; Depositional loading: load casts	Field observations
133	Oberhohndorf	50°42'36.77"N 12°31'37.27"E	5241 Zwickau Ost		Rotliegend rocks overlain by till	Mietzsch & Credner 1875; BGR Geoviewer 2019		
134	Piskowitz	51°6'2.89"N 13°26'42.17"E	4846 Meißen	2667 Meißen	Elsterian meltwater deposits	Steding et al. 1996b; Geoviewer.Sachsen 2019; Field observations		
135	Pöhla	50°59'49.56"N 12°16'26.58"E	5039 Kayna	2665 Zeitz	Elsterian meltwater deposits overlain by Weichselian loess	Liebe 1878; Koch et al. 1996c; Antares.Thueringen 2019		

## 9. Appendix

136	Pomßen	51°13'36.58"N 12°36'54.10"E	4741 Naunhof Otterwisch	2566 Wurzen	Saalian meltwater deposits overlain by Saalian till	Müller et al. 1995b; Geoviewer.Sachsen 2019; Field observations	Cryoturbation features: ball- and-pillow structures,	Field observations
137	Pratzschwitz	50°58'14.74"N 13°54'12.14"E	5049 Pirna	2669 Bautzen	Saalian meltwater deposits overlain by Weichselian fluvial sand	Beck & Credner 1889; Pietzsch 1913; Lorenz 2000; Geoviewer.Sachsen 2019		
138	Puschwitz	51°27'49.82"N 13° 5'41.37"E	4544 Belgern	2467 Bad Liebenwerda	Elsterian meltwater deposits	Picard 1930; Hellwig & Müller 1998;	Glaciotectonic features: conjugate deformation bands	Field observations
139	Ramsin 1	51°36'48.60"N 12°14'45.29"E	4339 Bitterfeld (West)	2465 Bitterfeld	Saalian meltwater deposits	von Linstow & Beyschlag 1913; Koch et al. 1996a		
140	Ramsin 2	51°36'38.53"N 12°15'10.87"E	4339 Bitterfeld (West)	2465 Bitterfeld	Saalian meltwater deposits	von Linstow & Beyschlag 1913; Koch et al. 1996a		
141	Renneritz	51°36'14.02"N 12°12'52.27"E	4339 Bitterfeld (West)	2465 Bitterfeld	Saalian meltwater deposits	von Linstow & Beyschlag 1913; Koch et al. 1996a;		
142	Reuden	51°40'29.46"N 12°12'52.63"E	4339 Bitterfeld (West)	2465 Bitterfeld	Saalian meltwater deposits	von Linstow & Beyschlag 1913; Koch et al. 1996a	Cryoturbation features: ice- wedge casts	Field observations
143	Sachsendorf	51°19'25.56"N 12°51'51.19"E	4643 Dahlen	2566 Wurzen	Saalian meltwater deposits (glacifluvial delta)	Grahmann & Kossmat 1925; Müller et al. 1995b; Lang et al. 2018		
144	Sandersdorf	51°37'25.27"N 12°14'55.21"E	4339 Bitterfeld (West)	2465 Bitterfeld	Saalian meltwater deposits	von Linstow & Beyschlag 1913; Koch et al. 1996a		
145	Schilda	51°36'34.17"N 13°25'6.44"E	4346 Schilda		Elsterian till and Saalian meltwater deposits	Geo.Brandenburg 2019		
146	Schkölen	51°2'0.25"N 11°49'27.23"E	4936 Camburg		Eocene-Oligocene fluvial sand and gravel	Seidel & Steinmüller 1994; Antares.Thuringen 2019; Field observations	Neotectonic features: deformation bands	Field observations
147	Sermuth 2	51°9'34.63"N 12°46'21.06"E	4842 Colditz	2666 Mittweida	Elsterian fluvial deposits	Koch et al. 1996b; Field observations	Cryoturbation features: sheared lenses, low-angle reverse faults	Field observations
148	Sermuth 1	51°8'58.53"N 12°46'36.74"E	4842 Colditz	2666 Mittweida	Elsterian fluvial and meltwater deposits	Siegert et al., 1900; Koch et al. 1996b; Field observations	Glaciotectonic features: ice- wedge casts, involutions	Field observations
149	Siebenhau- sen	51°41'49.92"N 12°14'1.00"E	4339 Bitterfeld (West)	2465 Bitterfeld	Saalian meltwater deposits	von Linstow & Beyschlag 1913; Koch et al. 1996a		
150	Steinbach	50°56'37.10"N 12°38'6.08"E	5041 Langenleuba- Niedershain	2766 Chemnitz	Elsterian meltwater deposits overlain by Weichselian loess	Dalmer et al. 1879; Wolf et al. 1998; Gläßer & Wiefel 1999; Field observations		
151	Stöbnig	51°3'41.78"N 12°48'21.08"E	4942 Rochlitz	2666 Mittweida	Elsterian meltwater deposits overlain by Weichselian loess	Dathe et al. 1876; Koch et al. 1996b; Geoviewer.Sachsen 2019		
152	Strauch	51°22'40.07"N 13°34'2.96"E	4647 Grossenhain- Skässchen	2568 Großenhain	Saalian meltwater deposits	Klemm & Credner 1886; Steding et al. 1995; Geoviewer.Sachsen 2019	Cryoturbation features: flame structures, involutions Glaciotectonic features: deformation bands, folds	Field observations

## 9. Appendix

<b>153</b>	Thierbaum	51°6'11.68"N 12°44'50.03"E	4842 Colditz	2666 Mittweida	Elsterian meltwater deposits overlain by Weichselian loess	Siegert et al. 1900; Koch et al. 1996b	Glaciotectonic features: deformation bands	Field observations
<b>154</b>	Tröbitz	51°37'3.35"N 13°25'42.77"E	4346 Schilda		Elsterian till and Saalian meltwater deposits	Geo.Brandenburg 2019		
<b>155</b>	Wendelstein	51°16'51.87"N 11°28'18.39"E	4734 Wiehe		Early Pleistocene to Elsterian fluvial gravel	Dames 1875; Geoviewer.Sachsen 2019		
<b>156</b>	Zeihscha	51°29'53.71"N 13°26'40.38"E	4446 Bad Liebenwerda	2467 Bad Liebenwerda	Elsterian meltwater deposits	Hellwig & Müller 1998; Geo.Brandenburg 2019		

## Acknowledgements

The years as researcher at the Leibniz University Hannover and the writing of this dissertation were a meaningful and learning but also a challenging time for me. Without the support, patience and guidance of the following people, this research would not have been possible. It is also to them that I owe my deepest gratitude.

First and foremost, I would like to thank Prof. Dr. Jutta Winsemann and Dr. Christian Brandes for giving me the opportunity to pursue my dissertation within two research projects.

Prof. Dr. Jutta Winsemann is thanked for her scientific advice, guidance, support and constructive critiques of this research work. I especially want to thank Prof. Dr. Jutta Winsemann for sharing her broad knowledge of sedimentology with me.

I am very grateful to Christian for his support during the last years. Thank you for your scientific advice, positivity, and encouraging words during stressful phases of paper submissions. Thank you for your help during fieldwork and thank you for the coffee breaks.

I am also very grateful to Prof. Dr. Manfred Frechen for discussion and for the co-examine of this thesis and Prof. Dr. Stefan Weyer for his support as a chairman of the examination committee.

The owners of the sand and gravel pits are thanked for the permission to work on their properties.

I would like to thank Prof. Dr. Thomas Spies, Dr. Thomas Lege, Dr. Diethelm Kaiser, Dr. Jörg Schlittenhardt and Dr. Manuel Hobiger from the BGR for discussion and constructive critiques that helped to improve this work.

I would like to thank Dr. Holger Steffen for his support and for the determination of the numerical simulations of glacial isostatic adjustment. Thank you Holger, for your collegiality. Dr. Ulrich Polom is thanked for discussion and introduction to the shear-wave seismic method. I am very grateful to Dr. Sumiko Tsukamoto and Dr. Yan Li for sharing their knowledge of luminescence dating with me and for their help and support during luminescence dating.

Prof. Dr. Hans-Joachim Franzke, Dr. David C. Tanner, Dr. Thomas Günther, Dr. Jan Igel, Prof. Dr. Małgorzata Pisarska-Jamrozły are thanked for paper discussion.

Sonja Riemenschneider, Gudrun Drewes, Petra Posimowski, Sabine Mogwitz and Astrid Techmer (LIAG) are thanked for their support during sample preparation and their collegiality. I would like to especially thank Sonja and Gudrun for their kindness. Runa Fälber is thanked for her help during fieldwork and DEM analysis. Runa, thank you for the nice weeks in Saxony. Furthermore, I would like to thank my colleagues Jörg, Deyan, Nils, Gang, George, Katharina, Uli, Philipp, Jill, and Meike for nice conversations, coffee breaks and their support during these years. Dr. Lena Steinmann, Linda Oppermann, Dagmar Müller, Oliver Böhm and Marco Büscher are thanked for proof-reading.

Last but not least I want to thank my family, especially my parents for endless support throughout the years and never stopping their belief in me. I am very grateful to have such great friends who always supported me, thank you Linda, Lena, Melanie, Svenja, Elisa, Malte and Tina, Bernie and Olli for everything.



## Curriculum Vitae

Name	Katharina Müller
Date of birth	25.07.1989
Place of birth	Neustadt am Rübenberge
Citizenship	German

### Education

10/2016 - 02/2022 **Doctoral programme** in Earth Sciences at Gottfried Wilhelm Leibniz Universität Hannover, Germany, *specialization geology*

10/2013 - 07/2016 **Master of Science** in Earth Sciences at Gottfried Wilhelm Leibniz Universität Hannover, Germany, *specialization geology*

10/2010 - 10/2013 **Bachelor of Science** in Earth Sciences at Gottfried Wilhelm Leibniz Universität Hannover, Germany, *specialization mineralogy*

### Practical experience

10/2016 - 02/2021 **Research assistant** at Institut für Geologie, Gottfried Wilhelm Leibniz Universität Hannover, Germany

03/2014 - 07/2016 **Student research assistant** at Institut für Geologie und Mineralogie, Gottfried Wilhelm Leibniz Universität Hannover, Germany

02/2013 - 04/2013 **Internship**, 6 weeks at Leibniz Institut für Angewandte Geophysik, Geozentrum Hannover, Germany, *division geothermal energy and information systems*

## Publications in peer-reviewed journals and peer-reviewed books

- Müller K**, Winsemann J, Kaiser D, Lege T, Spies T, Brandes C (submitted) Re-examination and neotectonic analysis of the N-S trending Regensburg-Leipzig-Rostock fault system between Leipzig and Cheb
- Müller K**, Winsemann J, Pisarska-Jamroży M, Lege T, Spies T, Brandes C (2021) The challenge to distinguish soft-sediment deformation structures formed by glaciotectonic, periglacial and seismic processes in a formerly glaciated area: a review and synthesis. In: *Steffen H, Olesen O. and Sutinen R. (eds): Glacially-Triggered Faulting, Cambridge University Press*
- Müller K**, Winsemann J, Tanner DC, Lege T, Spies T, Brandes C (2021) Glacially-Induced Faults in Germany. In: *Steffen H, Olesen O and Sutinen R (eds): Glacially-Triggered Faulting, Cambridge University Press*
- Munier R, Adams J, Brandes C, Brooks G, Dehls J, Gibbons SJ, Hjartardóttir ÁR, Hogaas F, Johansen TA, Kvaerna T, Mattila J, Mikko H, **Müller K**, Nikolaeva SB, Ojala A, Olesen O, Olsen L, Palmu J-P, Ruskeenieni T, Ruud BO, Sandersen PBE, Shvarev SV, Smith CA, Steffen H, Steffen R, Sutinen R, Tassis G (2020) International database of Glacially Induced Faults. *Pangaea* <https://doi.pangaea.de/10.1594/PANGAEA.922705>.
- Müller K**, Polom U, Winsemann J, Tsukamoto S, Steffen H, Igel J, Günther T, Spies T, Lege T, Frechen M, Franzke H-J, Brandes C (2020) Structural style and neotectonic activity along the Harz Boundary Fault, northern Germany: A multimethod approach integrating geophysics, outcrop data and numerical simulations. *International Journal of Earth Sciences* 109:1811-1835
- Brandes C, Igel J, Loewer M, Tanner DC, Lang J, **Müller K**, Winsemann, J (2018) Visualisation and analysis of shear-deformation bands in unconsolidated Pleistocene sands using ground-penetrating radar: Implications for paleoseismological studies. *Sedimentary Geology* 367:135-145

## Conference contributions (Abstracts)

- Müller K**, Winsemann J, Pisarska-Jamroży M, Lege T, Spies T, Brandes C.: Limitations of soft-sediment deformation structures as indicator for paleo-earthquakes in formerly periglacial and glaciated areas, *EGU General Assembly 2020, online*
- Müller K**, Winsemann J, Polom U, Steffen H, Tsukamoto S, Günther T, Igel J, Spies T, Frechen M, Brandes C: Neotectonics and paleoseismicity - The reactivation potential of faults in northern Germany due to glacial isostatic adjustment, *BGE - Tage der Standortauswahl 2019, Braunschweig, Germany*
- Brandes C, Igel J, Loewer M, Tanner D, Lang J, **Müller K**, Winsemann J: 3-D analysis of shear-deformation bands in unconsolidated Pleistocene sands with ground-penetrating radar: Implications for paleoseismological studies. *INQUA, 2019, Dublin, Ireland*
- Müller K**, Winsemann J, Polom U, Frechen M, Tsukamoto S, Igel J, Spies T, Lege T, Steffen H, Brandes C: Lateglacial reactivation of the Harz Boundary Fault (northern Germany) caused by glacial isostatic adjustment. *INQUA, 2019, Dublin, Ireland*
- Müller K**, Winsemann J, Polom U, Igel J, Tsukamoto S, Steffen H, Spies T, Lege T, Frechen M, Brandes C: Paleoseismological investigation of northern Germany. *EGU General Assembly, 2019, Vienna, Austria*
- Müller K**, Polom U, Winsemann J, Tsukamoto S, Steffen H, Spies T, Lege T, Frechen M, Franzke H-J, Brandes C: Active faults and paleoseismicity in northern Germany induced by glacial isostatic adjustment: An example from the Harz boundary fault zone. *Symposium on Postglacial faults, 2018, Kautokeino, Norway*
- Müller K**, Brandes C, Polom U, Tsukamoto S, Spies T, Lege T, Frechen M, Winsemann J: Neotectonic analysis of the Harz boundary fault (northern Germany). *EGU General Assembly, 2018, Vienna, Austria*
- Brandes C, Igel J, Loewer M, Tanner DC, Lang J, **Müller K**, Winsemann J: Visualisation and 3-D structural analysis of shear-deformation bands in unconsolidated Pleistocene sands with ground-penetrating radar. *EGU General Assembly, 2018, Vienna, Austria*
- Müller K**, Brandes C, Polom U, Tsukamoto S, Spies T, Lege T, Frechen M, Winsemann J: Paleoseismological analysis of the Harz boundary fault, northern Germany. *5<sup>th</sup> International Colloquium Historical Earthquakes, Paleoseismology, Neotectonics and Seismic Hazard; 2017, Hanover, Germany*